Lecture Notes in Electrical Engineering 290

Electronic Navigation
Research Institute
Editor

Air Traffic Management and Systems

Selected Papers of the 3rd ENRI International Workshop on ATM/CNS (EIWAC2013)

Springer

For further volumes:
http://www.springer.com/series//7818

Electronic Navigation Research Institute (ENRI)
Editor

Air Traffic Management and Systems

Selected Papers of the 3rd ENRI International Workshop on ATM/CNS (EIWAC2013)

Springer

Editor
Electronic Navigation Research
Institute (ENRI)
Tokyo, Japan

ISSN 1876-1100 ISSN 1876-1119 (electronic)
ISBN 978-4-431-54474-6 ISBN 978-4-431-54475-3 (eBook)
DOI 10.1007/978-4-431-54475-3
Springer Tokyo Heidelberg New York Dordrecht London

Library of Congress Control Number: 2014930335

Preface

The Electronic Navigation Research Institute, ENRI, is a national laboratory in Tokyo, Japan. ENRI specializes in air traffic management, communication, navigation, and surveillance, i.e., ATM and CNS, for aviation. As one of its contributions to aviation, ENRI organizes a workshop titled "ENRI International Workshop on ATM/CNS (EIWAC)" to develop civil aviation by exchanging and sharing updated information about ATM/CNS in the world. The third EIWAC, EIWAC2013, was held in February 2013 in Tokyo. The agenda of EIWAC2013 included keynote speeches by opinion leaders in civil aviation, a panel discussion, and technical presentations by specialists. In addition, the exhibitions by institutes or companies from the aviation field provided good opportunities for exchange and discussion of samples or data.

This book is designed to provide a view of current and future ATM and related systems discussed at EIWAC2013. The topics that appear in this book span a wide area, ranging from the EIWAC keynote speeches and mathematical models of aircraft trajectory to error analysis of systems in the field. The technical topics were selected from the proceedings presented in the technical sessions for EIWAC2013. The presentations were appreciated for their usefulness by attendees from the areas of ATM and CNS. In addition, the presentations were recognized by reviewers as works with significant contributions on new proposals, methods, experience, or surveys summarizing essential papers in related areas. After the selection process, the articles were compiled for this book.

An introduction to EIWAC2013 is provided in Part I. The papers on ATM such as conflict detection, separation assurance, trajectory prediction, and optimization are included in Part II. Papers on tools and evaluation for ATM are in Part III, and those on theory and experience for improving CNS are in Part IV. More than ten papers in the CNS area were presented at EIWAC2013 but only two of those are found in this Part. Most contents of the papers not in this book will appear in other publications such as related project reports on CNS systems. Finally, Part V contains a paper that is refined material for a tutorial session.

I hope that this book will be a good record of what researchers achieved at EIWAC2013 in the way of drafting the future for ATM and CNS. I hope, also, that

this book will be distributed so as to allow these excellent research results to be accessible to readers throughout the world.

I would like to express my deep appreciation to the members of the EIWAC2013 Technical Program Committee and the Associate Editors for their special support in drafting the editorial policy. They are listed in this book with special thanks.

Tokyo, Japan Shigeru Ozeki

Contents

Committee Member List

EIWAC 2013 Technical Program Committee

Editor in Chief
Shigeru Ozeki [Electronic Navigation Research Institute (ENRI), Japan]

Editors
Jean-Marc Loscos [Direction des Services de la Navigation Aérienne (DSNA), France]
Dong Min Kim [Korea Aerospace Research Institute (KARI), Korea]
Masatoshi Harigae [Japan Aerospace Exploration Agency (JAXA), Japan]
Takeshi Tsuchiya [University of Tokyo, Japan]
Ken Ito [ENRI, Japan]
Masato Fujita [ENRI, Japan]

Associate Editors
Claus Gwiggner [Universität Hamburg, Germany]
Sachiko Fukushima [ENRI, Japan]
Kota Kageyama [ENRI, Japan]
Mark Brown [ENRI, Japan]
Naruto Yonemoto [ENRI, Japan]
Susumu Saito [ENRI, Japan]

Part I
Introduction

Introduction to the Third ENRI International Workshop on ATM/CNS (EIWAC 2013)

Kazuo Yamamoto

Abstract ENRI organized the third ENRI International Workshop on ATM/CNS (EIWAC 2013) in Tokyo to share comprehensive information on the latest ATM/CNS technologies and operations among EIWAC participants. In this chapter, the overview of EIWACs, the speaker, title and summary of each keynote speech in EIWAC 2013 are presented. The contents of discussion in the EIWAC panel session are summarized. The discussion in the EIWAC has demonstrated the problems that present aviation system is facing and the prospective solutions for realizing future aviation system.

Keywords ATM • CNS • EIWAC • ENRI • Global air navigation plan

1 Introduction

Electronic Navigation Research Institute (ENRI) is an Independent Administrative Institution in Japan funded mainly from the Ministry of Land, Infrastructure, Transport and Tourism. ENRI has been conducting research, development and test on electronic navigation systems for more than 45 years. ENRI expanded its area of activity and is now an only institute in Japan specialized in Air Traffic Management (ATM), Communication, Navigation and Surveillance (CNS) for aviation.

Demand for increasing air traffic capacity, efficiency and safety has become more and more conspicuous in the world. It is said that the solution to the demand is a fully-harmonized global air navigation system based on modern performance based technologies and procedures. However, it is not necessarily easy for the people in aviation society in Japan to share comprehensive information on the latest ATM/CNS technologies and operations for the above system. In addition to that,

K. Yamamoto (✉)
Electronic Navigation Research Institute (ENRI), Chofu182-0012, Japan
e-mail: yamamoto@enri.go.jp

Electronic Navigation Research Institute (ENRI), *Air Traffic Management and Systems*, Lecture Notes in Electrical Engineering 290, DOI 10.1007/978-4-431-54475-3_1,

ENRI has been expected to contribute to realizing safer, more efficient and seamless Asian sky. Thus ENRI decided to organize an international workshop discussing ATM/CNS technologies, operations and the Asian sky improvement. We named the workshop "ENRI International Workshop on ATM and CNS" (EIWAC). The first workshop was held in 2009 and the newest one (EIWAC 2013) was held in February 2013 in Tokyo.

The purpose of this book is to provide distinguished subjects presented and discussed in EIWAC 2013. In this chapter, the overview of EIWACs is described first. The speaker, title and summary of each keynote speech in EIWAC 2013 are presented. Then, the panelists, topics and the contents of discussion in the EIWAC panel session are summarized. Selected and revised papers from the contributions presented in the technical sessions will be provided in the following chapters.

2 Overview of EIWACs

In March 2009, ENRI organized the first ENRI International Workshop on ATM and CNS [1] in Tokyo with the theme "Towards Future ATM/CNS." It was the first international workshop specialized in ATM/CNS and related topics in Japan. The EIWAC consisted of the plenary session where keynote speeches were performed and the technical sessions. Twenty-two presentations in six sessions including four keynote speeches were performed. The second EIWAC [2] was held at Tokyo Akihabara in 2010. Forty-five presentations in 19 sessions including seven keynote speeches were performed. A panel session was added in the second EIWAC to discuss future automated ATM. The workshop was a great success by many impressive presentations and very active discussion with more than 500 participants. The third EIWAC [3] was held at Tokyo Odaiba on February 19–21, 2013.

Table 1 is a brief summary of the EIWAC series. It shows that keynote speeches and foreign guests are increasing in number and the variety of keynote speeches is expanding with each event. The quality of presentations has been improved from one event to next because in the second EIWAC, reviewing process was introduced to submitted contributions. Then, more precise reviewing was done by more specialists not only from ENRI but from other institutions in the third EIWAC. The number of supporters is also increasing from one event to next.

Challenges we offered first in the EIWAC 2013 were as follows:

- Invitation of outstanding and influential keynote speakers from International Civil Aviation Organization (ICAO), operators, and an aircraft manufacturer,
- Very innovative topics and discussion in the panel session,
- Many young researchers and students in the technical and poster sessions,
- Tutorial concerning mathematical modeling and applications to trajectory optimization problems,
- Many speakers and audience from Asian countries especially from Republic of Korea and Thailand, and
- Close review of selected contributions for this publication.

Table 1 Summary of the EIWAC series

Serial Number	1	2	3
Name	EIWAC 2009	EIWAC 2010	EIWAC 2013
Date, Year	March 5–6, 2009	November 10–12, 2010	February 19–21, 2013
Venue	Ohtemachi Sankei Plaza, Tokyo	Akihabara convention hall, Tokyo	Odaiba Miraikan hall, Tokyo
Theme	Towards future ATM/CNS	Safety, efficiency and environment	Drafting future sky
Keynote speakers	4	7	9
Panel session		Title: "Future of Automation in ATM", six panelists	Title: "Future ATM: Centralized, de-centralized or best mixed", four panelists
Other sessions			Poster session and Tutorial
Technical sessions	6	19	17
Total presentations	22 including 13 foreign speakers	45 including 33 foreign speakers	46 including 33 foreign speakers
Participants	480 including 20 foreign guests	550 including 60 foreign guests	540 including 80 foreign guests
The states of participants	7	14	13
Proceedings	ENRI International Workshop on ATM/CNS, March 2009	The second ENRI International Workshop on ATM/CNS, November 2010	The third ENRI International Workshop on ATM/CNS, February 2013
The number of organizing/programming committee members and their affiliations	11 from ENRI	16 from ENRI, University of Tokyo (UoT) and Japan Aerospace Exploration Agency (JAXA)	20 from ENRI, UoT, JAXA, Japan Civil Aviation Bureau, Direction des Services de la Navigation Aérienne and Korea Aerospace Research Institute
Supporters	4	6	13

Above summary and challenges show that more and more people in the world have been interested in the EIWAC with each event. The topics in the EIWAC have become more and more updated, refined and important. Therefore, we believe that EIWAC has become one of the most attractive symposiums about ATM/CNS and related topics in the world.

3 Keynote Speeches

Keynote speakers and presentations at the plenary sessions in EIWAC 2013 are summarized in this section. The presentations are available at ENRI website [3].

3.1 Nancy Graham, "The ICAO Approach to Global Air Navigation Plan"

Nancy Graham is director of air navigation bureau of ICAO. Her presentation can be divided into two topics as summary of the 12th Air Navigation Conference and the steps which should be taken after the conference. In the 12th Air Navigation Conference, held at ICAO headquarters from 19th to 30th November 2012, four important milestones were presented as "Global Air Navigation Plan (GANP)", "2012 Safety Report", "ASBU Block 0 iKit" and "Air Operator Certificates (AOC) iKit." Where, Aviation System Block Upgrade (ASBU) shows the target availability timelines for a group of operational, technological and procedural improvements to realize a fully-harmonized global air navigation system.

Figure 1 depicts the ASBU composing of four Blocks (Block 0–3) and four performance improvement areas [4]. Where, smaller white squares in each block are called "Modules" representing operational performance to be attained and the means to be realized.

Secondly, she presented several steps to be taken after the conference. Most of these steps are aiming to promote Block 0 implementation. Followings are examples of these steps:

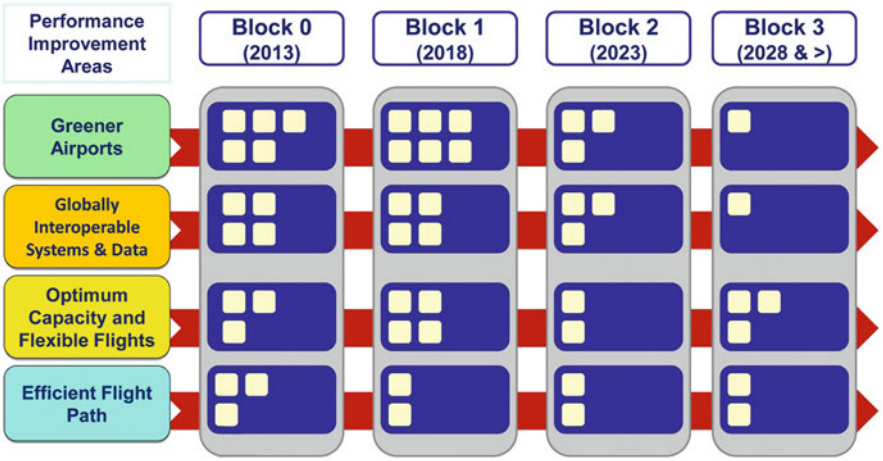

Fig. 1 Aviation system block upgrade (ASBU)

- Environmental and operational assessments of Block 0 modules,
- Technical meetings to help promote Block 0 and Block 1,
- Incentives and financing policies for operators and Air Navigation Service Providers (ANSPs) to introduce new technologies and procedures,
- End-to-end demonstration of new ATM concepts, and
- Reinforcement of Block 0 implementation strategies.

From her presentation, we can conclude that ASBU has become an important guideline for our future ATM policies. We have to take into account implementation of already developed technologies in practical operations on a step by step manner.

3.2 Mark Reeves, "Developments in NextGen"

Next Generation Air Transportation System (NextGen) is a comprehensive initiative that United States government is promoting to introduce next generation air transportation system to US airspace by 2025. Mark Reeves, director of Federal Aviation Administration (FAA) presented several examples for operational upgrade that NextGen will bring as:

- From ground based Navigation & Surveillance to Satellite based Navigation & Surveillance,
- From Air Traffic Control (ATC) communication by voice to by digital communication,
- From disconnected information systems to more readily accessible systems, and
- From fragmented weather forecasting to forecasts embedded into decisions.

Then he described recent operational improvements and successes based on NextGen as:

- Expansion of Automatic Dependent Surveillance Broadcast (ADS-B) and Performance Based Navigation (PBN),
- Optimized profile descents,
- Greener skies over Seattle by fewer emissions and by PBN arrival procedures,
- Better access to small airports, and
- Surface data-sharing for more efficient ground operations.

As a near future plan, he explained Mini-Global Demonstration in 2014 which is designed to show the validity of System Wide Information Management (SWIM).

From his presentation, we could obtain the update of NextGen activities and the current topics that NextGen is focusing. The information will help us harmonize our R&D plans with NextGen.

3.3 *Patrick Souchu, "From SESAR to Standardization"*

Single European Sky ATM Research (SESAR) is an ATM improvement program involving all aviation players for defining, committing to and implementing a pan-European program for Single European Sky. Patrick Souchu, Direction des Services de la Navigation Aérienne (DSNA) and council chair of European Organisation for Civil Aviation Equipment (EUROCAE) as well, reported five major SESAR activities recently released as:

- Traffic Synchronization: (a) Development of streaming techniques including point merge procedures in a multi airport terminal control area, (b) Development of ATC assistance tools in the application of initial 4D (i4D) concept and upgraded airborne system,
- Airport Integration and throughput: (a) Detection and alert of runway incursion and infringements of restricted areas by aircraft and vehicles, (b) Linking airport operations plan with network operations plan for better surface management,
- Moving from Airspace to 4D trajectory management: Coordination between Air Traffic Service (ATS) units through flight objects exchange mechanisms,
- Conflict management and automation: Introduction of short term conflict alert system using Mode S Down-linked aircraft parameters, and
- Network collaborative management and demand capacity balancing: (a) Development of the short term air traffic flow and capacity management procedures, (b) Enhancement of flight plan processing based on 4D profiles and aircraft performance.

As council chair of EUROCAE, he described EUROCAE and its activities as well. EUROCAE is a non-profit organization with an objective of developing technical standards in support of the aviation society mainly in Europe. He explained a brief history of EUROCAE, working group activities and the relations with other bodies such as ICAO, the Radio Technical Commission for Aeronautics (RTCA), SESAR Joint Undertaking and European Aviation Safety Agency (EASA). He stressed the gaps among R&D, standardization and implementation in many aviation systems.

When the SESAR R&D activities are compared with the NextGen presented by Mark Reeves in Sect. 3.2, we found several topics that were emphasized in one project but not in the other. It shows that the environmental differences between USA and EU will cause different highlights of the problems. Thus, we must examine the problems we are now facing and estimate the importance and urgency in Japanese sky.

3.4 *Kazuo Yamamoto, "JCAB CARATS and ENRI's R&D Activities"*

Kazuo Yamamoto, former director of research planning and management of ENRI described the relationship between Japan Civil Aviation Bureau's (JCAB)

Collaborative Actions for Renovation of Air Traffic Systems (CARATS) and ENRI's R&D activities. In the presentation, he provided the overview of JCAB CARATS and ENRI's major R&D projects and the results. Some practical outcomes derived from the cooperation between ENRI and CARATS were also presented.

3.5 Martin Eran-Tasker, "Future ATM – From Asian Operator's Point of View"

Martin Eran-Tasker is technical director of Association of Asia Pacific Airlines (AAPA). The first half of his presentation was concerning the facts about current Asian air traffic and business environment as:

- 655 million passengers, 18 million tons of cargo per year and 4,984 aircraft,
- Moderate global economy and volatility oil price,
- Increasing passenger traffic but stagnated cargo demand, and
- Significant and rapid traffic growth in the long run.

Under such environment, Martin Eran-Tasker described how future ATM system should be to keep pace with Asian traffic growth. He first pointed out that as "Cost of No Action", congestion, delay, degradation of aviation safety and lack of capacity for growth would be brought about in Asia Pacific sky. Thus, he said that "do nothing" is not an ATM option and common political will and policy solutions must be shared in Asia Pacific region. Then he presented near term wish list by Asia Pacific airlines as:

- Promotion of seamless airspace between north Asia and rest of Asia Pacific,
- Adoption of PBN for en-route implementation of Required Navigation Performance (RNP) 4 and for approach of Non Precision Approach (NPA), Approach Procedure of Vertical guidance (APV) and GPS Landing System (GLS),
- Rapid implementation of ADS-B out and surveillance based separation assurance, and
- Regional but globally harmonized and interoperable thinking and solutions.

He concluded that the lack of seamless Asian sky is causing inefficient and constrained airspace, increasing operational cost and fuel consumption. We then have to recognize that ATM safety and operational efficiency go beyond national airspace and/or borders, thus globally harmonized and interoperable policies and solutions are indispensable.

3.6 Yoichi Nakamura, "MRJ Features and Navigation Perspective"

Mitsubishi Regional Jet (MRJ) is a new passenger airplane that Mitsubishi Aircraft Corp. has developed and is now in the process of final assembly after a long blank

of passenger airplane production in Japan. Yoichi Nakamura of Mitsubishi Aircraft Corp. presented the general specification/features of MRJ family and its expected operations.

First, key concepts of MRJ were presented about efficiency, operational performance and accommodation. Then, major features of MRJ for operation were presented as:

- Equipment of almost all the latest CNS systems as Aeronautical Telecommunication Network (ATN) Baseline 1, RNP10/RNAV2&1, RNP Authorization Required (AR), Satellite Based Augmentation System (SBAS), Localizer Performance with Vertical (LPV) guidance, ADS-B out etc. for meeting future ATM,
- Flight deck with future CNS/ATM environment and improved situation awareness by large and high density Primary Flight Display (PFD) and navigation displays,
- Flight Management System (FMS) with all navigation functions and capabilities to control RNAV/RNP and SBAS or Wide Area Augmentation System (WAAS) operations, and
- Vertical Situation display, graphical flight planning and the route window displaying the progress of planned flight.

His presentation suggested that future operation will be more dependent on the performance of aircraft CNS/ATM systems than that of present airplanes.

3.7 Blair Cowles, "Aircraft Operator's ATM Overview"

Blair Cowles, assistant director of the International Air Transport Association (IATA) described the role of IATA, important facts of present world air transport and market forecast. Then, he explained Safety, Operations and Infrastructure (SO&I). As the means of infrastructure enhancement, he proposed the implementation of PBN, continuous descent operations (CDO) and continuous climb operations (CCO). Environments that may cause inefficiencies and delays were also pointed out as:

- Fragmented air navigation services,
- Regulations to equip many CNS systems, and
- Non-harmonized skies.

He emphasized the necessity of harmonized ATC and regional air navigation service network in Asia Pacific region to attain seamless skies. He said the necessity of political leadership and mandate as well for establishing Asia Pacific regional plan.

He concluded that we should plan for the future growth, consider future regional structures to manage the transition to future ATM system. He called for infrastructure improvement in states and between states to realize seamless ATM in Asia Pacific.

3.8 Franck Giraud, "Certification & Oversight of Air Navigation Service in EU System"

Franck Giraud is director of international cooperation of French civil aviation authority. He first described that formerly in Europe, Air Navigation Services (ANSs) were provided by EU public entities. However, during 1998–2004, EU decided to separate ANSs and regulatory functions in the context of Single European Sky. After 2004, European states reorganized their own ANSs.

Franck Giraud then presented EU principles of certification and surveillance of ANS after 2004. The EU principles are based on three concepts and activities as:

- Certification of ANSP, which means that an ANSP must be certified by the national supervisory authority,
- Continuous safety oversight, which means that once an ANSP gets initial certification, a process of continuous oversight of the ANSP must be performed,
- Specific applications to technical systems in three ways of supervision as:
  - Guarantee the safety of changes in a system,
  - Apply specific regulation to operation software in a system, and
  - Apply specific requirements for interoperability of systems all around Europe.

He showed practical procedures for a technical system certification. For example, when an ANSP conducts safety analysis of the ATM system that has been changed or updated, the ANSP will identify the items that may affect safety and analyze them to get the results. The results will be sent to the authority for approval.

His presentation provided important information about future roles of an ANSP and the authority. It also showed that the core of certification requirements is based on Safety Management System (SMS) retained by each ANSP.

3.9 Akbar Sultan, "NASA NextGen Operations Research"

Akbar Sultan is deputy director of Airspace Systems Program, National Aeronautics and Space Administration (NASA) headquarters. His presentation covered NASA's Airspace System Programs (ASPs). He showed current major projects belonging to the ASPs as:

- Automation technologies to mitigate traffic bottlenecks and weather restrictions,
- Dynamic weather routing,
- Spot and runway departure advisor, airspace model tools, and
- Future ATM Concepts Evaluation Tool (FACET).

Recent international partnerships for bi-lateral benefits were also presented:

- NASA/FAA research transition teams,
- ASP Industry Days and technical interchange meetings, and
- ATM technical demonstrations.

Before concluding his remark, he addressed the importance of partnership of researchers belonging to different organizations. ENRI is now discussing practical topics for future ENRI–NASA collaboration with him.

4 Panel Session

EIWAC 2013 Panel was held on February 19th 2013 with the theme "Future ATM: Centralized, decentralized or best mixed?" The objective of the panel is to provide EIWAC 2013 participants with the idea on post ASBU operation. The panelists were Patrick Souchu of DSNA, Todd Lauderdale of University of California, Shinji Suzuki of University of Tokyo and Blair Cowles of IATA. And the moderator was Shigeru Ozeki of ENRI.

In the panel, Shigeru Ozeki summarized the current status and future ATM plans discussed in ICAO, NextGen, SESAR and CARATS. Several key technologies and future ATM plans appeared in these projects were: (a) Airborne participation in collaborative ATM, (b) Traffic complexity management, (c) Airborne self separation, (d) Full 4D trajectory based operation, (e) SWIM, (f) Performance based operation, and so on.

Then, each panelist was asked to express his opinions about the future ATM plans.

Prof. Suzuki addressed from aircraft dynamics point of view, that predictability of aircraft trajectory will be greatly influenced by wind. As the range of efficient speed control of present airplanes is strictly limited, centralized traffic control will need enormous meteorological data for timely and precise speed control, he said.

Mr. Souchu expressed his opinion from ANSP's point of view that air traffic will greatly depend on the operation environment. If airspace is not very crowded and the possibility of conflict is low, decentralized operation will achieve better performance than centralized one. On the contrary, if traffic density is very high, centralized operation will be more efficient. He said that standardized flight procedures will be indispensable depending on the traffic density in airspace.

Mr. Cowles presented his opinion from an aircraft operator's point of view that no matter what flight procedures are introduced, we should take advantage of present aircraft's navigation performance and avoid expensive additional equipage. He stressed that most present FMSs have primary performance of trajectory based operation and we should pursue more efficient operation under current FMS performance.

Dr. Lauderdale expressed his opinion from a traffic researcher's point of view. He said that distributed autonomous system is flexible but will be difficult to bring about optimum solutions for total traffic. On the other hand, centralized system can bring total optimum solutions but easily be affected by uncertainties. He suggested that appropriate harmonization of centralized and distributed or autonomous systems will be an answer.

Fig. 2 EIWAC 2013 panelists and moderator (Mr. Ozeki, Prof. Suzuki, Mr. Souchu, Dr. Lauderdale and Mr. Cowles from left to right)

These opinions showed the necessity of function sharing of different aviation systems for future ATM. A panelist pointed out if such function sharing is to be introduced, human factor will be more and more important because each system will be operated by different people.

Finally, moderator Mr. Ozeki addressed that the discussion suggested post ASBU ATM framework and the prospects for future air traffic would be bright. He finally expressed his gratitude to the panelists and the participants in the session for their proactive and fruitful discussion. Figure 2 shows the moderator and panelists.

5 Conclusions

The third ENRI International Workshop on ATM and CNS (EIWAC 2013) was held in February 2013 for the purpose of sharing comprehensive information on the latest ATM/CNS technologies and operations among EIWAC participants from all over the world and of seeking potential partners for collaboration.

History and overview of the EIWAC series were described first. Then, the topics and opinions presented by the keynote speakers belonging to different organizations

as regulator, ANSP, operator, R&D institute and university were summarized. The keynote speeches have shown that the speakers have common recognition about the problems that present aviation system is facing, but have diverse views for solving the problems and for realizing the future aviation system.

Noteworthy opinions and major conclusions in the panel session titled “Future ATM: Centralized or Decentralized or Best mixed?” were presented. The discussion in the panel focused on several key technologies based on centralized operation and decentralized or distributed autonomous operation. An important conclusion of the discussion was to construct an appropriate function sharing framework between centralized and decentralized operations for future aviation system. We can say that the panel has suggested us post ASBU ATM environment.

ENRI is now planning to hold next EIWAC in 2015. The next EIWAC will also attract many people in the aviation society worldwide and can contribute to the advancement of global aviation system.

References

1. EIWAC 2009 homepage, http://www.enri.go.jp/eiwac/2009/en/
2. EIWAC 2010 homepage, http://www.enri.go.jp/eiwac/2010/en_EIWAC2010siryou.html
3. EIWAC 2013 homepage, http://www.enri.go.jp/e_EIWAC2013siryou.html
4. International Civil Aviation Organization, “2013–2028 Global Air navigation Capacity & Efficiency Plan, 2014–2016 Triennium Edition,” DOC 9750, 2014, pp 10–11

Part II
Air Traffic Managements

Probabilistic Conflict Detection in the Presence of Uncertainty

Yoshinori Matsuno and Takeshi Tsuchiya

Abstract In order to satisfy the increasing demand in air traffic, the automated air traffic control systems are necessary for facilitating and alleviating the work of air traffic control. The primary concern of air traffic control is to maintain safe separation between aircraft, and one of the major safety critical situations is a midair conflict. In this paper, for the automated air traffic control systems, the problem of probabilistic conflict detection in the presence of various uncertainties during flight is considered. The aircraft dynamics are described by using stochastic differential equations, and the future aircraft's trajectory is determined by solving the stochastic optimal control problem. A computationally efficient numerical algorithm combining the pseudospectral method with the generalized polynomial chaos method to solve the stochastic trajectory optimization problems is proposed. By using the stochastic trajectory optimization method, the novel probabilistic conflict detection algorithm is proposed. Through the numerical simulations for trajectory prediction and conflict detection, the performance and effectiveness of the algorithms are illustrated.

Keywords Air traffic management • Conflict detection • Stochastic optimal control • Generalized polynomial chaos

1 Introduction

The demand in air traffic has been growing mainly in the Asia-Pacific region, and current air traffic management (ATM) system is under considerable stress. To satisfy the increasing demand, the International Civil Aviation Organization (ICAO)

Y. Matsuno (✉) • T. Tsuchiya
Department of Aeronautics and Astronautics, The University of Tokyo,
7-3-1 Hongo, Bunkyo-ku, Tokyo 113-8656, Japan
e-mail: 0669922514@mail.ecc.u-tokyo.ac.jp; tsuchiya@mail.ecc.u-tokyo.ac.jp

Electronic Navigation Research Institute (ENRI), *Air Traffic Management and Systems*,
Lecture Notes in Electrical Engineering 290, DOI 10.1007/978-4-431-54475-3_2,

published a new operational concept of global ATM in 2005 [9]. NextGen [5] and SESAR [4], the two major ATM programs initiated by the United States and Europe, respectively, are currently ongoing in order to support the new era of air transportation. In Japan, CARATS [16], the long-term vision for air traffic systems, was also proposed in 2010. In these ATM programs, the automated air traffic control (ATC) systems are necessary to meet future growth in air traffic by facilitating and alleviating the work of ATC. The primary concern of ATC is to maintain safe separation between aircraft, and one of the major safety critical situations is a midair conflict. When the minimum separation standard between aircraft is violated, a conflict occurs. The protected zone of an aircraft is generally defined as follows: the minimum allowed horizontal separation of en route airspace is 5 nm, and the vertical separation requirement is 1,000 ft. Air traffic controllers currently monitor the trajectories of aircraft and whether there are some potential conflicts within a lookahead time horizon.

There are two interconnected procedures to predict a midair conflict, i.e., trajectory prediction and conflict detection. In addition, typically, most of the proposed methods to solve the problems of trajectory prediction and conflict detection can be categorized into two approach, i.e., deterministic and probabilistic [11]. Because all problems in the real world contain uncertainties which arise due to disturbances, modeling and estimation errors, we cannot predict the future position of the aircraft completely. Therefore, in this study, we consider the problem of probabilistic conflict detection and propose the novel stochastic conflict detection algorithm by considering various uncertainties during flight, which is the key element for the realization of the future air traffic systems.

For trajectory prediction and conflict detection in a probabilistic setting, the empirical distribution model of future aircraft's positions [12,17,24], the dynamical model by using stochastic differential equations that describe the aircraft motion [8,19], or other probabilistic aircraft model [2,14] is applied to the aircraft's motion model. In this paper, we model the aircraft dynamics by using stochastic differential equations, and determine the future aircraft's trajectory by solving the stochastic optimal control problem. The previous work in the area of stochastic optimal control includes the following. Blackmore et al. proposed the particle control method using mixed integer linear programming techniques [1]. However, their proposed approach relies on linear system dynamics, and is therefore difficult to apply to nonlinear aircraft dynamics. Liu and Hwang solved stochastic optimal control problems by discretizing the aircraft's continuous dynamics to get a controlled Markov chain and then finding an optimal control law [15]. But the problem becomes intractable as the number of discrete states grows. Application of various statistical tools to the stochastic optimization problems is another commonly used approach. Lecchini-Visintini et al. proposed a Markov chain Monte Carlo framework to determine an approximate optimal control input [13]. Kantas et al. applied Bayesian optimal design and sequential Monte Carlo method to automatically generate optimal and safe maneuvers [10]. Prandini et al. also employed the Monte Carlo simulation [19]. However, using these statistical methods takes much computation time, and it is very difficult to implement them in the real applications of ATC.

Therefore, to reduce the computational burden, we employ a recently developed computationally efficient method, generalized polynomial chaos (gPC) [22, 23], to solve the stochastic trajectory optimization problems. The gPC method applied to the stochastic trajectory optimization problem by Cottrill and Harmon [3], however their application is limited to a very little number of uncertainties or random variables. Therefore to overcome this disadvantage, we employ other approach which can be used for the larger number of random variables ($\geq$5), and propose the stochastic optimization method. By using the stochastic trajectory optimization method, the novel conflict detection algorithm is proposed.

The paper is organized as follows. Section 2 presents the stochastic trajectory optimization method for trajectory prediction. In Sect. 3, probabilistic conflict detection algorithm is provided. Section 4 gives the numerical results and the effectiveness of our proposed algorithms is illustrated. Finally, conclusions and future research direction are provided in Sect. 5.

2 Trajectory Prediction

Our proposed stochastic optimization method combines the deterministic optimization method with the gPC method. In this section, we first introduce the deterministic trajectory optimization method, thereafter we propose the computationally efficient stochastic approach.

2.1 Deterministic Optimization Method

The following general continuous-time optimal control problem in Bolza form is considered. Determine the state variables, $x(t) \in \mathbb{R}^{n_x}$, the control variables, $u(t) \in \mathbb{R}^{n_u}$, the initial time, t_0, and the terminal time, t_f, on the time interval, $t \in [t_0, t_f]$, that minimize the cost function given by:

$$J = \phi_B(x(t_0), x(t_f)) + \int_{t_0}^{t_f} g(x(t), u(t), t)dt \tag{1}$$

subject to the dynamic constraints:

$$\frac{dx}{dt} = f(x(t), u(t), t) \tag{2}$$

the inequality path constraints:

$$c_{min} \leq c(x(t), u(t), t) \leq c_{max} \in \mathbb{R}^{n_c} \tag{3}$$

and the boundary conditions:

$$b_{min} \leq b(x(t_0), x(t_f)) \leq b_{max} \in \mathbb{R}^{n_b} \tag{4}$$

where ϕ_B and g define the Mayer and Lagrange terms in the cost function, respectively, f is the system dynamics, c defines the path constraint functions, and b expresses the boundary condition functions.

In this research, we apply the direct collocation pseudospectral method, which has increased in popularity for solving optimal control problems in recent years. Especially the Radau pseudospectral method [18] is employed to solve the optimal control problems. In the pseudospectral method, the dynamic variables (the state variables, $x(t)$, and the control variables, $u(t)$), which depend on time, are approximated and parameterized using Lagrange polynomials. The cost function (Eq. (1)) and the constrains (Eqs. (2)–(4)) are also discretized using a quadrature rule, and the continuous-time optimal control problem is discretized and transcribed into a nonlinear programming (NLP) problem, then an NLP solver, such as sequential quadratic programming (SQP), is applied to determine the optimal solution.

In this paper, we employ the General Pseudospectral Optimization Software (GPOPS) [20], which is performed in MATLAB and using SNOPT [7] as the NLP solver. Using GPOPS, the continuous-time optimal control problem is transformed into the NLP problem for SNOPT NLP solver which finds the optimal solution. Therefore, GPOPS is employed as the deterministic solver in the gPC algorithm described in the next subsection.

2.2 Stochastic Optimization Method

Uncertainties during flight are considered as random variables, and the aircraft's motion is described as stochastic differential equations. One of the most commonly used methods for solving stochastic differential equations is Monte Carlo method, or one of its variants such as the quasi Monte Carlo method. Monte Carlo method generates random samples of random variables based on their prescribed probability density function. Each random sample is inserted into the stochastic differential equations, and the stochastic problem is transformed into the deterministic problem that can be solved using deterministic methods. Using a set, or ensemble, of deterministic solutions, the statistical information (e.g., expected value (mean), variance and covariance) can be calculated. The Monte Carlo method is straightforward to implement because it only requires repetitive application of deterministic solvers. However, it is well known that the mean converges slowly and a large number of executions are needed for accurate results, which implies excessive computational burden.

The gPC method is also easy to implement by using sample points of the random variables and repetitive executions of deterministic simulations as in the Monte Carlo method. However, to reduce the computational burden, the gPC algorithm

uses the collocation points as the sample points and a polynomial approximation to determine the solution as described in detail later. By the gPC method, the stochastic solutions are expressed as orthogonal polynomials of the random variables, and the different types of orthogonal polynomials, such as Hermite and Legendre, can be chosen to achieve better convergence.

There are two main methods of the gPC algorithm, i.e., the Galerkin and the stochastic collocation. With respect to the implementation, a disadvantage of the Galerkin method is that it can be cumbersome and difficult to implement for complex and nonlinear systems [23]. In contrast, the stochastic collocation approach is straightforward and easier to implement because it can be solved by using the deterministic numerical solvers [22]. Therefore, in this paper, the stochastic collocation form of the gPC method is employed. The stochastic collocation form of the gPC algorithm is explained as follows.

By the gPC method, the solution $z(p)$ is approximated by the summation of the orthogonal polynomial of independent random variables $p = (p_1, \ldots, p_N) \in \mathbb{R}^N$. The Mth order approximation of the solution $z_M(p)$ is written as the following equation.

$$z_M(p) = \sum_{m=1}^{M} C_m \Phi_m(p) \tag{5}$$

where C_m is the coefficient, and $\Phi(p)$ represents the N-dimensional orthogonal polynomial basis function obtained from the one-dimensional basis function of each random variable $\phi(p_i)$ $(i = 1, \ldots, N)$ by the tensor product rule.

$$\Phi_m(p_1, \ldots, p_N) = \prod_{i=1}^{N} \phi_i^{l_i}(p_i) \ (m = 1, \ldots, M, \ l_i = 1, \ldots, P) \tag{6}$$

where P is the total degree of one-dimensional bases ϕ^{l_i}, and M is the total number of tensor product basis functions and determined by the following binomial coefficient.

$$M = \binom{N+P}{N} \tag{7}$$

In this paper, the normalized orthogonal polynomial basis is used by satisfying the following orthogonality condition.

$$E[\phi^j(p_i)\phi^k(p_i)] = \int \phi^j(p_i)\phi^k(p_i)\rho_i(p_i)dp_i = \delta_{jk} \tag{8}$$

where δ_{jk} is the Kronecker delta function, and $\rho_i(p_i)$ is the probability density function corresponding to the ith random variable p_i.

In addition, the coefficient C_m in Eq. (5) is determined by the following equation.

$$C_m = E[z(p)\Phi_m(p)] = \int z(p)\Phi_m(p)\rho(p)dp \tag{9}$$

where $\rho(p)$ is the joint probability density function given by:

$$\rho(p) = \prod_{i=1}^{N} \rho_i(p_i) \tag{10}$$

Applying the stochastic collocation method, the integral in Eq. (9) can be approximated by using Gaussian quadrature. A set of collocation points and quadrature weights is chosen based on the quadrature rule. Though the N-dimensional quadrature is derived from the one-dimensional quadrature by the tensor product rule in the research by Cottrill [3], we employ the sparse grid quadrature based on extensions of one-dimensional or univariate Gaussian quadrature [6]. In general, as the number of random variables gets larger, the tensor product grid suffers the curse of dimensionality. However, the sparse grid with Q collocation points p^j $(j = 1, \ldots, Q)$ and associated weights α^j $(j = 1, \ldots, Q)$ consists of a very small number of the collocation points, and it can reduce the computational burden and increase the number of random variables or uncertainties. As in the Monte Carlo method, the stochastic problem is transformed into the deterministic problem on each collocation point, and can be solved by repetitive application of the deterministic method.

The approximation of Eq. (9) based on the quadrature rule is given by the following equation.

$$C_m \approx \sum_{j=1}^{Q} z(p^j)\Phi_m(p^j)\alpha^j \tag{11}$$

where $z(p^j)$ denotes the deterministic solution using the jth collocation point p^j of the random variables.

The approximate stochastic solution is determined by Eqs. (5) and (11) as the orthogonal polynomials of the random variables. The stochastic solution is a distribution function of the random variables and can be evaluated for any given random inputs. In addition, the statistical information of the stochastic solution can be calculated by using the coefficients given by Eq. (11), and evaluates how the solution varies with the random variables. The expected value of the solution is described as the following equation.

$$E[z(p)] \approx E[z_M(p)] = \int \left[\sum_{m=1}^{M} \mathbf{C}_m \Phi_m(p) \right] \rho(p)dp = C_1 \tag{12}$$

The variance is calculated by the following equation.

$$var[z(p)] = E[(z(p) - E[z(p)])^2] \approx E[(z_M(p) - E[z_M(p)])^2]$$
$$= \int \left[\sum_{m=1}^{M} C_m \Phi_m(p) - C_1 \right]^2 \rho(p) dp$$
$$= \sum_{m=2}^{M} [C_m]^2 \tag{13}$$

By the theory of the gPC method, the stochastic solution including the statistical information (expected value and variance) is approximated and determined. Using the gPC algorithm mentioned above, in this paper, the gPC method with GPOPS as the deterministic trajectory optimization solver is applied to the stochastic trajectory optimization problems.

2.3 Stochastic Trajectory Prediction Algorithm

In this study, the time of arrival at the waypoint from the aircraft's current position is predicted by using our proposed stochastic optimization algorithm. The procedures of the algorithm are listed as follows.

1. Generate a set of collocation points p^j $(j = 1, \ldots, Q)$ and associated weights α^j $(j = 1, \ldots, Q)$.
2. Calculate the values of the orthogonal polynomial basis functions $\Phi_m(p^j)$ $(m = 1, \ldots, M,\ j = 1, \ldots, Q)$.
3. Solve the Q deterministic trajectory optimization problems using the Q collocation points p^j $(j = 1, \ldots, Q)$, and determine the solution $z(p^j)$ $(j = 1, \ldots, Q)$ (z is the time of arrival or the terminal time t_f of the trajectory optimization problem in this paper).
4. Calculate the coefficients C_m $(m = 1, \ldots, M)$.
5. Calculate the statistics of the approximate solution, the expected value $E[z(p)]$ and the variance $var(z(p))$, from the coefficients C_m.

2.4 Numerical Simulation

In this subsection, numerical simulation is conducted to verify the effectiveness and performance of our proposed stochastic trajectory optimization method.

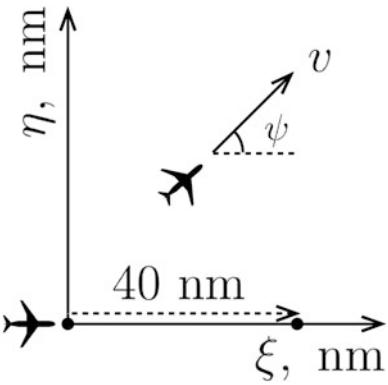

Fig. 1 Problem setting for trajectory prediction

2.4.1 Problem Setting

We consider the aircraft flying in two-dimensional plane, the ξ and η coordinate frame as shown in Fig. 1. The state variables are defined as $x(t) = (\xi, \eta, \psi)^T$ where ψ is the heading angle, and the control variable $u(t)$ is the bank angle. The control variable is bounded as $|u(t)| \leq 35^\circ$. The aircraft dynamics are described in the following equations.

$$\begin{aligned} \dot{\xi} &= v\cos\psi + w_\xi \\ \dot{\eta} &= v\sin\psi + w_\eta \\ \dot{\psi} &= \frac{g}{v}\tan u \end{aligned} \tag{14}$$

where g is the acceleration of gravity: $9.8\,\mathrm{m/s^2}$, v is the airspeed (true airspeed), and (w_ξ, w_η) are the wind velocities in the ξ and η directions. v is assumed to be the constant speed of 480 knots.

As shown in Fig. 1, the initial and terminal conditions (t_f is the terminal time) are as follows.

$$\begin{aligned} x(0) &= (0,0,0)^T \\ x(t_f) &= (40,0,0)^T \end{aligned} \tag{15}$$

For solving the optimal control problems, the cost function J is minimized and given by the following equation.

$$J = 10^{-4}\cdot t_f + \int_0^{t_f} u(t)^2 dt \tag{16}$$

Furthermore, as the uncertainties during flight or random variables for the gPC method, the wind prediction error, the airspeed measurement error, and the current

Table 1 Comparison between gPC and Monte Carlo methods

Algorithm	Total number of sample points	$E[t_f]$ (s)	$\sqrt{var[t_f]}$ (s)	Computation time
gPC	51	300.24	7.04	45 s
Monte Carlo	20,000	300.21	7.08	5.5 h

position estimation error are considered. In this paper, we consider the aircraft flying in two-dimensional horizontal plane, and the wind prediction error and the current position estimation error are divided into two components, i.e., the longitude and latitude directions. Then, we consider five random variables. In addition, we assume that these uncertainties are modeled as the standard deviations of the Gaussian distributions, and the values are $5.17\,\mathrm{m/s}$ for the wind prediction errors, $2.57\,\mathrm{m/s}$ for the airspeed measurement error and $50\,\mathrm{m}$ for the current position estimation errors [2, 17, 21, 24]. The wind prediction error represents uncertainty in the meteorological prediction, and for simplicity the only wind prediction error is considered. Because the Gaussian distributions are used for the uncertainties in this paper, Hermite polynomial basis functions collocated at Gauss-Hermite quadrature points are selected for the gPC method as suggested in the paper by Xiu [22].

The stochastic solution of the terminal time t_f is calculated by using our proposed stochastic approach. In addition, to verify the effectiveness and performance of our proposed method, the stochastic solution is computed by using Monte Carlo method, one of the most commonly used methods for solving stochastic differential equations, and compared with the solution that is calculated by using our proposed approach.

2.4.2 Simulation Results

Table 1 shows the expected value $E[t_f]$ and standard deviation $\sqrt{var[t_f]}$ (derived from the variance $var[t_f]$) of the terminal time t_f by using the gPC and Monte Carlo methods. The estimated solutions given by the gPC and Monte Carlo methods (i.e., $E[t_f]$ and $\sqrt{var[t_f]}$) closely match each other. It indicates that the gPC algorithm can estimate a reasonable solution. In addition, as shown in Table 1, by using the Monte Carlo method, the estimation of the solution converges after 20,000 iterations, requiring about five and a half hours. On the other hand, the gPC method requires only 51 collocation points for five random variables by using the sparse grid quadrature. The total number of multidimensional bases M and one-dimensional bases P are 56 and 3, respectively. Computation time is approximately 45 s for solving the 51 trajectory optimization problems and determining the solution by constructing the gPC approximation. Our proposed algorithm performs much faster than the Monte Carlo method does. Therefore our proposed gPC method provides an accurate approximate solution of the stochastic trajectory optimization problem while dramatically reducing computational cost.

3 Conflict Detection

By using the trajectory prediction algorithm described in Sect. 2, we propose the estimation method of the conflict probability between aircraft in this section. First, the conflict probability between aircraft is defined, thereafter the estimation method of the conflict probability is described.

3.1 Conflict Prediction

In this study, the specific conflict scenarios, the merging situations at the waypoint (merging point), are considered. As described in Sect. 2, the time of arrival at the merging point from the aircraft's current position can be predicted. Based on this trajectory prediction algorithm for two or multiple aircraft, a possible conflict between aircraft is detected. A conflict (not a collision) is defined as a situation where two or more aircraft come within the required minimum separation standard between each other. We consider multiple aircraft flying at the same altitude, and the required minimum separation is set to 5 nm horizontally. For simplicity, it is assumed that all aircraft pass at the merging point at the same speed of V knots. Therefore, the minimum distance separation can be transcribed into the minimum time separation $\Delta T_{sep} = 5 \cdot 3600/V$ s.

The purpose of the conflict prediction is to compute the probability that any two aircraft will be in conflict at the merging point. By using the stochastic trajectory prediction algorithm, the expected value and variance (or standard deviation) of the time of arrival at the merging point are calculated. The probability distribution of the time of arrival is assumed to be the Gaussian distribution. Therefore, we can determine the Gaussian distributions of the two aircraft, labeled A and B, $P_A(t)$ and $P_B(t)$, respectively. The conflict probability between the two aircraft can be determined by using these Gaussian distributions. The estimation method of the conflict probability is described in the next subsection.

3.2 Conflict Probability Estimation

We use the convolution integral to estimate the conflict probability. The conflict probability CP_{A-B} between the aircraft A and B is given by the following equations.

$$CP_{A-B} = \int_{-\Delta T_{sep}}^{\Delta T_{sep}} P_{A-B}(\tau) d\tau \tag{17}$$

$$P_{A-B}(\tau) = \int_{-\infty}^{\infty} P_A(t) P_B(t+\tau) dt \tag{18}$$

where $P_{A-B}(\tau)$ given by Eq. (18) expresses the conflict probability when the time separation (the time difference of the time of arrival) at the merging point between the aircraft A and B is τ. Therefore, by using Eq. (18), the conflict probability is described in Eq. (17), because the conflict occurs when τ satisfies the following condition: $-\Delta T_{sep} \leq \tau \leq \Delta T_{sep}$.

By the theory of the convolution integral, $P_{A-B}(\tau)$ given by Eq. (18) is expressed as the Gaussian distribution. Therefore, by using Eqs. (17) and (18), the conflict probability between any two aircraft can be estimated.

4 Numerical Simulation

In this section, numerical simulation is conducted to verify the effectiveness and performance of our proposed stochastic approach to detect conflicts. We consider various conflict scenarios, especially merging situations, between two or multiple aircraft.

4.1 Problem Setting

We consider the aircraft flying in two-dimensional horizontal plane. The two cases are considered: the meteorological prediction for the aircraft dynamics is not considered in Case 1, and considered in Case 2. The meteorological prediction data are provided by the Japan Meteorological Agency as a grid format of longitude and latitude. Therefore, to obtain the required wind predictions, linear and bilinear interpolations are applied. In addition, because the meteorological prediction data are provided as a grid format of longitude and latitude, the longitude θ and latitude ϕ coordinate frame is considered in Case 2, whereas the ξ and η coordinate frame is considered in Case 1. The state variables are defined as $x(t) = (\xi, \eta, \psi)^T$ in Case 1 and $x(t) = (\theta, \phi, \psi)^T$ in Case 2, and the control variable $u(t)$ is the bank angle. The control variable is bounded as $|u(t)| \leq 35^\circ$. The aircraft dynamics in Case 1 are given by Eq. (14), and the dynamics in Case 2 are described in the following equations.

$$\begin{aligned} \dot{\theta} &= \frac{v\cos\psi + w_\theta}{(R+h)cos\phi} \\ \dot{\phi} &= \frac{v\sin\psi + w_\phi}{R+h} \\ \dot{\psi} &= \frac{g}{v}\tan u \end{aligned} \tag{19}$$

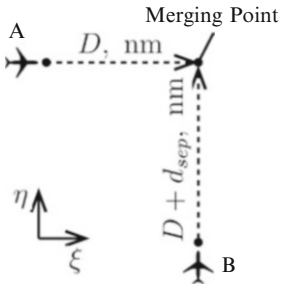

Fig. 2 Problem setting for conflict detection in Case 1

where R is the Earth's radius: 6.37×10^6 m, h is the altitude, and (w_θ, w_ϕ) are the wind velocities in θ and ϕ directions. The altitude is assumed to be a constant 35,000 ft.

As the uncertainties during flight, the wind prediction error, the airspeed measurement error, and the current position estimation error are also considered as described in Sect. 2.4.1. In addition, Hermite polynomial basis functions collocated at Gauss-Hermite quadrature points are chosen for the gPC method. Furthermore, for solving the optimal control problems, the cost function J given by Eq. (16) is minimized.

For the gPC method, the number of collocation points for five random variables is set to 51 by using the sparse grid quadrature, and the deterministic trajectory optimization problems are solved repetitively. In addition, the total number of multidimensional bases M and one-dimensional bases P are 56 and 3, respectively. The solutions including the statistical information such as the expected value and variance (or standard deviation) are calculated. The merging situations in Case 1 and 2 are explained as follows.

4.1.1 Merging Scenario in Case 1

As illustrated in Fig. 2, we consider the merging scenarios of the two aircraft, labeled A and B, flying at the same altitude and the same speed of $V = 480$ knots (true airspeed). The distance between the position of the aircraft A and the merging point is set to D nm, and the distance between the position of the aircraft B and the merging point is longer and set to $D + d_{sep}$ $(d_{sep} \geq 0)$ nm. The initial and terminal conditions of the aircraft A and B are as follows.

$$\begin{aligned} x_A(0) &= (-D, 0, 0)^T \\ x_A(t_{fA}) &= (0, 0, 0)^T \\ x_B(0) &= (0, -(D + d_{sep}), \pi/2)^T \\ x_B(t_{fB}) &= (0, 0, \pi/2)^T \end{aligned} \tag{20}$$

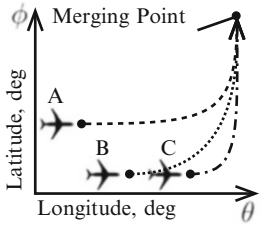

Fig. 3 Problem setting for conflict detection in Case 2

where t_{fA} and t_{fB} are the terminal time (or the time of arrival at the merging point) of the aircraft A and B, respectively.

We can generate various merging situations with various combinations of D and d_{sep}. In this paper, D is set to 80 and 160 nm and d_{sep} is set to 5 and 10 nm, and the total number of the merging scenarios is four. For each combination, the conflict probability is estimated and evaluated by using our proposed stochastic method described in Sect. 3.

4.1.2 Merging Scenario in Case 2

As shown in Fig. 3, the merging scenario of the three aircraft, labeled A, B, and C, flying at the same altitude (35,000 ft) and the same speed of $V = 450$ knots (true airspeed) is considered. The initial and terminal conditions of the aircraft A, B, and C are as follows.

$$\begin{aligned} x_A(0) &= (138.5, 34.75, 0)^T \\ x_A(t_{fA}) &= (140, 35.5, \pi/2)^T \\ x_B(0) &= (139, 34.25, 0)^T \\ x_B(t_{fB}) &= (140, 35.5, \pi/2)^T \\ x_C(0) &= (139.5, 34.25, 0)^T \\ x_C(t_{fC}) &= (140, 35.5, \pi/2)^T \end{aligned} \tag{21}$$

where t_{fA}, t_{fB}, and t_{fC} are the terminal time (or the time of arrival at the merging point) of the aircraft A, B, and C, respectively.

Using our proposed stochastic approach described in Sect. 3, the conflict probability between the pairwise aircraft is estimated and evaluated.

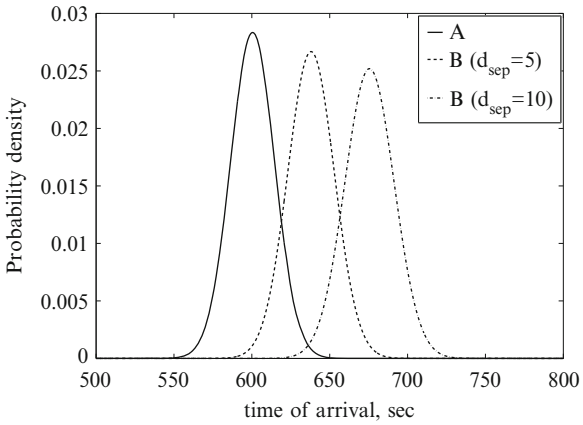

Fig. 4 Probability distribution of time of arrival in Case 1 ($D = 80$ nm) (mean value: 600.49 (A), 638.02 (B ($d_{sep} = 5$ nm)), 675.55 (B ($d_{sep} = 10$ nm)), standard deviation: 14.07 (A), 14.95 (B ($d_{sep} = 5$ nm)), 15.83 (B ($d_{sep} = 10$ nm)))

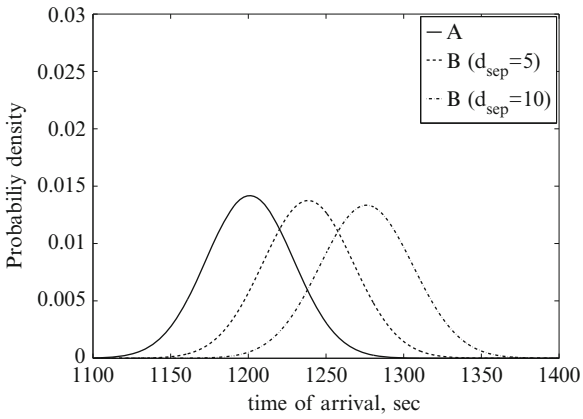

Fig. 5 Probability distribution of time of arrival in Case 1 ($D = 160$ nm) (mean value: 1200.97 (A), 1238.50 (B ($d_{sep} = 5$ nm)), 1276.03 (B ($d_{sep} = 10$ nm)), standard deviation: 28.14 (A), 29.02 (B ($d_{sep} = 5$ nm)), 29.90 (B ($d_{sep} = 10$ nm)))

4.2 Simulation Results

In Case 1, Figs. 4 and 5 show the probability distributions of the time of arrival at the merging point for the combinations of D and d_{sep}. Table 2 indicates the conflict probabilities for the combinations of D and d_{sep}. As shown in Table 2, when d_{sep} is 10 nm, the conflict probability is lower than that of when d_{sep} is 5 nm due to the longer time separation between the aircraft A and B. When d_{sep} is 10 nm, as D becomes larger, the conflict probability becomes much higher. On the other hand, when d_{sep} is 5 nm, the conflict probability of when D is 160 nm is not much different from that of when D is 80 nm. The reasons of this are as follows. As shown in Figs. 4 and 5, when D becomes larger, the standard deviation of the time of arrival gets larger and the probability distribution grows wider. Accordingly, when d_{sep} is 10 nm, the range in which the two probability distributions overlap each other is much larger. In contrast, when d_{sep} is 5 nm, the range of when D is 80 nm is not much different from that of when D is 160 nm. As a result, when d_{sep} is 10 nm, the

Table 2 Conflict probability in Case 1

(D, d_{sep}) (nm)	Conflict probability
$(80, 5)$	0.49928
$(80, 10)$	0.038099
$(160, 5)$	0.467965
$(160, 10)$	0.177118

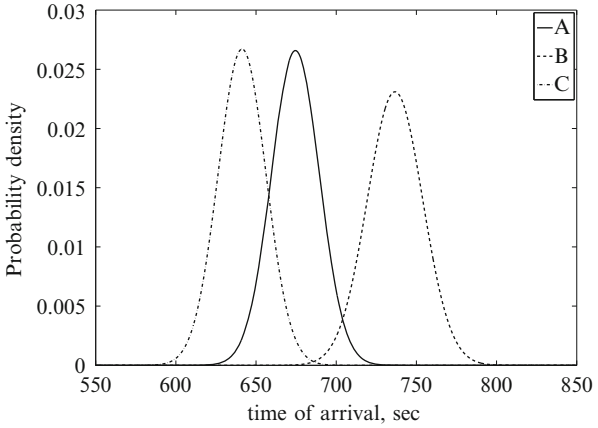

Fig. 6 Probability distribution of time of arrival in Case 2 (mean value: 674.55 (*A*), 736.66 (*B*), 641.28 (*C*), standard deviation: 15.01 (*A*), 17.27 (*B*), 14.94 (*C*))

Table 3 Conflict probability in Case 2

Combination of aircraft	Conflict probability
A and B	0.16687
A and C	0.37491
B and C	0.0076496

conflict probability of when D is 160 nm is higher than that of when D is 80 nm. On the other hand, when d_{sep} is 5 nm, the conflict probability of when D is 160 nm is not much different from that of when D is 80 nm.

In addition, the computation time for calculating the time of arrival and each conflict probability is about 1 min. Our proposed probabilistic approach can provide reasonable solutions while dramatically reducing computational cost.

In Case 2, Fig. 6 shows the probability distributions of the time of arrival at the merging point for the three aircraft. The position of the aircraft C is nearest to the merging point among the three aircraft and the mean value of the time of arrival of the aircraft C is the smallest as shown in Fig. 6. On the other hand, the position of the aircraft B is farthest to the merging point and the mean value of the time of arrival of the aircraft B is the longest. As shown in Fig. 6 and Table 3, the distributions of the three aircraft and the conflict probabilities are effectively calculated. In addition, the computation time for calculating the time of arrival is approximately 1 min. In Case 2, the conflict probabilities and the time of arrival can be calculated by using our proposed computationally efficient method.

Therefore, through the numerical simulations in Case 1 and 2, we can confirm the effectiveness and performance of our probabilistic algorithm for detecting possible conflicts by using the computationally efficient gPC method.

5 Conclusions and Future Work

In this paper, we proposed the gPC method for solving the stochastic trajectory optimization problem and estimating the conflict probability. As the sample problems, the numerical simulation for the trajectory prediction demonstrated that our proposed computationally efficient method can generate the accurate approximation of the solution of the stochastic trajectory optimization problem by determining and characterizing the statistical information, i.e., the expected value and variance. In addition, we estimated and evaluated the conflict probability between the pairwise aircraft in two merging scenarios by using the stochastic trajectory prediction algorithm. Through the numerical simulations for trajectory prediction and conflict detection, the performance and effectiveness of our novel probabilistic approach was evaluated and verified.

The purpose of trajectory prediction and conflict detection is to resolve an impending conflict. For conflict resolution, we need to decide the time to initiate a resolution maneuver and select the maneuver to execute. For solving the problem of conflict resolution, knowledge of the conflict probability help to establish the optimal time to initiate the resolution maneuver as well as the characteristics of the maneuver. Further research will focus on applying stochastic trajectory optimization for conflict resolution problems. Besides, for improving our stochastic algorithms, our proposed stochastic method is currently being extended for three-dimensional aircraft dynamics. In addition, the random variables will be assumed to have the different kinds of probability density function, and it will lead to a mix of the different kinds of polynomials in the gPC method. Furthermore, we will consider the time-varying random variables such as time-varying wind prediction error. By introducing the time-varying random variables, the number of random variables and computational burden will be increased, however, our stochastic approach has a potential for solving such a difficult problem.

References

1. Blackmore L, Ono M, Bektassov A, Williams BC (2010) A probabilistic particle-control approximation of chance-constrained stochastic predictive control. IEEE Trans Robot 26:502–517
2. Chaloulos G, Lygeros J (2007) Effect of wind correlation on aircraft conflict probability. J Guid Control Dyn 30:1742–1752
3. Cottrill GC, Harmon FG (2011) Hybrid Gauss pseudospectral and generalized polynomial chaos algorithm to solve stochastic trajectory optimization problems. In: AIAA guidance, navigation, and control conference

4. Council of the European Union (2012) European ATM master plan, 2nd edn
5. Federal Aviation Administration Joint Planning and Development Office (2010) Concept of operations for the next generation air transportation system, Version 3.2
6. Genz A, Keister BC (1996) Fully symmetric interpolatory rules for multiple integrals over infinite regions with Gaussian weight. J Comput Appl Math 71:299–309
7. Gill PE, Murray W, Saunders MA (2005) SNOPT: an SQP algorithm for large-scale constrained optimization. SIAM Rev 47:99–131
8. Hu J, Prandini M, Sastry S (2005) Aircraft conflict prediction in the presence of a spatially correlated wind field. IEEE Trans Intell Transp Syst 6:326–340
9. International Civil Aviation Organization (2005) Global Air Traffic Management Operational Concept. Doc 9854AN/458
10. Kantas N, Lecchini-Visintini A, Maciejowski JM (2010) Simulation-based Bayesian optimal design of aircraft trajectories for air traffic management. Int J Adapt Control Signal Process 24:882–899
11. Kuchar J, Yang L (2000) A review of conflict detection and resolution methods. IEEE Trans Intell Transp Syst 1:179–189
12. Lauderdale TA (2012) Probabilistic conflict detection for robust detection and resolution. In: AIAA aviation technology, integration, and operations conference
13. Lecchini-Visintini A, Glover W, Lygeros J, Maciejowski JM (2006) Monte Carlo optimization for conflict resolution in air traffic control. IEEE Trans Intell Transp Syst 7:470–482
14. Liu W, Hwang I (2011) Probabilistic trajectory prediction and conflict detection for air traffic control. J Guid Control Dyn 34:1779–1789
15. Liu W, Hwang I (2012) Probabilistic aircraft conflict resolution: a stochastic optimal control approach. In: American control conference
16. Ministry of Land, Infrastructure, Transport and Tourism Study Group for the Future Air Traffic Systems (2010) Long-term vision for the future air traffic systems - changes to intelligent air traffic systems
17. Paielli R, Erzberger H (1997) Conflict probability estimation for free flight. J Guid Control Dyn 20:588–596
18. Patterson MA, Rao AV (2012) Exploiting sparsity in direct collocation pseudospectral methods for solving optimal control problems. J Spacecr Rockets 49:364–377
19. Prandini M, Hu J, Lygeros J, Sastry S (2000) A probabilistic approach to aircraft conflict detection. IEEE Trans Intell Transp Syst 1:199–220
20. Rao AV, Benson D, Darby CL, Mahon B, Francolin C, Patterson M, Sanders I, Huntington GT (2011) User's manual for GPOPS version 5.0: a MATLAB software for solving multiple-phase optimal control problems using hp-adaptive pseudospectral methods. University of Florida, Gainesville
21. Schwartz B, Benjamin S, Green S, Jardin M (2000) Accuracy of RUC-1 and RUC-2 wind and aircraft trajectory forecasts by comparison with ACARS observations. Weather Forecast 15:316–326
22. Xiu D (2009) Fast numerical methods for stochastic computations: a review. Commun Comput Phys 5:242–272
23. Xiu D (2010) Numerical methods for stochastic computations. Princeton University Press, Princeton
24. Yang L, Kuchar J (1997) Prototype conflict alerting system for free flight. J Guid Control Dyn 20:768–773

Automated Separation Assurance with Weather and Uncertainty

T.A. Lauderdale and H. Erzberger

Abstract There are three major components to automating the tasks of air-traffic controllers: resolving aircraft-to-aircraft conflicts, providing arrival scheduling, and helping to ensure that aircraft remain clear of severe weather. The Advanced Airspace Concept provides functionalities to address all three of these components in an integrated fashion and provides redundant systems to handle uncertainties and failures. This paper discusses recent enhancements to components of this system to efficiently handle complex weather environments and to reduce the effect of aircraft performance uncertainties. The weather avoidance functionality incorporates an understanding of aircraft operations by limiting the complexity of the proposed solutions. To capture this understanding, the algorithm uses geometric calculations instead of a grid-based approach. Current research using this new functionality is discussed. Also discussed are methods to increase the robustness of the system to unavoidable differences between predicted aircraft trajectories and the trajectories that are actually flown.

Keywords Separation assurance • Weather avoidance • Robust automation

1 Introduction

Future air transportation systems are expected to rely upon increased automation for separation assurance and trajectory management to increase airspace capacity. There are many proposed designs to provide this increased level of automation including providing enhanced tools to air-traffic controllers and moving some of the responsibility for separation assurance to the flight deck.

T.A. Lauderdale (✉) • H. Erzberger
Aviation Systems Division, NASA Ames Research Center, Moffett Field, CA 94035, USA
e-mail: Todd.A.Lauderdale@nasa.gov; Heinz.Erzberger@nasa.gov

Electronic Navigation Research Institute (ENRI), *Air Traffic Management and Systems*, Lecture Notes in Electrical Engineering 290, DOI 10.1007/978-4-431-54475-3_3,

One concept for automated ground-based separation assurance is the Advanced Airspace Concept (AAC) [4] made up of the Autoresolver strategic separation algorithm [6, 7] and the Tactical Separation-Assured Flight Environment (TSAFE) [12] for tactical conflict resolution. This paper is a sequel to [5], which describes new developments in the evolution of the Autoresolver. A new algorithm for automated avoidance of complex weather scenarios is presented along with a synopsis of recent research to increase the system's robustness to trajectory prediction errors.

A new weather avoidance algorithm was developed and added to the Autoresolver recently. Convective weather cells are modeled by polygons, and the algorithm uses efficient geometric calculations to determine lines of tangency to these weather polygons. It generates weather-conflict-free paths through complex arrangements of such cells. A first implementation of the weather avoidance algorithm was presented for a single cell in [6]. This paper presents the more complete design for avoiding multiple cells.

Increasing the robustness of the algorithm to errors in predictions of future aircraft states is the other research area discussed here. Accurate trajectory predictions are the foundation of the Autoresolver, but even the highest fidelity trajectory prediction system will not be completely accurate due to unknowable or uncertain information. The algorithm has been shown to be especially sensitive to errors around the top-of-descent point [10], and one method to improve the algorithm in that area will be discussed. Also discussed is a method to improve system performance by including knowledge of past trajectory prediction accuracy.

2 Autoresolver

The AAC Autoresolver is designed to automate many of the tasks that an air-traffic controller currently performs. The Autoresolver detects and provides resolutions for potential losses of separation between aircraft. It also provides conflict-free, continuous-descent trajectories for aircraft merging at an arrival-metering fix. The Autoresolver handles predictions and resolutions of weather incursions as well. The resolution trajectories are created in an integrated fashion so that a resolution for one type of problem does not result in a new conflict of a different type. As a strategic trajectory-planning tool, it provides efficient resolutions by minimizing delay, fuel burn, or a combination of both [1]. As a result of this integrated approach to airspace problems the Autoresolver can also be used to analyze flight plan change requests from flight crews or airline operation centers to ensure that they do not create new conflicts.

Accurate predictions of aircraft trajectories are required to ensure that the Autoresolver generates safe and efficient solutions. The Autoresolver has been designed to separate the resolution process from the trajectory prediction process. Thus the Autoresolver generates simplified route, altitude, and speed change commands and sends them to an independent trajectory prediction system. This process of generating simplified trajectory changes and sending them to an independent

system that computes high-fidelity trajectories is called "trial planning". Since these two functionalities have been separated, the Autoresolver can more easily adapt to improvements in trajectory prediction capabilities. Also, separating the trajectory prediction and resolution processes allows the Autoresolver to function with different types of aviation software systems, including fast-time simulations, real-time simulations, and operational airspace automation tools.

3 Complex Weather Avoidance

The Autoresolver is designed to solve airspace problems on the order of 20–2 min before the problem occurs. As mentioned previously, one class of problems that must be dealt with in this time frame is resolutions to avoid severe weather regions. An approach to avoiding such weather conflicts will now be presented.

3.1 Algorithm Inputs and Assumptions

The primary inputs to the weather avoidance algorithm are polygons representing regions of airspace to avoid. One possible source of these weather avoidance polygons has been provided by researchers at MIT Lincoln Laboratories with their Convective Weather Avoidance Model (CWAM) [3]. CWAM provides avoidance polygons that are based on weather observation data such as precipitation intensity and cloud tops. The avoidance polygons are created by studying historical trajectories and historical weather to create a probabilistic prediction of the likelihood that pilots will avoid regions with certain weather characteristics.

The weather avoidance polygons can be of arbitrary shape and have arbitrary positions relative to the path of the aircraft (Fig. 1). Several techniques have been developed for other applications to create paths through fields of polygons. For example, Dijkstra's algorithm could be used to find the shortest path through a gridded model of the airspace. Instead of using these grid-based methods, which are susceptible to generating multiple dog-legged trajectories we solve the problem geometrically where limits on the complexity of maneuvers are built into the solution process.

Since weather is an unpredictable, dynamic process, forecasts play an important role in this weather avoidance procedure. At the time the avoidance route is created, the precise position and shape of downstream weather cells is not know, but the current prediction of that future weather can be used. For example, when looking for weather conflicts at a point 10 min into the future along a predicted trajectory, polygons capturing the current forecast for weather 10 min into the future can be used. To simplify the subsequent discussion, the fact that downstream weather cells are actually forecasts is not highlighted.

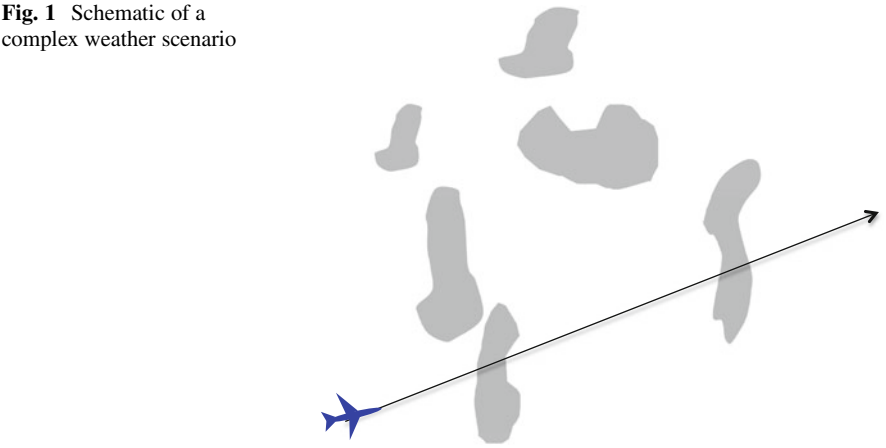

Fig. 1 Schematic of a complex weather scenario

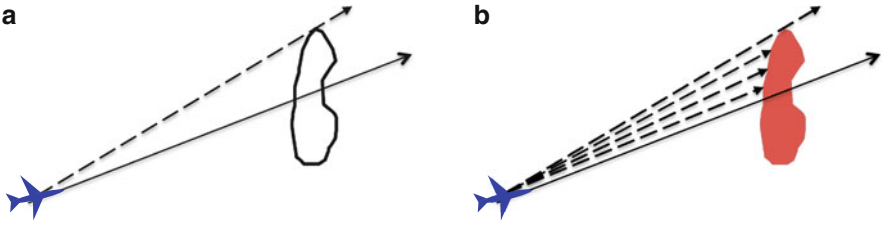

Fig. 2 Tangents can be found using a polygon (**a**) or a search if the polygon is not known (**b**)

The core of the geometric solution relies on two simple algorithms: the first determines tangent lines from a point to the boundary of a (possibly) non-convex polygon, and the second calculates tangent lines between non-intersecting, non-convex polygons. Algorithms to calculate these lines for randomly shaped polygons are freely available. If, instead of a polygon, a bitmap such as a weather radar image is available, an approximate direction of a tangency line can still be determined. To accomplish this, the predicted trajectory must by overlaid on the bitmap and then for any point on the trajectory that lies in a forbidden color of the bitmap. By probing for cell penetration through incremental heading changes as illustrated in Fig. 2 the tangency point can be determined.

One key constraint imposed on the resolution path is that route changes generated by the algorithm be limited to at most two additional route waypoints. Such a constraint is necessary in order to limit pilot workload. A third waypoint may be added to resolve aircraft-to-aircraft conflicts that arise from the re-route around the weather.

In general, the algorithm attempts to generate up to four possible resolution routes depending on the number of additional waypoints required. There will be one to each side of the weather cell and two between the cells. The final route selected by the algorithm is the one that is predicted to have the least airborne delay.

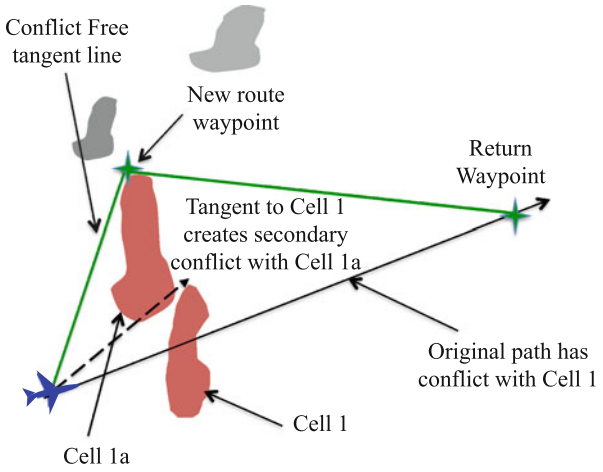

Fig. 3 Route must avoid initial and subsequent polygons

Another important aspect of the procedure is that, like all Autoresolver functions, it relies upon an external trajectory prediction system to determine if a proposed solution actually solves the problem. Simplified geometric calculations are performed by the Autoresolver to determine paths that are theoretically weather-conflict free, but these simplified paths are then passed to the external trajectory prediction system; the external system can generate high-fidelity trajectory predictions and check these trajectories against current and forecast weather as well as for aircraft-to-aircraft conflicts.

3.2 Avoidance Procedure

The current position of the aircraft is used as the origin of the weather avoidance route, and a suitable downstream waypoint is chosen as the return waypoint. In the example shown in Fig. 3, Cell 1 triggered the initial weather-conflict detection. Generally paths on both sides of this weather cell will be found, but, for illustration purposes, the subsequent discussion will focus only on the path to the left. For this path, the tangent from the current position to the left of that weather cell is created. If, as in the figure, the tangent line is not conflict-free to the tangent point of Cell 1, but, instead, happens to intersect another cell (Cell 1a), then that cell replaces Cell 1 as the primary conflict cell and a tangent line to that cell is found. Replacement of weather cells that initially triggered the resolution process but were subsequently replaced by a different cell is a standard procedure used in all the following steps. The intersection of the two tangent lines from the current position and the return waypoint to Cell 1a is used as a new waypoint in the route. If this new trajectory is free of weather conflicts, then this route is a valid candidate for the weather avoidance route.

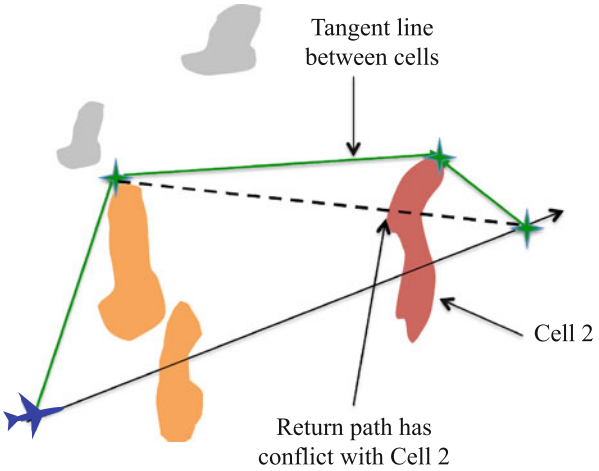

Fig. 4 Tangents between two cells are added if return route is blocked

If the route between the primary weather cell and the return waypoint is not conflict free (Fig. 4), then the tangent line between the two active cells is determined and two waypoints are used for the resolution. In this case, the first waypoint is located at the intersection of the tangent line from the current position to the primary weather cell and the tangent line between the two cells. Similarly, the second waypoint is located at the intersection of the tangent line from the return waypoint to the second weather cell and the tangent line between the cells.

Since more than two additional waypoints are not allowed, and if, as in Fig. 5, a conflict is detected on the tangent path, then an iteration process is followed. The position of the first waypoint is varied along its initial tangent line in increments from the point of tangency. For each trial waypoint, the tangent line to the new conflict cell is calculated and the intersection with the return waypoint tangency line is used as the second waypoint. Among these trajectory iterations, the conflict-free trajectory with the minimum delay is used as the weather avoidance route.

The entire process discussed above is repeated for the other tangency point of the original conflict polygon, which in this case would result in a turn to the right. Also, whenever two waypoints are needed to solve the problem (Fig. 4), interior tangency paths between the two weather polygons are included using the procedure, discussed previously, for exterior tangent lines. Figure 6 shows the four resulting weather avoidance paths. The entire path-finding algorithm can be repeated for different return waypoints, within a reasonable distance, to improve efficiency if desired.

Since weather is often moving and changing, as discussed previously, this process relies on forecast weather for downstream cells. These forecasts are inherently uncertain, so it can be important to ensure some additional space around each weather cell. To create this space, a horizontal buffer distance may be used. Any time a waypoint is found in the resolution process, it is moved a prescribed distance away from the weather cell. The line bisecting the angle formed by the

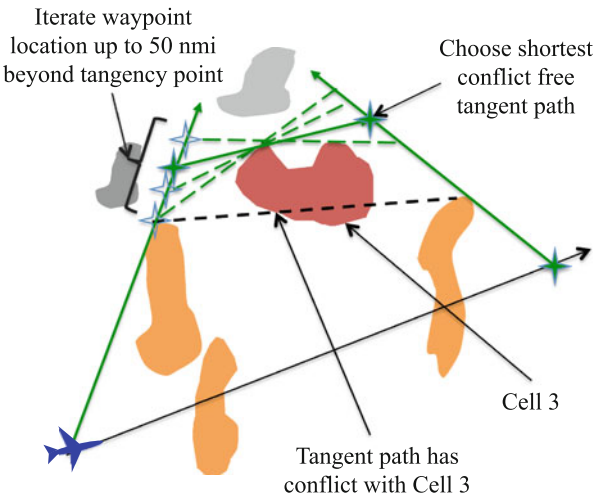

Fig. 5 Iteration is required for blocked tangent lines

Fig. 6 Four possible weather resolution paths

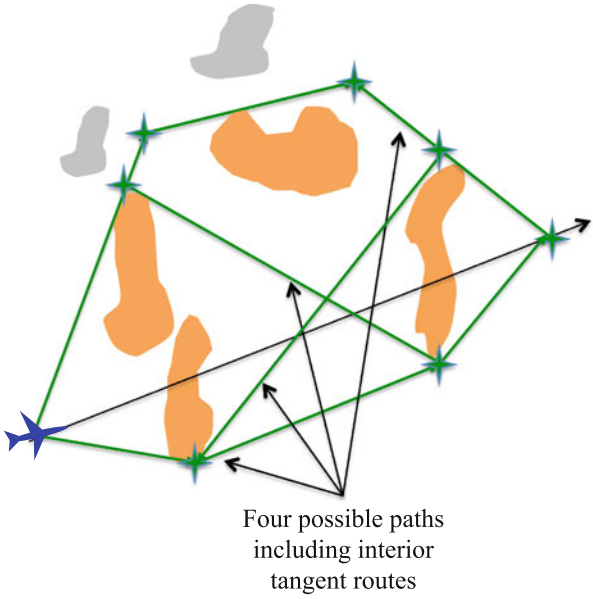

two tangent lines defines the direction of motion. If, as shown in Fig. 7, this buffer distance causes a new weather cell to be active, then the tangent to that cell is found, and the resolution process continues. This buffer should be sized based on weather forecast accuracy such that it is unlikely that the aircraft will have to be rerouted due to motion and changes of the weather. Of course, all trajectories are constantly being scanned for weather conflicts in case the weather changes more than estimated.

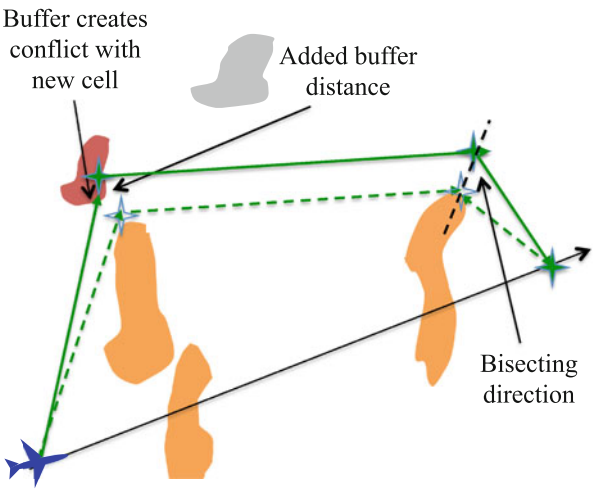

Fig. 7 Additional buffer added to handle changing weather

After the weather routes are created they are checked for predicted separation violations with other aircraft. If conflicts are found, they are resolved using the core Autoresolver functionality by maneuvering the other aircraft, adding an additional route waypoint, or temporarily changing the cleared altitude of the flight along the weather avoidance route. Also, for aircraft near their arrival fix, weather resolutions are performed and the schedule to the arrival fix is adjusted to reflect that change. Finally, it is important to note that all resolutions for aircraft-to-aircraft conflicts and arrival-metering trajectories are checked to ensure that they are free of weather conflicts.

3.3 Evaluation and Operating Concepts

This weather avoidance procedure was developed, evaluated, and refined in a fast-time simulation platform, the Airspace Concept Evaluation System [8], using CWAM weather polygons and realistic traffic patterns. Figure 8a shows an example of a one-waypoint resolution around weather from one of these fast-time simulations. For this resolution, the larger cell triggered the resolution, but the smaller cell became important. A buffer was used in this resolution process that placed the waypoint away from the boundary of the smaller cell.

A more complex resolution scenario from the same simulation is depicted in Fig. 8b. In this case, the return waypoint is located behind two weather cells. In constructing the tangent lines, other weather cells closer to the aircraft cause a two-waypoint solution to be required. Again, the additional buffer is evident in the

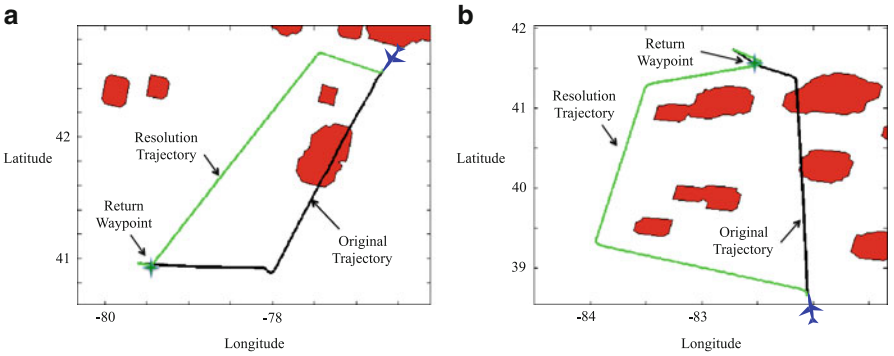

Fig. 8 (**a**) An example one waypoint resolution from simulation, and (**b**) a more complex resolution involving multiple weather cells and requiring two waypoints

solution in the distance of the final trajectory from the weather cells and in the fact that the resolution did not attempt to pass between the weather cells.

The weather resolution process in the Autoresolver is integral to a concept for improving the efficiency of routes through changing weather, known as Dynamic Weather Routes (DWR) [11]. In evolving weather situations aircraft routes, often planned up to an hour in advance, can become inefficient as the weather moves and changes in intensity. These routes are usually designed to travel longer distances to circumnavigate areas of weather. In the DWR concept, a system continually (approximately every 12 s) evaluates the routes of aircraft in weather by checking for possible shortcuts to downstream waypoints. If one of these shortcuts is free of weather and provides enough flight-time savings, then the airline operations center can uplink the revised route to the aircraft for execution. If the shortcut has a weather conflict the shortcut trajectory can be sent to the Autoresolver to create a conflict-free route. If this new route saves enough time over the current route, then this route can be sent to the aircraft.

Results of real-time evaluations of the DWR concept show an average of around 10 min of savings for many aircraft in varied weather conditions [11]. NASA is currently evaluating the DWR system in the field in collaboration with an airline. In this evaluation the Autoresolver weather-avoidance algorithm is a critical component.

4 Robustness to Trajectory Uncertainty

The Autoresolver algorithm relies on accurate predictions of future aircraft states to efficiently maintain safety. Unfortunately, perfect trajectory predictions will never be possible due to unknowable or uncertain information, so the Autoresolver system must be designed to be robust to these errors. For weather resolutions the impact of

trajectory prediction error is usually overshadowed by the uncertainty of the position of the weather, so a simple buffer around weather as discussed previously is used.

Maintaining separation between aircraft, on the other hand, is very sensitive to trajectory prediction errors, and the main goal of the research discussed in this section is to design the Autoresolver such that it can maintain aircraft separation under various types of trajectory prediction errors in the most efficient way possible.

Two recent, related approaches to deal with these uncertainties will be discussed in the following sections. One is to increase vertical separation requirements around the predicted top-of-descent point. The other is to use historical performance characteristics of the trajectory prediction system to improve conflict detection performance and to select more robust resolutions.

4.1 Top-of-Descent Vertical Buffers

An analysis of the Autoresolver algorithm in the presence of different sources of trajectory prediction errors showed that the system was most susceptible to errors in prediction around the aircraft's top-of-descent point [10]. In this analysis, aircraft were assumed to be performing Flight Management System based continuous descent approaches where the aircraft would determine the top-of-descent point. Errors in the ground-based system's ability to predict this top-of-descent point can lead directly to losses of separation because aircraft are already flying exactly at their required vertical separation. Conflicts arising from such errors are often detected with only short times to loss of separation and may be difficult resolve. Also, the ground-based top-of-descent predictions generally do not improve as the aircraft approaches its descent point.

To improve the system's robustness to these types of errors, a special vertical buffer was added around the predicted top of descent. This buffer is illustrated by the difference between the vertical separation requirement around the top-of-descent points in Fig. 9a, b. Details of how this buffer was created are presented in [2]. The basic idea of this buffer is to provide a measure of safety in case the aircraft descends earlier or later than was predicted. The effect of the buffer is to clear out the airspace immediately below and in front of the predicted descent point. Since these buffers will clear more airspace than is needed compared to a perfectly known descent point, the sizes of these buffers should be tailored to the accuracy of the trajectory prediction system.

These top-of-descent buffers were added to the Autoresolver and simulated in fast time with different levels of trajectory-prediction error [2]. The buffers reduced the total number of losses of separation due to top of descent errors by over 80 %, but also increased the total number of maneuvers by about 50 %. Research is ongoing to tailor the buffers more precisely to the amount of trajectory prediction error. A long-term solution is for aircraft to downlink their top of descent points for use by the ground system, thereby largely eliminating the need for the buffers.

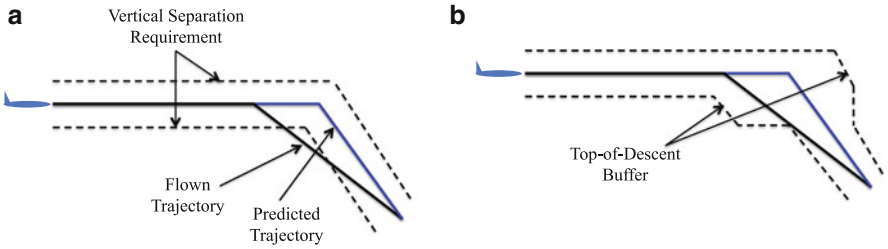

Fig. 9 (**a**) The standard separation criteria and (**b**) the tailored vertical buffer around the top-of-descent point

Fig. 10 Illustration of trajectory predictions with associated uncertainties

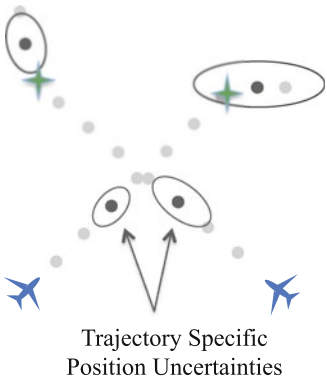

4.2 Probabilistic Conflict Detection

A more general method of dealing with trajectory prediction errors uses the knowledge of past performance of the trajectory prediction system to influence the detection and resolution processes directly. One way to do that is to create a probabilistic conflict detection system where the probability of conflict between two aircraft depends on their predicted trajectories and a characterization of the probable quality of those trajectories.

Figure 10 shows two trajectories with ovals representing confidence bounds of select trajectory points. These confidence bounds depend on the trajectory prediction system and the trajectories being predicted. For instance, a specific system may do a better job of modeling one type of aircraft than another, it may predict entirely level trajectories more accurately than trajectories that contain altitude transitions, or it may have increased lateral uncertainty around turns.

In [9] a mathematical framework is presented that integrates this type of uncertainty information to provide a probability that any two trajectories will result in a loss of separation. In the paper, doing conflict detection based on this system provided a benefit by reducing both missed alerts and false alerts by over 5% each as compared to the performance of a deterministic conflict detection system.

An additional benefit of using probabilistic detection in an automated separation assurance system is that the probability that a proposed conflict resolution maneuver will result in a conflict can also be calculated. This information can be used to select resolutions that are less likely to result in a subsequent conflict. Using a combination of delay and probability of conflict to select among a set of candidate resolutions reduced both the total number of resolutions and the total delay in a simulation [9].

5 Conclusions

This paper presented the advances made in two important areas of research for the AAC ground-based automated separation assurance system. First, a description of a new algorithm to avoid complex weather situations was shown. The algorithm enables selection of efficient routes around arbitrary combinations of weather regions using an algorithm based on geometric calculations. Second, recent efforts to enhance the robustness of the separation assurance system to trajectory prediction errors were presented. Handling these unavoidable errors is necessary to ensure a reliable and efficient automation system.

References

1. Bowe AR, Santiago C (2012) An approach for balancing delay and fuel burn in separation assurance automation. In: AIAA aviation technology, integration, and operations conference, AIAA-2012-5416, Indianapolis, IN
2. Cone AC, Bowe AR, Lauderdale TA (2012) Robust conflict detection and resolution around top of descent. In: AIAA aviation technology, integration, and operations conference, AIAA-2012-5644, Indianapolis, IN
3. DeLaura R, Robinson M, Pawlak M, Evans J (2008) Modeling convective weather avoidance in enroute airspace. In: 13th conference on aviation, range, and aerospace meteorology (ARAM), New Orleans, LA
4. Erzberger H (2006) Automated conflict resolution for air traffic control. In: 25th international congress of the aeronautical sciences
5. Erzberger H (2009) Separation assurance in the future air traffic system. In: The second ENRI international workshop on ATM/CNS, Tokyo
6. Erzberger H, Lauderdale TA, Cheng Y (2010) Automated conflict resolution, arrival management and weather avoidance for ATM. In: 27th international congress of the aeronautical sciences, Nice
7. Erzberger H, Lauderdale TA, Cheng Y (2012) Automated conflict resolution, arrival management and weather avoidance for ATM. J Aerosp Eng 226(8):930–949
8. George S, Satapathy G, Manikonda V, Palopo K, Meyn L, Lauderdale TA, Downs M, Refai M, Dupee R (2011) Build 8 of the airspace concept evaluation system. In: AIAA modeling and simulation technologies conference, AIAA-2011-6373, Portland, OR
9. Lauderdale TA (2012) Probabilistic conflict detection for robust detection and resolution. In: AIAA aviation technology, integration, and operations conference, Indianapolis, IN
10. Lauderdale TA, Cone AC, Bowe AR (2011) Relative significance of trajectory prediction error on an automated separation assurance algorithm. In: 9th USA/Europe air traffic management R&D seminar, Berlin

11. McNally D, Sheth K, Gong C, Love J, Lee C, Sahlman S, Cheng J (2012) Dynamic weather routes: a weather avoidance system for near-term trajectory-based operations. In: 28th international congress of the aeronautical sciences (ICAS), Brisbane
12. Paielli RA (2011) Evaluation of tactical conflict resolution algorithms for enroute airspace. AIAA J Aircr 48(1):324–330

Reduced Wake Vortex Separation Using Weather Information

Naoki Matayoshi

Abstract Current wake vortex separation minima are a major impediment to increasing traffic capacity since they require greater separations than radar separation minima. The concept of dynamic wake vortex separation, which allows reduced separations in favorable weather conditions when wake durations on flight paths become shorter, would allow an increase in capacity. The Japan Aerospace Exploration Agency (JAXA) has developed a methodology that calculates a reduced wake vortex separation that is equally safe as current separation minima. The methodology uses a probabilistic wake vortex prediction model to probabilistically assure that the wake vortex encounter risks at reduced separations do not exceed those at current separation minima. JAXA has also developed an airport terminal traffic simulation environment to demonstrate the traffic capacity gain at a congested airport when reduced wake vortex separations are introduced and take-off/landing sequences are optimized. The simulation result showed a greater than 10 % capacity gain, and confirmed the effectiveness of the proposed methodology.

Keywords Aircraft separation • Wake vortex • Weather information

1 Introduction

The demand for air travel continues to grow, and there is a strong demand to reduce aircraft separations to increase traffic capacity. The wake vortex separation minima are a major impediment to this since they require 4–6 nm separations, which are greater than radar separation minima of 2.5–3 nm that specify minimum separation under radar surveillance (Table 1). However, these wake vortex separation minima were established in the 1970s when knowledge of wake vortices was limited, and

N. Matayoshi (✉)
Japan Aerospace Exploration Agency (JAXA), Chofu, Japan
e-mail: matayoshi.naoki@jaxa.jp

Electronic Navigation Research Institute (ENRI), *Air Traffic Management and Systems*, Lecture Notes in Electrical Engineering 290, DOI 10.1007/978-4-431-54475-3_4,

Table 1 ICAO wake vortex separation minima

Leading aircraft	Following aircraft	Radar	Non-radar	
			Departure	Arrival
Heavy (≥136 ton)	Heavy	4 nm	2 min	2 min
	Medium	5 nm	2 min	2 min
	Light	6 nm	2 min	3 min
Medium (≥7 ton)	Heavy	–	–	–
	Medium	–	–	–
	Light	5 nm	–	3 min
Light	All categories	–	–	–

might therefore be overly conservative, assuming the worst case. During the past few decades, knowledge of wake vortices has greatly increased thanks to advances in lidar measurement and CFD analysis techniques [1, 2]. Based on this, the concept of dynamic wake vortex separation, which allows reduced separations in favorable weather conditions when wake durations on flight paths become shorter, has been studied intensively [3–6]. In this concept, the current wake vortex separation minima are considered to be adequately safe, and the wake vortex encounter (WVE) risks at reduced separations must be equal to or lower than the risks at current separations. Here, the WVE risk means a probability that a following aircraft encounters a leading aircraft's wake vortex which is strong enough to be hazardous to flight. However, there are still only a limited number of researches that discuss how to control the WVE risk at reduced separations, apart from a few studies that mainly discuss wake vortex advection due to crosswinds and so are applicable only to crosswind conditions [5, 6].

This paper discusses methods to probabilistically assure that the WVE risks at reduced separations do not exceed those at current separations for a wide range of weather conditions by using a probabilistic wake vortex prediction model which can consider more complicated wake decay and advection processes than crosswind advection. First, we introduce the concept of dynamic separation according to weather conditions. Second, we describe a method to control the hazard probability that the WVE risks at reduced separations exceed those at current separations by quantifying the errors in the WVE risk evaluation. Finally, we demonstrate the expected separation reduction and capacity gain by introducing dynamic separation.

2 Concept of Dynamic Separation

Wake durations on flight paths largely vary according to the surrounding weather conditions such as prevailing wind, turbulence intensity and atmospheric stability. The WVE risk therefore varies with the surrounding weather conditions even if aircraft maintain a constant separation as current separation rules require (Fig. 1).

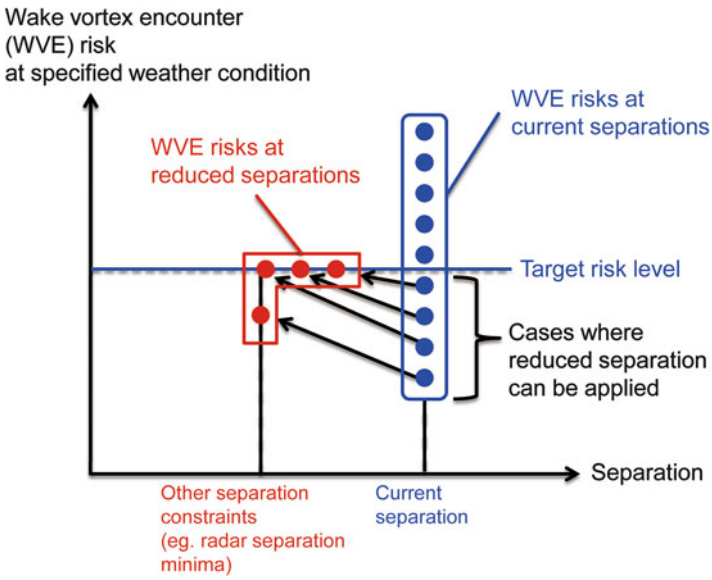

Fig. 1 Concept of dynamic separation

However, based on a long history of safe aircraft operations, these various risks at current separations are all considered to be practically safe. If we determine a target risk level within these risks at current separations and reduce separations until the expected risks at reduced separations reach the target risk level, the WVE risks at reduced separations would be acceptably safe since the maximum risk at reduced separations, equal to the target risk level, is within the risks experienced at current separations (Fig. 1). Other separation constraints such as radar separation minima remain active in this separation reduction process. This concept of dynamic separation according to weather conditions is proposed as a candidate of the next separation standard in International Civil Aviation Organization's (ICAO) global air navigation capacity and efficiency plan (GANP) [7].

3 WVE Risk Evaluation Considering Wake Vortex Prediction Errors

To realize dynamic separation, it is necessary to calculate WVE risks in various weather conditions by predicting wake vortex behaviors. However, we have to be aware that the WVE risk calculation process may have errors, mainly due to wake vortex prediction errors. If we underestimate the WVE risks at reduced separations, the true WVE risks at reduced separations might exceed the target risk level. Likewise, if we overestimate the WVE risks at current separations, the target risk level based on those overestimated WVE risks might exceed the true WVE

risks at current separations. Therefore, if we have errors in WVE risk calculation either at current separations or at reduced separations, it may lead to the WVE risks at reduced separations becoming higher than those at the current separations. Although the concept of dynamic separation is widely accepted as a candidate of the next separation standard, the methodology to calculate the WVE risk and to reduce separations considering the risk calculation errors is not yet established. Here, we propose a method to probabilistically assure that the WVE risks at reduced separations do not exceed those at current separations.

3.1 Errors in WVE Risk Calculation

The WVE risk is defined as a probability that a following aircraft enters the hazard area of a wake vortex generated by a leading aircraft. The hazard area indicates an area that wake-induced turbulence can be hazardous to flight. To calculate the WVE risk, we need probability density distributions (PDDs) of aircraft position, wake vortex position and circulation intensity (product of wake-induced wind velocity and distance from wake vortex's core). In our method, the PDDs of aircraft position are considered as prescribed distributions based on flight procedure standards. The WVE risk calculation errors therefore derives mainly from errors in the PDDs of wake vortex position and circulation intensity that are predicted using a probabilistic wake vortex prediction model.

3.2 WVE Risk Evaluation Considering Wake Vortex Prediction Errors

The PDDs of wake vortex position and circulation intensity are produced based on a database of several thousand wake vortex observations acquired in various weather conditions. We must consider the following two major PDD error sources:

1. The uncertainty of the PDD: The PDD has an uncertainty since it is based on a finite number of observations. The reliability of the PDD increases with the number of observations from which it is derived.
2. The uncertainty of the surrounding environmental conditions: The PDDs are derived from wake vortex observation data normalized by using the leading aircraft (wake vortex generator) flight conditions and the weather conditions that prevailed when the observations were conducted. Thus, the accuracy of a PDD depends on the accuracies of the information about these conditions.

Such PDD errors can be quantified by the confidence interval of the PDDs [8]. Using this confidence interval information, we can calculate the reduced separations whose WVE risks do not exceed those at current separation as follows (Fig. 2):

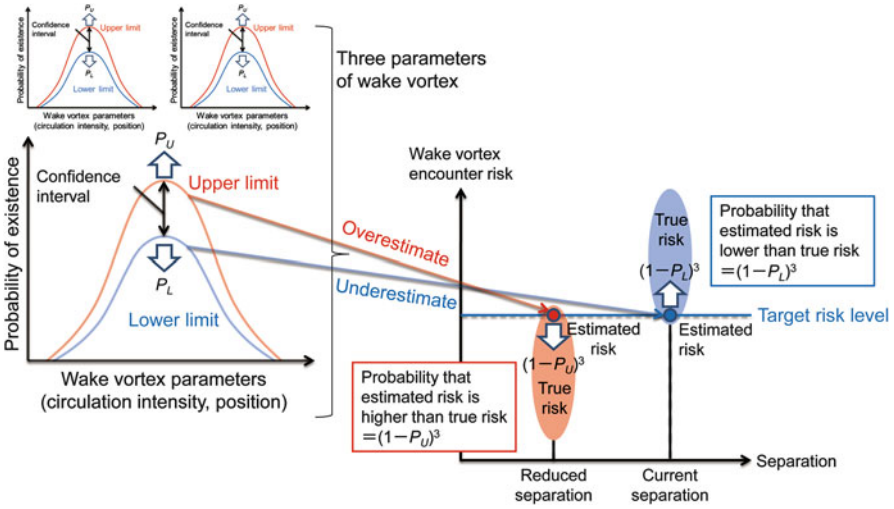

Fig. 2 WVE risk evaluation method

Step 1: Calculate the confidence intervals for each of the PDDs of the wake vortex position and circulation intensity based on [8]. The lower limits of the PDD's confidence interval (PDD_L) satisfy the requirement that the probability that "true PDD is higher than PDD_L for all ranges" is "$1-P_L$". In the same manner, the upper limits of the PDD's confidence interval (PDD_U) satisfy the requirement that the probability that "true PDD is lower than PDD_U for all ranges" is "$1-P_U$". P_U and P_L are configurable parameters that specify the confidence levels of the confidence intervals.

Step 2: Estimate the WVE risk at current separation under various weather conditions (P_{Cur_Est}) by using the PDD_L. The probability that the true WVE risk (P_{Cur}) is lower than the estimated risk (P_{Cur_Est}) is P_L. We then set the target risk level within the estimated WVE risks at current separation.

Step 3: Estimate the WVE risk at a reduced separation under a target weather condition (P_{Rdc_Est}) by using the PDD_U. The probability that the true risk (P_{Rdc}) is higher than the estimated risk (P_{Rdc_Est}) is P_U. Therefore, when we reduce wake vortex separation to the point at which the estimated risk at the reduced separation becomes equal to the target risk level based on the estimated risk at current separation ($P_{Rdc\_Est} = P_{Cur\_Est}$), the hazard probability (P_{Hzr}) that the true WVE risk at reduced separation exceeds the true risk at current separation ($P_{Rdc} > P_{Cur}$) is expressed as shown in Eq. (1).

$$1 - P_{Hzr} > (1 - P_L)(1 - P_U) > 1 - P_L - P_U \tag{1}$$

where, "$1-P_{Hzr}$" is a probability of "$P_{Rdc} \leq P_{Cur}$"; "$1-P_U$" is a probability of "$P_{Rdc} < P_{Rdc\_Est}\ (= P_{Cur\_Est})$"; "$1-P_L$" is a probability of "$P_{Cur\_Est} < P_{Cur}$".

In fact, there are three wake vortex parameters: circulation intensity and lateral/vertical positions. We therefore have to modify Eq. (1) accordingly by applying the above procedure to all three variables.

$$1 - P_{Hzr} > \left((1 - P_L)(1 - P_U)\right)^3 > 1 - 3(P_L + P_U) \tag{2}$$

As shown in Eq. (2), we can control the hazard probability by changing the confidence levels of the PDD confidence intervals used in the WVE risk evaluations. Although we do not consider the errors of the PDDs of aircraft position in this paper, such errors can be handled in a similar manner.

4 Airport Terminal Traffic Simulation with Reduced Separation

Here, we describe the airport terminal traffic simulation environment to demonstrate the expected capacity gain by introducing reduced separations based on our proposed methods.

4.1 Target Airport

We selected Tokyo international (Haneda) airport as the target airport since wake vortex separation is a major constraint to capacity at this airport, especially when southerly winds prevail [9]. As shown in Fig. 3, RWY16L/R are used for departures and RWY22 and 23 are used for arrivals when southerly winds prevail. In this configuration, there are three situations where wake vortex separation limits aircraft separations: (1) between successive landings on RWY22; (2) between successive take-offs from RWY16L/R; (3) between take-off from RWY16L and landing on RWY23. Table 2 shows the current separations with and without wake vortex

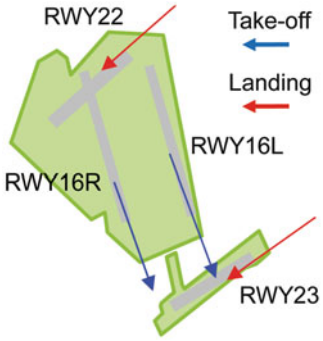

Fig. 3 Runway operations for southerly winds at Tokyo international airport

Table 2 Required separations with/without wake vortex separation

Situation	Wake vortex separation	
	Without	With
Successive landings on RWY22	115 s	120 s
Successive take-offs from RWY16L/R	95 s	120 s
Take-off from RWY16L and landing on RWY23	47 s	102 s

Table 3 Specifications of JAXA's non-hydrostatic mesoscale weather forecasting model

Item	Specification
Basic equations	Non-hydrostatic, compressible with terrain-following coordinates
Prediction range	164 km × 164 km
Grid resolution	2 km × 2 km × 300 m
Inputs	GPV (20 km resolution; provided by the Japan Meteorology Agency)
Outputs	Wind, pressure, temperature, relative humidity, icing/turbulence index
Output rate	Every 10 min

separations for these three situations. The required separations without wake vortex separation are mainly due to radar separation minima and runway occupation time constraints. In particular, the separation between "take-off from RWY16L and landing on RWY23" varies largely by wake vortex separation existence. In such cases, we can expect a large capacity gain by introducing reduced wake vortex separation.

4.2 Weather Condition

Weather information around the target airport is necessary to simulate wake vortex behaviors. In this simulation, JAXA's non-hydrostatic mesoscale weather forecasting model (Table 3) was used to produce realistic weather data around the airport such as prevailing winds, turbulence intensity and atmospheric stability. A domain size of 164 km × 164 km with a grid distance of 2 km was used, which covers the whole of the airport's terminal airspace. Using this model, one year of weather data around the airport were generated and approximately 1,000 cases where southerly winds prevailed were chosen for the simulation.

4.3 Probabilistic Prediction of Wake Vortex

There are several parametric wake vortex prediction models such as D2P/P2P/S2P developed by DLR [10–12], DVM/PVM developed by UCL [13], and the AVOSS model developed by NASA/NWRA [14]. These models output a wake vortex's circulation intensity and position considering its generation, decay and

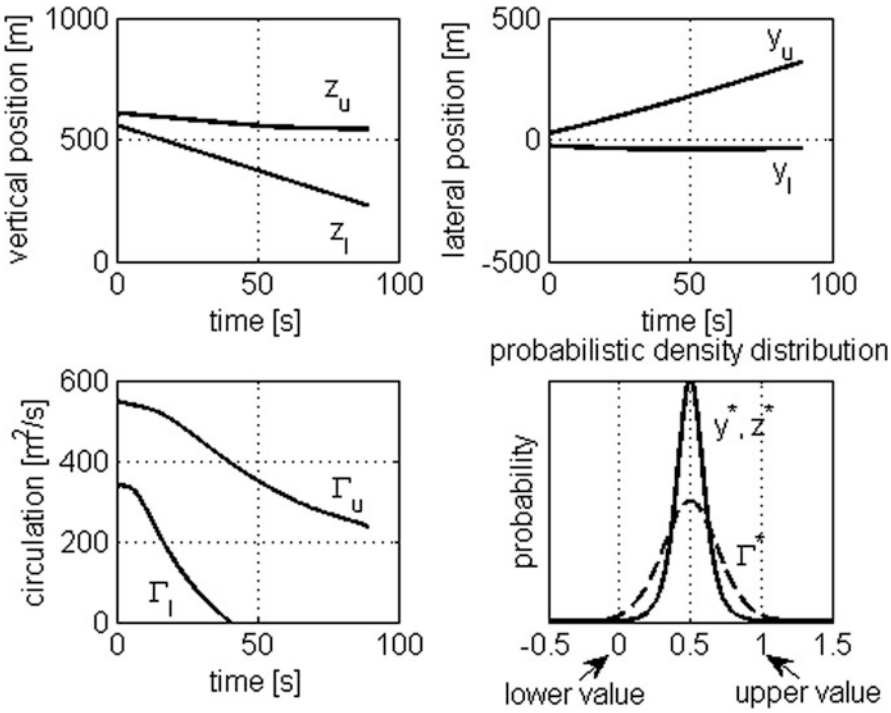

Fig. 4 Wake vortex generated by a "heavy" aircraft on approach to an airport. Measured values are normalized by the equation: $X^* = (X_{meas} - X_l)/(X_u - X_l)$, $X = y, z, \Gamma$, where X^* is a normalized value, X_{meas} is a measured value, X_u is a upper value, X_l is a lower value

advection processes. The initial vortex intensity depends on aircraft parameters such as lift (weight) and airspeed. Ambient atmospheric parameters such as wind speed/direction, turbulence intensity and stratification govern the decay and advection processes. The ground effect is also modeled as a function of the wake vortex's circulation intensity, its height above the ground and the time elapsed since its generation.

In our simulation, the S2P model is employed since it is capable of providing PDDs of wake vortex circulation intensity and vertical/lateral positions in real-time. Considering wake decay and advection processes, the S2P model predicts the uncertainty bounds (the upper and lower limits) of wake vortex parameters, and then applies the prescribed PDDs normalized by the calculated uncertainty bounds to express wake vortex random behaviors (Fig. 4). Since the uncertainty bounds account for wake vortex deterministic behaviors influenced by flight conditions and local weather conditions, the PDDs are independent of these. We therefore require only a single PDD for each wake vortex parameter derived from the wake vortex observation database. In our simulation, the PDDs based on about 2,400 wake vortex observation data presented in [11] were used. However, we must consider the PDD

Table 4 Accuracy level of available weather information

Parameter	Errors (1σ)	
	Case 1	Case 2
EDR ($m^{2/3}/s$)	0.05	0.025
Brunt–Väisälä frequency (1/s)	0.005	0.0025
Wind (m/s)	3.0	1.5

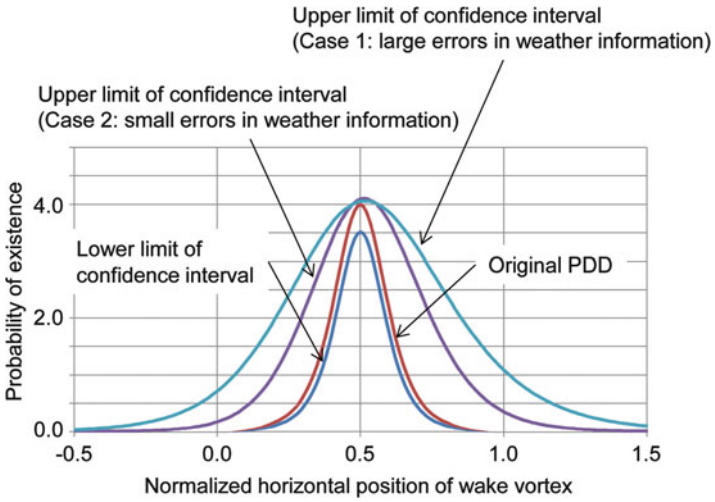

Fig. 5 PDD confidence intervals of wake vortex horizontal position

errors when we estimate WVE risks as we discussed. We calculated the confidence interval of the PDDs with a condition of $P_U = P_L = 10^{-3}/6$. By using these confidence intervals in the WVE risk evaluations, we can control the hazard probability P_{Hzr} to be lower than 10^{-3}. In addition, we assume two different accuracy levels of available weather information in wake vortex prediction. The wake vortex behavior heavily depends on weather parameters listed in Table 4. The eddy dissipation rate (EDR) indicates atmospheric turbulence intensity and the Brunt–Väisälä frequency indicates atmospheric stability. Both parameters mainly affect wake vortex decay process. The wind mainly determines wake vortex advection process. Therefore, the accuracy of wake vortex prediction largely changes according to the accuracy levels of available weather information. The first case in Table 4 assumes the current weather forecast accuracy commonly available in Japan. The second case assumes a near-future weather forecast accuracy whose errors are set to be half of the first case.

Figure 5 exemplifies the calculated confidence intervals of the PDD of the wake vortex horizontal position. The vertical axis shows the probability of existence and horizontal axis shows the horizontal position normalized by the predicted horizontal position. The value of 0.5 on the horizontal axis means that the predicted position matches the actual position perfectly. The envelope of the PDD becomes larger if available weather information accuracy degrades. This means that the WVE

risks are overestimated and the expected separation reduction is smaller. Thus, we can obtain an appropriate safe separation margin according to the accuracy of the available weather information.

4.4 Aircraft Trajectory Model

The nominal routes of departure/arrival traffic were set based on the Aeronautical Information Publication (AIP) and flight procedure standards published by the Japan Civil Aviation Bureau. The PDDs of aircraft positions around the nominal paths were produced based on radar surveillance data and a probabilistic trajectory model used in the risk collision model for the ILS landing [15]. In our simulation, the PDDs of the aircraft position remain constant regardless of surrounding weather conditions and aircraft types.

4.5 Aircraft Types

The aircraft types considered in the simulation are heavy and medium category aircraft in current wake vortex separation rules. These two categories are dominant among aircraft types flying at the target airport. A B747 size aircraft was used as a leading aircraft, since a heavier aircraft makes a stronger wake vortex and makes it difficult to reduce separations. As following aircraft, the lightest aircraft type was chosen from each of the heavy and medium categories: a B767 size aircraft was chosen from a heavy category and a B737 size aircraft from a medium category.

4.6 Hazard Area of Wake Vortex

The size of a hazard area of wake vortex depends on the wake vortex circulation intensity and the flight characteristics of a following aircraft. In our simulation, a hazard area was defined as an area where aircraft rolling moment induced by wake vortex could be more than $5^\circ/s^2$. Based on JAXA's flight simulation results, we set the hazard area size as shown in Fig. 6. Since two cores of wake vortex are not necessarily located at the same altitude due to surrounding weather conditions such as vertical windshear [10–12], the highest altitude of hazard area is set to be Δz higher than a higher wake vortex core and vice versa as shown in Fig. 6. The vertical extent of the hazard area is larger for medium category aircraft than heavy category aircraft since lighter aircraft are more prone to wake vortex disturbance. On the other hand, the horizontal extent of the hazard area is larger for heavy category aircraft since heavy category aircraft have a longer wing span than medium category aircraft.

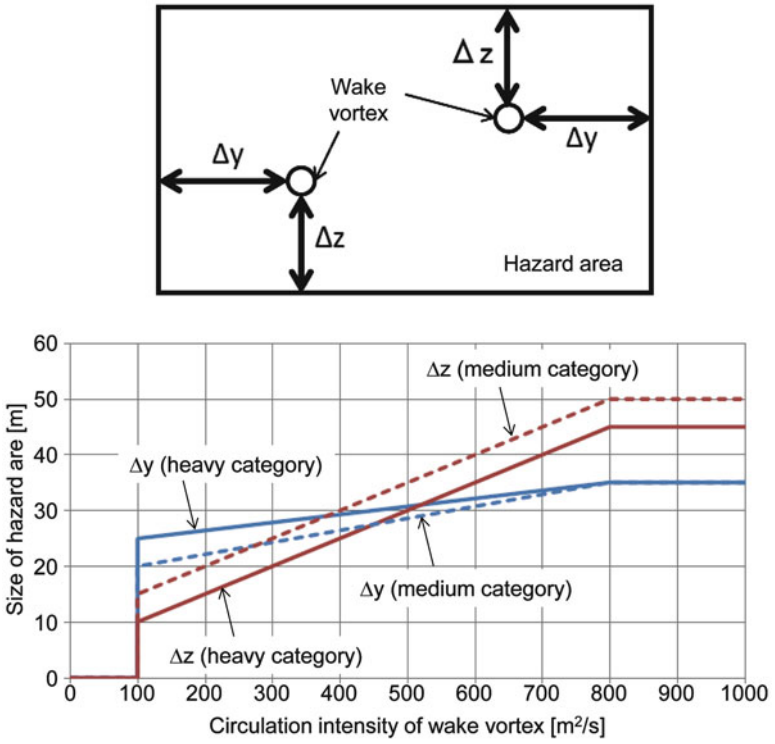

Fig. 6 Hazard area of wake vortex

4.7 WVE Risk Calculation

As previously mentioned, the WVE risk is defined as the probability that a following aircraft enters the hazard area of the wake vortex generated by a leading aircraft. In other words, the WVE risk equals to a probability that a wake vortex exists within a region of the hazard area whose center is the position of a following aircraft. This probability is calculated as follows:

Step 1: The probability $P_{W\Gamma}(\Gamma, y_L, z_L)$ that "a wake vortex generated by a leading aircraft located at (y_L,z_L) and whose circulation intensity is Γ exists within a hazard area whose center is the position of a following aircraft" is expressed as shown in Eq. (3) below. $P_{W\Gamma}$ is a function of Γ since the size of the hazard area varies according to Γ:

$$P_{W\Gamma}(\Gamma, y_L, z_L) = \int_{-\infty}^{+\infty}\int_{-\infty}^{+\infty} P_{WF}(\Gamma, y, z)\, p_F(y, z)\, dydz \tag{3}$$

where $P_{WF}(\Gamma,y,z)$ is the probability that a wake vortex whose circulation intensity is Γ exists within the hazard area whose center coordinate is (y,z), and $p_F(y,z)$ is the probability that a following aircraft exists at the coordinate

(y,z). The former probability is calculated using the probabilistic wake prediction model (S2P model) and hazard area size information. The latter probability is calculated using the aircraft trajectory model.

Step 2: The probability $P_{WL}(y_L,z_L)$ that "a wake vortex generated by a leading aircraft located at (y_L,z_L) exists within a hazard area whose center is the position of a following aircraft" is expressed as shown in Eq. (4) below:

$$P_{WL}(y_L, z_L) = \int_0^{+\infty} P_{W\Gamma}(\Gamma, y_L, z_L)\, p_\Gamma(\Gamma)\, d\Gamma \tag{4}$$

where $p_\Gamma(\Gamma)$ is the probability that the wake vortex circulation intensity is Γ. This probability is calculated using the probabilistic wake prediction model.

Step 3: The probability P_W that "a wake vortex generated by a leading aircraft exists within a hazard area whose center is the position of a following aircraft" is expressed as shown in Eq. (5) below:

$$P_W = \int_{-\infty}^{+\infty}\int_{-\infty}^{+\infty} P_{WL}(y,z)\, p_L(y,z)\, dydz \tag{5}$$

where $p_L(y,z)$ is the probability that a leading aircraft exists at the coordinate (y,z). This probability is calculated using the aircraft trajectory model.

The obtained probability P_W is the WVE risk. Note that we use the lower limits of the confidence intervals of the wake parameters' PDDs to calculate the WVE risk at current separations, and use the upper limits to calculate the WVE risk at reduced separations.

5 Simulation Results and Discussion

5.1 WVE Risk Distribution

Figure 7 shows the simulated WVE risk distributions in one year of southerly wind operations (about 1,000 different weather conditions) for three situations shown in Table 2. Each point in Fig. 7 expresses the maximum WVE risk during an approach or a departure in one weather condition. The lateral axis shows the maximum WVE risk and the vertical axis shows the altitude of a following aircraft where the maximum risk is expected. The aircraft separation between leading and following aircraft was fixed to 120 s for all situations.

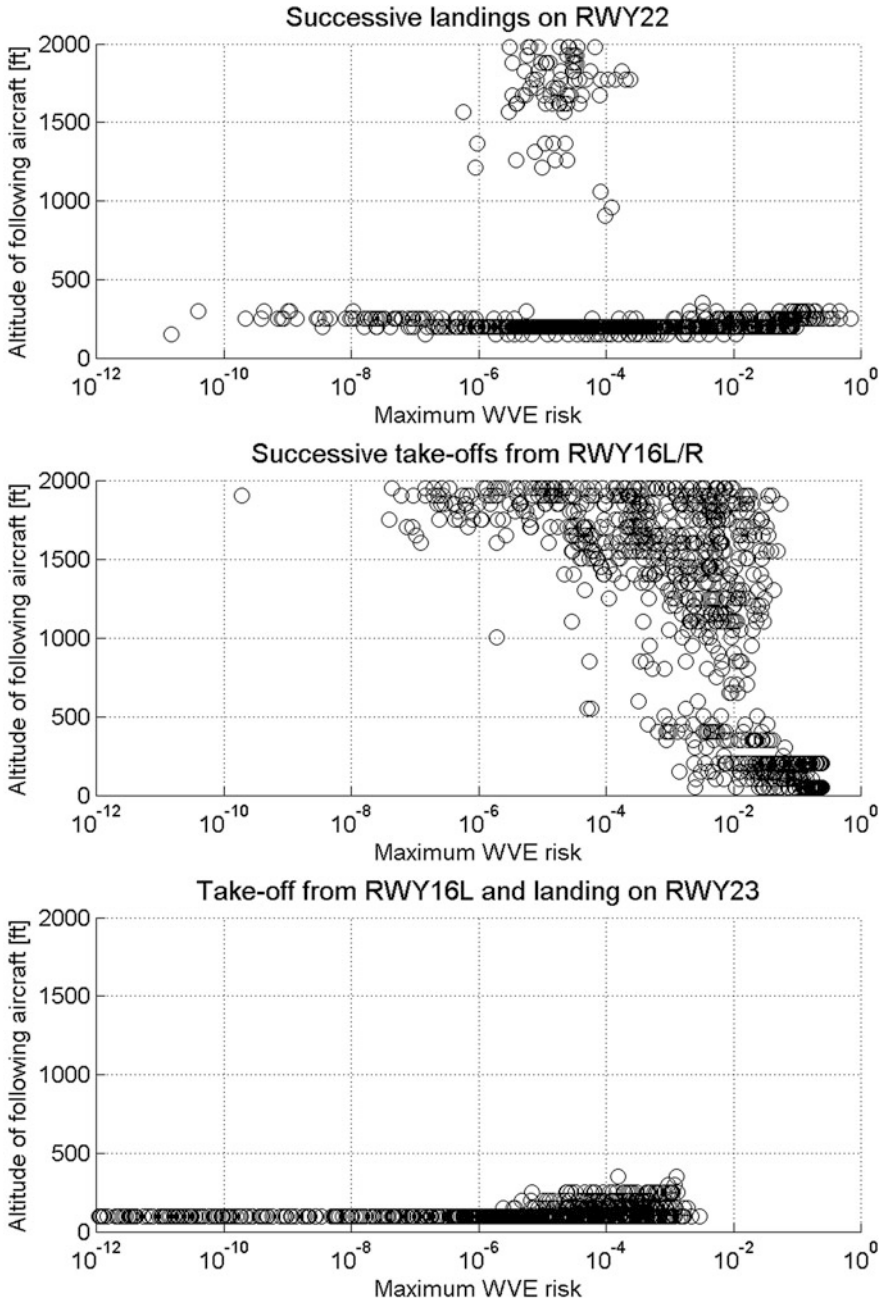

Fig. 7 Maximum WVE risk distributions

5.1.1 WVE Risk Variation due to Weather Conditions

Figure 7 indicates that the WVE risks vary largely due to weather conditions from 10^{-1} to 10^{-12}. From this, we can expect the separation reduction in many favorable weather conditions whose WVE risks are quite low. Figure 8 compares weather parameters between high WVE risk conditions (higher than the yearly averaged risk) and low WVE risk conditions (lower than the yearly averaged risk) for successive take-offs from RWY16L/R. The comparison result indicates that strong crosswinds and large EDRs are effective to mitigate WVE risks. This is because wake vortices are drifted away from the flight path by strong crosswinds and wake vortex decay is accelerated under turbulent atmosphere expressed by large EDRs.

5.1.2 Vertical Distribution of WVE Risk

Successive Landings on RWY22 and Take-Offs from RWY16L/R

Figure 9 shows the vertical profile of the occurrence frequency of the maximum WVE risk. In successive landings or take-offs where leading and following aircraft fly the same path, the maximum WVE risks are mainly occurred at either above 1,500 ft or below 500 ft. The WVE risk increases at above 1,500 ft since the variations of aircraft position are larger than lower altitudes. For example, the WVE risk increases if a following aircraft flies lower than a leading aircraft since wake vortex has a tendency to descend by itself. The occurrence probability of such situation becomes higher as the variation of aircraft position becomes larger. On the other hand, the WVE risk increases at below 500 ft since descent of wake vortex is blocked by ground surface and wake vortex lingers near the flight path. To mitigate these two WVE risk peaks at high and low altitudes, GBAS-based flexible flight paths such as dual thresholds or curved approach would be beneficial since leading and following aircraft can fly different flight paths.

Take-Off from RWY16L and Landing on RWY23

The maximum WVE risk mostly occurs at below 100 ft since the flight paths of take-off from RWY16L and landing on RWY23 intersect over RWY23 (Fig. 3).

5.2 Separation Reduction

Table 5 shows the simulated separation reduction for three situations shown in Table 2. The reduction shown is averaged over one year of southerly wind operations (about 1,000 different weather conditions). We employed three different target WVE risk levels: 50 % / 70 % / 90 % cumulative values of the WVE risks at current

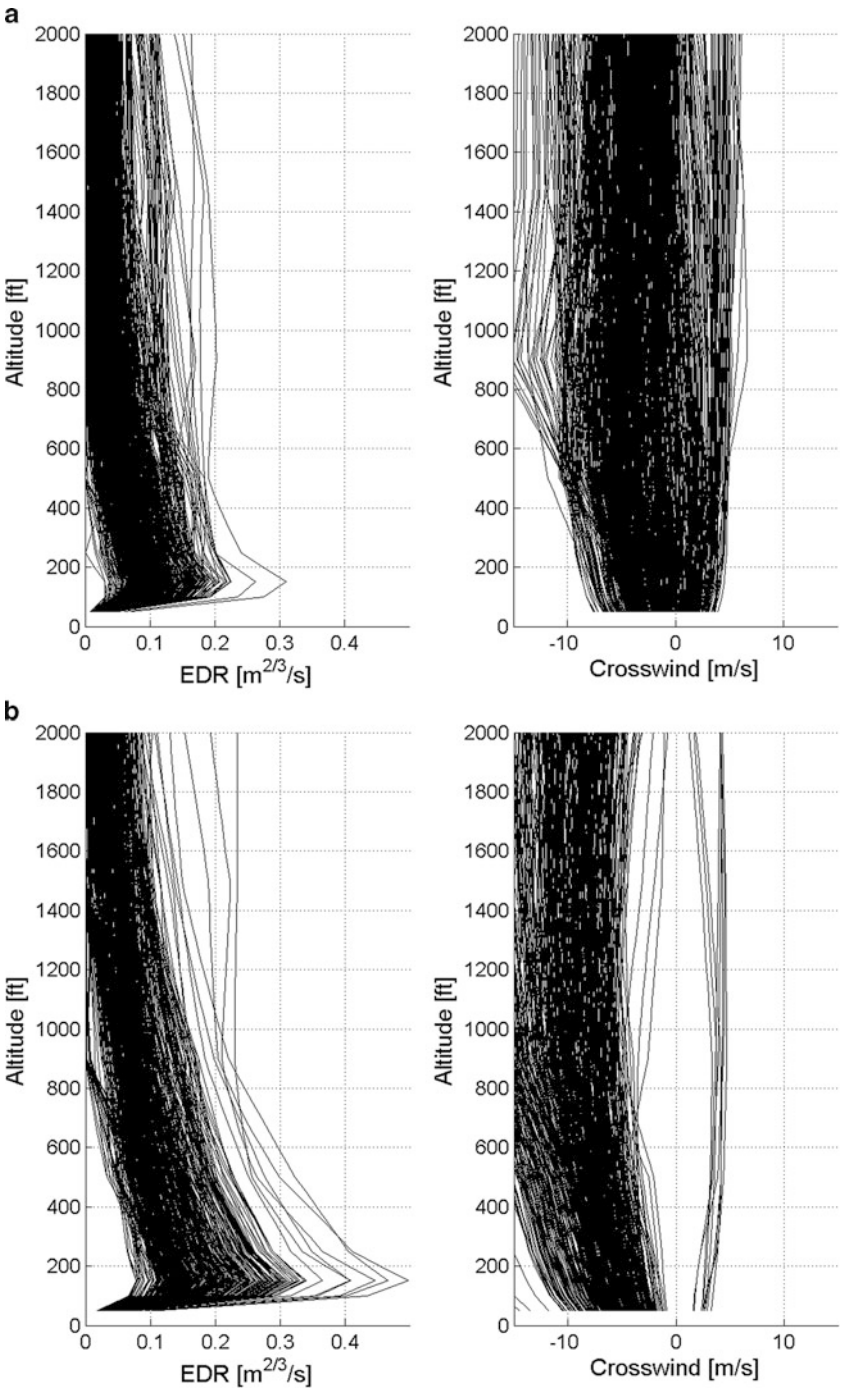

Fig. 8 Comparison of weather parameters between high and low WVE conditions (successive take-offs from RWY16L/R). (**a**) High WVE risk conditions. (**b**) Low WVE risk conditions

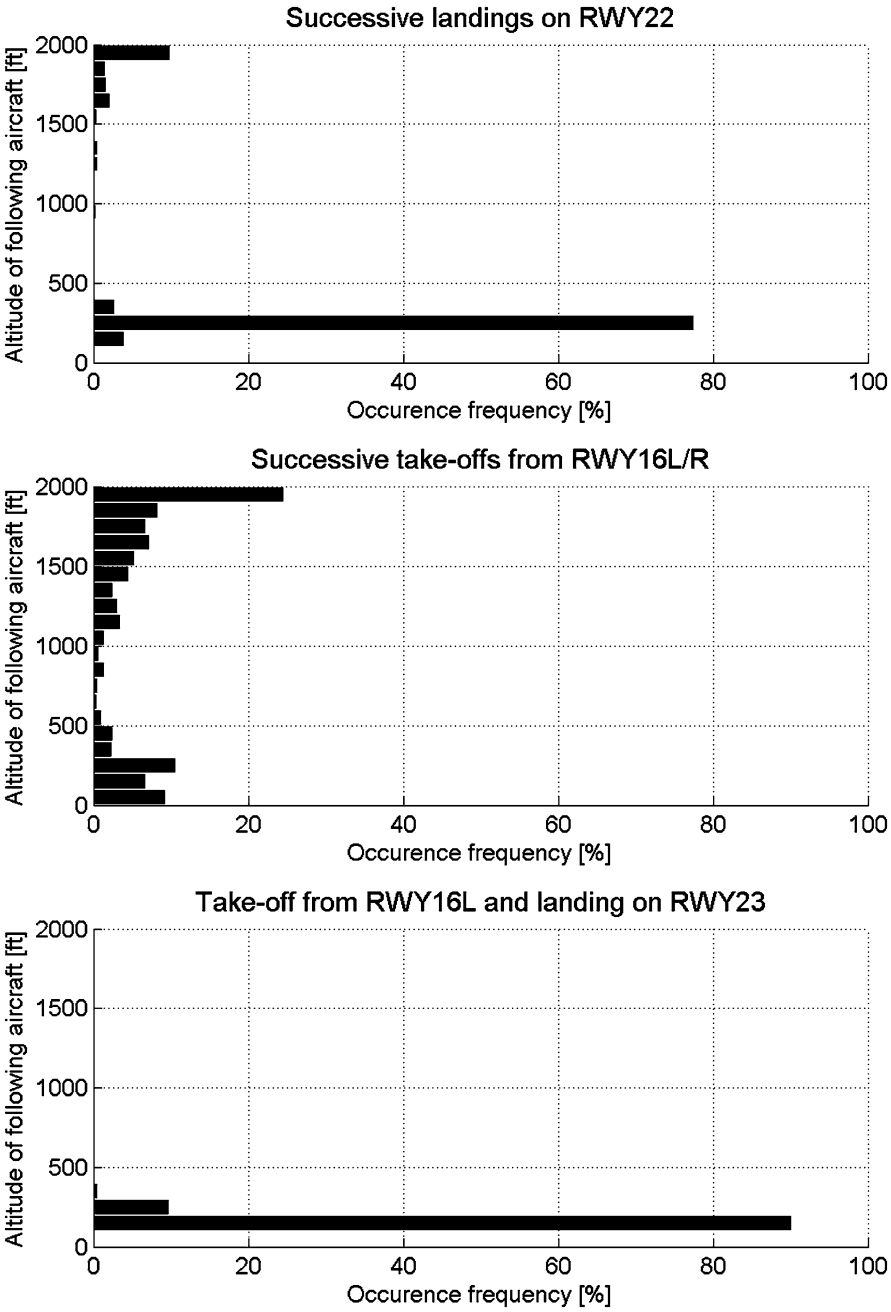

Fig. 9 Vertical profile of the occurrence frequency of the maximum WVE risk

Table 5 Simulated separation reductions (averaged over approximately 1,000 different weather conditions)

Situation	Errors in weather information	Target risk level (cumulative risk value at current separations)		
		50 %	70 %	90 %
(1) *Following aircraft: Heavy category*				
Successive landings on RWY22	Case 1	0 s	0 s	2 s
	Case 2	0 s	1 s	3 s
Successive take-offs from RWY16L/R	Case 1	3 s	5 s	10 s
	Case 2	4 s	7 s	13 s
Take-off from RWY16L and landing on RWY23	Case 1	0 s	1 s	7 s
	Case 2	1 s	7 s	16 s
(2) *Following aircraft: medium category*				
Successive landings on RWY22	Case 1	0 s	0 s	2 s
	Case 2	0 s	1 s	3 s
Successive take-offs from RWY16L/R	Case 1	3 s	5 s	10 s
	Case 2	4 s	7 s	13 s
Take-off from RWY16L and landing on RWY23	Case 1	0 s	2 s	8 s
	Case 2	1 s	7 s	17 s

separations. For example, if we employ the 50 % cumulative values as the target risk level, we have chances to reduce separation at 50 % of all take-off/landing operations unless other separation constraints prohibit. Here, we discuss three factors affecting separation reduction.

5.2.1 Target Risk Level

The separation reduction depends heavily on the target risk level. The highest target risk level of 90 % cumulative value leads to over 10 s reduction in two situations. On the other hand, the lowest target risk level of 50 % cumulative value brings reductions of only a few seconds. As a natural consequence, a higher target risk level brings a larger separation reduction since it gives more chances to reduce separations. However, the total amount of the WVE risks does increase if we employ the higher target risk level. Although the safety of reduced separations remains acceptable while the target risk level is set to be within the risks at current separations, we have to realize that the selection of the target risk level is a trade-off between the separation reduction and the WVE risks.

5.2.2 Type of Following Aircraft

The type of following aircraft (heavy or medium category) makes little difference to the separation reduction, since the size of hazard area does not greatly vary by aircraft type.

5.2.3 Accuracy of Available Weather Information

Poor accuracy of available weather information decreases separation reduction. In particular, the reduction of the separation between "take-off from RWY16L and landing on RWY23" is largely affected by the weather information accuracy. In this case, the flight paths of leading and following traffic are different. The flight paths of following traffic are therefore located at the tails of the PDDs of the wake vortex positions in most weather conditions except for strong crosswinds. Meanwhile, the prediction results of wake vortex position are widely spread when the accuracy of the available weather information is poor. In such cases, the probability of wake vortex existence at the tail of the PDD increases as shown in Fig. 5, and the WVE risk therefore increases.

5.3 Expected Capacity Gain

The airport capacity gain expected from the separation reduction shown depends on the airport operating conditions such as aircraft types and take-off/landing sequences. We obtained the maximum 4.5 % capacity gain when we assumed the airport operating conditions at the most congested time period (8–9 a.m.) of the target airport. In this time period, the ratio of heavy to medium category aircraft was almost one to one. In addition, the capacity gain increased up to 14.5 % when we optimized the take-off/landing sequences. Wake vortex separations can be reduced by increasing the opportunities of successive take-offs/landings of the same category aircraft. This result demonstrates the effectiveness of dynamic separation using weather information and the optimization of the take-off/landing sequences.

6 Conclusions

This paper presented a methodology that calculates a reduced wake vortex separation that is equally safe as current separation minima. We proposed that the wake vortex encounter risk at reduced separation should be estimated using the upper confidence interval of the PDDs of wake vortex parameters, and the risk at current separation estimated by using the lower confidence interval. By doing this, we can control the hazard probability that the wake vortex encounter risks at reduced

separations exceed those at current separation to be lower than a threshold value. We also presented an airport terminal traffic simulation environment to demonstrate the traffic capacity gain for a congested airport by introducing reduced wake vortex separations and optimizing take-off/landing sequences. The simulation result shows a 14.5 % capacity gain. This result supports the effectiveness of the proposed methodology.

To realize dynamic separation according to weather condition, our proposed methodology would greatly help since it can calculate reduced separations with acceptable safety level using probabilistic weather information. However, it might be difficult to achieve sufficient safety level only by such probabilistic risk assessment especially at the introduction phase of dynamic separation. One possible solution is to utilize a real-time wake vortex monitoring system combined with our proposed methodology as a "safety net". Such real-time wake vortex monitoring system has been studied by several organizations [16]. Another factor to be considered is how to produce the detailed weather information around the airport with probabilistic accuracy information which is necessary for probabilistic wake vortex prediction. JAXA has started a development of a new weather forecasting model that is capable of providing probabilistic forecast accuracy information according to weather conditions.

References

1. Gerz T, Holzäpfel F, Darracq D (2001) Aircraft wake vortices: a position paper. Wakenet
2. WakeNet2-Europe (2006) Wake vortex research needs for 'improved wake vortex separation ruling' and 'reduced wake signatures'. Final report of the thematic network 'WakeNet2-Europe'. 6th Framework Program, NLR-CR-2006-171. National Aerospace Laboratory, Amsterdam
3. Holzäpfel F, Gerz T, Frech M, Tafferner A, Kopp F, Smalikho I, Rahm S, Hahn K-U, Schwarz C (2007) The wake vortex prediction and monitoring system WSVBS – Part I: Design. In: 1st CEAS European air and space conference, Berlin
4. Gerz T, Holzäpfel F, Gerling W, Scharnweber A, Frech M, Wiegele A, Kober K, Dengler K, Rahm S (2007) The wake vortex prediction and monitoring system WSVBS – Part II: Performance and ATC integration at Frankfurt Airport. In: 1st CEAS European air and space conference, Berlin
5. Lang S (2009) Wake turbulence mitigation for departures (WTMD) and wake turbulence mitigation for arrivals (WTMA). In: Global wake conference, Brussels
6. Treve V (2011) Crosswind dependent separations (CROPS). In: Wakenet 3 specific workshop 'WV concepts & capacity,' London
7. Anon (2012) Global air navigation capacity & efficiency plan 2013–2028. ICAO Doc 9750 Draft 2014–2016 Triennium Edition
8. Sugiura M, Matayoshi N (2011) Accuracy estimation of probabilistic wake vortex prediction considering weather information errors. In: 3rd AIAA atmospheric space environments conference, Honolulu, June 2011 (AIAA 2011–3195)
9. Matayoshi N, Okuno Y, Sugiura M, Kono M, Yoshii T, Hirata T (2010) Airport terminal traffic simulation applying reduced wake vortex separation. In: 10th AIAA aviation technology, integration and operations conference, September 2010 (AIAA 2010–9338)

10. Holzäpfel F (2003) Probabilistic two-phase wake vortex decay and transport model. J Aircraft 40(2)
11. Holzäpfel F (2006) Probabilistic two-phase aircraft wake-vortex model: further development and assessment. J Aircraft 43(3)
12. Holzäpfel F, Steen M (2007) Aircraft wake-vortex evolution in ground proximity: analysis and parameterization. AIAA J 45(1)
13. Jackson W, Yaras M, Harvey J, Winckelmans G, Fournier G, Belotserkovsky A (2001) Wake vortex prediction—an overview. Phase 6 and project final report, Transport Canada and its Transportation Development Center, TP 13629e.pdf. www.tc.gc.ca/tdc/summary/13600/13629e.htm
14. Robins RE, Delisi DP (2002) NWRA AVOSS wake vortex prediction algorithm, version 3.1.1. NASA/CR-2002-211746
15. Anon (1980) Manual on the use of the collision risk model (CRM) for ILS operations. ICAO Doc 9274
16. Barbaresco F, Orlandi F, Juge P (2013) European FP7 Project: Ultra-fast wind sensors for wake vortex hazards mitigation. In: WakeNet-Europe workshop 2013

Basic Analysis of Winds Aloft Forecast Used for En-Route Trajectory Prediction

Hiroko Hirabayashi and Yutaka Fukuda

Abstract This paper provides the impact of a meteorological forecast model on the trajectory of aircraft for future Air Traffic Management based on trajectory operation. The ground speed of aircraft was calculated under the influences of seasonal wind conditions and meteorological forecast accuracy during cruise flights on the waypoints in the course towards Tokyo International Airport. Aspects of wind conditions of cruise altitude vary from season to season depending on the position of the waypoint, and whether jet stream exists or not. Aircraft ground speed tends to vary based on the direction of aircraft movement in addition to wind conditions. The predictions of ground speed were calculated using meteorological forecast data of 15 h prior or later. The results show that prediction accuracy of ground speed improves if recent prediction data is used. And ground speed prediction accuracy becomes lower and high RMS values overlap when and where wind speed widely varies.

Keywords Air traffic management • Meteorological forecast • Trajectory

1 Introduction

Trajectory-Based Operation (TBO) is the axis of a global Air Traffic Management (ATM) concept which is being developed by the International Civil Aviation Organization (ICAO) to accommodate a demand for safe, efficient and environmentally-friendly flights through technical advances in the air transport industry with increasing traffic volume [1]. For the purpose of realization of the TBO, prediction of aircraft trajectory is required not only in the aircraft on-board

H. Hirabayashi (✉) • Y. Fukuda
Electronic Navigation Research Institute, 7-42-23 Jindaijihigashi-machi, Chofu, Tokyo 182-0012, Japan
e-mail: h-hirabayashi@enri.go.jp

Electronic Navigation Research Institute (ENRI), *Air Traffic Management and Systems*, Lecture Notes in Electrical Engineering 290, DOI 10.1007/978-4-431-54475-3_5,

system but also in the ground system. One of the applicable aircraft performance models to predict aircraft trajectory is Base of Aircraft Data (BADA), which the Eurocontrol Experimental Centre provides [2]. To create a precise prediction of aircraft trajectory, a prediction model reflecting regional variations is being developed by comparison between predicted trajectory and actual measurement data [3–5].

The impact factors for the prediction of aircraft trajectory are aircraft kinetics, intentions of the pilot or air traffic controller, atmospheric conditions, and so on. The atmospheric conditions such as wind speed, wind direction and temperature are one of the key factors for predicting aircraft trajectory because atmospheric conditions affect aircraft speed during flight. Reflecting close to real conditions where aircraft is passing will help in developing a high-accuracy prediction model of aircraft trajectory, and the advancement of the wind prediction model for aircraft trajectory has been studied [6]. One high-altitude atmospheric condition data to be used is Numerical Weather Prediction (NWP) that the Japan Meteorological Agency (JMA) provides. NWP uses mathematical models of the atmosphere and oceans to predict the weather based on current weather conditions. The NWP model performance is checked whenever new atmospheric models are developed [7]. However, the impact on aircraft speed has never been analyzed. In order to clarify the impact of the meteorological forecast model on the trajectory, aircraft ground speed (GS) during cruise flights were calculated using values in the NWP model.

2 Methods

2.1 Aircraft Ground Speed Calculation

GS, which is the speed of the aircraft relative to the ground, was calculated in this study. The measurement and indication of airspeed are ordinarily accomplished on board connected to a pitot-static system. True airspeed (TAS) is the speed of the aircraft relative to the atmosphere. Figure 1 shows the vector relationship between the TAS and GS. The formula is as follows:

$$V_{GND} = V_{TAS}\, cos\, \varnothing_D + W\, cos\, (\varnothing_W - \varnothing_T) \tag{1}$$

where $\boldsymbol{V_{GND}}$ is ground speed, $\boldsymbol{V_{TAS}}$ is true airspeed, $\boldsymbol{W}$ is wind speed, $\varnothing_W$ is wind vector angle, $\varnothing_T$ is track vector angle and $\varnothing_D$ is drift angle, the drift angle is calculated as follows:

$$\varnothing_D = sin^{-1}\left(\frac{W}{V_{TAS}} sin\, (\varnothing_W - \varnothing_T)\right) \tag{2}$$

The simplest way to calculate TAS is by using a function of Mach numbers as follows:

$$V_{TAS} = M \times \sqrt{\gamma \cdot R \cdot T} \tag{3}$$

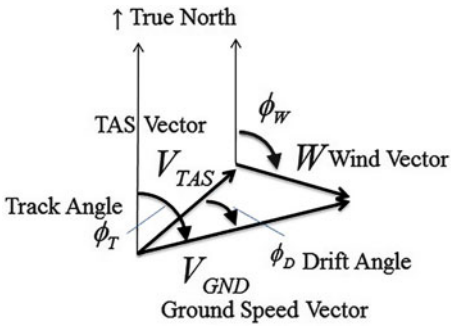

Fig. 1 Relation between track direction and wind direction

where M is Mach number, γ is adiabatic index of air, R is Real gas constant of air and T is Temperature.

Generally, aircraft maintain a constant Mach number during cruise flight. GS was calculated using the constant Mach number 0.84 in this study.

2.2 Target Waypoints

In the case of Japan, air traffic flow concentrates on Tokyo International Airport from each part of the country. Three main traffic flows were targeted in this study, from New Chitose (Sapporo), Fukuoka and Naha to Tokyo. Fixed waypoints, HPE (Hanamaki), IGOSO and SHIBK, located 200–300 NM (1 NM = 1,852 m) from the departure airport, were chosen as the points where GS was calculated, as shown in Fig. 2.

2.3 Meteorological Model

The JMA has currently operated several NWP models to cover various types of forecasts. The Meso-Scale Model (MSM) is intended for use in basic data for prediction of disasters and for aviation with higher horizontal resolution. East–west and north–south direction of wind elements and temperature are gained from the Japan Meteorological Business Support Center online data service. Wind speed and wind direction were calculated from east–west and north–south directions of wind elements. Table 1 shows a brief overview of MSM Grid Point Value (GPV). Three pressure altitudes (300, 250 and 200 hPa) which are close altitudes that jet aircraft fly at as a cruising altitude in general, were used for this study. Forecast hours 15, 12, 9, 6, 3 and 0 were used for the meteorological forecast data analysis.

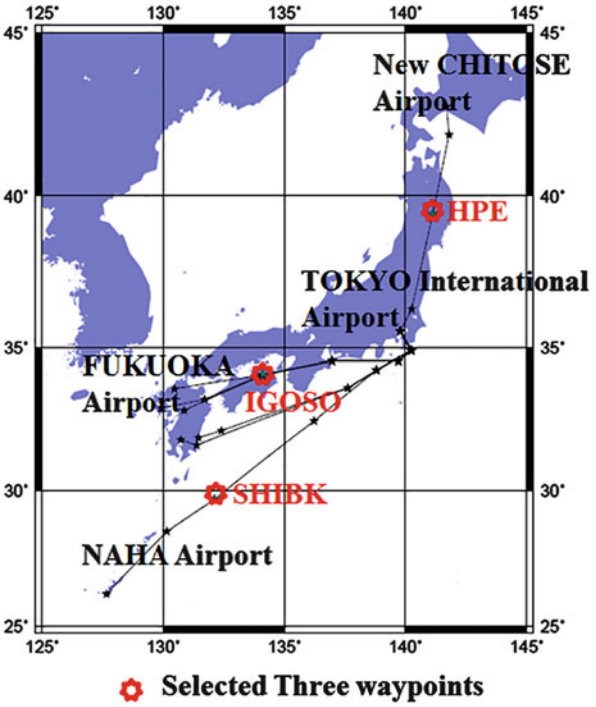

Fig. 2 Flight course and target waypoints

Table 1 Summary of MSM (GPV)

Delivered range	Northern latitude between 22.4° and 47.6°		
	Eastern longitude between 120° and 150°		
Grid system	Latitude and longitude intervals		
	Latitude 0.1° × longitude 0.125°		
Initial value	00, 03, 06, 09, 12, 15, 18, 21 UTC (eight times a day)		
Forecast hours	15 h forecast (00, 06, 12, 18 UTC)		
	33 h forecast (03, 09, 15, 21 UTC)		
	3 h intervals		
Pressure altitude hPa (feet in ISA; 1 foot = 0.3048 m)	100 (53,083 ft)	150 (44,647 ft)	200 (38,662 ft)
	250 (33,999 ft)	300 (30,065 ft)	400 (23,574 ft)
	500 (18,289 ft)	600 (13,801 ft)	700 (9,882 ft)
	800 (6,394 ft)	850 (4,781 ft)	900 (3,243 ft)
	925 (2,500 ft)	950 (1,773 ft)	975 (1,061 ft)
	1,000 (364 ft)		

2.4 Applicable Period

For the purpose of examination of seasonality in high altitudes, 140 days (4 weeks from each of the five seasons as defined below) of MSM (GPV) data in 2011 were used.

- Winter: January 23 to February 19,
- Spring: April 24 to May 21,
- Summer: July 24 to August 20,
- Typhoon season: September 1 to September 28 and
- Autumn: October 23 to November 19; total 140 days

In the case of Japan, typically four seasons are characterized by atmospheric temperature difference and position of air mass. The months with the lowest temperature are January/February and the highest are July/August, which were defined as winter and summer respectively in this study. In addition to the four seasons, the typhoon season was also considered. Several cyclones with disturbance wind averagely pass through the Japanese archipelago in September. Two typhoons passed through the Japanese archipelago in September, 2011.

Every 3 h of the three pressure altitudes, 3,360 GS were calculated at each waypoint at one forecast hour, totaling 60,480 GS.

3 Wind Aspect at High Altitudes

There is a strong westerly wind that is a jet stream near the tropopause where jet aircraft fly at cruising altitude. The width of a jet stream is typically a few hundred kilometers and its vertical thickness is often less than 5 km. The condition of the wind near the tropopause varies due to the influence of the jet stream.

Figure 3 represents the wind speed and wind direction of 250 hPa at each waypoint. The dots are terminal points of one wind vector. The main stream of upper wind at each waypoint is westerly wind. Strong westerly winds are shown in the winter at IGOSO and SHIBK, meanwhile wind at HPE is weak and broadens widely throughout the season.

4 Seasonal Tendency of Aircraft Ground Speed

4.1 Seasonally-Varying GS

GS was calculated using values in the NWP. Table 2 shows mean and standard deviations of GS in each season assuming that aircraft maintains Mach number 0.84 during cruise flight at 250 hPa. There is not much difference in GS along each

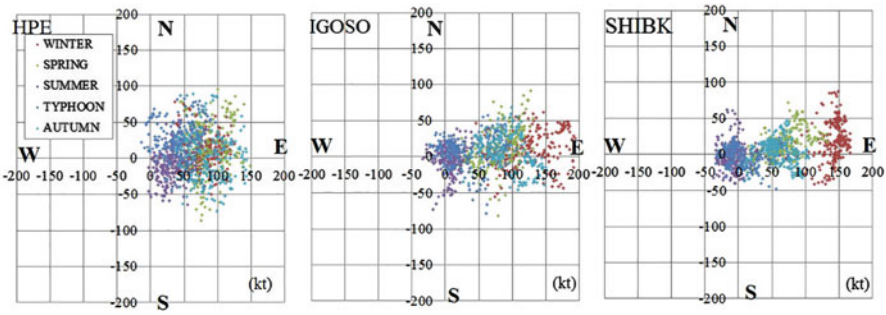

Fig. 3 Terminal points of wind vectors

Table 2 Aircraft ground speed at each waypoint at 250 hPa (kt)

Waypoint		Winter	Spring	Summer	Typhoon season	Autumn
HPE	Mean	454	449	497	463	461
	SD	23	34	25	27	29
IGOSO	Mean	613	572	506	531	584
	SD	44	32	15	31	28
SHIBK	Mean	611	558	493	507	544
	SD	32	27	17	22	18

waypoint during the summer whereas it varies between IGOSO/SHIBK and HPE in other seasons. The variation among these waypoints is caused by flight direction to the destination airport. Especially in the winter, the gap of mean GS between IGOSO/SHIBK and HPE is wide. GS varies widely in the winter in the case of SHIBK and IGOSO, and in the spring in the case of HPE according to standard deviation.

Figure 4 shows distributions of GS at 250 hPa at each waypoint [probability density functions (PDF) and cumulative distribution functions (CDF)]. The peak of GS varies among seasons at IGOSO/SHIBK whereas peaks at HPE do not vary much from season to season. At SHIBK and IGOSO, GS is fast and varies widely especially in the winter.

4.2 Ground Speed Change in Three Hours

Table 3 shows the mean and maximum changes in GS over a period of 3 h. GS varies widely in the winter especially at IGOSO (Table 2), and the change in 3 h varies widely in the spring at HPE. The largest change is 57 knots (1 knot = 0.5144 m/s) in 3 h at HPE in autumn.

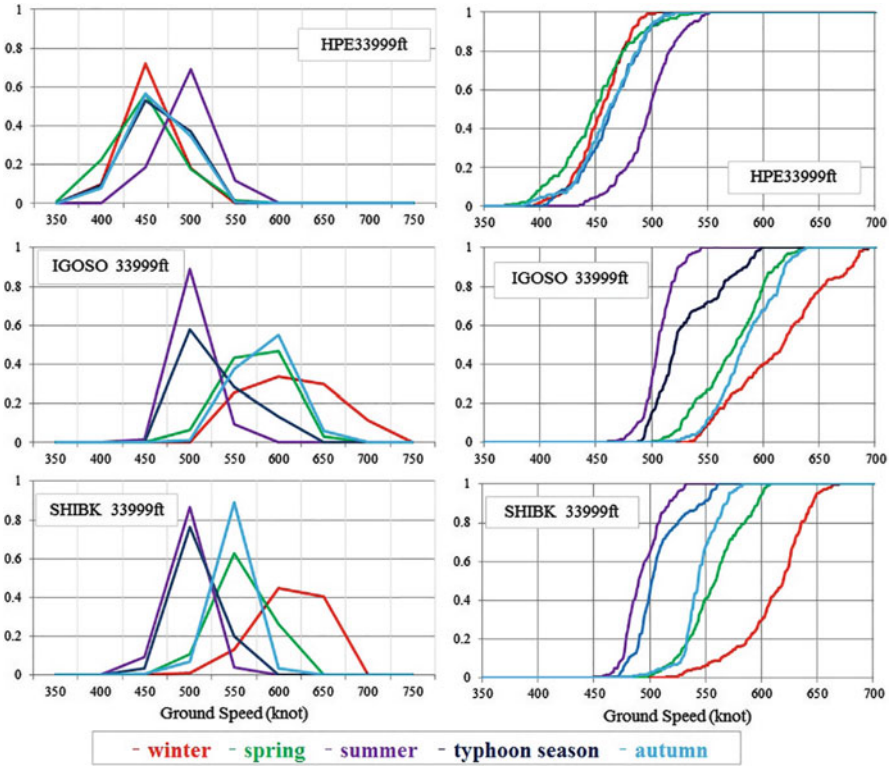

Fig. 4 GS distributions

Table 3 Mean and maximum change of GS in 3 h (kt)

	HPE	IGOSO	SHIBK
Mean			
Winter	8	8	6
Spring	10	8	6
Summer	6	5	5
Typhoon season	6	5	5
Autumn	8	5	4
Maximum			
Winter	45	33	21
Spring	47	42	29
Summer	32	32	25
Typhoon season	34	27	24
Autumn	57	34	22

5 Meteorological Forecast Data Analysis

5.1 Weather Prediction Errors

Meteorological forecast data at zero hour is assumed as a true value in this study. Differences between data of forecast hours (FT = 15, 12, 9, 6 and 3) and zero are regarded as prediction errors. Wind speed prediction errors, wind direction prediction errors and temperature prediction errors are distributed symmetrically and their peaks are almost zero (Fig. 5).

Ninety-five percent of temperature prediction errors are within $\pm 2^{\circ}$. Inside ± 7 knots of wind speed, prediction errors are satisfied in 94 % of the FT3 and 76 % of the FT15. Accuracy of wind direction prediction errors drop in the summer and the typhoon season. One of the reasons for lower accuracy of wind direction predictions in the summer and the typhoon season is that the motion of typhoons which bring strong swirling wind is difficult to predict.

5.2 Ground Speed Prediction Errors

Prediction accuracy of GS improves when using weather data predicted in more recent hours. Differences between GS calculated using meteorological forecast hours (FT = 15, 12, 9, 6 and 3) data and that of zero hour data were defined as GS prediction errors in this study. Figure 6 shows the distribution of GS prediction errors of FT15, FT9 and FT3. The mean of prediction error are -0.2 knots in the

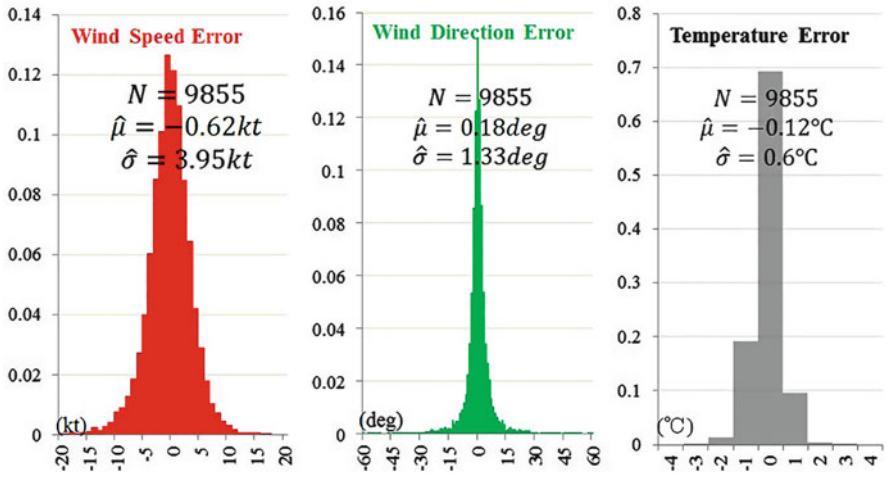

Fig. 5 Weather prediction error distributions

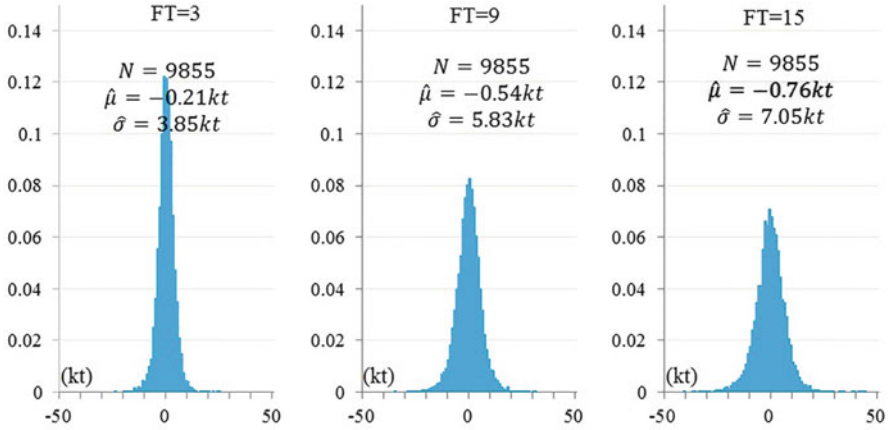

Fig. 6 GS prediction error distributions

Table 4 The percentage of prediction errors within ±7 kt

	Winter (%)	Spring (%)	Summer (%)	Typhoon season (%)	Autumn (%)
Wind speed prediction error within ±7 kt					
HPE	96	91	91	84	93
IGOSO	90	92	96	94	95
SHIBK	95	92	96	94	96
Ground speed prediction error within ±7 kt					
HPE	98	94	93	96	97
IGOSO	88	93	96	96	94
SHIBK	96	92	94	94	96

FT3, −0.5 knots in the FT9 and −0.8 knots in the FT15 respectively. More than 90 % of GS predictions fit within ±15 knots in the FT15, ±9 knots in the FT9 and ±6 knots in the FT3.

5.3 Seasonal Tendencies of Errors

Table 4 is the percentage of prediction errors of FT3 data both of wind speed and GS, which are within ±7 knots. Seasonal tendency of wind speed prediction errors are similar to that of GS prediction errors. The lowest-accuracy season is winter at IGOSO in both GS prediction errors and wind speed prediction errors. Table 5 is RMS values of GS prediction errors of FT3 data. The prediction accuracy becomes lower in the winter and RMS values are high.

Table 5 RMS of GS prediction errors (kt)

	Winter	Spring	Summer	Typhoon season	Autumn
HPE	3	4	4	4	3
IGOSO	5	4	3	4	4
SHIBK	4	4	4	4	3

Table 6 Days showing a maximum value of GS prediction error (kt)

		FT3	FT6	FT9	FT12	FT15
HPE	Date and time	September 28 00Z	September 28 03Z	July 27 06Z	September 5 00Z	September 5 00Z
	MAX GS prediction error	25	28	35	41	42
IGOSO	Date and time	November 5 21Z	May 3 03Z	November 5 21Z	September 2 18Z	September 3 03Z
	MAX GS prediction error	24	29	29	38	53
SHIBK	Date and time	September 20 06Z	September 20 06Z	May 19 03Z	September 20 06Z	September 20 06Z
	MAX GS prediction error	22	34	30	40	44

5.4 Large Error Situations

Days showing high-level GS prediction error are in Table 6. The largest GS prediction error was 53 knots at IGOSO on September 3. A typhoon passed through the Japanese archipelago on that day and the timing of a large error overlapped with the centre of the typhoon as it passed (Fig. 7). Upon viewing other days' meteorological analysis charts, the areas where high GS prediction errors were calculated were areas where air turbulence potentially occurs in most of the cases. Turbulence is caused by unstable atmosphere conditions such as typhoons (tropical cyclones) with a high cumulonimbus cloud, near the trough with horizontal/vertical wind shear along a strong jet stream, convective cloud area caused by unstable air and so on. A large change in wind speed and direction in a short time occur when those unstable atmosphere areas move. The mean of the amount of change in ground speed in 3 h is 23 knots on the days in Table 6. It is three or four times larger than the mean of all the days in Table 3.

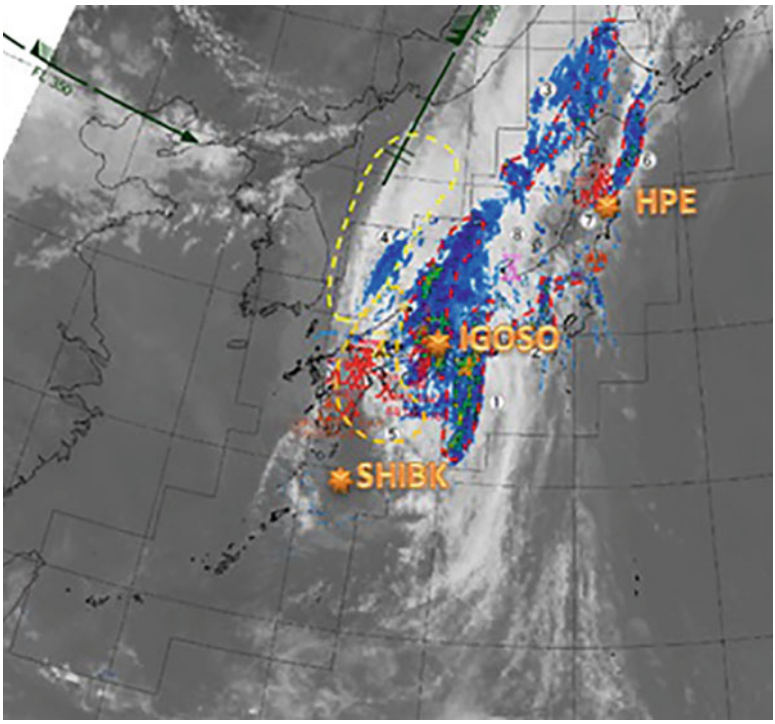

Fig. 7 Analysis chart for aviation (ABJP) valid 03 UTC of September 3, 2011

6 Discussion

Prediction of aircraft trajectory accuracy is the key in the implementation of TBO for future ATM. Meteorological conditions affect aircraft attitude and speed during flight. The purpose of this study is to be able to analyze GS influenced by seasonal changes in atmospheric conditions and meteorological forecast accuracy.

6.1 The Impact of Jet Stream

The existence of a jet stream is important for aviation because of its strong wind speed. Airline industries not only reduce the flight hours but also save fuel when the flight course is set by utilizing a jet stream, especially for east–west long-range flights. It is also known as clear air turbulence (CAT) caused by horizontal and vertical wind shear connected to the jet streams. In the northern hemisphere, the polar jet stream moves southward to approximately 25° at farthest during the winter and northward to approximately 45° during the summer in a meandering shape.

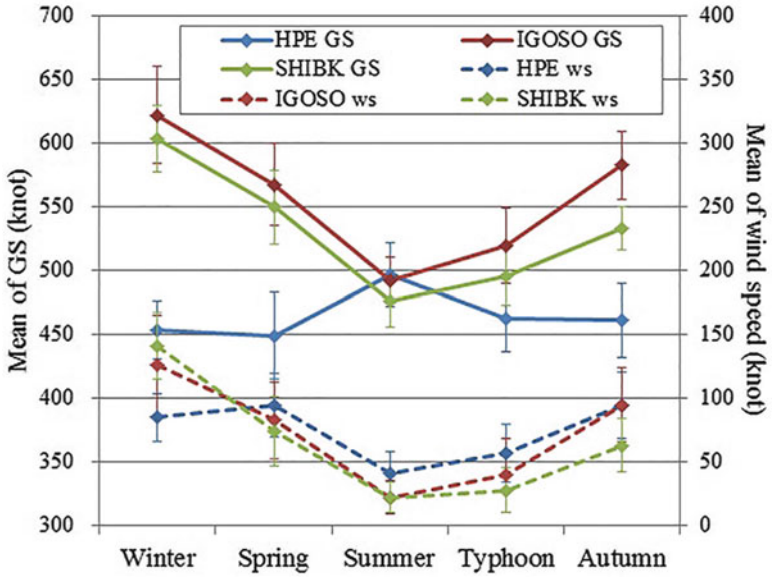

Fig. 8 Mean of aircraft ground speed and wind speed at each waypoint (250 hPa)

Aspects of wind conditions at cruising altitude vary in each season depending on the position of the waypoint, and whether a jet stream exists or not.

GS during cruising flights varies due to both seasonal changes in wind and flight direction. Figure 8 represents the mean of GS and wind speed in each season in the same chart. GS of IGOSO/SHIBK are shown as lines with similar wind speed at each season, whereas GS of HPE is a contrasting line. The fastest GS was calculated in the winter for east-bound aircraft, and in the summer for southwest-bound aircraft.

6.2 GS Prediction Accuracy

GS prediction accuracy improves if recent weather forecast data is used. The mean of prediction error is −0.2 knots in the FT3. The zero hour weather data of MSM (GPV) is not an actual measured value of the atmosphere. It is the calculated value for the default used in predicting future atmospheric conditions, and serves as a useful reference value for determining the average atmospheric condition in the grid area. There are unpredictable atmospheric disturbances such as turbulences occurring in small local areas that do not show up in the MSM. Currently, data-link communication between aircraft during flight and ground-based systems has improved. By reflecting actual atmosphere tendencies from measured meteorological elements by aircraft during flight into algorisms of ground prediction systems, the accuracy of trajectory prediction will improve even more.

It is expected that the required time tolerance will be 30 s at the en-route waypoint in the initial 4D trajectory data link of operations [8]. The difference of 9 or 10 knots during cruise flight rises by approximately 30 s at 200 NM away. And a 7-knot peak of wind vector error is required to satisfy the 6-knot longitudinal error in trajectory accuracy requirements [9]. In en-route phase, the planned TAS by the airline relatively fits with the actual TAS. The mean of the difference between the actual TAS and the planned TAS was −4 knots [10]. GS prediction error shows up as the sum of TAS prediction error and wind prediction error. Although there were a few large GS prediction error areas, the mean of GS prediction error was small and relatively matched within ranges of trajectory prediction requirements, under the no TAS error condition in this study. Therefore, GS prediction error appears mainly to be due to the aircraft kinetic model error such as TAS prediction.

When it comes to a climbing or descending phase, it has been clarified that the estimate error of wind, especially wind direction, is large under a height of 20,000 ft (1 foot = 0.3048 m) by the estimation of TAS/CAS from radar data [10]. Atmospheric conditions in a climbing or descending phase also have an effect on aircraft trajectory, however there is not much impact in comparison with cruising altitude. The mean and standard deviations of wind speed at 20,000 ft in the winter, the season the wind speed is strongest, were approximately 60 and 20 knots respectively in an additional study. The wind speed was approximately half compared to cruising altitude.

When and where the GS prediction accuracy became lower overlapped with when and where wind speed widely varied. The largest GS prediction error was 53 knots in this study. In most of these large error cases, the area where a high GS prediction error was calculated was where air turbulence potentially occurs. Turbulence is caused by unstable atmosphere conditions. To make short intervals to update the atmospheric conditions forecast with the assistance of actual weather data from aircraft during flight by data-link, the accuracy of predictions will improve in the future. The first step, to examine atmospheric conditions which have the possibility to cause large prediction errors will be helpful to determine an indicator in regard to trajectory prediction accuracy depending on weather conditions.

6.3 Comparison of Accuracy Between GS and Weather Prediction Errors

For the purpose of determining which weather prediction errors impact GS prediction errors, the correlation of the accuracy, which is the percentage of prediction error contained in a certain range of error, of weather prediction errors and GS prediction errors was assessed. Figure 9 shows the correlation between GS prediction accuracy and weather prediction accuracy at IGOSO. Wind speed prediction accuracy shows the most matched linear relationship with GS prediction accuracy rather than that of wind direction and temperature prediction accuracy. Stronger

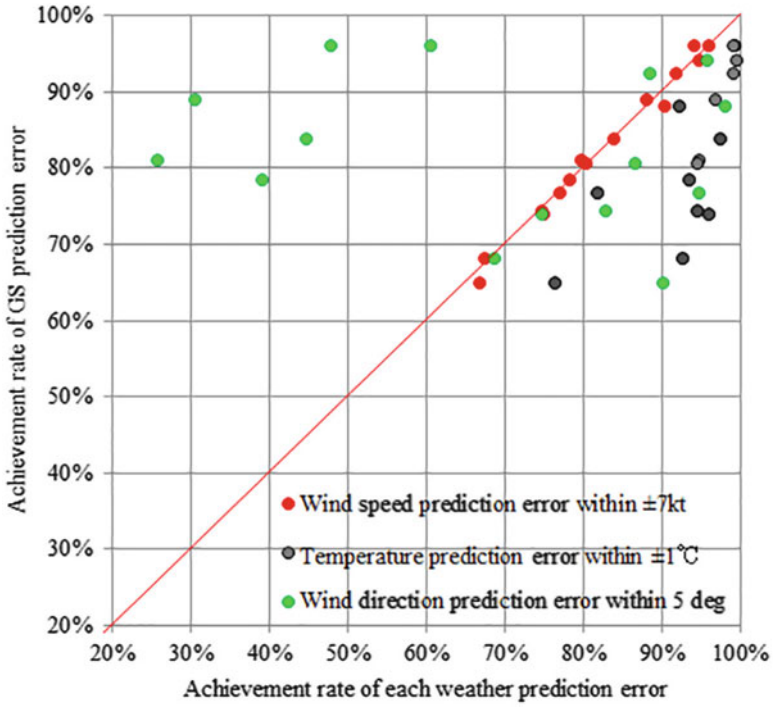

Fig. 9 Comparison of accuracy between GS prediction errors and weather prediction errors

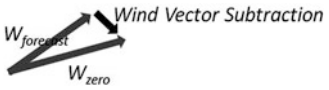

Fig. 10 Wind vector subtraction

wind blows at aircraft cruising altitude than at ground height in most of the cases, so wind speed prediction errors have an influence on GS prediction errors at cruising altitude.

A wind vector contains both wind speed factors and wind direction factors. The difference between the forecast hour wind vector ($\boldsymbol{W_{forecast}}$) and the zero hour wind vector ($\boldsymbol{W_{zero}}$) is one degree of exactness of prediction (Fig. 10). As wind vector subtraction ($|\boldsymbol{W_{forecast}} - \boldsymbol{W_{zero}}|$) increases, prediction accuracy lowers. So, a similar analysis was conducted between GS prediction errors and wind vector subtraction. The coefficient of determination ($\boldsymbol{R}^2$) of wind speed prediction accuracy and GS prediction accuracy within ±7 knots was 0.91, 0.99 and 0.96 at HPE, IGOSO and SHIBK respectively. The relationship between the GS prediction accuracy and the wind vector subtraction within ±9 knots was 0.97, 0.91 and 0.96 respectively in a similar analysis. Wind vector subtraction within ±9 knots derived a higher coefficient than that of within ±7 and ±10 knots.

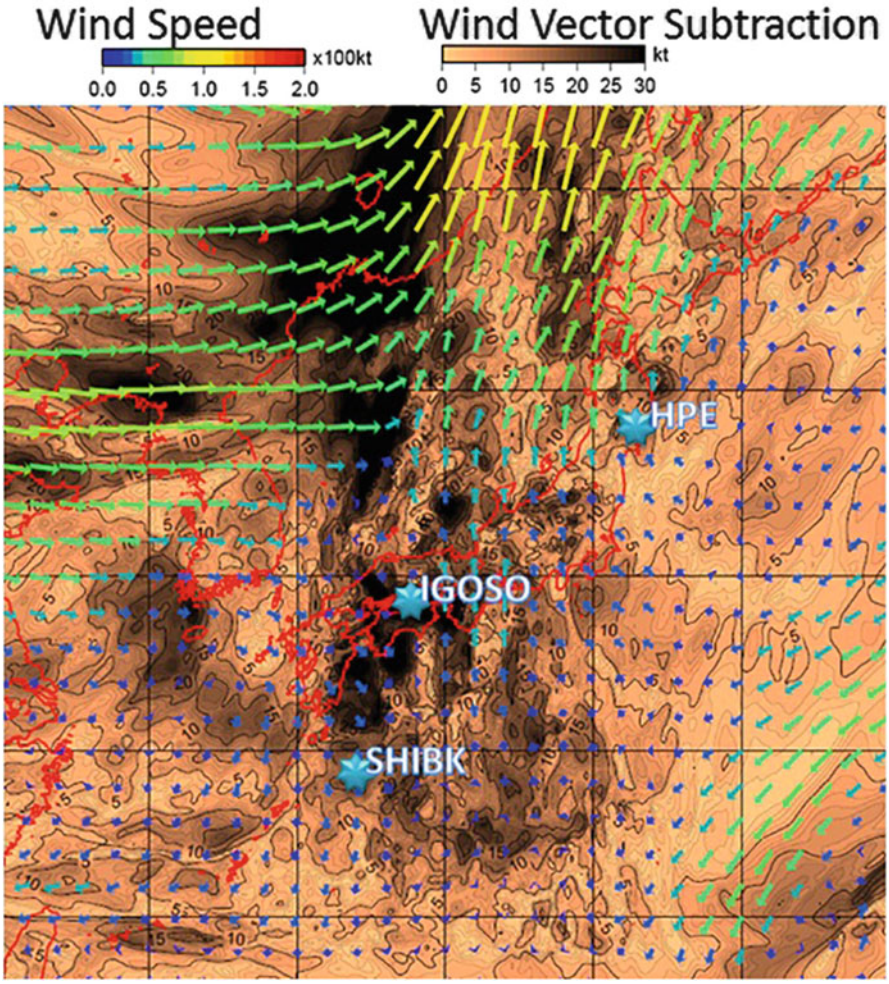

Fig. 11 Wind vector subtraction between FT15 and FT10

As described above, the wind speed was the most influential component in GS prediction, and the correlation of wind vector subtraction and GS prediction accuracy was also high. Figure 11 represents the contour of wind vector subtraction between FT15 and zero with a brown color scale at the time of the largest GS prediction error (the same day as in Fig. 7). When the wind speed is high, the wind vector subtraction tends to be large. Even when the wind speed is weak, wind vector subtraction tends to be large when whirling wind (i.e. cyclones) moves, because it is difficult to predict the movement accurately.

Wind vector subtraction is capable to express dynamic wind vector change such as cyclones, even when the wind speed is weak. One of the indexes to express

weather forecasts uncertainty is “ensemble”, and a time-lagged ensemble of weather model forecasts were estimated and used to estimate the level of uncertainty in hypothetical aircraft trajectory predictions [11]. One possible next step of this study would be inserting the wind forecast uncertainty index into the wind vector subtraction value to define “hot spot” which have the possibility to cause large prediction errors.

7 Conclusion

GS was calculated under the influences of seasonal wind conditions and meteorological forecast accuracy during cruise flight on three way points towards Tokyo International Airport from north, west and southwest directions. The prediction of aircraft trajectory at cruising altitude is more likely to be affected by wind factors than during climb or descent phases because of a jet stream, that is a strong westerly wind. Aspects of wind conditions at cruising altitude varied in each season depending on the position of the waypoint, and whether a jet stream existed or not. The tendency of GS varied by direction of aircraft in addition to the wind conditions.

The results showed that prediction accuracy of GS improved by using weather data predicted in more recent hours, as expected. Although there were a few large GS prediction error areas, the mean of GS prediction error was small and relatively matched within ranges of trajectory prediction requirements, under the no TAS error condition in this study. There was also a new finding of relation between prediction accuracy and meteorological conditions, when and where the GS prediction accuracy became lower overlapped with when and where wind speed widely varied.

The wind speed component was the dominant element in making an impact on aircraft ground speed prediction errors among meteorological prediction errors. Also wind vector subtraction is one degree of exactness of prediction. Wind vector subtraction is capable to express dynamic wind vector change such as cyclones, even when the wind speed is weak. The results lead to suggest that one possible next step in this study would be inserting the wind forecast uncertainty index into the wind vector subtraction value to define “hot spots” which have the possibility to cause large prediction errors.

References

1. ICAO (2005) Global air traffic management operational concept. ICAO Doc 9854AN/458
2. Eurocontrol Experimental Centre (2012) Use manual for the Base of Aircraft Data (BADA). Revision 3.10, EEC Technical/Scientific Report No. 12/04/10-45
3. Coppenbarger RA (1999) Climb trajectory prediction enhancement using airline flight-planning information. In: AIAA-99-4147, AIAA guidance, navigation, and control conference

4. Gong C, McNally D (2004) A methodology for automated trajectory prediction analysis. In: AIAA 2004-4788, AIAA guidance, navigation, and control conference and exhibit
5. Fukuda Y, Shirakawa M, Senoguchi A (2010) Development of trajectory prediction model. In: ENRI international workshop on ATM/CNS
6. Cole RE, Green S, Jardin M, Schwarts BE, Benjamin SG (2000) Wind prediction accuracy for traffic management decision support tools. In: Third USA/Europe air traffic management R&D seminar
7. Japan Meteorological Agency (2013) Outline of the operational numerical weather prediction at the Japan meteorological agency
8. Eurocontrol (2008) Initial 4D–4D trajectory data link (4DTRAD) concept of operations. European Organization for the Safety of Air Navigation
9. Eurocontrol (2010) Specifications for trajectory prediction. EUROCONTROL-SPEC-0143
10. Shirakawa M, Fukuda Y, Senoguchi A, Brown, AM (2012) Estimation of the aircraft air speeds with the ground radar data. In: JSASS 50th aircraft symposium (Japanese)
11. Lee AG, Weygandt SS, Schwarts B, Murphy JR (2009) Performance of trajectory models with wind uncertainty. In: AIAA modeling and simulation technologies conference

Flight Trajectory Optimization for Modern Jet Passenger Aircraft with Dynamic Programming

Navinda Kithmal Wickramasinghe, Akinori Harada, Hironori Totoki, Yuto Miyamoto, and Yoshikazu Miyazawa

Abstract Future Air Transportation Systems (ATS) would eventually have to treat the ever increasing demands in aviation industry. Fuel consumption and flight time could be significantly reduced by modifying the current sector based system into a more relaxed user priority based ATS. Trajectory Based Operations (TBO) is considered as one of the key technologies in this transition. This paper concentrates on a proposed flight trajectory optimization tool based on Dynamic Programming (DP), meteorological data and an aircraft performance model to obtain fuel minimum 4D-optimal flight trajectories for a single jet passenger aircraft considering the effect of wind conditions. Major drawbacks such as "Curse of Dimensionality" in DP are overcome with a unique method called "Moving Search space Dynamic Programming (MS-DP)" method. A quantitative evaluation has revealed that an average reduction of 9% in fuel consumption could be achieved with a tradeoff of flight time which exceeds at an average of 7% compared to a series of flight data measured by a commercial GPS receiver in an airliner cabin.

Keywords Aircraft performance optimization • Flight time • Fuel consumption

1 Introduction

Future Air Transportation Systems (ATS) would eventually have to treat the ever increasing air traffic, sky-rocketing fuel prices, CO_2 emission, noise pollution concerns and economic instability in the aviation industry with effective solutions

N.K. Wickramasinghe (✉) • A. Harada • H. Totoki • Y. Miyamoto
Graduate School of Engineering, Kyushu University, Fukuoka 819-0395, Japan
e-mail: navinda@aero.kyushu-u.ac.jp; a-harada@aero.kyushu-u.ac.jp; totoki@aero.kyushu-u.ac.jp; yuto-m@aero.kyushu-u.ac.jp

Y. Miyazawa
Department of Aeronautics and Astronautics, Kyushu University, Fukuoka 819-0395, Japan
e-mail: miyazawa@aero.kyushu-u.ac.jp

Electronic Navigation Research Institute (ENRI), *Air Traffic Management and Systems*, Lecture Notes in Electrical Engineering 290, DOI 10.1007/978-4-431-54475-3_6,

to provide a reliable, safe and efficient service to its customers [1]. The current ATS is considered as a safe system but the aging operational procedures and ground based Air Traffic Control (ATC) systems will overrun the capacity it was originally designed for in the next couple of decades. Especially, in terminal airspaces of busy airports, aircraft are bound to follow vector control procedures to maintain a smooth air traffic flow. International flight routes such as North Pacific (NOPAC) Composite Route System (CRS) and Pacific Organized Track System (PACOTS) are relatively more relaxed than domestic flight routes and are optimized daily according to weather forecasts and air traffic conditions, which are called as User Preferred Routes (UPR). Hence, a study on benefits obtained in a futuristic domestic airspace is vital to understand the necessary solutions to meet the future demands with a cost effective and efficient approach.

Collaborative Action for Renovation of Air Traffic Systems (CARATS) is the proposed long term research plan for the improvement of Japan ATS. It has introduced 4D-Trajectory Based Operations (TBO) as one of the key technologies to realize the transformation of sector based Air Traffic Control (ATC) system into a more relaxed and efficient Air Traffic Management (ATM) system. This is a core solution in the "Free Flight" concept, which is considered as a safe flight operating capability and would let the operators to select the optimal flight path and speed in real time [1]. 4D-flight trajectory optimization is formulated as an optimal control problem to be proposed in TBO and had been extensively studied over the last few decades [2–4]. Various mathematical programming approaches such as calculus of variations and direct method have been proved to have positive impact on the optimization process [5, 6]. On the contrary, these methods possess disadvantages in providing the global optimum and predicting the computational time due to iterative calculation methods they use in the process. Therefore, a reliable numerical optimization method is a necessity to obtain optimal solutions to be applied in TBO concept. Therefore, Dynamic Programming (DP) is considered as one of the most suitable tools to evaluate the global optimum while contemplating the required constraints [7].

This research is dedicated to contribute towards a futuristic ATS with the objective of developing a 4D-flight trajectory optimization tool for a single jet passenger aircraft to minimize the fuel consumption by considering the presence of wind conditions. DP is utilized in the optimization process to obtain the global optimum and a unique calculation method is proposed in order to overcome the drawbacks of DP. A quantitative evaluation is implemented to generate optimal trajectories along one of the busiest domestic flight routes between Haneda and Fukuoka, and obtained results are compared with a series of flight data measured in airliner cabin by using a commercial GPS data logger. Air data are estimated by applying meteorological data from Japan Meteorological Agency (JMA) to assure the clarity of measured GPS data. The aircraft performance is analyzed with the application of Base of Aircraft Data (BADA) aircraft performance model by the European Organization for the Safety of Air Navigation (EUROCONTROL).

2 Optimal Trajectory Design

Generally, an aircraft's motion is expressed by six degree of freedom (6 DOF) equations of motion. In this study, state variables are reduced by using point mass approximations and omitting the state variables which represent the aircraft's attitude. Furthermore, the dynamics of velocity direction change is neglected while the dynamics of velocity change which is directly related to energy is considered.

2.1 Equations of Motion

An aircraft's 3D-translational motion is reviewed in Fig. 1. The azimuth angle relative to air ψ_a, path angle relative to air γ_a and the engine thrust T are used as control variables and the equations of motion are solved with respect to the state variables of latitude ϕ, longitude θ, geo-potential altitude H and true airspeed V_{TAS}.

$$\frac{d\theta}{dt} = \frac{1}{(R_0 + H)\cos\phi}\left(V_{TAS}\cos\gamma_a \sin\psi_a + W_x\right) \tag{1}$$

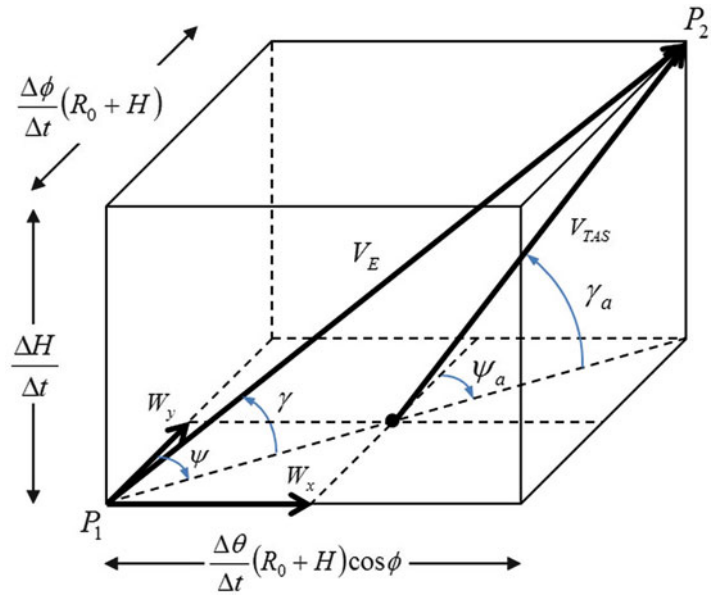

Fig. 1 Definition of point mass equations

$$\frac{d\phi}{dt} = \frac{1}{R_0 + H}\left(V_{TAS}\cos\gamma_a \cos\psi_a + W_y\right) \tag{2}$$

$$\frac{dH}{dt} = V_{TAS}\sin\gamma_a \tag{3}$$

$$m\frac{dV_E}{dt}\cos\left(\gamma_a - \gamma\right)\cos\left(\psi_a - \psi\right) = T - D - mg\sin\gamma_a \tag{4}$$

m	Aircraft mass	γ	Path angle
g	Gravity acceleration	ψ_a	Azimuth angle relative to air
R_0	Earth radius	ψ	Ground track angle
D	Aerodynamic drag	W_x	Zonal wind component
γ_a	Path angle relative to air	W_y	Meridional wind component

Southerly winds and westerly winds are considered as positive and the vertical wind component is assumed negligible. The aircraft's position is defined by latitude, longitude and geo-potential altitude and the aircraft's speed is given with true airspeed and speed V_E which is on Earth-centered Earth-fixed coordinate system. Each velocity direction is calculated by path angle and azimuth angle relative to air and, path angle and ground track angle respectively. Speed V_E is considered due to the effect of wind vector on the acceleration of aircraft. This acceleration vector is parallel to V_E and its cosine component is added to Eq. (4) to evaluate the required engine thrust which is parallel to V_{TAS} vector. Parameters relative to aerodynamic system are depicted with index a.

2.2 Meteorological Data

The Japan Meteorological Agency (JMA) provides a variety of weather data on global and domestic atmospheric conditions. These are known as Numerical Weather Prediction (NWP) models and periodically updated weather data are available for commercial use. Physical variables shown in Table 1 are provided by two main NWP models, Global Spectral Model (GSM) and Meso Scale Model (MSM) in a grid point value (GPV) format on a coordinate frame defined by longitude, latitude and barometric pressure surface. The precision of these data was reviewed by referring to an airline onboard flight data [8]. Results depict that numerical data provided by GSM model are more precise than MSM model and is suitable to be used in trajectory optimization analysis. This difference emerges according to so called *position error* which occurs in weather prediction by MSM model due to its fine mesh resolution [9]. Hence, GSM model for Japan region was applied in this study and its fundamental properties are given in Table 1.

Table 1 GSM Japan region model fundamental properties [10]

Article	Model properties
Data format	GRIB2
Initial time value	00, 06, 12, 18 (UTC)
Region	Longitude: 120–150°, latitude: 20–50°
Resolution	Longitude direction: 0.25° Latitude direction: 0.2°
Barometric pressure levels	12 levels {mean sea level 100 hPa}
Physical variables	Geopotential altitude, temperature, vertical flow, relative humidity, wind velocity

Table 2 Operational limitations for performance optimization

Limitation	Value
Maximum operating calibrated airspeed	310 kt
Stall speed (for reference mass)	149 kt
Minimum operating calibrated airspeed	Stall speed × 1.3 kt
Maximum operating Mach number	0.84
Maximum operating altitude	43,100 ft

2.3 Aircraft Performance Model

Generally, a model capable of providing sufficient and precise data is essential to discuss an aircraft's performance, especially to conjecture the fuel consumption at a specific flight condition. Base of Aircraft Data (BADA) model 3.9 developed and maintained by European Organization for the Safety of Air Navigation (EUROCONTROL) is applied in the proposed optimization model to evaluate the aircraft's performance [11]. The operational limitations provided in BADA model for the subjected aircraft are given in Table 2 and are used to sustain the validity of obtained solutions.

A review on the variations in thrust, fuel consumption, airspeed and other parameters is a necessity when performing a dynamic optimization for a complete flight profile. Models which are defined in the BADA model are used to estimate these variations. The aerodynamic model provides useful equations to calculate the lift and drag coefficients and the fuel consumption model provides unique computational algorithms to obtain the fuel flow for each phase of flight. The nominal fuel flow is a function of true airspeed and the minimum fuel flow is a function of altitude which applies for idle thrust conditions. The thrust model provides the maximum thrust available at each flight phase. According to a numerical analysis we could understand that the numerical error of evaluating the fuel consumption is ±5% compared to an airliner onboard flight data [12]. Therefore, the same model was applied to calculate the fuel consumption of both reference trajectories and corresponding optimal trajectories to reduce the effect by this error.

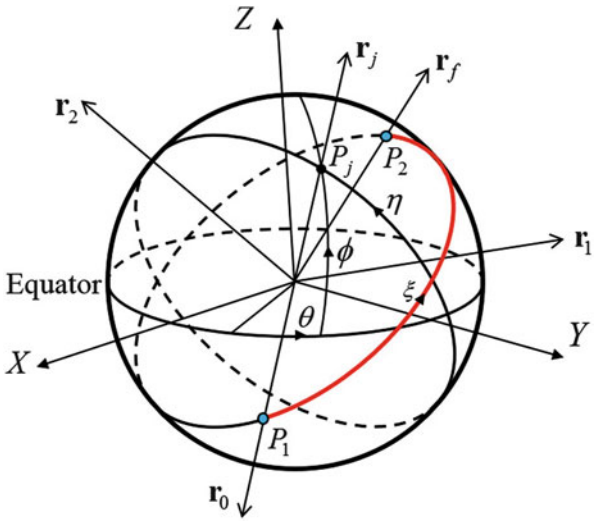

Fig. 2 Transition from Earth-centered Earth-fixed coordinate system to polar coordinate system

2.4 Dynamic Programming Approach

Generally, a steady or quasi-steady flight of an aircraft is assumed by categorizing its flight into climb, cruise and descent phases in order to evaluate the performance optimization. In case we assume that prognostic wind data is in possession, it creates a further necessity of dynamic optimization to achieve a flight trajectory which could minimize the fuel consumption. Hence we apply the DP method in our optimization analysis because of its unique qualities provided in [13].

2.4.1 Application of DP

State variables ϕ and θ are transformed to ξ and η in the Polar coordinate system and they represent downrange angle and cross range angle respectively as shown in Fig. 2. This provides a feasible calculation platform for our proposed optimization model.

The downrange angle which transits monotonously with time, depicts the progress angle from initial point P_1 along the Great Circle Route (GCR), which is the shortest aerial path between the initial point P_1 and terminal point P_2. The cross range angle provides the lateral deviation from GCR at an arbitrary point P_j. Unit vectors $\mathbf{r}_0$ and $\mathbf{r}_f$ are along the initial and terminal points respectively and unit vectors $\mathbf{r}_1$ and $\mathbf{r}_2$ are used in the coordinate system transformation process. Then the three state variables H, η and calibrated airspeed V_{CAS} are discretized and applied in the optimization model. Note that state variable V_{TAS} is transformed to V_{CAS} and is expressed as V.

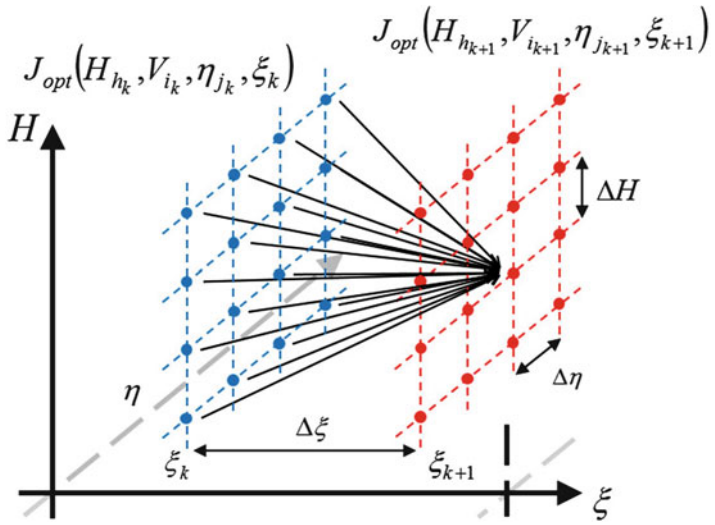

Fig. 3 DP logic on trajectory transition (dimension of velocity is omitted to simplify the image)

2.4.2 Performance Index

The total fuel consumption is defined as the performance index J, which is the integral of fuel flow FF during the flight time $t_f - t_0$ as shown in Eq. (5).

$$J = \int_{t_0}^{t_f} FF(t)\ \mathrm{d}t \tag{5}$$

Then the optimal performance index J_{opt} is derived with H, V, η and ξ which could be expressed as $J_{opt}(H,V,\eta,\xi)$. The global optimum is obtained by solving the combinatorial optimization problem for all transitions between the grid points. According to DP algorithm, the principle of optimality is defined as follows:

$$J_{opt}\left(H_{h_{k+1}}, V_{i_{k+1}}, \eta_{j_{k+1}}, \xi_{k+1}\right) = \min_{\substack{h_k \to h_{k+1} \\ i_k \to i_{k+1} \\ j_k \to j_{k+1}}} \left[\left(H_{h_k}, V_{i_k}, \eta_{j_k}, \xi_k\right) + \Delta J\right] \tag{6}$$

$$\Delta J = FF\Big|_{\xi_k}^{\xi_{k+1}} \Delta t \tag{7}$$

The increment of performance index for each transition is derived by $\triangle J$ where the fuel flow is assumed to be constant in each transition. Figure 3 depicts the DP logic on trajectory transition in the state space grid.

Although DP possesses various advantages as an optimization method, it also has several major drawbacks [13, 14]. To reduce these effects we have utilized a unique method called "Moving Search space Dynamic Programming (MS-DP)", constructed by integrating the concept of gradient method and DP. Since the number of calculations is proportional to the square of number of grid points on the plane of independent variable, it could be drastically reduced if the search area in state space is limited. In this method, optimization calculations are implemented in a partial space around a reference trajectory to reduce the computational time. If a solution is obtained in the partial search space, a new search space is generated around the solution and optimization calculation continues until the solution is converged, where the new solution is identical to the previous reference trajectory. The validity of this unique calculation method is thoroughly discussed in [13].

2.5 GPS Data Analysis

A series of flight data were used in this study as reference data to understand the benefits obtained by the proposed optimization tool. A commercial GPS data logger was used inside the cabin of an airborne aircraft (after departure warnings are turned off and before landing warnings are turned on) to measure the aircraft's 3D-position (latitude, longitude and geometrical altitude) and ground speed. An analysis was implemented to confirm the validity of these data before utilizing them as reference data in the optimization process [15].

2.5.1 Lateral Deviation from Airway

The maximum deviation from the airway was recorded only at a magnitude of several dozen meters [15] and large deviations were noticed near the waypoints due to the performed maneuvers in order to maintain its predetermined flight course and heading angle change procedures.

Figure 4 illustrates the quantitative evaluation on the deviation of a series of flight routes from its corresponding airways. The bias error from the radius of fuselage is considered in this analysis for clarity because the data are measured at the airliner cabin window seat.

2.5.2 Estimation of Air Data

Pressure altitude and Mach number are estimated with the application of weather data to understand the current flight procedures. Figure 5 resembles not only a quantitative evaluation of the deviation from predetermined pressure altitude but also the accuracy of weather prediction data. Also, from the BADA model we are aware that the subjected aircraft generally performs at a cruising speed of

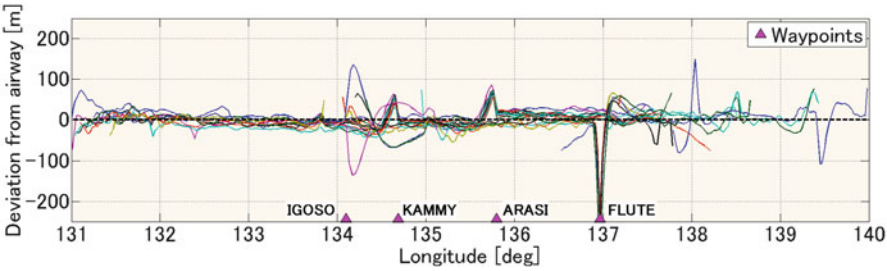

Fig. 4 Quantitative evaluation for lateral deviation from airway

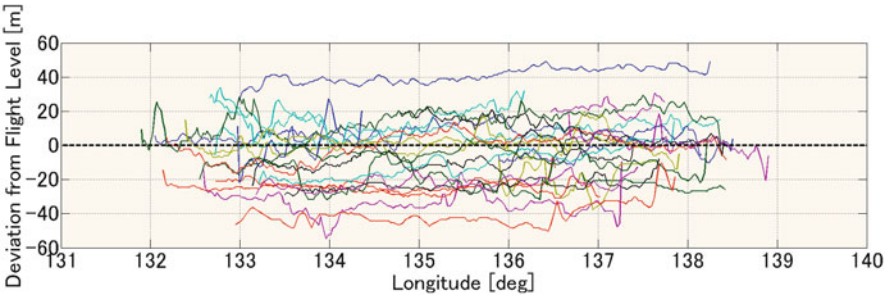

Fig. 5 Quantitative evaluation for deviation from cruising pressure altitude

Mach 0.84. Yet a quantitative evaluation for the deviation of Mach number could not be achieved because we were not aware of the precise Mach number setting for each flight case [15].

From the obtained results we could confirm that GPS measured flight data are sufficiently reliable to be used as reference data. We could also confirm that present day passenger aircraft are,

- Capable of maintaining flight profiles with high precision along the airway and the cruising pressure altitude according to provided onboard flight data on its Flight Management Systems (FMS).
- Bound to follow vector control procedures before entering the terminal airspace of busy airports in order to adjust the arrival sequence.

3 Results

A total of 14 flights are analyzed with seven flights each from Haneda (RJTT) to Fukuoka (RJFF) and Fukuoka (RJFF) to Haneda (RJTT) which are shown in Table 3. The estimated flight profile in the optimization process for each flight case is given in Table 4. Initial and terminal values of altitude and calibrated airspeed are set to be identical at each flight case to perform a fair evaluation.

Table 3 Reference GPS data

Flight case (FC)	Year/month/day	Departure/destination	Data record time (JST)	
			Initial time	Final time
01	2011/6/18	RJFF/RJTT	14:02	15:20
02	2011/6/19	RJTT/RJFF	20:00	21:48
03	2011/6/26	RJTT/RJFF	19:58	21:28
04	2011/7/31	RJTT/RJFF	19:59	21:30
05	2011/8/28	RJTT/RJFF	18:50	20:31
06	2011/9/02	RJFF/RJTT	09:53	11:30
07	2011/9/24	RJFF/RJTT	10:57	12:20
08	2011/10/01	RJFF/RJTT	15:04	16:22
09	2011/10/02	RJTT/RJFF	19:54	21:41
10	2011/10/08	RJFF/RJTT	16:11	17:29
11	2011/10/10	RJTT/RJFF	11:22	12:59
12	2011/10/15	RJFF/RJTT	16:04	17:42
13	2011/10/17	RJTT/RJFF	10:20	12:00
14	2011/10/21	RJFF/RJTT	9:55	11:20

Table 4 Estimated flight profile

Variable	Description
Flight route	RJTT: 35.5483°N 139.9078°E
	RJFF: 33.8903°N 130.3317°E
Down range	Resolution: 31 grid points
Altitude	Minimum: 3,000 m, maximum: 13,000 m
	Resolution: 101 grid points
Calibrated airspeed	Minimum: 100 ms^{-1}, maximum: 160 ms^{-1}
	Resolution: 61 grid points
Cross range	2.5° on each side of Great Circle Route
	Resolution: 101 grid points

3.1 Quantitative Evaluation

This section discusses the results obtained 4D-flight trajectory optimization tool. They are compared with the previously discussed flight data and achieved benefits are reviewed. Figure 6 depicts the total reference data used in the analysis and data plots in Fig. 7 illustrate the achieved efficiency in fuel consumption with respect to exceeded flight time compared to reference GPS data.

We could achieve an average of 9% for fuel consumption efficiency with exceeding the flight time with an average of 7%. The GPS logger does not provide data regarding the aircraft mass at respective measuring points. Hence, we have utilized the reference mass value of 208,700 kg as the initial mass at all cases.

The results in Fig. 7 show that the optimal routes tends to spend more flight time than the reference GPS route in order to reduce the fuel consumption. In case of flights from RJTT to RJFF, it is reasonable that most of the optimal trajectories

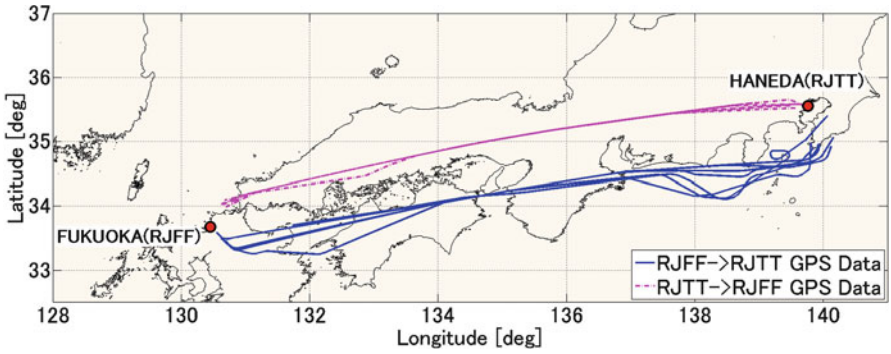

Fig. 6 GPS measured data over Haneda (RJTT) ↔ Fukuoka (RJFF) flight route

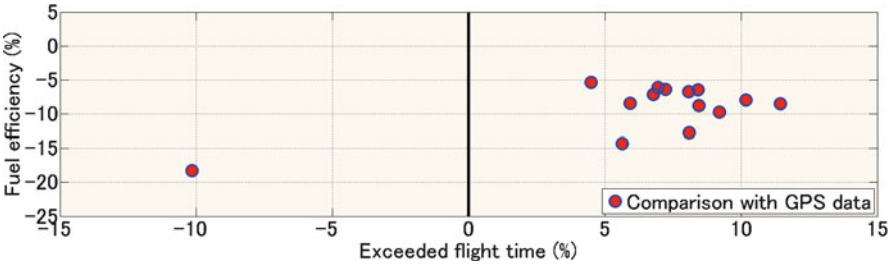

Fig. 7 Tradeoff between fuel consumption and exceeded flight time

tend to exceed flight time largely compared to their respective reference trajectories because both reference trajectory and optimal trajectory perform close to GCR. Furthermore, in flight cases from RJFF to RJTT, the flight time excess is smaller or negative. From this quantitative evaluation it could be considered that current flight plans in FMS give higher priority to save flight time than saving the amount of fuel consumed. Critical points of the optimization process are explained in detail in the next subsections with particular flight cases and obtained optimal results at each respective case.

3.1.1 Preference of Descent Speed

Subfigures a–i in Fig. 8 illustrate several parameters related to aircraft's performance based on FC: 10. The most prominent feature of this analysis is the selection of speed and altitude as shown from Fig. 8a–d. Aircraft on the reference trajectory (refers to as *ref. aircraft*) tends to perform a longer cruise phase and a descent with steep rate. Also the *ref. aircraft* performs the cruise phase at a predetermined flight altitude and at high speeds in all phases of flight. On the contrary, aircraft on the optimal trajectory (refers to as *opt. aircraft*) performs at a higher altitude and a relatively lower airspeed. This is because aircraft achieve efficient performance

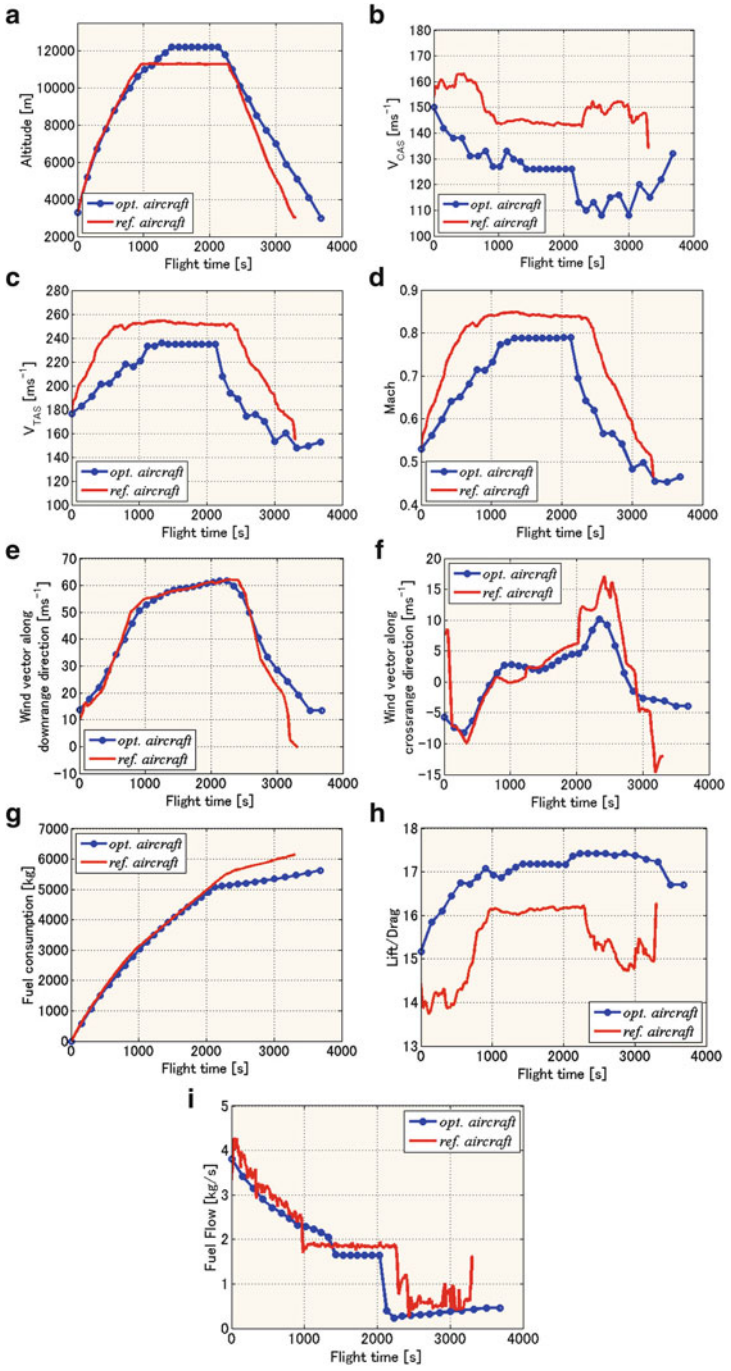

Fig. 8 Characteristics comparison for FC: 10. (**a**) Flight altitude. (**b**) Calibrated airspeed. (**c**) True airspeed. (**d**) Mach number. (**e**) Wind vector along downrange direction. (**f**) Wind vector along cross range direction. (**g**) Fuel consumption. (**h**) Lift drag ratio. (**i**) Fuel flow

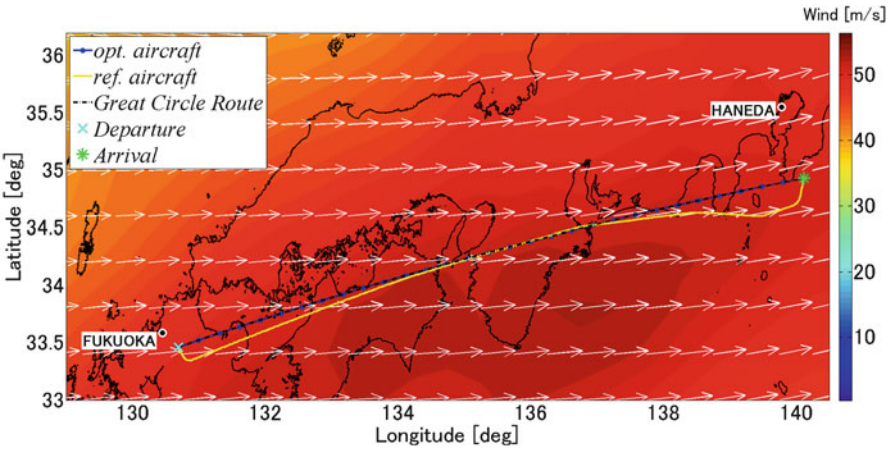

Fig. 9 Lateral flight profile comparison for FC: 10

when flying close to the service ceiling of flight envelope according to BADA model. Furthermore *opt. aircraft* uses tailwinds efficiently to reduce the aircraft speed which are depicted in Fig. 8e, f. This results a reduction of fuel consumption as illustrated in Fig. 8g and a higher lift drag ratio as shown in Fig. 8h compared to *ref. aircraft*. The reduction of fuel consumption is also visible from the fuel flow comparison in Fig. 8i. Furthermore, the aircraft applies idle thrust settings at descent phase at both cases to save unnecessary fuel burn. Slower speed and smooth descent rate results the *opt. aircraft* to spend more flight time to reach the destination. Due to the existence of strong uniform tailwinds, *opt. aircraft* tends to follow the GCR to minimize the flight range while the *ref. aircraft* is bound to vector control procedures near Haneda airport as shown in Fig. 9. The color bar represents the wind magnitude along the flight space at cruising altitude of *opt. aircraft*.

In this comparison, *ref. aircraft* performs with 6,152.6 kg of fuel consumption at a flight time of 3,305 s while the *opt. aircraft* performs with 5,630.2 kg of fuel consumption at a flight time of 3,683 s which results an efficiency of 8.5% in fuel consumption with a tradeoff of 11% in exceeding flight time.

3.1.2 Vector Control Procedures

This subsection discusses results compared to FC: 12 which the *ref. aircraft* experiences vector control and holding procedures at the terminal airspace of Haneda airport. From Fig. 10a it is visible that *ref. aircraft* had to maintain a level flight during its descent as a result of vectoring. On the other hand, the *opt. aircraft* performs a typical flight mission upon the assumption of relaxed ATC procedures. Similar to results on FC: 10, the *opt. aircraft* tends to perform at a higher altitude to obtain greater performance. Furthermore, from Fig. 10b, c it is

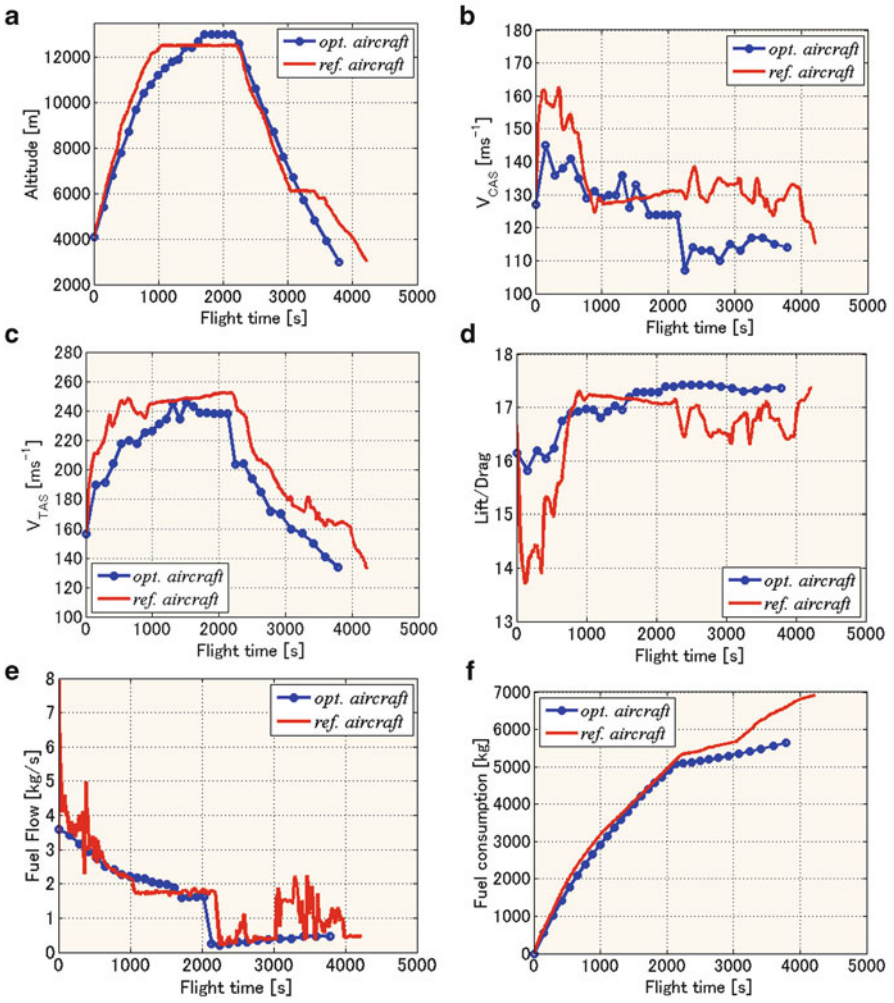

Fig. 10 Characteristics comparison for FC: 12. (**a**) Flight altitude. (**b**) Calibrated airspeed. (**c**) True airspeed. (**d**) Lift drag ratio. (**e**) Fuel flow. (**f**) Fuel consumption

understood that *ref. aircraft* climbs at a steep rate and performs a longer cruise and descent with a holding at relatively high speeds. This results a lower lift drag ratio and also additional fuel flow as depicted in Fig. 10d, e. Hence, the reduction in fuel consumption is clearly visible from Fig. 10f. Also according to current ATC procedures, aircraft approaching Haneda airport from West direction have to pass through the initial fix located at South of airport. Yet, with the assumption of ATC constraints free ATS system is applied, Fig. 11 indicates that *opt. aircraft* tends to use the advantage of tailwinds and laterally deviates from GCR which results a significant reduction of fuel consumption and flight time compared to *ref. aircraft*.

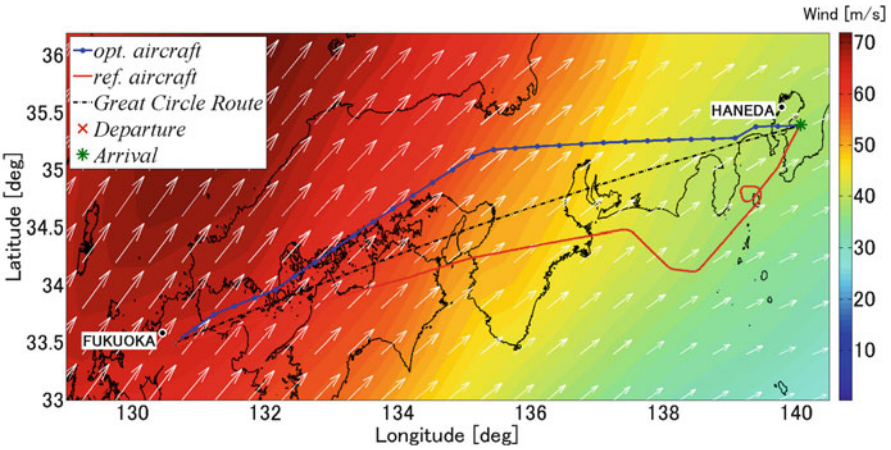

Fig. 11 Lateral flight profile comparison for FC: 12

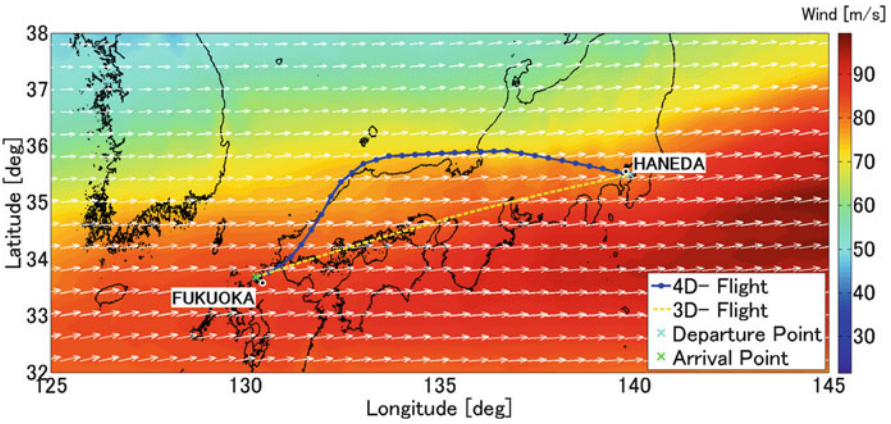

Fig. 12 Lateral flight profile at 25,000 Pa barometric pressure altitude

The *opt. aircraft* performs with 5,643.7 kg of fuel consumption at a flight time of 3,791 s while the *ref. aircraft* performs with 6,905.5 kg of fuel consumption at a flight time of 4,220 s which results an efficiency of 18.3% in fuel consumption and an efficiency of 10.1% in flight time. This flight case results the largest reduction of fuel consumption and also reduction in flight time.

3.1.3 Effect of Wind Shear

To clarify the effect of wind shear on lateral deviation of an aircraft in our proposed model, a comparative analysis was performed by creating two optimal trajectories in the presence of strong wind shear, one with the ability to laterally deviate (refers

to as 4D-flight) and the other without this ability (refers to as 3D-flight). The lateral flight profile is given in Fig. 12 with the magnitude of wind shear. According to the BADA model, aircraft achieves high performance at high altitudes. Therefore both optimal flight paths tend to perform at high altitudes close to the service ceiling. Yet, in the presence of strong headwinds in the region we could understand that the aircraft would try to pass through where the effect of headwinds is relatively small. Hence, the 4D-flight has taken the tradeoff with flight range into consideration and as a result, the flight range has become larger compared to 3D-flight but has been able to reduce the fuel consumption and flight time. This example clearly indicates that the strong wind shear could have a great impact on flight trajectory optimization to succeed future demands in an effective approach.

In this case, 3D-flight performs with 9,651.1 kg of fuel consumption at a flight time of 6,031 s while the 4D-flight performs with 9,349.9 kg of fuel consumption at a flight time of 5,948 s which results an efficiency of 3.12% in fuel consumption and 1.38% in flight time.

4 Conclusions

We conclude this study with an overview of this research followed by a discussion on obtained results and future works to be accomplished [16].

Flight trajectory optimization of a jet passenger aircraft for climb, cruise and descent phases has been formulated as an optimal control problem by considering its inherent performance characteristics by assuming no ATC constraints are engaged. The aircraft's 3D-position and airspeed were considered as state variables to implement the optimization in a provided grid space with heading angle, flight path angle and engine thrust as control variables.

Dynamic Programming method was introduced as a suitable optimization tool because of its unique qualities. Also a unique calculation method called "Moving Search Space Dynamic Programming (MS-DP)" method was proposed to overcome DP's drawbacks and demonstrated its validity through a numerical analysis [12]. Other utilized models were also checked for their validity to be applied in the optimization process.

A commercial GPS logger was used in airliner cabin to measure a series of flight data and their reliability was thoroughly checked by estimating several air data.

A quantitative evaluation was performed and its benefits were reviewed. An average of 9% fuel efficiency could be obtained with a tradeoff of 7% exceeding flight time by creating optimal trajectories for 14 flight cases between Haneda (RJTT) and Fukuoka (RJFF). In a free arrival time optimization process we could understand that the aircraft on optimized routes adjusts the Top of Descent (TOD) setting and performs the descent phase with a smoother rate compared to conventional operating procedures. It is also a fact that present ATC system bounds the aircraft through vector control procedures which results additional fuel burn and

flight time. By providing a more relaxed airspace, pilots would be able to perform efficient flight missions such as,

- Flying at minimum flight distance at the presence of uniform headwinds or tailwinds.
- Adjust the descent airspeed to maintain a high lift drag ratio as a continuous descent approach.
- Perform lateral deviations from predetermined airway to use strong tailwinds or avoid strong headwinds to reduce unnecessary fuel burn.

The constrained workspace of this study has to be emphasized, namely providing free airspace for a single passenger aircraft to perform a 4D-optimal trajectory neither considering any ATC restrictions nor constraints. However, the main objective of this research is to generate a fundamental, yet reliable optimal flight trajectory model to lay the foundation for future studies in the field of Air Traffic Management. Considering multiple aircraft influences the optimal control problem to be more complicated. By enhancing the scope of DP applications such as to analyze optimal flight trajectories with arrival time constraints [17] and Conflict Detection and Resolution (CD&R) methods for multi objective optimization strategies, one could achieve an overall optimization of the system.

References

1. Nolan MS (2011) Fundamentals of air traffic control, 5th edn. Delmar, New York
2. Franco S, Rivas D, Valenzuela A (2010) Minimum fuel cruise at constant altitude with fixed arrival time. J Guid Control Dynam 33(1):280–285
3. Soler M, Zapata D, Olivares A, Staffetti E, Cegarra J (2010) Comparative analysis of commercial aircraft trajectory performance. In: 2nd international conference on engineering optimization, Lisbon
4. Burrows JW (1983) Fuel-optimal aircraft trajectories with fixed arrival times. J Guid Control Dynam 6(1):14–19
5. Betts JT, Cramer EJ (1995) Application of direct transcription to commercial aircraft trajectory optimization. J Guid Control Dynam 18(1):151–159
6. Hargraves CR, Paris SW (1987) Direct trajectory optimization using nonlinear programming and collocation. J Guid Control Dynam 10(4):338–342
7. Hagelauer P, Mora-Camino F (1998) A soft dynamic programming for on-line aircraft 4D trajectory optimization. Eur J Oper Res 10(1):87–95
8. Totoki H, Kozuka T, Miyazawa Y, Funabiki K (2013) Comparison of JMA numerical prediction GPV meteorological data and airliner flight data. Aero Tech Japan Trans Japan Soc Aero Space Sci 12:57–63 (in Japanese)
9. Ninomiya K (2004) Fundamental understanding on numerical prediction. Ohmsha, Tokyo (in Japanese)
10. Japan Meteorological Business Support Center Online Data Service (2006) (in Japanese). http://www.jmbsc.or.jp/hp/online/f-online0a.html
11. Eurocontrol Experimental Center (2011) User manual for the Base of Aircraft Data (BADA). Revision 3.9, EEC Technical/Scientific Report, No. 11/03/08-08

12. Harada A, Miyamoto Y, Miyazawa Y, Funabiki K (2013) Accuracy evaluation of an aircraft performance model with airliner flight data. Aero Tech Japan Trans Japan Soc Aero Space Sci 11:79–85
13. Harada A, Miyamoto Y, Wickramasinghe NK (2013) Flight trajectory optimization tool with dynamic programming developed for future air transportation system. In: The 3rd ENRI international workshop on ATM/CNS (EIWAC 2013)
14. Bellman R (1965) Dynamic programming, 4th edn. Princeton University Press, Princeton
15. Totoki H, Wickramasinghe NK, Hamada T, Miyazawa Y (2012) Estimation of flight trajectories by using GPS measured in airliner cabin. Aero Tech Japan Trans Japan Soc Aero Space Sci 11:43–50 (in Japanese)
16. Wickramasinghe NK, Harada A, Miyazawa Y (2012) Flight trajectory optimization for an efficient air transportation system. In: 28th International Council of the Aeronautical Sciences (ICAS2012)
17. Miyazawa Y, Wickramasinghe NK, Harada A, Miyamoto Y (2013) Passenger aircraft optimal trajectory with an arrival time constraint. Aero Tech Japan Trans Japan Soc Aero Space Sci 12:31–38 (in Japanese)

Part III
Tools and Evaluation for Air Traffic Managements

Evaluation of an Automated Taxi Concept in a Distributed Simulation Environment

Stephan Kocks, Astrid Oehme, Tobias Rad, Boris Budweg, and Thomas Feuerle

Abstract Taking into account the actual predictions for the growth of air traffic in Europe in the next 20 years, major hub airports will become more and more the bottlenecks in the overall air transport network. Amongst other factors, current taxi procedures and the dependency on airfield view for both, controllers and flight crews, have a large impact on an airport's efficiency and capacity. The ROLF project (Rollführung, Taxi Guidance), a sub-project of the research project iPort (Innovative Airport) within the scope of the German Aeronautical Research Program (LuFo IV), aimed at operational changes at airports to meet future requirements regarding the arising European airspace demand by introducing an increased level of automation. Following the project's objectives, a concept of operations was developed by the ROLF partners that describes in detail the systems and procedures necessary for automated taxi operations. This paper focuses on a human-in-the-loop evaluation of the operational concept in order to investigate its feasibility and the general acceptance by its users from flight deck perspective. At first, the operational concept is introduced in the context of an Advanced Surface Movement Guidance and Control System (A-SMGCS). A simulation environment spatially distributedover multiple locations in Germany is described, which was

S. Kocks (✉) • T. Rad • T. Feuerle
Institute of Flight Guidance, Technische Universität Braunschweig, Hermann-Blenk-Str. 27, 38108 Braunschweig, Germany
e-mail: s.kocks@tu-braunschweig.de; t.rad@tu-braunschweig.de; t.feuerle@tu-braunschweig.de

A. Oehme
HFC Human-Factors-Consult GmbH, Köpenicker Str. 325, Haus 40, 12555 Berlin, Germany
e-mail: oehme@human-factors-consult.de

B. Budweg
Diehl Aerospace GmbH, An der Sandelmühle 13, 60439 Frankfurt am Main, Germany
e-mail: boris.budweg@diehl-aerospace.de

Electronic Navigation Research Institute (ENRI), *Air Traffic Management and Systems*, Lecture Notes in Electrical Engineering 290, DOI 10.1007/978-4-431-54475-3_7,

the base for the evaluation study. Finally, the conducted simulation study and evaluation results are presented. Several positive effects with regard to automated taxi procedures were observed.

Keywords A-SMGCS • Automated taxi operations • Surface management system • Cockpit display system • Electronic flight bag • Taxi guidance application • Data link • Simulation environment • Human-in-the-loop evaluation

1 Introduction

Despite the global economic recession since 2008, air traffic in Europe is expected to have doubled in the next 20 years. This positive economic development will lead, however, to a capacity bottleneck and increasing accident risks especially at major congested hub airports. According to the most-likely scenario of the current EUROCONTROL long-term forecast [3], approximately two million flights will not be accommodated in 2030 — around 10% of the demand.

Due to strict regulations in terms of environment protection as well as spatial restrictions, it becomes nearly impossible to expand existing airports, especially in areas with a high population density like Europe. As a consequence, a change of current taxi procedures and the integration of novel Air Traffic Management (ATM) technologies and concepts such as Advanced Surface Management Guidance and Control Systems (A-SMGCS) [6] are needed to obtain the required safety, capacity, and efficiency.

1.1 Current Taxi Operations

Surface operations constitute a demanding and high-workload task for both Air Traffic Control (ATC) and flight crews as various tasks have to be accomplished simultaneously. Today, ground movement operations are primarily based on visual surveillance by ATC and the use of ground surveillance radar. For this purpose, the controllers observe all movements on the maneuvering area and issue clearances to the individual aircraft via voice radio. The flight crews have to interpret their given taxi instruction, confirm it, and mentally integrate this detached information with the other information necessary for taxiing. At the same time, they are required to visually monitor surrounding traffic for possibly arising conflicts and to configure the aircraft for departure.

Navigation on aerodrome surface is typically based on visual aids such as signs, painted markings, and lighting. Furthermore, paper copies of airport charts help the flight crews to locate themselves on the ground. Guidance support via individual lighting, if available, is operated manually and activated depending on local procedures based on visibility conditions. Consequently, the flight crews have

to continuously observe the maneuvering surface in order to find visual cues and compare the followed route with regard to the issued clearances until the final taxi destination. However, this might be difficult at complex and unfamiliar airports. Especially during low visibility conditions the risk of disorientation by the pilots will increase, which again might lead to hazardous accidents including runway incursions. Simultaneously, the capacity of the airport decreases because of greater separation distances and lower taxi speeds.

1.2 The ROLF Project

The ROLF project (Rollführung, Taxi Guidance), a sub-project of iPort (Innovative Airport) within the German Aeronautical Research Program (LuFo IV) aimed at innovations and operational changes at airports to meet future requirements regarding the arising European airspace demand. In continuation of Roll:MOPS (Rollverkehr: Management- und Optimierungssysteme, Ground Traffic: Management and Optimization Systems) [4, 10], ROLF focused on a higher level of automation in surface traffic management and visual guidance via ground and onboard solutions in order to

- increase resources,
- increase safety,
- reduce environmental impact of ground traffic, and
- reduce the dependency on direct airfield view.

Within the scope of the project, a concept of operations (ConOps) was developed that describes in detail the systems and procedures necessary for automated taxi operations. Special effort has been made to take the changing role of the human actors into account. Simulation trials were conducted with airline pilots in order to validate the operational concept in terms of safety, efficiency, and usability and work performance. For this purpose, a simulation environment was set up containing an ATC simulator and three cockpit simulators equipped with the developed systems and applications. The individual components were located at multiple locations in Germany.

ROLF-ConOps supports the key goals proposed by the Single European Sky ATM Research (SESAR) program [8]. Considering automation to be an enabler for a safer and more efficient operational environment, it represents one possible solution for future surface management procedures.

1.3 About

This paper focuses on the human-in-the-loop evaluation of the concept of operations with the goal to investigate its feasibility and the general acceptance by its users from flight deck perspective. Section 2 introduces the operational concept developed

by the ROLF consortium and provides a detailed description of its respective ground and onboard systems as well as procedures. Section 3 presents the spatially distributed simulation environment, which was the base for the validation study. The conducted simulation study is described in Sect. 4, followed by a presentation of the evaluation results in Sect. 5.

2 Concept of Operations

ROLF-ConOps addresses the ATM community, including airport operators, air traffic controllers, pilots, system developers, suppliers, researchers, and authorities. Following the project's objectives, the concept concentrates on an increased level of automation in ground traffic management based on integrated surveillance sensor technology with the goal to submit a complete, generic system concept for automated ground traffic control. ROLF-ConOps contains a detailed description of systems and processes, and their corresponding interactions and information flows, concerned actors, their roles and responsibilities from final approach and landing to take-off. Thus, each phase of the taxi process defines a distinct use case, which is elaborated for two levels of automation.

The main components are a Surface Management System (SMAN), Airfield Ground Lighting (AGL), and two different kinds of Onboard Display Units (ODU): a Cockpit Display System (CDS) and an Electronic Flight Bag (EFB). The SMAN is the core system and provides a central A-SMGCS information platform that coordinates the traffic of the airport. The AGL provides individual guidance for each aircraft. Both onboard systems depict the own-ship position, surrounding traffic as well as the dedicated route on an Airport Moving Map (AMM). The communication between the SMAN and CDS/EFB is realized via a digital data link. The systems are described in detail in Sect. 2.2.

In order to enable a successive implementation, care was taken to ensure that the concept in a first step is able to support cooperative as well as non-cooperative traffic. During its preparation, the users of the novel components, i.e. controllers and pilots, have been constantly involved.

2.1 Addressed Levels of Automation

ROLF-ConOps envisions two levels of automation: The semi-automated level includes procedures comparable to an automation level 2–6 of the automation scale proposed by Wickens et al. [11]. The 10-point scale describes the allocation of decision making and action selection when a task is jointly performed by a human and a system. It ranges from low automation with manual performance only (1) to full automation without the possibility of intervention for the operator (10).

The highly-automated procedures in ROLF strive for full automation and include automation level 7–10 use cases.

Semi-automated procedures support mixed traffic as currently present. The controller is indeed supported by a ground management system, which assists decision making in providing a narrowed set of alternative options. However, he/she is responsible for action selection and execution and communicates via voice with the pilots of non-cooperative aircraft. Additionally, controller and pilot are informed in parallel via dedicated Human Machine Interfaces (HMI) about the current situation. By using data link with cooperative aircraft, aural misunderstandings of controller and pilot are reduced.

In high-level procedures, the controller role is a more passive one. General procedures and route assignments are automatically processed via SMAN and therewith highly flexible, supporting a more efficient surface management. Only if procedures are not complied with, the resulting conflicts have to be resolved via direct communication of human controller and pilot. System failures will be remedied by manual control procedures. Thus, the controller remains a fallback system and will be mainly confronted with conflict resolution. The pilot will have to comply with instructions given via airfield lighting and onboard system.

Being in operation in the near future, semi-automated procedures are of high interest regarding hitherto unexplored feasibility and human factors issues. Thus, we concentrated on these levels of automation in our simulation study.

2.2 Systems

In the subsequent sections the basic system components providing the functionalities necessary for ROLF-ConOps procedures are presented. The components are consortium-specific, i.e. they possibly have to be adapted to the respective operational concept of other airports and users.

As already mentioned, two different approaches have been investigated concerning the onboard units: the integration of software into already existing Cockpit Display Systems and the use of external Class 2 Electronic Flight Bags. While a CDS application must ensure a very high certification level to guarantee that no safety-relevant system will be disturbed, an EFB can be installed in addition to already available cockpit instrumentation involving an easier and faster certification process. Therefore, an EFB is more suitable for the retrofit market, while the integrated solution is focusing on new aircraft developments.

2.2.1 Surface Management System

The SMAN is a back end software system that provides automation services for surveillance, routing, guidance, and control. Designed especially for large and

medium sized airports, the SMAN coordinates all aircraft on the maneuvering area with the goal to optimize traffic flow enabling safe and efficient taxi operations.

The routing function allows to create, store, retrieve, edit, delete, and assign taxi routes for all flights. Each taxi route is a directed path between any two defined points located on the centerline of a runway, taxiway, or stand. When calculating an individual route, the SMAN takes into account the current traffic situation as well as various objectives and constraints such as distances, routing preferences, restricted areas, and physical limitations.

The primary guidance function is to support the flight crews in quickly leaving the runway and following their assigned inbound or outbound taxi routes. In addition, it indicates to taxiing pilots and drivers to hold short of an active runway and crossing taxiway.

The primary control task is to predict and detect potential conflicts as well as to support controllers in providing lateral separation by sequencing converging traffic at intersections. During take-off and landing, the SMAN automatically controls the runway stop bars to prevent aircraft or vehicles from entering a runway. In low visibility operations, the SMAN can be used to provide longitudinal spacing between following aircraft by dynamically switching intermediate stop bars.

The Integrated Controller Working Position (ICWP) represents the HMI for the ATC controller working on an airport equipped with a SMAN. It supports the controller in monitoring the aerodrome surface by displaying the positions of aircraft and vehicles and their relevant flight plan information as well as indicating the status of the all stop bars. In case the SMAN detects a conflict situation, appropriate warnings and alerts are issued. Also, the ICWP provides for means of interacting with the SMAN. At any time, the controller can assign and modify routes or enter clearances and advisories for the individual aircraft. The ICWP of Frankfurt/Main airport is depicted in Fig. 1.

2.2.2 Airfield Ground Lighting

The AGL visually guides the flight crews along their assigned taxi routes by dynamically switching taxiway centerline lights in front of the aircraft (individual Follow-the-Greens). It provides unambiguous guidance for each flight from the runway to the parking stand and vice versa.

During taxiing, the SMAN continuously updates the individual route segments and transmits them to the Airfield Lighting Control System (ALCS) taking into account upcoming holding points at intersecting runways and taxiways as well as preceding aircraft. The ALCS converts the information into individual commands in order to switch the corresponding centerline lights. The lights behind the aircraft are automatically switched off.

Fig. 1 Integrated controller working position

2.2.3 Cockpit Display System

The CDS is represented by a taxi guidance application that has been designed for the integration into one of the center displays of the Main Instrument Panel (MIP). Unlike the traditional interaction via keyboard and/or trackball, it can be operated via touch screen.

The main goal of the CDS is to improve the flight crews' situational awareness and to reduce their mental workload during ground movement operations by dynamically rendering the own-ship position as well as surrounding traffic on a high-resolution airport map. The map is based on an Aerodrome Mapping Database (AMDB) that contains highly reliable and precise information about the geometry of an airport. The AMDB complies with the ARINC 816 specification [1], which is already in use in the Onboard Airport Navigation System (OANS) of the Airbus A380.

The CDS fully supports data link communication. For this purpose, the system establishes a connection to the SMAN during approach in order to exchange tactical routing data such as requests, clearances, confirmations, and other information necessary to perform taxi operations.

As shown in Fig. 2, a significant feature of the CDS is the ability to visualize assigned taxi routes and cleared taxi route segments graphically and textually. The routing functionality is based on a taxi network that is generated from AMDB data and supplemented by manual airport specific adjustments, e.g. to account for missing connections. By knowing the own-ship position, the route to follow, and the upcoming holding points, the system detects and warns the flight crew about possible conflicts such as route deviations or unauthorized holding point overruns.

Fig. 2 HMI of the taxi guidance application (CDS)

All incoming instructions are ordered by priority and depicted in a message box with their respective arrival time. Dependent on the type of message, they must be confirmed to the SMAN, i.e. acknowledged or rejected, manually by the pilots. In case a new message arrives, the CDS informs the pilots visually and acoustically in order to draw their attention to the display. Reports and requests, e.g. for start-up and taxi, can be communicated via an interactive menu.

An interface to the Radio Management Panels (RMP) of the flight deck allows the CDS to monitor the current active radio frequencies as well as to automatically set the active/standby frequencies issued by the SMAN. As radio communication is considered as backup only in automated taxi operations, this functionality eases the frequency change for the pilots and always guarantees that the correct radio frequency is selected in case of an emergency situation. However, the pilots can change a preset frequency at any time.

2.2.4 Electronic Flight Bag

The EFB is represented by a software application that does not only focus on surface operations but supports the flight crews in all phases of flight. Following the concept of a paperless cockpit in terms of aeronautical information, the so called Gate-to-Gate software provides all required information in one single application. Depending on the flight phase, all operational relevant information are selected and seamlessly presented in a graphical and textual way to the pilots required to perform the current task [7].

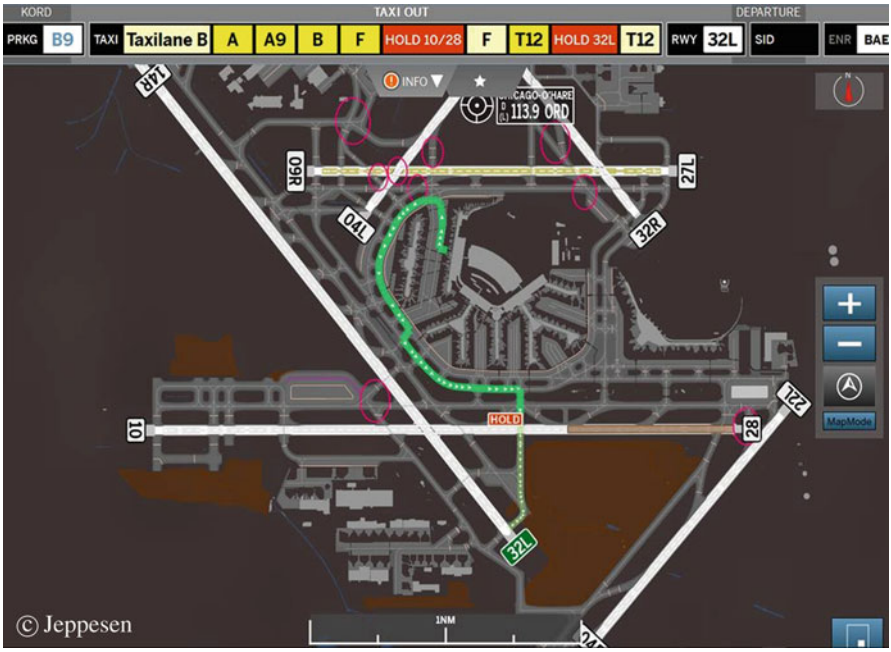

Fig. 3 HMI of the Gate-to-Gate application (EFB) [7]

Operated via touch screen, the application facilitates two modes: the live mode and the planning mode. While in live mode the application automatically adjusts the actual map area according to the current aircraft position and flight phase, in planning mode the user can browse through the different phases in order to familiarize with the relevant information of the current or a planned flight. The HMI layout orientates on the different flight phases [9].

Concerning the taxi phase, the global objectives of Gate-to-Gate correspond to the ones of the CDS application in terms of an increase of situation awareness and a workload reduction. For that purpose, the EFB depicts an airport map with the own-ship position as well as the current traffic situation (cf. Fig. 3).

A data link connection enables the system to communicate with the SMAN, even though the data exchange is limited to the reception of the assigned taxi route. Consequently, focusing on supporting situational awareness instead of providing guidance information, Gate-to-Gate depicts the overall taxi route until the final taxi destination without indicating the cleared taxi route segment. However, in case a route is about to cross an active runway, the respective runway holding point is automatically highlighted by the system and added to a textual route strip at the top of the HMI. New arriving route messages are chronologically listed in the JOBS tab. In order to visualize an issued route on the AMM, the corresponding message has to be selected by the pilot first.

Usually, the Gate-to-Gate application will be executed on two EFB devices, one for each crew member. Both EFBs are provided with identical information and display the same content, but can be operated individually.

Gate-to-Gate is also able to graphically depict relevant Notice to Airmen (NOTAM) messages, e.g. runway or taxiway closures, as well as actual weather for each individual phase of flight. This has already been investigated in [9] and was not part of our study.

2.3 Execution of Procedures

The ConOps comprises general, optional, and abnormal procedures (procedure violations) for inbound and outbound movements. General procedures are described from final approach and landing to take-off. Optional procedures include taxiway sequencing and route modification, while abnormal procedures address for instance route deviations or an overrun of holding point indication devices.[1] Additionally, fallback procedures were detailed for a set of system failures such as SMAN or data link breakdown.

2.3.1 Semi-automated Procedures

The semi-automated procedures support the processing of cooperative and non-cooperative traffic, while radiotelephony (R/T) is the backup for fully equipped aircraft, e.g. when procedure violations occur and a conflict has to be solved.[2] SMAN provides conventional guidance, i.e. the manual or semi-automatic switching of stop bars to indicate traffic to stop. In addition, SMAN continuously and dynamically updates information about released route segments for each aircraft to enable individual Follow-the-Greens. The controller receives route proposals, has to assess them and select and execute as he/she prefers. The route proposals are transmitted via data link to the CDS/EFB and the pilot has to confirm their reception. SMAN, CDS, and AGL detect and predict potential hazards, i.e. procedure violations or abnormal procedures. Primarily, SMAN provides and distributes alerts for ICWP, AGL, and CDS because it continuously scans the airport state for actual or potential conflicts. CDS and AGL trigger respective system alerts for controller and pilot as

[1] Generic terms were used to support adaptation to the conditions of different airports.

[2] From the controller/SMAN point of view an aircraft is fully equipped, if all tactical routing data can be exchanged with the onboard component via data link, e.g. requests, reports, routes, clearances, and confirmations. The aircraft is considered as not equipped, when it does not support data link communication at all or only parts of it. In this case, all taxi instructions are to be issued via voice radio.

well, if either component predicts/detects a respective hazard first. The component then transfers the information to SMAN, which distributes the information to the remaining component.

The semi-automated procedures were evaluated in the study described in Sect. 4.

2.3.2 Highly- and Fully-Automated Procedures

In highly-automated procedures SMAN provides advanced guidance, i.e. an automatic control of the airfield lighting based on surveillance data as well as ATC clearance/advisory input (automation level 10 in [11]). Conflict detection and exchange with CDS are the same as for semi-automated procedures. Conflicts are resolved via voice communication.

The procedures at full automation level have not been tested in the simulation study.[3]

3 Simulation Environment

In order to enable a human-in-the-loop evaluation of the operational concept and its systems, a complex simulation environment was required consisting of both ATC and cockpit simulators. Due to the fact that such simulators were available at the individual partners' sites, we decided to use the existing hardware to conserve project resources and to adapt it to our needs. The overall simulation environment was spatially distributed across Germany and composed of one ATC simulator located in Freiburg and three cockpit simulators located in Braunschweig, Darmstadt, and Frankfurt/Main. Furthermore, a couple of auxiliary systems were provided as described in Sect. 3.3. Figure 4 schematically depicts the architecture of the simulation environment.

The communication between the facilities was handled via internet. Primarily, the following data were exchanged:

- aircraft state vector data of the cockpit simulators
- surveillance/traffic data
- flight plan data
- airfield lighting data
- data link communication data
- voice communication data

[3] At the time the study was prepared, especially conflicts and their resolution were not defined in detail (switch from full automation mode to manual control with voice communication and back).

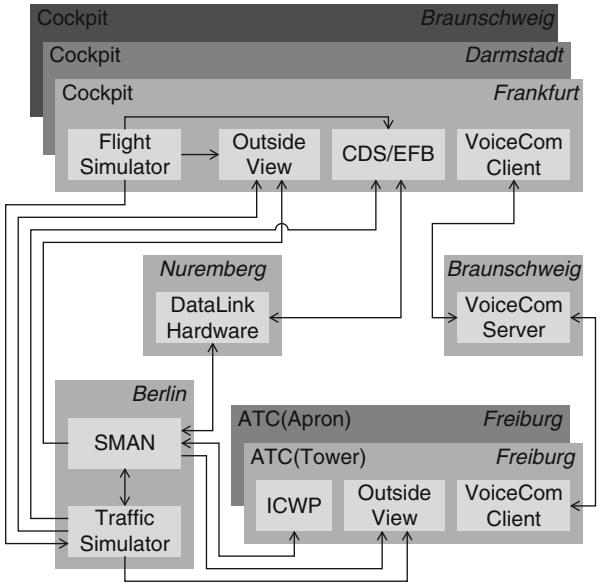

Fig. 4 Architecture of the simulation environment

3.1 ATC Simulator

The ATC simulator comprised two controller working positions each equipped with a 24″pen touch display. While the first ICWP was configured to represent an apron working position responsible for pushback and taxiing, the second ICWP represented a tower working position responsible for landing, runway crossing, line-up and take-off as well as taxiing in the vicinity of the runways. On both positions, the operational version of the ICWP was running connected to the operational one of the SMAN (executed on a dedicated server in Berlin).

3.2 Cockpit Simulators

All three cockpit simulators were based on modern sidestick controlled aircraft operated by two pilots. They provided the necessary controls, actuators, indicators, and navigation aids to operate the aircraft during final approach, landing, taxi, and take-off. The key components of the simulators orientated on their real counterparts, which gave the pilots the ability to concentrate on the changes introduced by the experimentation setup. The cockpits came with a cylindrical or spherical screen with a viewing angle of approximately 180°. In order to guarantee a consistent outside view including individual AGL visualization, it was generated by the same

Fig. 5 Cockpit simulator in Frankfurt with integrated CDS

rendering software at all locations. For the voice communication, operable RMPs were installed as well as headsets and push-to-talk (PTT) keys.

The cockpit layout, flight simulation engine and system simulation itself varied through the three locations. While the simulator located in Braunschweig was a full replica of an Airbus A320, Darmstadt was running a generic Airbus like flight deck. The third simulator in Frankfurt represented an Airbus like cockpit with single sided controls only.

The CDS application was integrated with a single instance into the center MIP of the cockpit simulators in Darmstadt and Frankfurt (cf. Fig. 5). As the CDS application fully supports data link communication, both simulators are classified as equipped from controller/SMAN point of view.

The EFB was mounted in a twin configuration at both sides of the simulator in Braunschweig (cf. Fig. 6). Due to the limited data link functionality of the EFB application, the simulator in Braunschweig was considered as not equipped by the controller/SMAN.

3.3 Auxiliary Systems

To support the distributed simulation, several auxiliary systems were needed. They are briefly described in the subsequent sections.

Fig. 6 Cockpit simulator in Braunschweig with integrated EFB

3.3.1 Outside View

The outside view was provided by a 3D real-time rendering engine that generates synthetic images from tower and cockpit perspective, i.e. buildings and aircraft with photo-realistic textures as well as realistic aircraft and airfield lights. Changing ambient light enables the simulation of airport operations at different times of day. Weather phenomena such as rain, snow, and fog can be activated in order to reduce visibility. For the trials described within this paper, fog was used to limit the horizontal visibility during degraded visibility conditions.

Via a direct connection to the SMAN, the outside view was also responsible to control the status of the airfield lighting system at the level of single lamps or sections in case of individual guidance. Based on the Roll:MOPS results, a maximum length of 300 m was chosen for the illuminated route sections.

3.3.2 Data Link

The data link used for the exchange of tactical routing data between the SMAN and CDS/EFB applications was based on the Universal Access Transceiver (UAT) technology. For each party participating in the communication process, a dedicated hardware device was available composed of a server unit and transceiver. The ground and onboard components were connected to the server unit located in Nuremberg via internet; the radio frequency part was realized by a cable connection.

The internal protocol used for connection establishment, handshakes as well as the transmission of payload was specified and already validated within the scope of the Roll:MOPS project. The specification of the data messages exchanged between the SMAN and the CDS/EFB was done in ROLF.

3.3.3 Traffic Simulator

The traffic simulator generated aircraft and vehicle movements according to a flight plan database following an event driven approach. Each aircraft/vehicle has a certain degree of autonomy within the simulation. In particular, an aircraft maintains its own longitudinal spacing and lateral separation to avoid collisions, holds at illuminated stop bars or runway holding points. All flight plan related data as well as position and movement information were provided to external systems via several outgoing data interfaces. The traffic simulator was running on a dedicated server in Berlin.

3.3.4 Voice Communication System

The purpose of the voice communication system was to realistically copy VHF R/T communication. This was realized by a Voice over IP (VoIP) solution which was adapted to the needs of the simulation. The overall system comprised one server located in Braunschweig and multiple clients connected to the individual ICWPs and RMPs. For each frequency in use, a half-duplex voice channel was provided. Voice transmission could be activated via PTT keys. A logging module allowed the recording of channel occupancy times.

4 Simulation Study

The simulation study was conducted in order to validate aspects of the ROLF-ConOps from flight deck perspective, especially concerning the differences between common procedures and procedures with a higher level of automation to be introduced in near future, i.e. semi-automated procedures. The study extends work of the former project Roll:MOPS, in which AGL and onboard systems were compared as to their support of pilots' situational awareness in field trials [10]. In the simulation study we focused on three blocks of high level objectives derived from SESAR key performance indicators: safety, efficiency, and usability and work performance. We expected that compared to a baseline, operations with a higher level of automation would lead to a decrease in workload, an increase in situational awareness, and a reduction of voice radio channel occupancy. Another goal was to assess the feasibility of such distributed simulations for follow-up projects.

4.1 Participants

Eleven male airline pilots with an average flight experience of 5,063 h (range: 300–11,000 h) took part in the study, including five captains, two senior first officers, and three first officers.[4] None of the participants had any experience with moving maps. Seven pilots participated twice in our test trials. As the study focused on investigations from flight deck point of view, no ATC controllers were involved.

4.2 Scenarios and Missions

The simulation scenarios consisted of combinations of the two independent variables *visibility* and *procedure*, which were varied in two levels each: high visibility (10,000 m), low visibility (300 m), baseline procedures (no individual AGL, CDS/EFB with AMM only and R/T communication), and (semi-)automated procedures (individual AGL, full CDS/EFB functionality and data link communication) resulting in the four scenario combinations HighVisBase, HighVisAuto, LowVisBase, and LowVisAuto. Within each scenario, all of the participating cockpit simulators at the three locations had to jointly follow eight missions, i.e. five inbound and three outbound missions with predefined start and end points, which were based on an authentic flight plan with dense traffic.

In order to test our hypotheses, the pilots had to give their opinion regarding perceived safety, automation trust, mental effort, situational awareness, perceived support, smoothness of procedures and communication as well as perceived efficiency via respective questionnaires and interview questions with open answering format after each scenario. Channel occupancy was assessed as well.

4.3 Setting and Procedure

The scenarios were conducted at a Frankfurt airport model in a planned expansion stage for 2014. Each cockpit simulator was operated by two pilots; the ICWPs were operated by one trained pseudo-controller each. Other traffic was controlled automatically by the traffic simulator. On each of three test days, the pilots had to perform three out of the four research scenarios with a length of 1 h each in a quasi-randomized order. Thus, each scenario was performed in a different frequency, with one elicitation for HighVisBase, two elicitations for LowVisBase, and three elicitations each for HighVisAuto and LowVisAuto. The trials were preceded by a day of technical and procedural tests. The daily procedure of a test day is visualized in Fig. 7.

[4] One not stated.

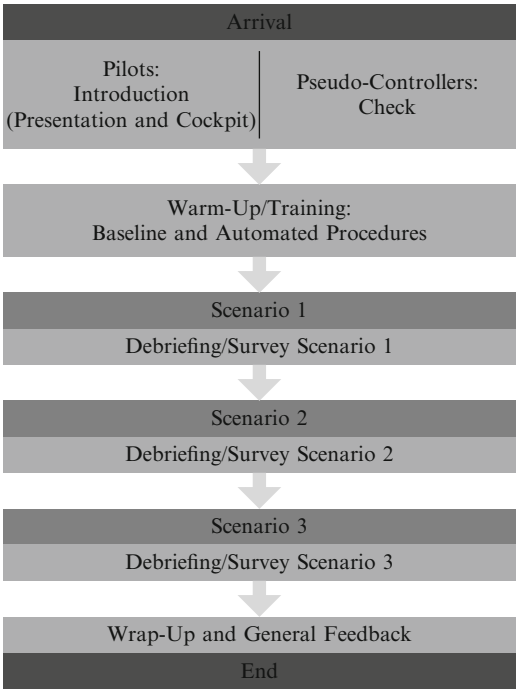

Fig. 7 Procedure of a test day

A test day started for the pilots with an introduction to the tasks, setup, and simulator, followed by a training phase for simulator handling and procedures. Taxi instructions were given by the pseudo-controllers. The flight plan information was given verbally by the test instructor. Subsequently, three scenarios were performed. After each scenario, a questionnaire was filled in by each pilot.

5 Simulation Results

Assessed data were mainly submitted to repeated measures analysis of variance (ANOVA) (e.g. [2])[5]. To remedy the unbalanced frequency of elicitations for each scenario (cp. Sect. 4.3), the data of LowVisBase, HighVisAuto, and LowVisAuto were aggregated. The results are reported following the three main objectives addressed with the simulation study. All parameters used in the subsequent sections are named in the following list:

[5] ANOVA is a statistical method to determine the differences between more than two group means. Repeated measures refers to successive measurements within one group, whose variation of means between measurements is analyzed.

d	Effect size
$F(x,y)$	Empirical test value of the F-test, which is used for comparing the group differences, with degrees of freedom x and y
f	Effect size
M	Mean value
p	Exceedance probability
SE	Standard error
$t(x)$	Empirical test value of the t-test, which is used for comparing the mean differences, with degrees of freedom x
Cronbach's α	Internal consistency of a scale
$(1-\beta)$	Test power

5.1 Safety

The perceived safety was assessed via seven items with the levels *low* (0) and *high* (6), e.g. *In the previous session there was a risk of taking the wrong intersection*. The internal consistency was satisfying with Cronbach's $\alpha = 0.75$, thus the items were aggregated to one scale via averaging. The factor *visibility* was not significant with $F(1,5) = 0.63$, $p = 0.46$, $f = 0.36$, $(1-\beta) = 0.10$. The factor *procedure* was significant with $F(1,5) = 22.65$, $p < 0.01$, $(1-\beta) = 0.96$ and a large effect of $f = 2.13$. The safety risks were rated higher in the baseline procedures than in the automated procedures: $M_{\text{Baseline}} = 2.59$, $SE_{\text{Baseline}} = 0.24$ vs. $M_{\text{Automation}} = 0.99$, $SE_{\text{Automation}} = 0.15$. The interaction between *visibility* and *procedure* was not significant.

As another safety aspect, automation trust was assessed via five items each for ODU and AGL, which were drawn from the Automation Trust Index SATI [5]. The items leveled between *none* (0) and *extreme* (6). The internal consistency for both system components were satisfactory with Cronbach's $\alpha_{\text{AGL-items}} = 0.83$ and Cronbach's $\alpha_{\text{ODU-items}} = 0.91$, which again supported aggregating to respective scales. Because of the small number of answers for the baseline scenarios, which was due to a lack of applicability of the items for these procedures, the ANOVA was conducted for the automation scenarios only. Main factors thus were *visibility* and *system*. *Visibility* again was non-significant with $F(1,16) = 0.15$, $p = 0.71$, $f = 0.10$, $(1-\beta) = 0.07$. The *system* assessments differed only by tendency with $F(1,16) = 3.55$, $p = 0.08$, $f = 0.47$, $(1-\beta) = 0.43$, while AGL was rated as slightly more trustable with $M = 5.35$ ($SE = 0.13$) than ODU with $M = 4.89$ ($SE = 0.21$). Note that the assessments for both systems were far above the neutral acceptance score of 3.00.

5.2 Efficiency

Efficiency was assessed via ratings of perceived efficiency and the measurement of the overall R/T communication.

The items for perceived efficiency did not reach acceptable internal consistency (Cronbach's $\alpha = 0.49$) and thus were analyzed individually. Each item varied between the levels *never* (0) and *always* (6). For the item regarding the *maintenance of continuous taxi speed* the factor *procedure* was significant by tendency with $F(1,5) = 5.29$, $p = 0.07$, $f = 1.03$, $(1-\beta) = 0.46$ and $M_{\text{Baseline}} = 3.42$ ($SE_{\text{Baseline}} = 0.46$) vs. $M_{\text{Automation}} = 4.28$ ($SE_{\text{Automation}} = 0.31$). There were no effects for the second item *having to stop due to other traffic*. The rating for *having to wait for a taxi clearance* was significant for the factor *procedure* with $F(1,5) = 10.35$, $p < 0.05$, $f = 1.44$, $(1-\beta) = 0.73$ and a higher level of *having to wait* during baseline procedures with $M = 3.38$ ($SE = 0.39$) than during automated procedures with $M = 2.78$ ($SE = 0.47$).

R/T communication was analyzed for usage frequency and average busy time for the factors *visibility*, *procedure*, and *group* (pilots vs. controllers). The controllers occupied the channel significantly more frequently than the pilots with $F(1,3) = 29.34$, $p < 0.05$, $(1-\beta) = 0.94$ and a large effect of $f = 3.18$. *Visibility* had no significant influence on R/T usage frequency with $F(1,3) = 0.45$, $p = 0.55$, $f = 0.39$, $(1-\beta) = 0.08$. *Automation*, i.e. using data link, decreased R/T usage by tendency with $M_{\text{Baseline}} = 93.44\,\text{s}$ ($SE_{\text{Baseline}} = 17.84\,\text{s}$) vs. $M_{\text{Automation}} = 27.85\,\text{s}$ ($SE_{\text{Automation}} = 10.00\,\text{s}$) and $F(1,3) = 6.30$, $p = 0.09$, $f = 1.45$, $(1-\beta) = 0.41$. No interaction between *visibility*, *automation*, and *group* was statistically significant. The *group*-factor was non-significant for the average R/T time ($F(1,3) = 1.91$, $p = 0.26$, $f = 0.80$, $(1-\beta) = 0.17$) as well as *visibility* ($F(1,3) = 0.31$, $p = 0.62$, $f = 0.32$, $(1-\beta) = 0.07$). *Procedure* was highly significant with a large effect of $f = 2.23$ and $F(1,3) = 14.99$, $p < 0.05$, $(1-\beta) = 0.73$. The average talking time was $M = 4.43\,\text{s}$ ($SE = 0.55\,\text{s}$) in automated procedures and $M = 5.20\,\text{s}$ ($SE = 0.45\,\text{s}$) in baseline procedures. The interaction between *visibility* and *procedure* was significant as well with $F(1,3) = 16.65$, $p < 0.05$, $f = 2.35$, $(1-\beta) = 0.77$: While the average R/T time was different in the HighVis conditions with increased R/T time in baseline procedures, both distributions overlapped in the conditions with constrained visibility (cf. Fig. 8).

5.3 Usability and Work Performance

Usability and work performance were assessed via subjective ratings of workload, situational awareness, and perceived support.

Workload items included the human processing stages of information acquisition and analysis, decision making, and action implementation (e.g., *In the previous session, how much effort did it take to understand and memorize ATC clearances?*).

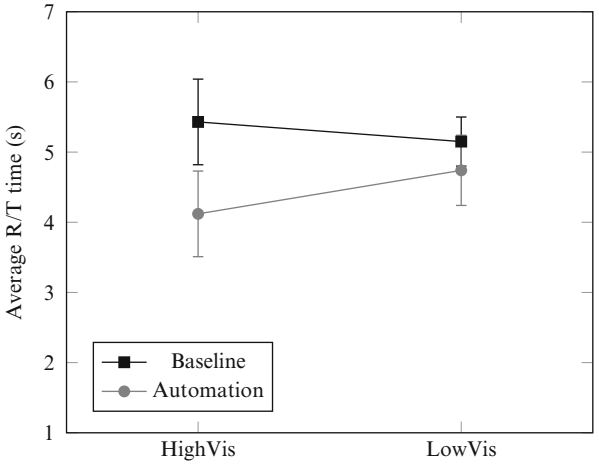

Fig. 8 Average R/T time: interaction between *visibility* and *procedure*

The seven items with levels between *none* (0) and *extreme* (6) had a good internal consistency of Cronbach's $\alpha = 0.88$ and thus were aggregated to an overall workload score. *Visibility* was highly significant for the workload assessment with $F(1,5) = 105.54$, $p < 0.01$, $f = 4.61$, $(1-\beta) = 1.00$ with higher scores in LowVis conditions ($M = 2.92$ ($SE = 0.18$)) compared to HighVis conditions ($M = 2.29$ ($SE = 0.19$)). *Procedure* was significant as well with $F(1,5) = 17.13$, $p < 0.01$, $f = 1.85$, $(1-\beta) = 0.91$ and higher mean score for the baseline procedures ($M = 3.38$ ($SE = 0.16$)) than for the automated procedures ($M = 1.83$ ($SE = 0.33$)). The interaction between *visibility* and *procedure* was statistically significant with $F(1,5) = 8.90$, $p < 0.05$, $f = 1.33$, $(1-\beta) = 0.67$. As Fig. 9 depicts, visibility conditions were influential in baseline procedures, whereas in automated procedures workload leveled quite similarly with $M_{\text{HighVis}} = 1.65$ ($SE_{\text{HighVis}} = 0.31$) and $M_{\text{LowVis}} = 2.01$ ($SE_{\text{LowVis}} = 0.34$).

Situational awareness was appraised with three items with the levels *never* (0) and *always* (6), which did not interrelate well (Cronbach's $\alpha = 0.59$). Thus, ANOVA were calculated for each item separately. The *awareness for the own position* varied significantly with *procedure*: $F(1,5) = 11.16$, $p < 0.05$, $f = 1.50$, $(1-\beta) = 0.76$, with higher scores for automated procedures ($M = 5.86$ ($SE = 0.07$)) compared to baseline procedures ($M = 4.92$ ($SE = 0.27$)). *Visibility* and the interaction between *procedure* and *visibility* were non-significant. The *awareness of other traffic in the vicinity* varied significantly with *visibility* with $F(1,5) = 10.97$, $p < 0.05$, $f = 1.48$, $(1-\beta) = 0.75$ and *procedure* with $F(1,5) = 10.23$, $p < 0.05$, $f = 1.43$, $(1-\beta) = 0.73$. In good visibility, the pilots rated to be more aware of other traffic ($M = 4.78$, $SE = 0.30$) than in low visibility ($M = 3.76$, $SE = 0.28$). Automated procedures increased the awareness for other traffic ($M = 5.25$, $SE = 0.10$) compared to the baseline procedures ($M = 3.29$, $SE = 0.55$). The interaction between the factors

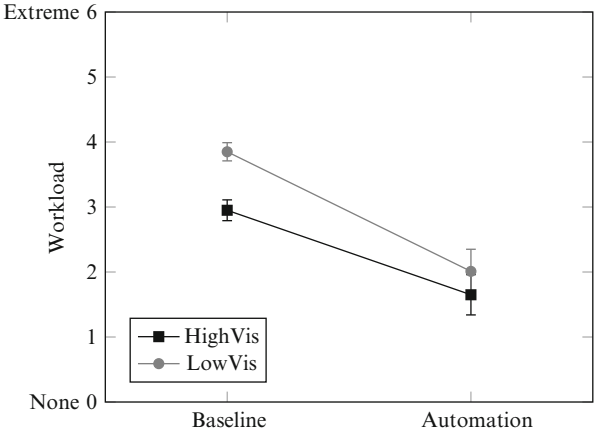

Fig. 9 Average workload ratings: interaction between *visibility* and *procedure*

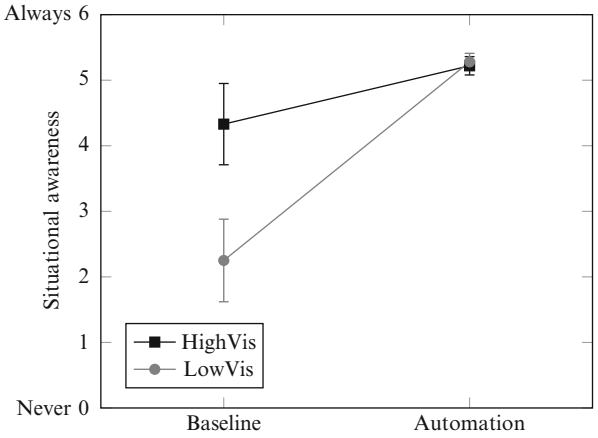

Fig. 10 Average ratings for situational awareness: interaction between *visibility* and *procedure* for item *I was aware of other traffic*

was significant as well with $F(1,5) = 12.33$, $p < 0.05$, $f = 1.57$, $(1-\beta) = 0.80$ (cf. Fig. 10). There were no significant effects for the third item, which related *to being surprised by unexpected events*.

The perceived support addressed the assistance in inbound and outbound processes by data link communication, AGL, and ODU. The assistance devices were assessed via single items with the levels *absolutely inappropriate* (0) and *absolutely appropriate* (6). Naturally, there were only a few answers for baseline conditions. The remaining completed visibility conditions with automated procedures were analyzed via t-test for paired comparisons. There were no significant differences between visibility conditions for data link communication with $t(17) = 0.42$,

$p = 0.68$, $d = 0.00$, AGL with $t(17) = -0.20$, $p = 0.85$, $d = 0.00$, and ODU with $t(17) = 1.53$, $p = 0.15$, $d = 0.00$. Comparisons between baseline and automation for both LowVis conditions were significant by tendency for AGL with $t(8) = -2.68$, $p = 0.03$,[6] $d = 1.00$, i.e. the support via AGL was rated higher in automated procedures than in baseline procedures. For the ODU, there was no significant difference between the two procedures in LowVis conditions with $t(7) = -1.17$, $p = 0.28$, $d = 0.00$.

5.4 Pilots' Comments

The onboard systems were assessed positively for baseline (9 out of 10) and automated procedures (16/25).[7] The moving map was stated to support situational awareness. AGL was not commented much, if so however, it received positive statements (e.g. *"intuitive lighting guidance"*). There were several suggestions for improvements of automated procedures, e.g. the usage of sound signals for changing taxi clearances in the ODU and possibilities for more requests in automated communication. Overall, the pilots were skeptic to rely on data link communication only, because they expect a reduction of situational awareness.

We received several critical comments to standard procedures (8/12) and communication (9/11) with pseudo-controllers, e.g. *"taxi-clearance was not precise"*. Pilots stated that the *"controllers were not completely used to standard phraseology"*.

6 Conclusions and Outlook

A concept of operations focusing on a higher level of automation in ground traffic management and visual guidance was introduced. It represents one possible solution to meet the future requirements concerning the expected growth in European air traffic. An evaluation study was conducted within a spatially distributed simulation environment in order to validate certain aspects of the operational concept with its respective systems and procedures from flight deck perspective.

We observed several positive effects with regard to our hypotheses: Automated procedures were frequently rated more advantageous in terms of perceived safety,

[6]Due to alpha-error inflation with multiple t-tests, a significance level of 0.025 was set as alpha-error correction.

[7]Example: *"Moving Map surely helps to improve pilots' situation awareness. Nevertheless the previous scenario* [LowVisAuto, A/N] *with an operable ALGS* [AGL, A/N] *in combination with an OBGS* [ODU, A/N] *made the whole operation safer and more effective. Misunderstandings with ATC confused us many times whereas the OBGS gave clear advices."*

workload, and efficiency than baseline procedures. Visibility only affected workload and the awareness for other traffic in that low visibility increased perceived effort and decreased the respective perception. However, some of the positive effects of automated procedures may have been due to the reported misunderstandings between pilots and pseudo-controllers in standard procedures.

R/T communication was reduced in automated procedures compared to the baseline scenarios. This might seem not surprising, because in automated procedures data link was applied for most communication processes. However, in badly designed automated procedures and with necessary switches between types of communication for requests, R/T time might have leveled the same for automated and baseline procedures or might even have been increased with automation. This was not the case in our study. Pilot comments suggest, however, that certain information should still be transmitted via voice in order to support situational awareness. Here, mere reduction of R/T time will not suffice as supportive argument for high levels of automation.

Overall, the distributed simulation was assessed as feasible and sufficiently realistic for research regarding operational procedures by the participating partners. As the concept was evaluated from flight deck point of view, a supplementary study with controllers or a full study with operators from both sites, air and ground, will yet have to show the benefits for ATC and the interaction between controllers and pilots regarding usability, acceptance, and workload.

Concerning the fully-automated taxi operations, the concept of operations is still under development. Once completed, a next step is to investigate the concept with specific scenarios with fully-automated procedures. Especially the drawbacks of a high level of automation with regard to the controller have to be thoroughly explored before a system providing for such procedures can come into effect.

Acknowledgements The ROLF project has been partially funded by the German Federal Ministry of Economics and Technology within the German Aeronautical Research Program (LuFo IV).

The authors would like to thank all ROLF partners and subcontractors for their support and trustful cooperation enabling this research (main contribution):

- ADB Airfield Solutions
- ATRiCS GmbH (ATC simulator, SMAN, ICWP, outside view, traffic simulator)
- DFS Deutsche Flugsicherung GmbH (ConOps)
- Diehl Aerospace GmbH (cockpit simulator, CDS, data link protocol, voice communication system)
- Fraport AG (ConOps)
- iAd GmbH (data link hardware)
- Jeppesen GmbH (EFB, AMDB)
- HFC Human-Factors-Consult GmbH (ConOps, pilot-data analysis)
- Institute of Flight Guidance, TU Braunschweig (cockpit simulator, CDS, voice communication system, RMP software)
- Institute of Flight Systems and Automatic Control, TU Darmstadt (cockpit simulator)

We would also like to give a special thanks to the airline pilots who participated in our simulation study for their valuable feedback.

References

1. ARINC (2006) Embedded interchange format for airport mapping database, ARINC Specification 816. Aeronautical Radio, Inc., Annapolis, MD
2. Bühner M, Ziegler M (2009) Statistik für Psychologen und Sozialwissenschaftler. Pearson, München
3. EUROCONTROL (2010) Long-Term Forecast: IFR Flight Movements 2010–2030. EUROCONTROL Statistics and Forecast Service (STATFOR)
4. Feuerle T, Kocks S, Hoffmann U, Langer B, Lutz A, Gärtner M (2008) Onboard display with data link connection. In: International symposium on precision approach and performance based navigation (ISPA), Bonn
5. Goillau P, Kelly C, Boardman M, Jeannot E (2003) Guidelines for Trust in Future ATM Systems: Measures. EUROCONTROL EATMP Guideline
6. ICAO (2004) Advanced Surface Movement Guidance and Control Systems (A-SMGCS) Manual, Doc 9830, 1st edn. International Civil Aviation Organization
7. Pschierer C, Sindlinger A, Barraci N, Wiesemann T, Gärtner M, Schiefele J (2011) Next generation EFB applications. In: Proceedings of the SPIE defense & security symposium, vol 8042, Orlando, FL
8. SESAR Consortium (2012) European ATM master plan—the roadmap for sustainable air traffic management, 2nd edn
9. Sindlinger A, Zimmer N, Wiesemann T, Li R, Andersson M, van der Stricht S (2010) Automated NOTAM processing for a graphical and textual integration on data link equipped aircraft. In: Integrated communications navigation and surveillance (ICNS) conference, Herndon, VA
10. Urvoy C, Oehme A, Drege C, Sendobry A, Klingauf U (2010) Conceptual validation of advanced pilot guidance-systems — a field test report. In: Proceedings of the 11th IFAC symposium on analysis, design, and evaluation of human-machine systems, Valenciennes, pp. 356–361
11. Wickens CD, Mavor A, Parasuraman R, McGee J (eds) (1998) The future of air traffic control: human operators and automation. National Academies Press, Washington, DC

A Visualization Tool for Analyzing Task Demands in En-Route Air Traffic Control

Daisuke Karikawa, Hisae Aoyama, Makoto Takahashi, Kazuo Furuta, and Masaharu Kitamura

Abstract For achieving effective utilization of advanced air traffic operation systems such as Air Traffic Flow Management (ATFM), harmonization with control activities of Air Traffic Control Officers (ATCOs) is one of the key issues to be tackled. In the present research, a process visualization tool of ATC tasks called COMPASi (COMPAS in interactive mode/COMPAS: COgnitive system Model for simulating Projection-based behavior of Air traffic controllers in dynamic Situations) has been applied to analyze the effects of air traffic flow control on ATC task demands. Through simulation-based experiments using COMPASi, beneficial and adverse effects of air traffic flow control on ATC task demands were successfully demonstrated in a couple of traffic situations where different control strategies of an ATCO were adopted. This result has indicated the applicability of COMPASi as a support tool for evaluating the effectiveness of ATFM with consideration of controllers' working methods.

Keywords Air traffic control • Air traffic flow management • Human factors • Visualization

D. Karikawa (✉) • H. Aoyama
Electronic Navigation Research Institute, 7-42-23 Jindaijihigashi-machi, Chofu, Tokyo 182-0012, Japan
e-mail: d-karikawa@enri.go.jp

M. Takahashi
Graduate School of Engineering, Tohoku University, Sendai, Japan

K. Furuta
Graduate School of Engineering, The University of Tokyo, Tokyo, Japan

M. Kitamura
Research Institute for Technology Management Strategy (TeMS), Sendai, Japan

Electronic Navigation Research Institute (ENRI), *Air Traffic Management and Systems*, Lecture Notes in Electrical Engineering 290, DOI 10.1007/978-4-431-54475-3_8,

1 Introduction

Rapid increase in air traffic demands in recent years requires higher levels of safety and efficiency of air traffic operations. In response to the increasing amount of air traffic, Air Traffic Management (ATM) involving advanced management of airspace, air traffic flow and capacity is being introduced in addition to traditional sector-based traffic control. One component of ATM is Air Traffic Flow Management (ATFM). ATFM aims at enhancing air traffic efficiency and reducing the workload of controllers in each sector by applying time-based control to air traffic at departure airports and specific points.

However, regardless of the introduction of ATFM, features and characteristics of Air Traffic Control (ATC) tasks in each sector are almost the same. Air Traffic Controllers (ATCOs) in charge of sectors are required to deal with multiple aircraft at the same time in constantly changing air traffic situations and weather conditions. For completing multiple controlling tasks safely in such a task environment, a controller needs to regulate task demands in his/her task execution process by adopting an appropriate air traffic control strategy, which can lead to the saving of the controller's cognitive resources for responding to unexpected situation changes. Thus, the authors consider that the effects of ATFM on working methods of controllers should be carefully analyzed as a part of the evaluation of ATFM. Mismatches between air traffic flow control by ATFM and a control strategy of an ATCO may lead to additional ATC task demands and put burden on the controller.

There is a lot of research aiming to reveal cognitive aspects of controllers. Rantanen et al. [1] and Yang et al. [2] conducted experimental studies with emphasis on controllers' temporal awareness affecting task prioritization and task performance. Several research works have analyzed features of controllers' conflict judgment [3–6]. However, there are only a few research efforts focusing on concrete and dynamic control activities of ATCOs such as adaptation of their working methods corresponding to traffic situations [7, 8]. In addition, a support tool that is capable of analyzing a controller's working methods is not common. Thus, the authors have developed a process visualization tool of ATC tasks for the purpose of analyzing ATCO's control activities and their effects on traffic flow. The process visualization tool called COMPASi (COMPAS in interactive mode/COMPAS: COgnitive system Model for simulating Projection-based behavior of Air traffic controllers in dynamic Situations) has functions to detect ATC tasks in a changing traffic situation and visualize them using color codes. The basic validity of COMPASi was evaluated through detailed comparison of two visualization results of ATC tasks: one was by COMPASi and the other was by an ATC training instructor [9]. COMPASi was also applied to a performance comparison of two different control strategies for the same traffic scenario [10].

The purpose of the present research is to examine applicability of COMPASi for evaluating effectiveness of ATFM with consideration of controllers' working methods. Several combinations of traffic situations and controllers' working methods with and without flow control by ATFM were simulated on COMPASi and analyzed

based on ATC task demands. The rest of this paper is organized as follows. First, a brief explanation of en-route ATC tasks and target sector is presented (Sect. 2). Second, the overview of COMPASi is introduced (Sect. 3). Third, simulation results are presented and discussed (Sects. 4 and 5).

2 En-Route ATC Tasks and Target Sector

En-route air traffic control is a part of ATC services provided for in-flight aircraft. In en-route control, a team of controllers takes charge of a divided airspace called a "sector". The present research has adopted an actual sector, i.e., Kanto-North (T03) sector in Japan, as the target sector. This chapter introduces a brief summary of the en-route ATC tasks and describes features of air traffic flow in sector T03.

The ATC tasks have two major purposes: to ensure the safety and efficiency of air transportation. The primary goal is to achieve the maintaining of safety by assuring a minimum separation of 5 nautical miles (NM) horizontally or 1,000 ft vertically between aircraft. Figure 1 shows sector T03 which is the northern part of the Tokyo region in Japan. The size of sector T03 is approximately 120×120 NM. The small white circles labeled with capital letters, i.e., GLAXY, SWAMP, and TLE, in Fig. 1 indicate geometrical points called fixes that are used for aiding in air navigation. Two hub airports, Tokyo (Haneda) International Airport and Narita International Airport, are located southward of sector T03. In addition, multiple smaller airports and air force bases are located in the surrounding area of this sector. Furthermore, overflight aircraft between North America and East Asia pass through this sector in an east–west direction. Thus this sector provides ATC services to various kinds of commercial and military flights as listed below:

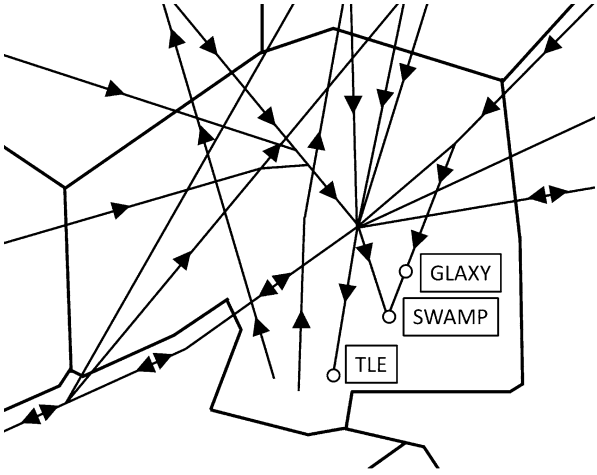

Fig. 1 Major traffic flows in T03 sector [9]. *Black triangles* indicate flight directions of aircraft on respective airways

- Departure/arrival flights from/to Tokyo airport and Narita airport (traffic flows in a north–south direction)
- Departure/arrival flights from/to other smaller airports and air force bases located in/around sector T03 (traffic flows in multiple directions)
- Overflight aircraft (traffic flows in an east–west direction)

In addition to assure minimum separation, regulations require an ATCO of sector T03 to achieve additional targets of altitude and separation of aircraft. For example, an aircraft arriving at Tokyo airport has to establish a 10 NM in-trail separation from another aircraft arriving at the same airport and also has to reach 13,000 ft by the TLE point (see Fig. 1). In order to achieve the target states of aircraft, the ATCO can issue speed, altitude, and heading/re-route instructions to the aircraft.

3 COMPASi

This chapter shows a brief description of COMPASi, a visualization tool of ATC tasks used in the present research.

3.1 Overview

COMPASi is a kind of PC-based ATC simulation tool equipped with a situation awareness model of a controller that is capable of detecting ATC tasks in a given traffic situation. Figure 2 shows the conceptual diagram of COMPASi. Given the initial states of traffic (e.g. aircraft's initial position, altitude, indicated air speed, and so on) and the log of ATC instructions, the COMPASi simulates air traffic flow with continuous performance calculation of aircraft and issuing of ATC instructions based on the instruction log file which contains altitude, speed, heading, reroute instructions to respective flights and the time of their issuance. The situation awareness model equipped with COMPASi analyzes a simulated air traffic situation and automatically detects ATC tasks in the situation. The detected tasks and issued ATC instructions are outputted as a time series graph (see Fig. 4). The graph illustrates issued ATC instructions and situation changes resulting from the instructions along the timeline, which is a visualization of the ATC task process. Further details of COMPASi are described in [9].

3.2 ATC Task Index

The ATC task index is an index for identifying ATC tasks and their execution states. Table 1, entitled "Task Demand Levels (TDL)", shows the ATC task levels used

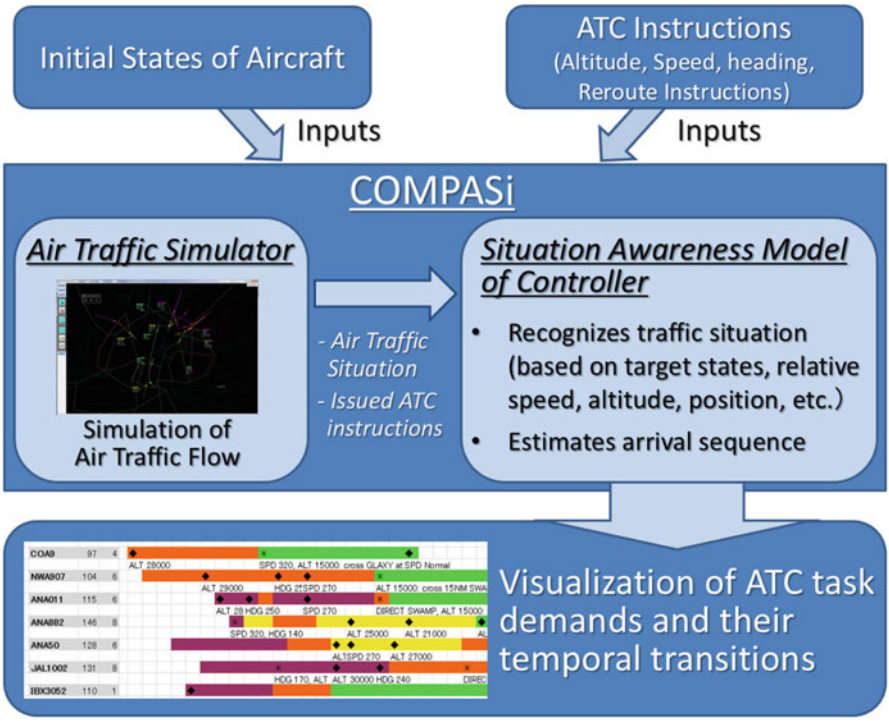

Fig. 2 Conceptual scheme of COMPASi [11]

Table 1 Task demand levels (adapted from [12])

Lv.	Situation/task demand	Display color on COMPASi
4	Time-critical situation in terms of conflict resolution(s)	Red
3+	Multiple separation assurances [conflict resolution(s)/in-trail spacing] between the target aircraft and two or more related aircraft	Magenta
3	Separation assurance (conflict resolution/in-trail spacing) between the target aircraft and one related aircraft	Orange
2	Altitude change	Yellow
1	(ATC tasks are completed)	Green

in the present research proposed by an experienced ATC training instructor in our research group [12, 13]. COMPASi detects ATC tasks based on TDL. TDL consists of four levels reflecting necessary ATC tasks for each aircraft as listed below:

- Lv. 1 indicates that all required ATC tasks for the target aircraft in the sector are completed.
- Lv. 2 indicates a local situation in which the target aircraft requires altitude change.

- Lv. 3 indicates a local situation in which the target aircraft requires a separation assurance task to be completed for conflict resolution or in-trail spacing.
- Lv. 3+ indicates multiple separation assurance tasks between the target aircraft and two or more related aircraft.
- Lv. 4 indicates a potentially risky situation that is a time-critical condition in terms of conflict resolution. The time horizon of Lv. 4 (3.5 min before loss of minimum separation occurs) is determined by the conflict alert displayed in an ATC console, which activates 3 min before loss of minimum separation occurs.

Aircraft coming from an upstream sector have various task levels ranging from Lv. 1 to Lv. 3+. By completing necessary ATC tasks in the sector, the TDL of each aircraft lowers to Lv. 1. In other words, TDLs of all aircraft have to be Lv. 1 before they enter a downstream sector.

TDLs can be utilized for comparative analyses of ATCO's control strategies in terms of safety and efficiency by specifying ATC tasks in an air traffic situation and their temporal transitions, which is called "Task Demand Level based performance Analysis (TDLA)" in this paper. For example, potential risk of loss of separation between aircraft is shown by TDLs at or above Lv. 3, i.e., Lv. 3, Lv. 3+, and Lv. 4. Thus, the durations, accumulations, and resolutions of these levels can reflect the effectiveness of proactive risk management of an ATCO, e.g., conflict prevention. In addition, since greater levels of TDLs generally indicate more complex tasks, the decrease of TDLs possibly implies the effectiveness of the ATCO's workload management by regulating task demands.

In order to evaluate the effectiveness of TDLA, it was applied to an analysis of results of a Human-In-the-Loop Simulation (HILS) experiment with professional participants [12]. Through the analysis, TDLA successfully visualized differences in task performance caused by varieties in adopted control strategies.

3.3 Input and Output

For simulating air traffic flow, COMPASi requires a set of aircraft performance data, flight plans, and inputs of ATC instructions. Aircraft performance data and flight plans are stored in Excel files. Thus, a user of COMPASi can easily modify contents in those files to change simulation settings. A flight plan contains data of an aircraft's initial position, altitude, speed, flight planned route, etc. ATC instructions, i.e., altitude, heading, speed, and re-route instructions to aircraft, can be issued automatically based on an instruction data file containing sets of timing and contents of ATC instructions. They can be also manually input by a user during a simulation run for modifying ATC instructions and traffic situations for the purpose of comparative analysis.

One of the output data from COMPASi is TDL. TDL of each aircraft is provided in two forms: color-coded call sign and lateral trajectory on a simulated radar display (Fig. 3), and a time series graph called Chart of ATC task Processing State (CAPS)

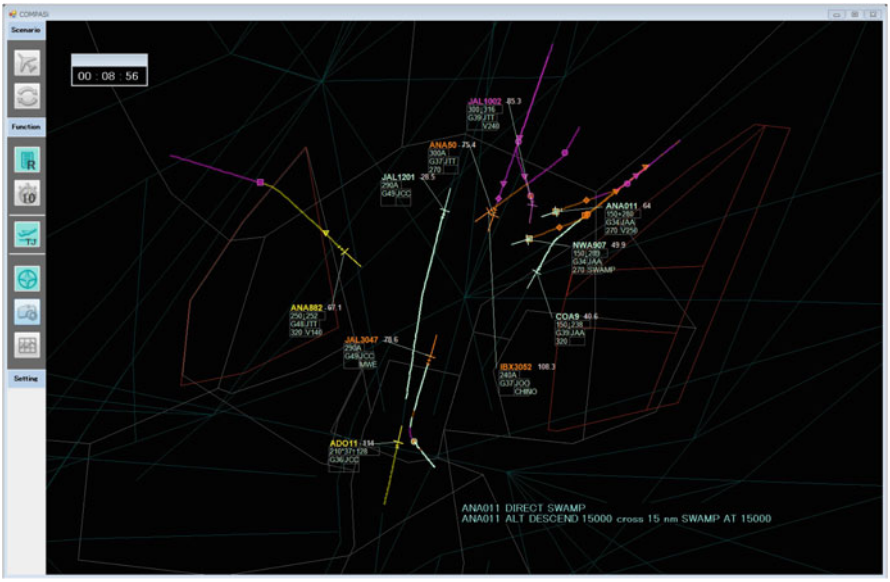

Fig. 3 Screenshot of COMPASi

(Fig. 4). CAPS also contains information of the contents and timings of ATC instructions [Fig. 4(1)], flight distance [Fig. 4(2)], and the number of instructions [Fig. 4(3)]. In addition, for supporting macroscopic evaluation of efficiency of air traffic flow, sums of flight distances and issued instructions are given for each flight type such as departure flights, arrival flights, over flights, and so on [Fig. 4(4)]. TDL and the number of instructions can reflect efficiency of ATC from the viewpoint of a controller. On the other hand, flight distance can reflect the efficiency of ATC from the viewpoints of a pilot since it is a major factor affecting fuel consumption of aircraft.

4 Simulation-Based Experiment

This chapter describes simulation-based experiments conducted to examine the applicability of COMPASi as a support tool for analyzing the effects of ATFM on ATC task demands. For the experiments, three examples of traffic situations including with and without flow control by hypothetical ATFM and two control strategies of ATCOs were prepared. Our basic assumption is that if COMPASi can visualize the difference of task demands resulting from combinations of control options of flow control and ATCO's control strategies, then COMPASi has the possible applicability as an analysis tool for identifying what types of traffic situations should be made or avoided by ATFM with consideration of controllers'

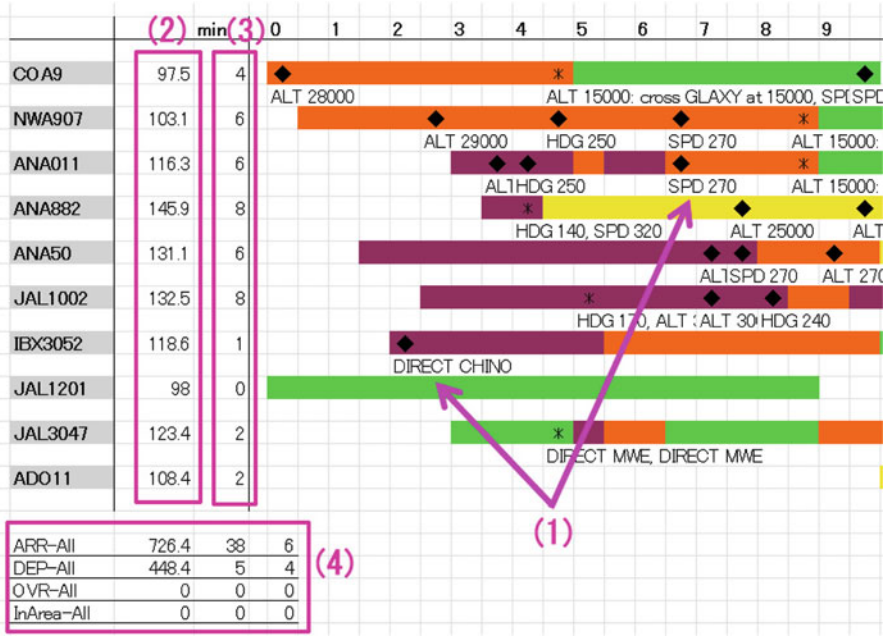

Fig. 4 Example of CAPS. (*1*) issued ATC instructions, (*2*) flight distance (each aircraft), (*3*) the number of ATC instructions (each aircraft), (*4*) the sums of flight distances, issued instructions, and the number of aircraft (each flight type)

working methods. A part of the results of the simulation-based experiments has already been reported in our previous research [14]. In this paper, findings of the previous research are summarized in Sect. 4.2. Simulation results of the present experiment are described in Sect. 4.3.

4.1 Traffic Scenario

Figure 5 shows a traffic scenario used in the simulation-based experiments. The scenario is a part of the air traffic scenario used in HILS research [13]. As illustrated in Fig. 6, the experiment simulated the effects of ATFM on air traffic by the modification of the traffic scenario. For example, a time-based control of a specific aircraft by ATFM that yields a 30 s delay can be simulated by moving the initial position of the aircraft back by 5 NM (which corresponds to the distance the aircraft flies in a little over 30 s).

As shown in Fig. 5, inbound flights are coming from upstream sectors to the target sector (sector T03). COA9, NWA907, and ANA011 are flights arriving at Narita International Airport. ANA882, ANA50, and JAL1002 are ones arriving at

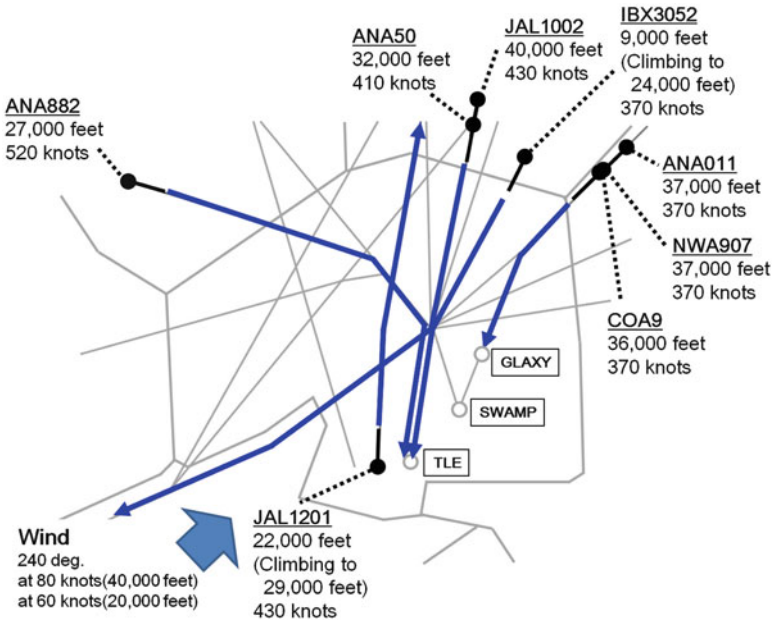

Fig. 5 Traffic scenario. Additional departure flights from Tokyo airport and Narita airport (ADO11 and JAL3047) appear several minutes later

Tokyo International Airport. In addition, departure flights from Tokyo airport, Narita airport (additional two flights, i.e., JAL3047 and ADO11, appear several minutes later), and Sendai airport exist around the south and north-east boundaries of the target sector. A controller in charge of sector T03 has to achieve target states of these aircraft following regulations while continuously assuring the minimum separation (1,000 ft vertical or 5 NM lateral). The simulated wind condition is 240° at 80 knots at 40,000 ft and 60 knots at 20,000 ft. The traffic scenario involves the following ATC tasks:

- Altitude change: Descent/climb clearance has to be issued to each aircraft so that the aircraft can reach its target altitude before passing specific geometrical points.
- In-trail spacing: 10 NM in-trail separations have to be assured for two aircraft groups consisting of three aircraft each. The Narita airport inbound flights are flying on the same airway. On the other hand, the Tokyo airport inbound flights are coming from different directions. In addition, JAL1002 (the following aircraft) is catching up to ANA50 (the leading aircraft) because the ground speed of JAL1002 is faster than that of ANA50.
- Conflict resolution: Expected lateral and vertical flight paths of departure flights intersect with those of some arrival flights. In such cases, ATC instructions are required to resolve conflicts for the purpose of assuring the minimum separation and achieving target states of each flight.

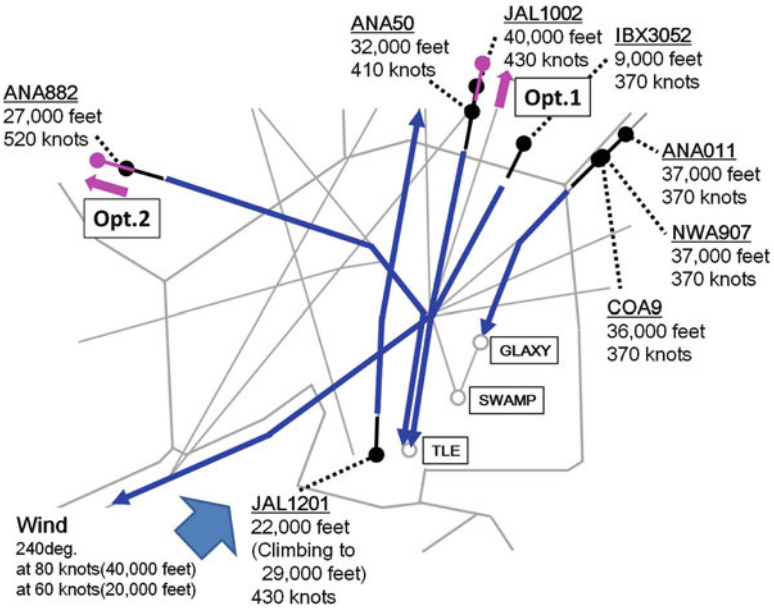

Fig. 6 Modification of traffic scenario for simulating ATFM

As described above, the traffic scenario covers somewhat diverse traffic situations including an aircraft group coming from multiple directions and a "catch-up" situation (following aircraft JAL1002 is faster than leading aircraft ANA50). It also contains all types of major ATC tasks listed in Table 1.

4.2 Experiment 1

This section summarizes the results of Experiment 1 conducted in our previous research [14]. In Experiment 1, two control options of ATFM affecting in-trail spacing tasks of three flights arriving at Tokyo airport, i.e., ANA882, ANA50, and JAL1002, were examined. The first option (Opt. 1) is that a 30 s delay is given to JAL1002 by ATFM (the situation was simulated by moving the initial position of JAL1102 back by 5 NM). The second one (Opt. 2) is that 30 s delay is given to ANA882, which is simulated by moving the initial position of ANA882 back by 5 NM. The simulated ATCO's control strategy for flights arriving at Tokyo airport is to line them up in the order of ANA882, ANA50, and JAL1002 for in-trail spacing. In order to achieve this sequence, flight distance of ANA882 is shortened by a shortcut instruction, while that of JAL1002 is extended by a radar vector instruction (Fig. 7). The control strategy described above is called "Strategy A (ST-A)" in this paper. Three cases of simulations listed in Table 2 were conducted in Experiment 1.

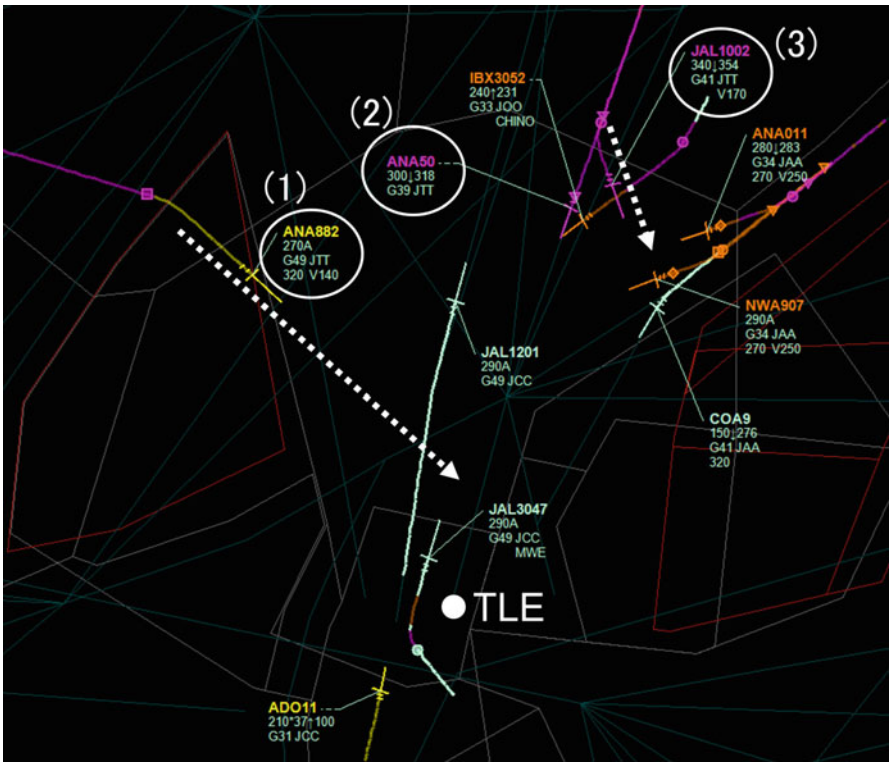

Fig. 7 Control Strategy A [11] adopted in Experiment 1. *Dotted arrows* indicate flight directions of ANA882 and JAL1002 following ATC instructions. The *numbers* indicate the arrival sequence of the Tokyo airport inbound flights

Table 2 Simulation cases in Experiment 1

	Control strategy	ATFM
Baseline Case A	ST-A	No
Case 1A	ST-A	Opt. 1
Case 2A	ST-A	Opt. 2

According to the comparison of Fig. 8 (Baseline Case A) and Fig. 9 (Case 1A), preventive and/or rapid decreases of TDLs were achieved by Opt. 1 of ATFM (Case 1A) as shown in Fig. 9 (1)(2). On the contrary, as indicated in Fig. 10 (3)(4), Opt. 2 of ATFM (Case 2A) caused Lv. 4 of TDL indicating a potential loss of minimum separation between ANA882 and ADO11 which did not appear in Baseline Case A. That is, Opt. 1 of ATFM harmonized with the ATCO's control strategy and contributed to reducing task demands. Opt. 2, on the other hand, conflicted with the ATCO's control strategy and caused additional task demands. This fact indicated that the appropriate combination of a control option of ATFM and the ATCO's control strategy is a key factor in achieving effective reductions in ATC task demands.

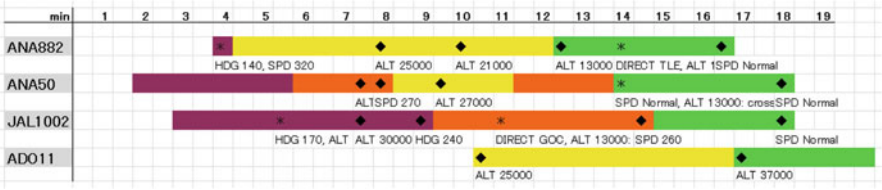

Fig. 8 CAPS of Baseline Case A

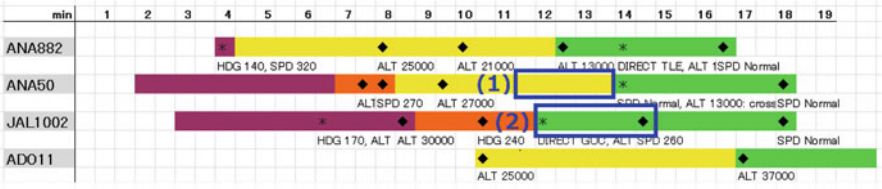

Fig. 9 CAPS of Case 1A. Boxes (*1*) and (*2*) indicate preventive and/or rapid decreases of TDLs by Opt. 1 of ATFM

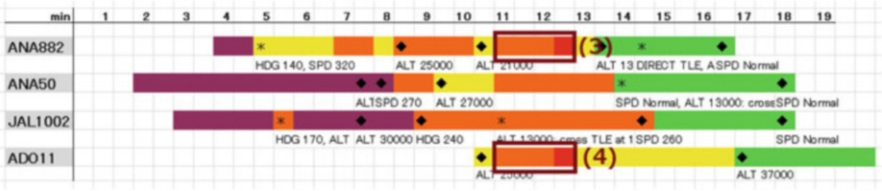

Fig. 10 CAPS of Case 2A. Boxes (*3*) and (*4*) indicate increases of TDLs by Opt. 2 of ATFM

4.3 Experiment 2

In addition to simulation cases in Experiment 1, further combinations of control options of ATFM and ATCO's control strategies were examined. The traffic scenario and two control options of ATFM used in Experiment 2 are completely the same as those in Experiment 1, but the control strategy for flights arriving at Tokyo airport is different. The control strategy adopted in Experiment 2 is to line up flights arriving at Tokyo airport in the order of ANA50, JAL1002, and ANA882. To achieve the sequence, ANA882 was vectored in an eastward direction so as to follow JAL1002 (Fig. 11). In this paper, this control strategy is called "Strategy B (ST-B)". Simulation cases in Experiment 2 are listed in Table 3.

Figures 12–14 show time series graphs of TDLs in three cases described in Table 3. In cases where ST-B was adopted, both of the two options of ATFM contributed to reducing task demands.

According to the comparison of Fig. 12 (Baseline Case B) and Fig. 13 (Case 1B), Opt. 1 of ATFM (Case 1B) lowered the TDL of ANA50 from Lv. 3+ to Lv. 3 at an earlier time frame than Baseline Case B as shown in Fig. 13 (1). Opt. 2 of ATFM

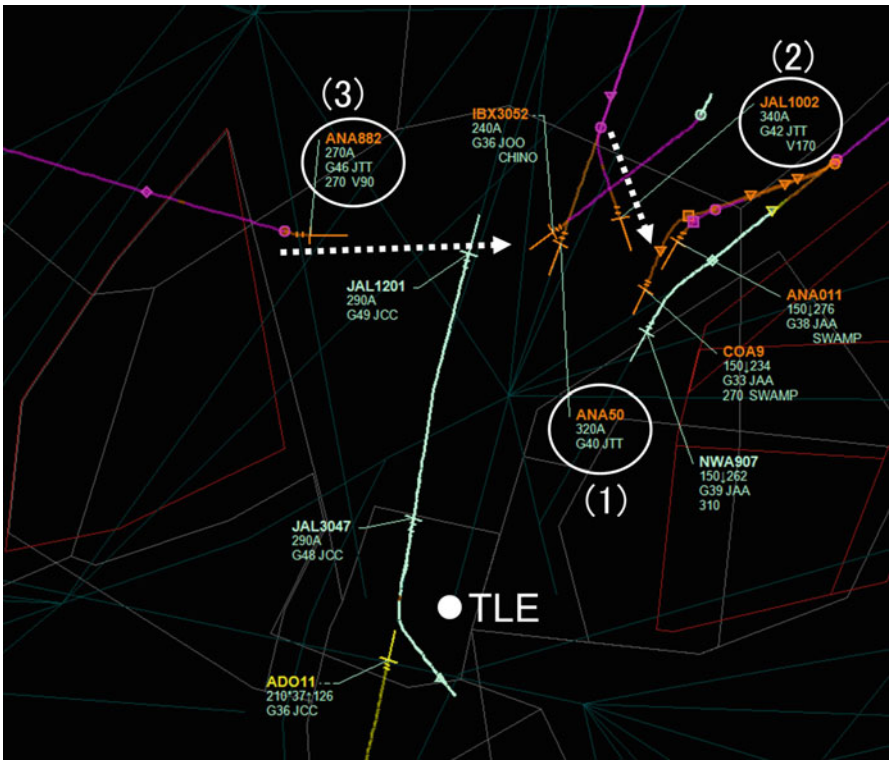

Fig. 11 Control Strategy B [11] adopted in Experiment 2. *Dotted arrows* indicate flight directions of ANA882 and JAL1002 following ATC instructions. The *numbers* indicate the arrival sequence of the Tokyo airport inbound flights

Table 3 Simulation cases in Experiment 2

	Control strategy	ATFM
Baseline Case B	ST-B	No
Case 1B	ST-B	Opt. 1
Case 2B	ST-B	Opt. 2

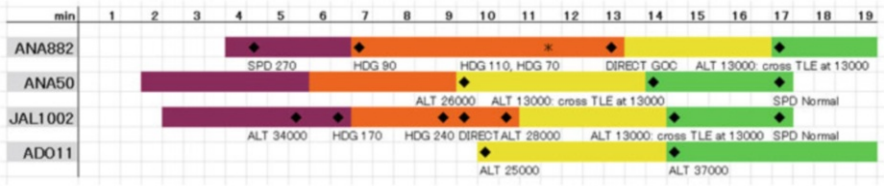

Fig. 12 CAPS of Baseline Case B

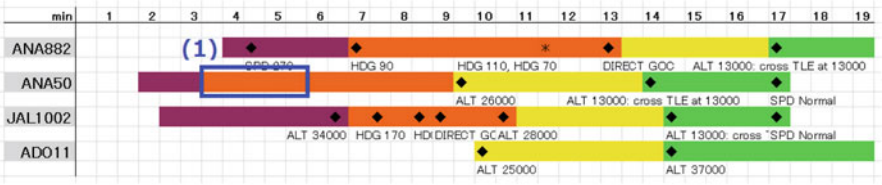

Fig. 13 CAPS of Case 1B. Box (*1*) indicates rapid decrease of TDL by Opt. 1 of ATFM

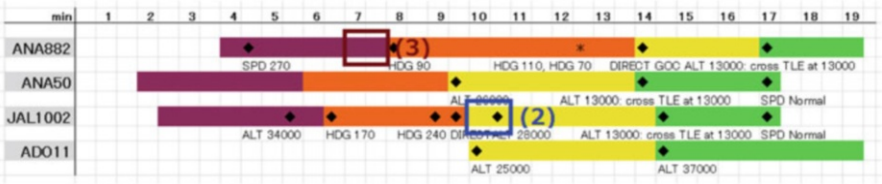

Fig. 14 CAPS of Case 2B. Boxes (*2*) and (*3*) indicate decrease and increase of TDLs respectively by Opt. 2 of ATFM

(Case 2B) also achieved an earlier drop of the TDL of JAL1002 from Lv. 3 to Lv. 2 [Fig. 14 (2)] although the adverse effect, i.e., the increase of TDL caused by Opt. 2, occurred [Fig. 14 (3)]. The TDLs of the rest of the parts in Figs. 13 and 14 are almost the same as those in Baseline Case B.

The effects of ATFM on ATC task demands in Experiment 2 are different from those in Experiment 1 although the traffic scenario and two control options of ATFM in both experiments are completely the same. This result demonstrates that COMPASi can visualize the difference of ATC task demands resulting from adopted control strategies.

5 Discussion

In Experiment 1 and Experiment 2, COMPASi successfully visualized beneficial and adverse effects of control options of ATFM on ATC task demands in a couple of traffic situations where different ATCOs' control strategies were adopted. This fact indicates the applicability of COMPASi as a supporting tool for analyzing ATC task demands under flow control by ATFM. As the results of both experiments have indicated, the appropriate combination of a control option of ATFM and the ATCO's control strategy is needed to achieve effective reductions in ATC task demands. Since COMPASi can analyze the difference of ATC task demands with consideration of ATCOs' control strategies, it may contribute to identify what types of traffic situations should be made or avoided by ATFM from controllers' position.

The simulation results also indicate the possibility that the introduction of ATFM may influence the choice of control strategies by ATCOs. Thus, ATCO's working

methods under ATFM should be carefully analyzed for supporting ATCOs, e.g., addressing human factor issues, providing necessary training programs, etc. The comparison of results of Experiment 1 and Experiment 2 has revealed that ST-B may have more tolerance or adaptability to situation changes caused by differences in control options of ATFM than ST-A. Nevertheless, it is very difficult to determine a recommended control strategy under flow control by ATFM in part because an appropriate control strategy strongly depends on the situation. For example, if JAL1002 is followed by another aircraft group arriving at Tokyo airport, adopting ST-B may cause additional tasks for in-trail spacing between the last aircraft in the arrival sequence of the leading group, that is ANA882 in ST-B, and the following aircraft group since ST-B requires a greater extension of flight distance of the last aircraft than ST-A. The authors consider that this kind of discussion for enhancing ATCOs' skills to the variety of situations should be emphasized in training programs for controllers working with ATFM.

6 Concluding Remarks

The present research attempted to visualize the effects of simulated flow control by ATFM on ATC task demands using COMPASi. In Experiment 1 and Experiment 2, beneficial and adverse effects of control options of ATFM on ATC task demands were analyzed in a couple of traffic situations where different control strategies of ATCOs were adopted. This fact has demonstrated the applicability of COMPASi as a support tool for evaluating the effectiveness of ATFM from the perspective of ATC task demands, and perhaps for estimating burden put on the controllers in the next-generation ATC environment including high density traffic and time-based air traffic management. Although we are still in the initial phase of these research projects, further analytical research using COMPASi will be conducted for exploring effective flow control methods of ATFM.

Acknowledgments The present research was supported by the Program for Promoting Fundamental Transport Technology Research of Japan Railway Construction, Transport and Technology Agency, and Grant-in-Aid for Scientific Research (B) 21310103 of the Japan Society for the Promotion of Science.

References

1. Rantanen EM, Yeakel SJ, Steelman KS (2006) Enroute controller task prioritization research to support CE-6 human performance modeling phase II: analysis of high-fidelity simulation data, Final technical report. Human Factors Division, University of Illinois. http://www.aviation.illinois.edu/avimain/papers/research/pub_pdfs/techreports/06-03.pdf
2. Yang J, Rantanen EM, Zhang K (2010) The impact of time efficacy on air traffic controllers situation awareness and mental workload. Int J Aviat Psychol 20(1):74–91. doi:10.1080/10508410903416037

3. Bisseret A (1981) Application of signal detection theory to decision making in supervisory control; the effect of the operator's experience. Ergonomics 24(2):81–94. doi:10.1080/00140138108924833
4. Rantanen EM, Nunes A (2005) Hierarchical conflict detection in air traffic control. Int J Aviat Psychol 15(4):339–362. doi:10.1207/s15327108ijap1504_3
5. Averty P (2005) Conflict perception by ATCS admits doubt but not inconsistency. In: Sixth USA/Europe air traffic management research and development seminar, Baltimore. http://www.atmseminar.org/seminarContent/seminar6/papers/p_105_HF.pdf
6. Loft S, Bolland S, Humphreys MS, Andrew N (2009) A theory and model of conflict detection in air traffic control: incorporating environmental constraints. J Exp Psychol Appl 15(2):106–124. doi:10.1037/a0016118
7. Sperandio JC (1971) Variation of operator's strategies and regulating effects on workload. Ergonomics 14:571–577
8. Fothergill S, Neal A (2008) The effect of workload on conflict decision making strategies in air traffic control. In: Proceedings of human factors and ergonomics society 52nd annual meeting, New York, pp 39–43
9. Karikawa D, Aoyama H, Takahashi M, Furuta K, Wakabayashi T, Kitamura M (2012) A visualization tool of enroute air traffic control tasks for describing controller's proactive management of traffic situations. Cogn Technol Work. doi:10.1007/s10111-012-0222-y
10. Karikawa D, Takahashi M, Aoyama H, Kitamura M, Furuta K (2011) A simulation-based analysis of "Resilience" in enroute air traffic control tasks. In: Proceedings of 4th symposium on resilience engineering, Sophia Antipolis, pp 135–141
11. Karikawa D, Aoyama H, Takahashi M, Furuta K, Ishibashi A, Kitamura M (2013) Analysis of the performance characteristics of controllers' strategies in en route air traffic control tasks. Cogn Technol Work. doi:10.1007/s10111-013-0268-5
12. Aoyama H, Iida H, Shiomi K (2010) An expression of air traffic controller's workload by recognition-primed decision model. In: Proceedings of 27th congress of international council of the aeronautical sciences, Nice, Paper ICAS 2010–11.10.2
13. Aoyama H, Iida H, Karikawa D (2010) Study on air traffic control system based on cognitive systems engineering IV (1). In: Proceedings of human interface symposium 2010, Kusatsu, pp 209–212
14. Aoyama H, Karikawa D, Iida H (2012) Development of resilience-oriented safety support methods (4). A consideration for evaluation and improvement of air traffic flow management. In: Proceedings of human interface symposium, Fukuoka, pp 53–58

Transitioning Resolution Responsibility Between the Controller and Automation Team in Simulated NextGen Separation Assurance

C.D. Cabrall, A.N. Gomez, J.R. Homola, S.M. Hunt, L. Martin, J. Mercer, and T. Prevot

Abstract As part of an ongoing research effort on separation assurance and functional allocation in NextGen, a controller-in-the-loop study with ground-based automation was conducted at NASA Ames' Airspace Operations Laboratory in August 2012 to investigate the potential impact of introducing self-separating aircraft in progressively advanced NextGen time-frames. From this larger study, the current exploratory analysis of controller–automation interaction styles focuses on the last and most far-term time frame. Measurements were recorded that firstly verified the continued operational validity of this iteration of the ground-based functional allocation automation concept in forecast traffic densities up to two times that of current day high altitude en-route sectors. Additionally, with greater levels of fully automated conflict detection and resolution as well as the introduction of intervention functionality, objective and subjective analyses showed a range of passive to active controller–automation interaction styles between the participants. Not only did the controllers work with the automation to meet their safety and capacity goals in the simulated future NextGen timeframe, they did so in different ways and with different attitudes of trust/use of the automation. Taken as a whole, the results showed that the prototyped controller–automation functional allocation framework was very flexible and successful overall.

Keywords Automation • Controller-in-the-loop • Functional allocation • NextGen • Separation assurance

C.D. Cabrall (✉) • A.N. Gomez • J.R. Homola • S.M. Hunt • L. Martin • J. Mercer
San Jose State University, NASA Ames Research Center, Moffett Field, CA, USA
e-mail: christopher.d.cabrall@nasa.gov; ashley.n.gomez@nasa.gov; jeffrey.r.homola@nasa.gov; sarah.m.hunt@nasa.gov; lynne.martin@nasa.gov; joey.mercer@nasa.gov

T. Prevot
NASA Ames Research Center, Moffett Field, CA, USA
e-mail: thomas.prevot@nasa.gov

Electronic Navigation Research Institute (ENRI), *Air Traffic Management and Systems*, Lecture Notes in Electrical Engineering 290, DOI 10.1007/978-4-431-54475-3_9,

1 Introduction

In the present day high altitude en-route environment of the United States National Airspace System, aircraft separation assurance is achieved by a highly labor intensive process of dutiful air traffic controllers on the ground. Monitoring the progress of aircraft across their display, the controllers scan their sector by watching each and every aircraft in order to identify potential separation risks and to mentally calculate conflict avoidance possibilities. From the time any aircraft checks in with one controller until it is handed off to the next, all clearances are devised mentally, manually, and individually by the controller and issued verbally over a radio frequency. With great scrutiny, attention, and positive personal control over each of the aircraft in their sector, en-route controllers have maintained a commendable safety record and contribute greatly to the overall US air traffic control system being the safest in the world [1].

Current forecasts by the Federal Aviation Administration (FAA) show continued growth in demand, in particular for the en-route centers, due to a faster growing commercial sector. The number of commercial aircraft is projected to grow from 2011 to 2032 at an average growth rate of about 1.5% or 127 aircraft annually. Similarly up to 2032, commercial IFR aircraft handled at FAA en-route centers has been projected to increase 2.4% annually [2]. These forecasts pose a problem for en-route controllers because they exceed monitor alert parameters (MAP) values which have been defined to limit the number of aircraft permitted in a sector as a safeguard prior to which performance is expected to decline. Natural cognitive processing limits of air traffic controllers have been accepted as potential bottlenecks against rising air traffic demand on account of the number of planes any person could reasonably be expected to track. Complementary to the FAA forecasts, the US Congress established the Joint Planning and Development Office (JPDO) to develop the Next Generation Air Transportation System (NextGen) which among its many visions, explicitly aims to overcome the capacity limits imposed by individually attended aircraft separation procedures of today and requires a restructuring of the roles of humans and automation and how they perform their respective functions to synergize human and automation performance [3].

To meet the forecast demand increase, separation management components of en-route NextGen environments are envisioned to rely on automation to augment human performance beyond today's limits by offloading workload from the human controllers onto automated functions for the majority of routine operations. Use of automated conflict detection and resolution decision aides that are seamlessly integrated within ground automation systems is planned to allow separation management tasks to move away from fixed human-based standards while always maintaining an unambiguous delegation of responsibility. Automation is anticipated to support a migration from tactical to strategic decision making as well as perform many routine tasks. With layers of protection that allow for graceful degradation of situations, automation reliance is planned to be coupled with modes that do not require full reliance on humans as backup. Building from today's current roles, the

corresponding NextGen roles for air traffic controllers that stand to benefit from use of automation include: identifying complex future conflicts, management of individual aircraft trajectories, and detecting and resolving conflicts via automation while eliminating residual conflicts [3]. Use of data communications that are integrated with ground automation is envisioned to reduce the number of voice communications and controller workload, and hence increase the controller's efficiency and ability to manage more traffic [4]. While providing tactical and strategic separation management, en-route trajectory based operations (TBO) automation is planned to provide the ability to request modifications of trajectories and support trajectory negotiation [5].

However, relying on automation to fully or partially replace a function previously carried out by a human operator means that automation need not be all or none, but can vary across a continuum of levels, from the lowest level of fully manual performance to the highest level of full automation. Furthermore, the specific function with its variant level of manual/automatic control, itself can range along a variety of human information processing sub-tasks or stages [6]. As a simple example, the function of detecting a conflict could be fully automatic, fully manual, or somewhere in between and this could exist along with different levels of automation for the subsequent separate function of conflict resolution, which could itself be fully automatic, fully manual, or somewhere in between. It has been shown that the flexibility of an automation system contributes to its use case as task load and complexity increase [7].

In addition to being flexible and multi-layered, other beneficial design factors can encourage effective trust and use within human–automation systems. Recent research suggests that humans respond socially to technology and reactions to computers can be similar to reactions to human collaborators [8]. In commonly observed effective human teamwork and collaboration, both parties walk a line to balance what they perceive the other is capable of while they, themselves, exhibit evidence of their own reliability in handling certain tasks. In general, someone's capability with simpler tasks is commonly held to reflect their capability with more complex tasks. Research on system credibility established within the context of simple decision tasks has been conducted and has shown that operators who experience an automated system's failures in easy tasks are less likely to comply with the automation's recommendations during a more difficult task [9]. Rather than taken on immediate face value, automation is scrutinized for its credibility through operator experiences with that automation, i.e. trust is learned. Considering that entire schools of cognitive theory have posited active participation as preferable over passive reception or observation, at least some sense of control is assumed to be of crucial importance for an operator to work with and appropriately trust automation. Automation surprises occur when technology autonomously performs tasks that cause a system to behave in a manner that the operator had not anticipated and it has been assumed that such a decrease in situation awareness arises from a non-satisfaction of a self-agency mechanism [10]. In other words, allowing the operator some form of control over the automation is expected to enhance the human–automation work dynamic.

2 Operational Concept

2.1 Ground-Based Automated Separation Assurance

Informed from the guidelines of the JPDO and human–automation functional allocation literature referenced above, our NextGen prototype instantiation of a ground-based automated separation assurance concept is next briefly described in this section. More detailed accounts of the precise characteristics and evolution of the concept can be found in the prior separation assurance (SA) research conducted at NASA Ames [11–18]. Additionally, complementary and collaborative airborne-based separation assurance concepts are detailed in research conducted at and with NASA Langley [19, 20].

Ground-based automated separation assurance involves automation components that monitor and/or manage nominal TBO equipped aircraft, while the controller handles off-nominal operations, provides additional services, and makes decisions when human involvement is needed. The primary difference from today's system is automated conflict detection and automated conflict resolution via data link. Controller involvement in routine conflicts is only required when an automatic trajectory change would exceed defined thresholds.

2.1.1 Enabling Environment

Each aircraft was assumed to be equipped with integrated data communications capabilities for route modifications, frequency changes, cruise altitude changes, and climb, cruise and descent speed modifications as well as high accuracy surveillance data provided via Automatic Dependent Surveillance Broadcast (ADS-B). Automated trajectory-based conflict resolutions were generated for conflicts with more than 3 min to initial loss of separation (LOS). For those with less time before LOS, a separate automated tactical conflict avoidance function (TSAFE) could generate a resolution and send heading changes to the aircraft directly.

2.1.2 Roles and Responsibilities

The automation detected conflicts, computed resolutions and/or alerted controllers. It nominally functioned by automatically sending instructions to aircraft via data link unless they exceeded a priori defined thresholds. The automation also augmented controller awareness and provided conflict status and probing tools. Primarily, the controller managed the automation, handled off-nominal situations and made decisions on situations when presented.

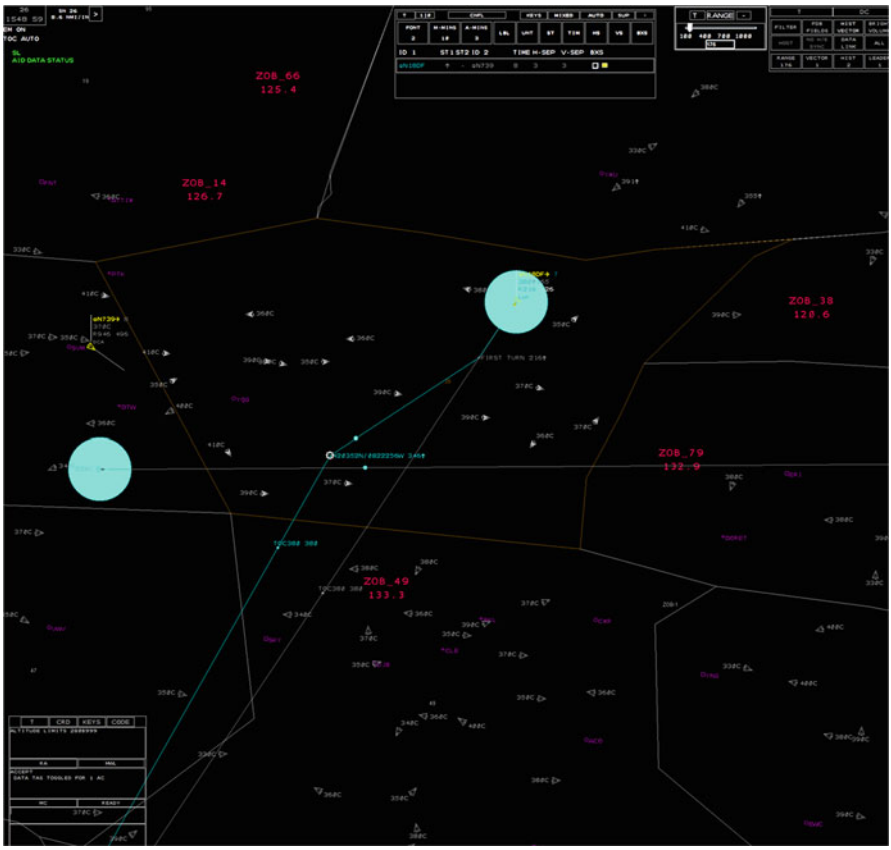

Fig. 1 Controller display with conflict list, an active conflict deferred by the automation to the controller (*yellow*), and a provisional resolution trajectory that currently conflicts with a third aircraft (*cyan*)

2.1.3 Air Traffic Controller Workstation

Figure 1 depicts the air traffic controller workstation prototype designed for the above distribution of roles and responsibilities. Aircraft that were managed by the automation and within the controller's sector are displayed in a brighter gray than low-lighted exterior aircraft. Additional information in data tags and colors were used to draw the controller's attention to a specific problem. The display was designed for general situation awareness and management by exception. The following figures present more detailed depictions of the various aspects of the interface controller's used to interact with the automation tools.

Nominally aircraft data tags were collapsed and appeared only as a chevron target with an altitude tag because routine aircraft operations such as frequency changes, hand-offs, climbs and descents, etc. were conducted automatically without controller involvement (Fig. 2).

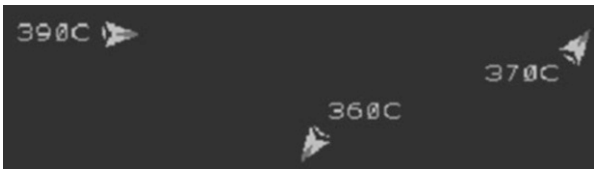

Fig. 2 Collapsed aircraft data tags as chevrons with altitude tags

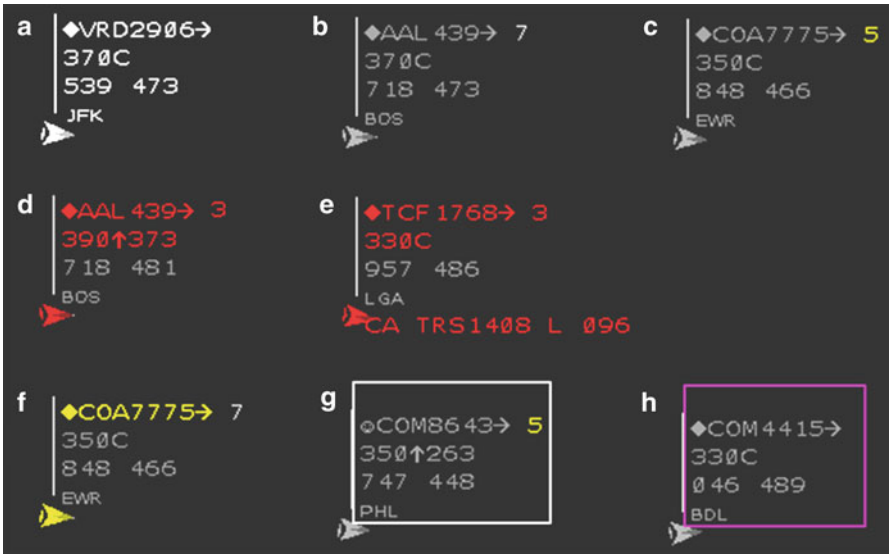

Fig. 3 Expanded data tag examples

Expanded data tags were used only in conjunction with situations requiring human attention. Figure 3 provides artificially arranged and ordered examples of what these looked like: (a) highlighted when manually expanded by the controller, (b) a "long-term" 7 min to LOS conflict number in gray, (c) a "medium-term" 5 min to LOS conflict number in yellow, (d) a "short term" 3 min to LOS with target symbol, data tag, and conflict number in red, (e) an auto-generated short term conflict resolution advisory in red, (f) a conflict deferred by the automation to the controller in yellow, (g) a conflict that the automation is still "thinking" about, and (h) an aircraft placed in an auto-uplink inhibited status by a controller.

Data tags contained items (Fig. 4) that controllers could left/right click on to initiate different trial plans/auto-resolution requests. For example, left clicking on the arrow opened a lateral trial plan; right clicking on the time to LOS requested an auto-resolution from the automation along the lateral dimension; right clicking on the altitude requested an auto-resolution along the vertical dimension. Also, controllers could click on the diamond to access a data communications menu.

Figure 5 depicts the conflict detection alert and automation status table. Each row represented a conflict and provided the callsigns of the involved aircraft, their datalink eligibility and their vertical status (climbing, descending, or level).

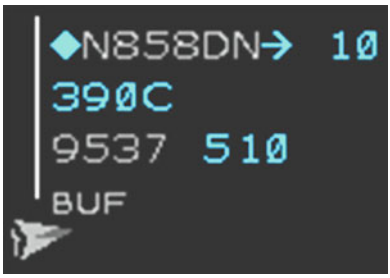

Fig. 4 Clickable data tag items

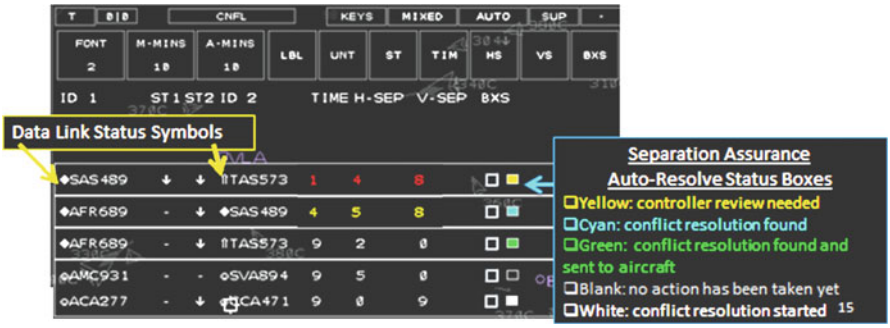

Fig. 5 Conflict detection alert and automation status table

The count down time to initial LOS was displayed in minutes, the predicted horizontal separation in nautical miles, and the predicted vertical separation in hundreds of feet. Last in the row, a dynamically color-coded box was used to indicate the current action-state of the automation in regard to that specific conflict.

2.1.4 Current Additions for Present Analysis

In line with the separation management standards and visions of the JPDO, the broader human factors research in human–automation functional allocation and trust introduced above, as well as participant comments from prior SA research, new adjustments and additions were made in the current study's human–automation interaction environment. Criteria thresholds for when the automation acted independently of the controller were changed and new intervention functionalities were introduced.

The thresholds were changed to provide a wider range of instances where the automation could uplink resolutions directly to aircraft without controller involvement (i.e. full-auto resolutions) while simultaneously increasing the amount of time available for a controller to observe or act prior to those uplinks by the automation. Specifically, full-auto resolution limits were increased to impositions on aircraft of up to 90 s or more of delay, 60 or more degrees of heading change, 2,200 or more feet of altitude change, and/or 200 or more knots of speed change.

Within these limits, the automation was permitted to directly issue an uplink resolution without involving the controller. Additionally, these criteria-bounded full-auto resolutions could only take place on conflicts that had no more than 8 min until LOS while the conflicts themselves could be displayed as early as 10 min until LOS. Furthermore, auto-generated TSAFE resolution advisories for short-term conflicts were eligible for direct uplink without controller involvement within 2 min to LOS. Suggested resolutions could be displayed as early as 3 min to LOS.

Based on prior feedback regarding the desire to maintain a certain level of control over the automation, new intervention functionalities were introduced that provided the controllers with an ability to inhibit/allow the automatic uplink aspect of the automation. At any point, a controller could input an "NU" (i.e., no uplinks) command and select one or more aircraft to put into a status where the automation was prohibited from uplinking conflict resolutions to the aircraft without their involvement. This status persisted for the aircraft until the same controller entered an "AU" (i.e., allow uplinks) command or the aircraft was handed off to the next controller.

2.2 Problem Statement of Current Analysis

The full-auto criteria adjustments described above combine to provide more opportunities for controllers to observe the automation successfully accomplish its work in handling simpler or "easy" conflicts. This complemented its already apparent proficiency with the routine hand-off and frequency changes. These opportunities are expected to support and engender actions from the controllers consistent with a perspective of reliability or trust in the automation. Such positive experience is assumedly essential as a precursor to effective interactions with the automation in more complex or critical situations. Furthermore, the addition of intervention functionality is expected to foster a sense of engagement, participation and control that should facilitate the controllers' confidence with and effective use of the automation.

First, verification that the prototyped human–automation functional allocation operational concept of this iteration of SA research continues to support the controllers in the NextGen envisioned environment by maintaining the FAA's safe separation standards and forecast levels of increased traffic densities is of principal interest to the current analysis. Next, the present analysis aims to provide a characterization of the transitioning separation assurance responsibilities between the controllers and the automation to explore the different interaction styles of controller trust and use of the automation, and lend insight towards possible factors that contribute to those shifting human–automation interaction styles.

3 Method

3.1 Apparatus

The entire operational environment was simulated using the Multi Aircraft Control System (MACS) software package [21] developed and maintained by the Airspace Operations Laboratory (AOL) software team. MACS is a java based scalable platform used for the prototyping of air traffic management displays and concepts that range from the current day and up through exploratory far term time frames. For each sector presently analyzed a radar controller (R-side) workstation consisted of a standard desktop PC with 75 cm Barco monitor and Display System Replacement (DSR) keyboard and trackball as input devices. These workstations were also equipped with tablet PCs that were used for voice communications similar to the presently fielded Voice Communications System (VCS). Seven pseudopilot stations with standard desktop PC setups were used for the management of flights within the simulation.

3.2 Design

The present analysis focuses on the last six runs of a larger human-in-the-loop SA study aimed to investigate the potential impact of introducing self-separating aircraft in progressively futuristic NextGen time-frames. The full study simulated four different time-frame environments and the last block of six runs were dedicated to representing the environment furthest into the future and with the most advanced human–automation operational paradigm. This portion of the study consisted of 2 days: one full day of training with a morning classroom briefing on the new environment assumptions and automation capabilities, hands-on learning activities, two training runs and discussion sessions followed by a second day of six different 40-min data collection runs.

Traffic scenarios were developed to present each controller participant with a varying range of aircraft densities for their sector over the course of a run to represent an approximate FAA NextGen forecast level of approximately twice that of current day levels (approx. 13–17 aircraft in a sector at any given point) resulting in peak instantaneous traffic counts of well over 30 aircraft in a sector. Scripted conflicts between aircraft trajectories were included in the density mix in addition to those that would naturally occur on account of the increased traffic levels.

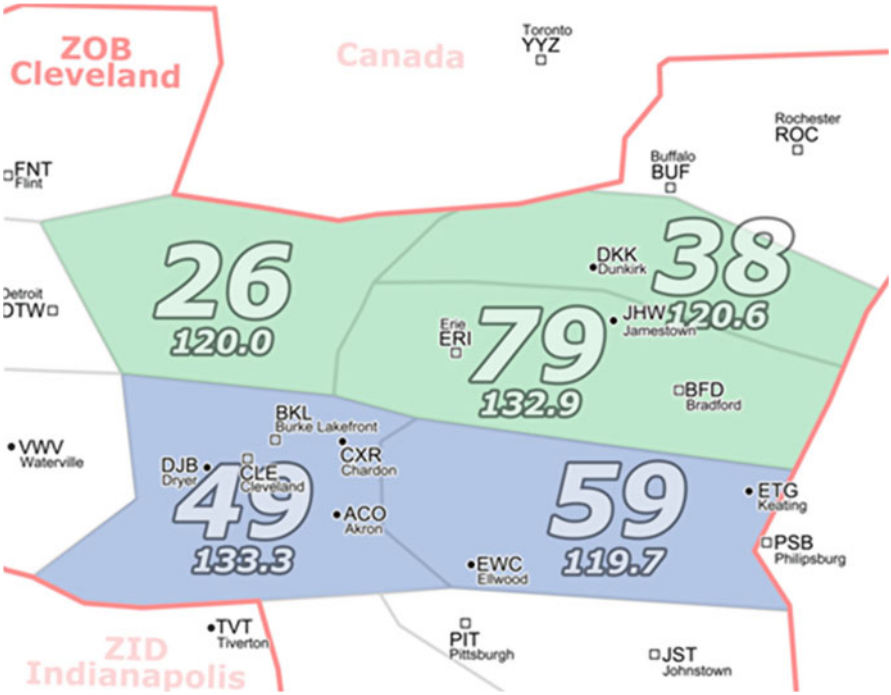

Fig. 6 Simulated airspace

3.3 Airspace

The airspace simulated five high altitude sectors from Cleveland Center (ZOB) in the central region of the United States: ZOB 26, ZOB 38, ZOB 79, ZOB 49 and ZOB 59. The floor of each sector was set at flight level (FL) 330 with confederate controllers handling the traffic outside of the five test sectors as well as the aircraft below. As seen in Fig. 6, each sector has unique geographic boundaries and different characteristics of aircraft density, traffic flows and complexity. Arrivals and departures from local area airports (e.g., Toronto-YYZ) contributed to these individual sector differences.

3.4 Participants

The participants consisted of seven current FAA front line managers, each from different enroute centers and current on radar rating and certification. Of these, five served as radar (R-side) controllers and two served as area supervisors that had five different recently retired confederate controllers available for on-call data (D-side)

control positions to support the R-sides. In addition to the D-sides, two other recently retired controllers served as confederate "Ghost" positions that managed the air traffic outside of the test area. Additional confederates included seven general aviation and student pilots that acted as pseudopilots and were assigned to each of the test sectors and surrounding areas.

3.5 Procedure

During the runs, the tasks of the control team were different in many respects from what they are today. As this was a functional allocation study of ground-based automated separation assurance, the main departures were along such lines: the automation was responsible for handoffs, transfers of communication, conflict detection, and conflict resolutions within defined parameters; the controllers were responsible for monitoring the automation's performance, handling conflict situations deferred by the automation, and exercising control of the automation to ensure an efficient and effective flow of traffic through the sector. Additional irregular events of varying situational awareness demand and potential consequence to automation acceptance, e.g. descent/climb requests from pilots due to turbulence however were not yet explicitly controlled for investigation within the current experimental conditions.

Data were collected on the performance of these tasks from a variety of sources throughout the study for later consolidation and analyses. During each run, screen recordings were taken on each of the workstations. Actions performed by participants within MACS and the various states and aspects of the traffic were recorded in real-time by MACS data collection processes. Participants completed post-run questionnaires after the conclusion of each data collection run as well as one post-simulation questionnaire administered at the end of the entire study.

4 Analysis Results

Because of the open-ended nature of human-in-the-loop simulations whereby actions of the controller participants can change the nature of the simulated traffic flows, the next section will first cover descriptive analyses of throughout and safety both on the whole and per the individual sectors (Sects. 4.1 and 4.2) before moving into the analyses of human–automation interaction styles (Sect. 4.3).

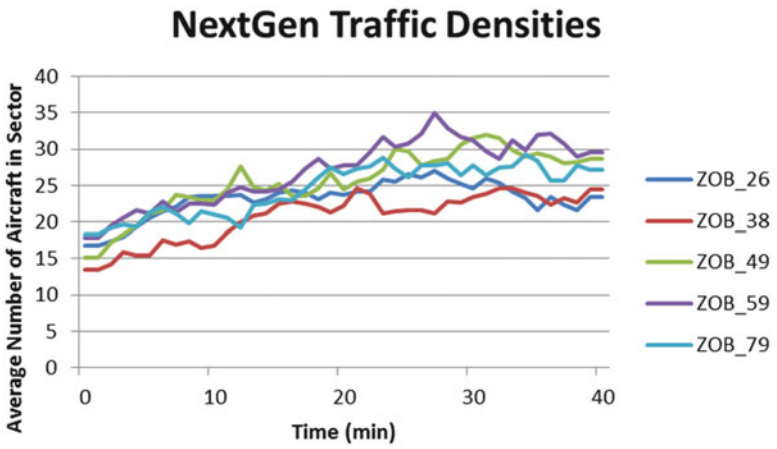

Fig. 7 Average aircraft counts across all six runs per sector

4.1 Capacity and Safety

Aircraft counts were calculated and recorded in real time at 1-min intervals for each sector during each run. Figure 7 shows the average aircraft counts collapsed across all six data collection runs. After an initial ramping up of traffic in the first quarter of a run, traffic densities increased to sustained average levels of approximately 23 aircraft for the narrowest and most local flow constrained sector (38) and approximately 29 aircraft for the larger and less local flow constrained sectors (49 and 59). These results verify that the targeted levels of aircraft counts were met and maintained by the test sector controllers across the simulated runs.

To assess the basic level of operational safety in the test airspace, LOS events were examined. A LOS was recorded anytime two aircraft were simultaneously closer than 5 nautical miles (nmi) laterally and less than 800 ft apart vertically. To be included in the following analysis, a LOS had to occur within one of the test sectors after the first 5 min of a run and last for more than 12 consecutive seconds (one full, simulated radar position update). LOS events were further categorized into Operational Errors (OE) and Proximity Events (PE) based upon the lateral separation at the closet point of approach measured along the diagonal between the aircraft. If that lateral separation distance was between 4.5 and 5.0 nmi horizontally, the LOS was counted as a PE; whereas if that distance was less than 4.5 nmi, the LOS was counted as an OE.

Across the 240 min of the six runs multiple LOS events were scripted to occur inside the test airspace. Only two LOS events actually occurred: both classified as PE. However, both LOS events were found to be attributable to simulation artifacts. Specifically, the first PE was due to a confederate pseudo pilot failing to comply with a controller's issued clearance to maintain a specified flight level. The other was due to a traffic scenario design error that unrealistically stacked two departure aircraft

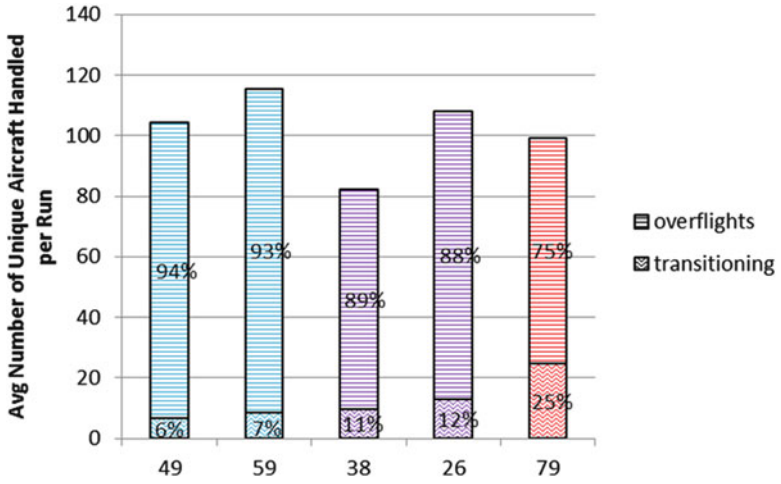

Fig. 8 Number of aircraft handled on average by a sector controller in a single run

together and did not provide the confederate ghost controller a fair amount of time to resolve prior to their entry into the test airspace. In sum, these results verify that appropriate levels of separation safety were maintained despite the increased levels of traffic and built in conflicts.

4.2 Individual Sector Differences

A priori differences in sectors in terms of a sector's demand for climbing and descending aircraft, average time and distances for aircraft to cross a sector, and the nature of the conflicts common to a sector were analyzed as potential contributing factors to a controller's interaction style with the automation. A characterization of each of these differences follows.

4.2.1 Transitioning Arrival and Departure Aircraft

Unique aircraft handled by each controller over the course of a run were counted and classified as either a transitioning aircraft or an overflight. These were averaged per run and the results can be seen in Fig. 8. Transitioning aircraft included those descending towards or climbing out of airports in the local vicinity of the test sectors (e.g., DTW, YYZ, BUF, etc.). These flights created additional complexity for controllers on account of the associated uncertainty and additional constraints and demands not attributed to overflights, which could nominally be left at the same altitude across a sector.

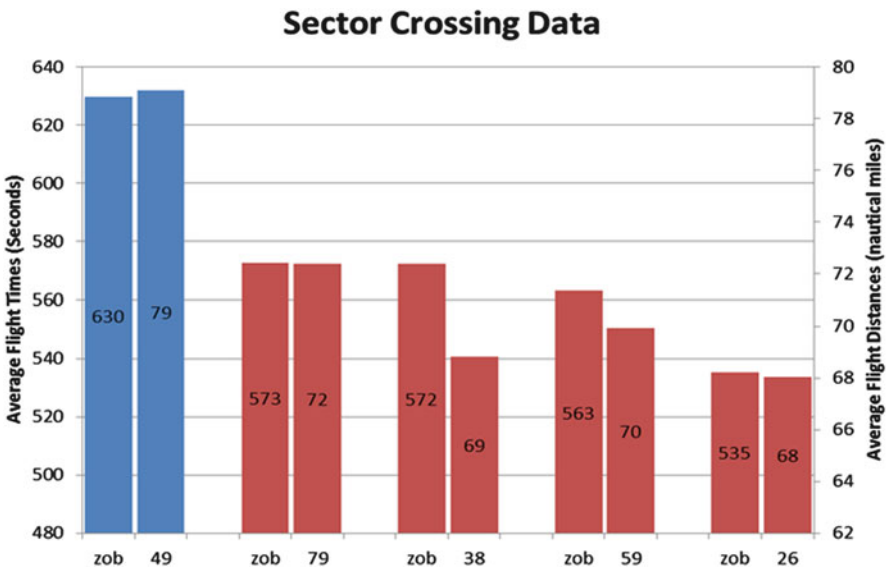

Fig. 9 Average aircraft sector crossing times (s) and distances (nm)

A single factor ANOVA was conducted to examine these differences and found a significantly higher proportion of transitioning aircraft for sector 79 over all the other sectors $F\ (4,25) = 39.35$, $p < 0.001$. Sectors 26 and 38 had the next highest proportion, which were in turn significantly higher than the proportions of transitioning aircraft for sectors 59 and 49.

4.2.2 Sector Crossing Time and Distance

One of the most visibly apparent individual differences between the controllers is the shape and size of the sector they controlled (Fig. 6). These aspects combine to affect how much time and what kind of space controllers' have to work with for aircraft in their sector before the aircraft is handed off to the next sector. Sector crossing data were recorded for each aircraft that transited a sector to capture how many seconds an aircraft spent in a sector and how far it flew within that sector.

A separate single-factor ANOVA was run to test for differences in both the transit times and transit distances of aircraft for each sector. In both cases, statistical significance was found indicative of more time and space for sector 49 when compared to any other sector; time: $F\ (4,1410) = 2.98$, $p < 0.05$, distance: $F\ (4,1410) = 3.49$, $p < 0.01$ with other comparisons failing to obtain significance (Fig. 9).

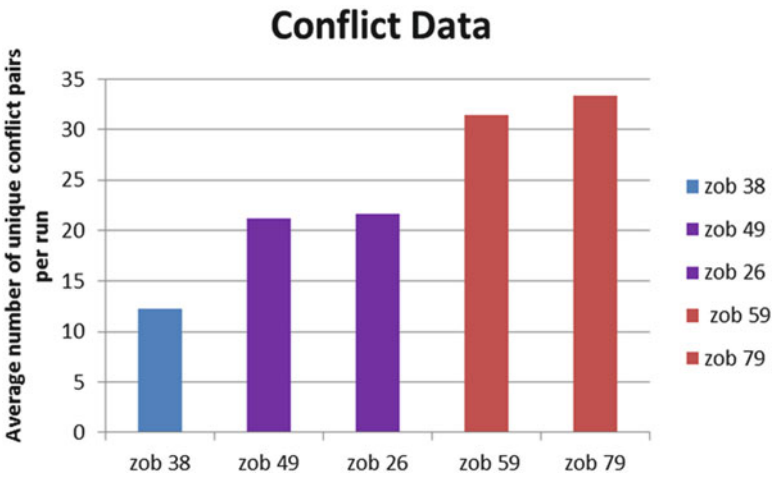

Fig. 10 Average number of conflicts per sector per run

4.2.3 Conflicts

During the simulation, a conflict event was logged at each track update where two aircraft were predicted to come into LOS at a future point in time in one of the test sectors. Figure 10 shows the average number of conflicts predicted for each sector across all six runs. A single-factor ANOVA was used to test for average conflict frequency differences among the five controllers. Average occurrences of unique conflict pairs differed significantly across the controllers, $F(4,25) = 12.43$, $p < 0.001$ with sectors 59 and 79 having significantly higher average number of conflicts per run than sectors 26 and 49 who in turn had a significantly higher average number of conflicts per run than sector 38 (Fig. 10).

Lastly, for each conflict pair the vertical state for each involved aircraft was recorded at that point in time. Conflict pairs were categorized as level conflicts if both aircraft were level, or transitioning conflicts if either aircraft in the pair was in a climb or descent. Figure 11 shows the average distributions of level conflicts on top of transitioning conflicts for each sector. A single factor ANOVA was used to test for differences in the average percentage of transitioning conflicts between the sectors. Sector 79 had a significantly higher proportion of conflicts that involved transitioning aircraft, $F(4,25) = 4.55$, $p < 0.01$. Comparisons between the other sectors did not obtain significant differences.

4.3 Human–Automation Interaction Styles

For the present analysis of human automation interaction styles, four major sources of information were investigated. These included route, altitude, and/or speed amendments uplinked by the automation without any controller involvement;

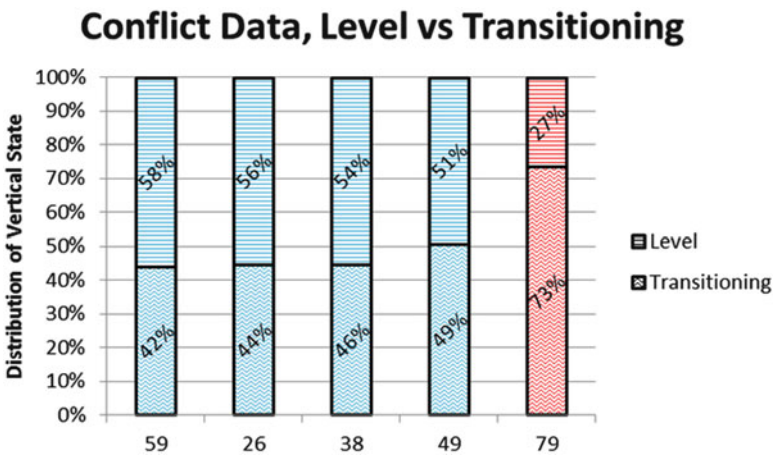

Fig. 11 Proportional number of conflicts that involved level versus transitioning aircraft

amendments uplinked by a controller with little to no automation involvement; interventions issued by a controller to inhibit the automation's ability to uplink to an aircraft; and subjective workload ratings and responses from questionnaires pertaining to participants' trust and use of the automation.

4.3.1 Uplinks

A total of 709 uplinks were counted across all five controllers and all six runs. 151 of these uplinks occurred without the presence of a conflict for the involved aircraft, whereas the remaining 558 uplinks concerned conflicts. From Fig. 12, it can be seen that sector 38 had the greatest percentage of non-conflict uplinks and sector 49 the least.

For uplinks where the automation detected conflicts, the status of the automation in resolving that conflict (Fig. 5) was recorded. Figure 13 shows the average proportions of different resolution automation states for each test sector.

4.3.2 Full-Auto Resolution Uplinks

288 of the conflict uplinks were full-auto resolutions not involving a controller and of these, 12.5% were tactical avoidance TSAFE resolutions and the remaining 87.5% were sent strategically with more than 3 min until LOS. A single-factor ANOVA was used to test for proportional full-auto resolution uplink differences among the five controllers. The average percentage of uplinks that were full-auto resolutions per run differed significantly across the controllers, $F(4,25) = 18.63$,

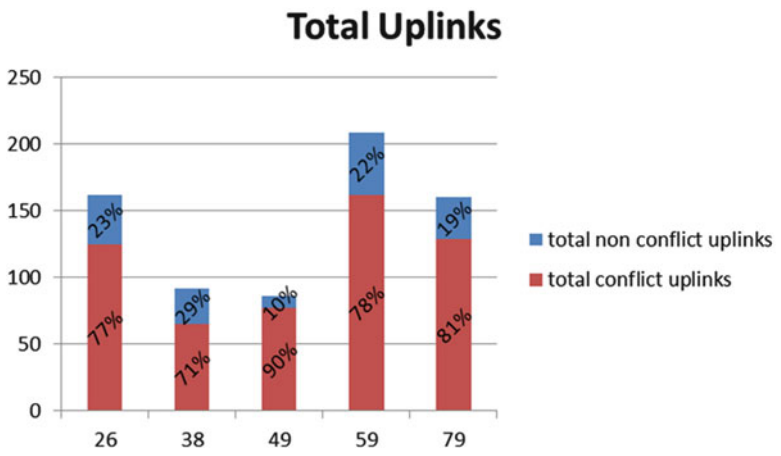

Fig. 12 Total uplinks categorized by conflict presence and sector

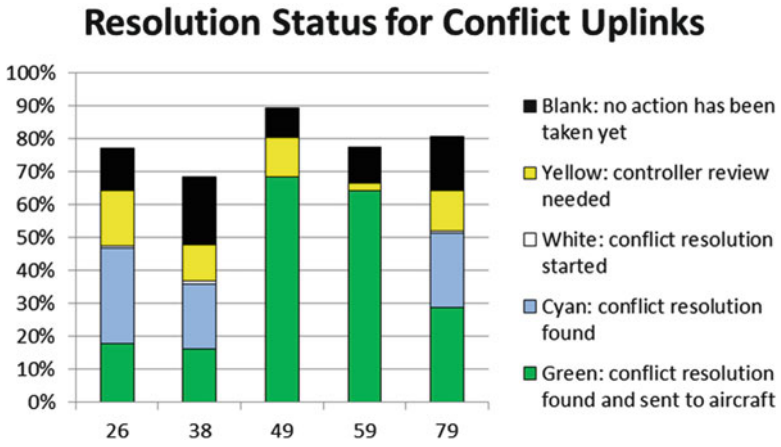

Fig. 13 Averaged proportions of status of resolution automation for uplinks involving conflicts

$p < 0.01$ with sectors 49 and 59 having significantly higher average percentages of full-auto uplinks than sector 79 who in turn had a significantly higher full-auto percentage than sectors 26 and 38 (Fig. 14).

4.3.3 Pro-active Controller Resolution Uplinks

Prior to the automation getting involved in the resolution of a conflict, a controller could issue a resolution on his/her own in response to a conflict alert or even, as mentioned above, without a conflict alert at all. In addition to the 151 non-conflict uplinks (Fig. 12), a total of 97 uplinks were issued by controllers across the runs

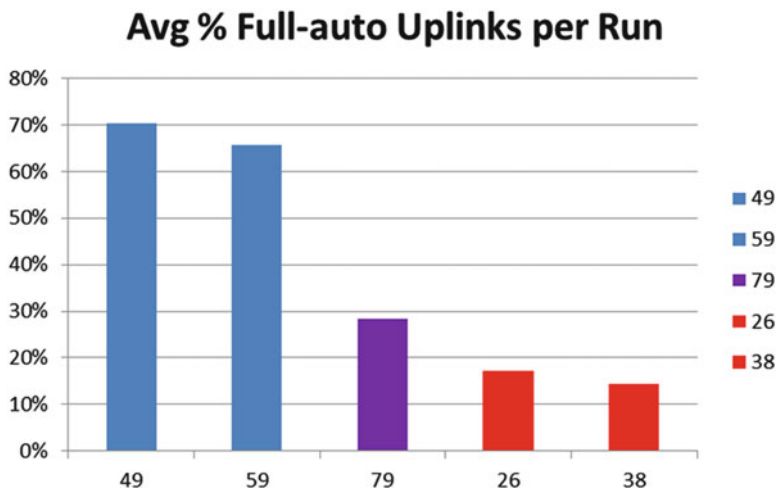

Fig. 14 Average percentage of uplinks in a run that were full-auto, i.e. the *green bars* from Fig. 13

while the conflict automation status box was still black/blank; i.e. indicative that the automation had not yet begun to work on resolving that conflict (Fig 13). Taking these two numbers together provides a measurement of how pro-active/preemptive a sector controller was in issuing resolution clearances.

A single-factor ANOVA was used to test for differences in the pro-activeness of sector controllers in resolution clearance uplinks. Average percentages of uplinks that were executed by controllers preemptive of automation differed significantly across the controllers, $F\ (4,25) = 3.95$, $p < 0.05$ with sector 38 showing significantly higher levels of pro-activeness than all the other sectors, and sector 49 the lowest (Fig. 15).

4.3.4 NU Intervention Frequency and Duration

An auto-uplink inhibit event "NU" was counted on a per plane basis and a total of 100 NU's were found issued by all test controllers across the six different runs. In 87% of these cases, controllers inhibited both aircraft involved in the conflict as opposed to just one. Figure 16 shows the total number of NU's for each sector as well as the proportionality of NU's that were issued on top of an active TSAFE advisory.

A single-factor ANOVA was run to test for differences in the number of NU's issued by controllers where the aircraft involved did not have an active T-SAFE advisory. Non-TSAFE NU's differed significantly across the controllers, $F\ (4,25) = 99.89$, $p < 0.001$ with sector 38 issuing significantly more NU's outside of TSAFE status on average per run than any other sector (Fig. 17).

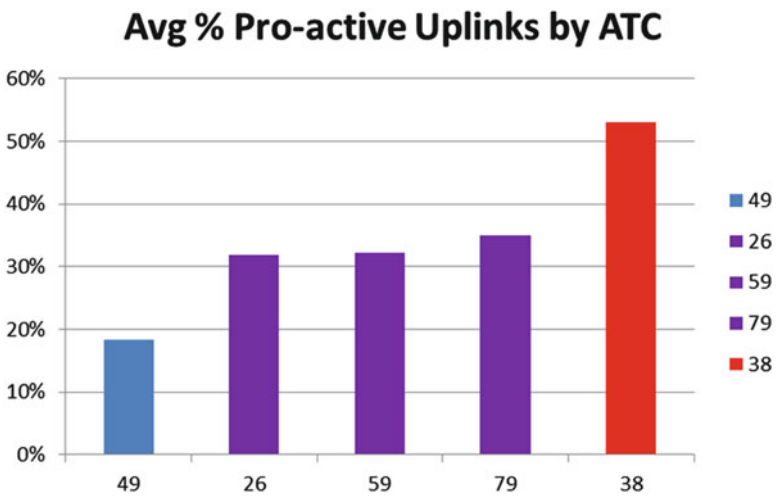

Fig. 15 Average percentage of uplinks in a run that were preemptive

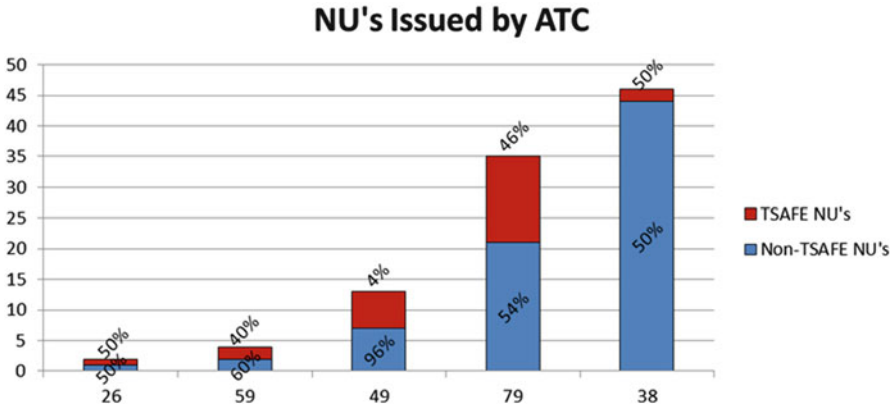

Fig. 16 Total NU's issued by a controller in the presence and absence of TSAFE advisories

Controllers could revert an aircraft from NU status back to automatic uplink eligibility status at any point or prolong their NU status indefinitely while under their ownership. Length of time in NU status was measured as the time between an NU and a subsequent AU for the same aircraft by the same controller. Initial results indicate that elapsed time in NU status ranged from as short as 20 s to as long as 379 s with an average duration of 115 s across all runs and controllers. Sectors 38 and 79 had the longest NU duration average at 145 s. Trends in the results indicate a positive relationship between number of NU's issued and length of time aircraft were kept in NU status (Fig. 18). In other words, controllers with more frequent use of NU left aircraft in NU status for longer durations on average versus less frequent users of NU who more quickly transitioned aircraft back out of NU status.

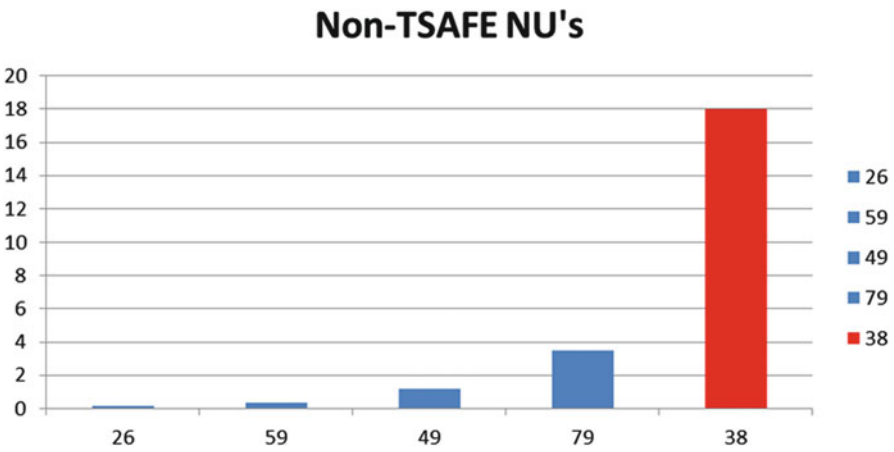

Fig. 17 Average number of non-TSAFE NU's issued per run

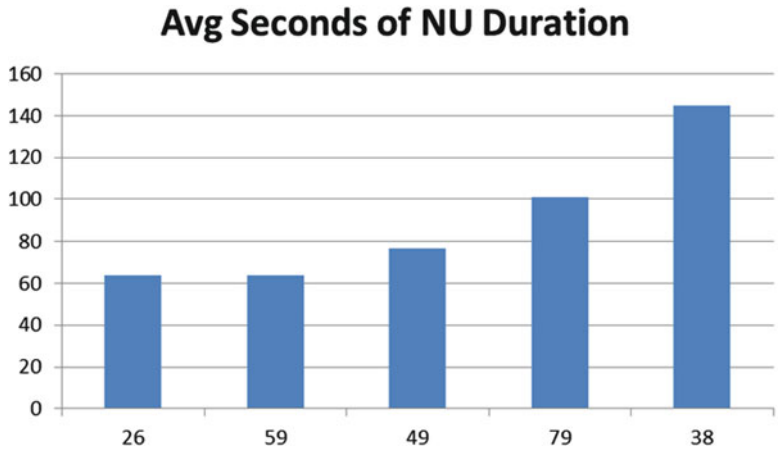

Fig. 18 Average number of seconds controller left aircraft in NU status before reverting with AU command

4.3.5 Subjectives: Workload

Throughout each 40-min run, self-assessment workload prompts appeared in the margin at the top of the controllers' display and lasted for 40 s for each prompt. Workload ratings were made on a "1" to "6" scale (1 = "Very Low Workload" to 6 = "Very High Workload") with averages computed per controller for each run. Notably, in spite of working about twice the level of present day traffic volume, participants still recorded favorable workload ratings. Furthermore, while average ratings for *all* participants fell on the lower end of the scale, statistical analyses still indicated significant differences between their ratings (Fig. 19), $F(4,360) = 14.02$,

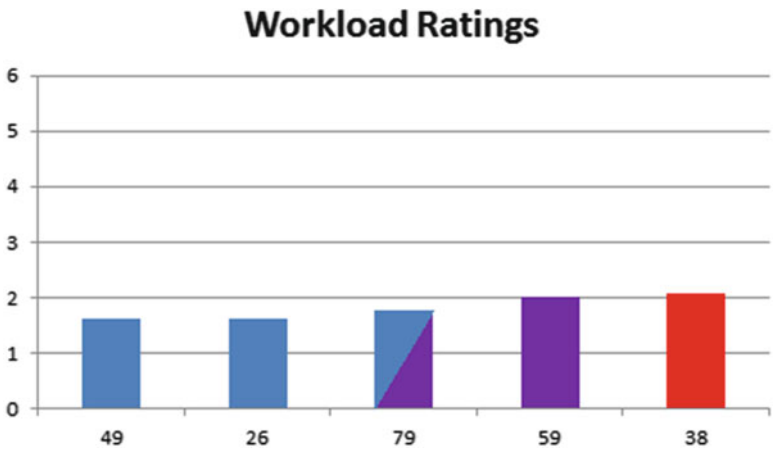

Fig. 19 Self-assessed workload ratings: 1–2 "Time on hands," 3–4 "In the groove," 5–6 "Overloaded"

$p < 0.001$. Sectors 49 and 59 were the only controllers to never rate their workload higher than a "2". Sector 49 provided a significantly lower rating than everyone else except 26, while sector 38's higher workload ratings obtained statistical significance as well.

4.3.6 Subjectives: Questionnaires

From their questionnaire responses on the topic of human–automation interaction styles, controllers showed some general consensus both as to what they liked and did not like about the automation tools. They also provided answers indicative of very different personal opinions on particular aspects.

For each of three different questions asking who should be responsible for the detection of conflicts, the generation of resolutions and the execution of resolutions, all controllers selected the answer "controller and ground automation should share." While the current analysis focuses only around the furthest "maximum" NextGen timeframe from the larger multi-timeframe experiment, the nature of the sequential design of the larger study lends itself to potential insights on controllers' developing attitudes over time and growing experience with the automation. While further analyses are planned to provide more detailed investigations, some relevant insight can still be seen at present that shed light on their "maximum" NextGen responses. Growth in controller confidence and trust of the automation can be seen from their increasing experience with it over time. Controllers' confidence grew in the trial planning tools as they used them. They were only "somewhat confident" when they used the tools in the minimum conditions ($m = 4$) but this confidence increased in the maximum conditions when they said they were "very confident" ($m = 6$).

Their confidence grew in a similar way when using the strategic conflict advisories: controllers were "quite confident" when they used the strategic advisories in the moderate conditions (m = 5.6) and this confidence increased to "confident" in the maximum conditions (m = 6). In the moderate condition, controllers' overall averaged opinion of the accuracy of the TSAFE advisories was that it was accurate (m = 4) and this increased slightly as they rated them as quite accurate (m = 4.66) in the maximum conditions.

In spite of the overall positive rating averages of the TSAFE tool, controllers did share some common reservations about its present implementation that limited its resolutions to using vectors without the possibility of using altitude resolutions. Example comments from controllers on sectors 38, 79, and 49 spoke directly to this: "I did not allow the computer to get to the point of needing a TSAFE resolution. The result of the computer applying a TSAFE was not acceptable to me."—38; "The better resolution was to stop the climb of one aircraft versus a turn"—79; "With climbing aircraft we had to be more aware to intervene before the computer vectored aircraft, when stopping at a lower altitude was a much easier, more efficient resolution"—49.

Despite where controller responses agreed with each other, other questionnaire answers alluded to striking differences in their overall experiences and dispositions. On one side of the spectrum, the sector 49 controller had a very easy time working with and trusting the automation. In a series of post simulation questions referencing a list of automation tools that asked what, if any, value was provided by that tool, this controller exclusively responded either "reduced my workload" or "increased my awareness." All other controllers selected answers that stated value was added to the operations (i.e., safer, more efficient) rather than to themselves or that a tool "had no added value." Additionally, for a question asked at the end of each run: "Did you feel rushed and that you did not have enough time to complete tasks? Or, did you feel that you did not have enough to do?" sector 49 marked the minimum value of "1 – very low time pressure" on the 7 point scale every time.

On the other hand, sector 38 indicated a personal preference and comfort for human control rather than trust of automation control in some areas. For example, "I don't always trust the solutions the computer comes up with, and never like the TSAFE resolutions" and "I think things will get easier as my comfort level increases. I do not always trust the solution or believe that they are in the best interest of the aircraft." Sector 38 answered "had no added value" to each of the three different value questions regarding TSAFE automation. At the end of a run, 38 was the only controller to answer "moderate compensation required to maintain adequate performance" to the question "how much did you have to compensate for the automation to make the tools and concept work?" all others selected either "minimal compensation" or "no controller correction." Another example of sector 38's confidence in himself over the automation comes from a question that asked at the end of a run for the controller to comment on whether or not they had enough time to resolve their most complex conflict, to which 38 responded "yes, only because I saw the potential loss of separation before the computer, put an NU on the involved aircraft, and separated them my way when the red fifth line appeared."

The questionnaire responses from sectors 26, 59 and 79 generally fell in between 49 and 38 with more moderate ratings and/or comments.

5 Discussion

Working within the human–automation interaction paradigm examined in the present analysis, controllers were able to maintain safe separation standards in spite of future levels of increased air traffic demand. From an absolute perspective of taking the group of participants on the whole, all the controllers worked well with and liked the automated tools. This can be seen from meeting the above goals along with low workload ratings and questionnaire responses that revealed they preferred sharing separation assurance responsibilities with a set of automated tools that they increasingly trusted as time and experience with them went on.

Exploring a relative comparison perspective between the controllers, the human automation interaction style measurements above observably divided the controllers along a spectrum with sector 38 placed towards a more manual end, sector 49 towards a more automated end, and the others falling somewhere in between. With the greatest proportion of non-conflict and pro-active trajectory uplinks, as well as the lowest proportion of full-auto uplinks, the highest number of NU's and non-TSAFE NU's, and the greatest average NU status durations, sector 38's objective data combine to stand out as a characterization of a more active approach to the human–automation team working dynamic. This higher level of engagement and activity is also reflected in the higher average workload ratings of sector 38 compared to the other sector controllers, though notably still well within the acceptable range of the workload scale. Sector 49 on the other hand, assumed a much more passive approach in the controller-automation dynamic, with the highest percentage of full-auto uplinks, lowest percentage of uplinks without automation involvement, and relatively low number and duration of automatic uplink interventions. Assuming such an approach, sector 49's peak workload ratings never exceeded a "2." The subjective questionnaire responses from 38 to 49 substantiate their differing styles of action, as their own words and ratings exhibit contrasting opinions of automation trust and use.

While individual differences in how much people trust and use automation will surely always exist based from their own personal experiences and attitudes, task characteristics like demand, pressure and complexity might reasonably be expected to influence a person's behaviors with automated tools. Individual sector differences from the pre-scripted traffic flows and sector geographic dimensions presented the controllers with very different and highly contextualized local work environments. Some of these factors exist on a level completely independent of a controller. For example, sectors 49 and 59 clearly had the most time and space to work with aircraft, as well as having to serve the lowest demand of transitioning aircraft. Other factors also reflect a local work environment that dynamically changes based on the actions taken from within that environment, as this is the nature of "human-in-the-loop."

For example, based on the pro-active resolution approach of the sector 38 controller, the lower number of conflicts certainly also reflect his solving of some conflicts early enough that they weren't recorded as conflicts. In contrast, sectors 59 (most likely by choice/comfort) and 79 (most likely by transitioning demand) had much higher levels of recorded conflict events.

Interestingly, sector 59 called out several instances in his questionnaire responses where he disapproved of the automation's handling of a situation. He also had approximately the same levels of sector crossing time/distances, and transitioning aircraft conflict demand as sector 38. However, unlike 38, we observed in his questionnaire comments a more passive approach like that of 49, i.e., "the hardest part will be to keep the controllers engaged"—59. Additionally, the arrangement of the simulation which had 59 co-located in the south area alone with 49 and separate from the other controllers, provided more opportunity for 59 to observe and be influenced by a functional passive approach than perhaps would have been afforded to him alone.

From the present analysis, the most clear and single mapping between individual sector characteristics and resultant human interaction style appears to be between lower levels of transitioning aircraft demand and lower levels of pro-active controller resolutions. Less transitioning aircraft have been observed to lead to fewer short-term conflicts and TSAFE advisories. The resultant trend in interaction with automation is underscored by the controller's expressed dislike that TSAFE resolutions were limited to the lateral dimension alone, which encouraged them to be more pro-active in assigning altitude stops themselves.

Several areas of future research are encouraged from the current analysis. While one can get some preliminary ideas of controller differences at present, more can be learned from subsequent tests in more precisely targeted and controlled studies. Most relevant to continuing from this exploratory vein of characterizing individually different controller–automation interaction styles would be a between-subjects designed study with either controller participants randomly rotated between or experimentally paired in specific sectors to ascertain relative effects of localized traffic and sector demands on a priori attitude towards trust/use of the automation. Additionally, further analysis of metrics to independently characterize traffic conflicts in open-loop runs would help to more accurately identify the variance in task or problem posed to each sector and speak towards levels of controller reliance on automation. Lastly, while flexible and accommodating to multiple styles of real-time usage, all the controllers in the present analysis shared the same underlying automation configuration parameters. In the future, this might not need to be the case. Individually tailored automation settings per the various localized sector environments and controller preferences for automation task sharing styles might be set ahead of time or flexibly adapted in real-time based on performance.

6 Conclusions

The automation's design was very flexible, with multiple interaction points for different stages of manual and automated control and so accommodated a variety of individually different passive to active work styles of the controller participants. The provision of increased ranges of opportunities for the automation to act independently and be previewed in doing so were well received by some sectors (49 and 59) while others felt much more comfortable with exercising the auto uplink intervention NU functionalities (38 and 79). Not only did the controllers work with the automation to meet their safety and traffic level goals in this simulated future NextGen timeframe, they also did so in different ways and with different attitudes of trust/use of the automation. The prototyped controller-automation functional allocation framework was on the whole very flexible and very successful.

Acknowledgements The authors greatly appreciate the support and collaboration of the NASA Airspace Program, the FAA, and particularly the controller participants. Gratitude is also owed to the entire research, development, and support staff in the AOL.

References

1. Federal Aviation Administration (2012) NextGen Briefing. Retrieved online November 2012 from http://www.faa.gov/air_traffic/briefing/
2. Federal Aviation Administration (2012) FAA Aerospace Forecasts Fiscal Years 2012–2032
3. Joint Planning and Development Office (2010) Concept of Operations for the Next Generation Air Transportation System [Draft version 3.2]
4. Joint Planning and Development Office (2011) Targeted NextGen Capabilities for 2025
5. Joint Planning and Development Office (2011) JPDO Trajectory-Based Operations (TBO) Study Team Report
6. Parasuraman R, Sheridan T, Wickens C (2000) A model for types and levels of human interaction with automation. IEEE Trans Syst Man Cybern A Syst Hum 30(3):286–297
7. Hou M, Kobierski R, Brown M (2007) Intelligent adaptive interfaces for the control of multiple UAVs. J Cogn Eng Decis Mak 1:327–362
8. Lee J, See K (2004) Trust in automation: designing for appropriate reliance. Hum Factors J Hum Factors Ergon Soc 46:50–80
9. Madhavan P, Wiegmann D, Lacson F (2006) Automation failures on tasks easily performed by operators undermine trust in automated aids. Hum Factors J Hum Factors Ergon Soc 48(2):241–256
10. Maille N, Sarrazin J (2012) Sense of control in supervision tasks of automated systems. Aerospace Lab Journal, AL04-09. Retrieved online November 2012 from http://www.aerospacelab-journal.org/
11. Erzberger H (2001, December) The automated airspace concept. In: Proceedings of the fourth USA/Europe air traffic management R&D seminar
12. Erzberger H (2009) Separation assurance in the future air traffic system. In: Proceedings of the ENRI international workshop on ATM/CNS (EIWAC 2009)
13. Homola J (2008) Analysis of human and automated conflict resolution capabilities at varying levels of traffic density. Master's thesis, San Jose State University, San Jose, CA

14. Prevot T, Homola J, Mercer J, Mainini M, Cabrall C (2009) Initial evaluation of NextGen air/ground operations with ground-based automated separation assurance. In: Proceedings of the eighth FAA/Eurocontrol R&D seminar
15. Homola J, Prevot T, Mercer J, Brasil C, Martin L, Cabrall C (2010) A controller-in-the-loop simulation of ground-based automated separation assurance in a NextGen environment. In: Proceedings of the ENRI international workshop on ATM/CNS (EIWAC 2010)
16. Prevot T, Mercer J, Martin L, Homola J, Cabrall C (2010) Function allocation for ground-based automated separation assurance in NextGen. In: Proceedings of the international conference on human-computer interaction in aerospace
17. Prevot T, Homola J, Martin L, Mercer J, Cabrall C (2011) Automated air traffic control operations with weather and time-constraints. In: Proceedings of the ninth FAA/Eurocontrol R&D seminar
18. Prevot T, Homola J, Martin L, Mercer J, Cabrall C (2012) Toward automated air traffic control – investigating a fundamental paradigm shift in human/systems interaction. Int J Hum Comput Interact 28(2):77–98
19. Wing D (2008) Performance basis for airborne separation. In: Proceedings of the 26th International Congress of the aeronautical sciences
20. Wing D, Prevot T, Murdoch J, Cabrall C, Homola J, Martin L, … Palmer M (2010) Comparison of ground-based and airborne function allocation concepts for NextGen using human-in-the-loop simulations. Paper presented at the 10th AIAA Aviation Technology, Integration, and Operations Conference, September, Fort Worth, TX
21. Prevot T (2002) Exploring the many perspectives of distributed air traffic management: the multi-aircraft control system (MACS). In: Chatty S, Hansman J, Boy G (eds) HCI-Aero 2002. AIAA Press, Menlo Park, pp 149–154

Part IV
Communication, Navigation and Surveillance

Joint Target Tracking and Systematic Error Correction for Wide Area Multilateration

J. Abbud and G. De Miguel

Abstract This work presents a method to estimate and correct undesirable effects caused by troposphere propagation and non-perfect ground station synchronization, in the context of target tracking with a Wide Area Multilateration (WAM) system. Correlation of opportunity traffic emissions is used to overcome the difficulty of installing reference beacons simultaneously visible to all the base stations. The architecture of this method is based on the possibility of decoupling the target position determination problem and the systematic error estimation problem. On one hand, given the non-linearity of the signal measurement (Time Difference of Arrival) with respect to the target state vector, the target position is determined by using an Unscented Kalman Filter (UKF). On the other hand, an Extended Kalman Filter (EKF) is used to estimate the systematic error in time. The relationship between both filters is established at their respective update stages. Experiments using deliberately adverse scenarios have been performed to test the reliability of this method.

Keywords Clock synchronization • Opportunity traffic • Target tracking • Troposphere propagation • Unscented Kalman Filter • Wide Area Multilateration

1 Introduction

In order to further optimize the use of airspace [1, 2], stricter aircraft positioning requirements can be expected in the near future.

The trend in Air Traffic Management (ATM) is to rely on ADS-B as the main source of aircraft positioning. It is therefore necessary to have an independent

J. Abbud (✉) • G. De Miguel
Grupo de Procesado de Datos y Simulación (GPDS-SSR),
Universidad Politécnica de Madrid, Madrid, Spain
e-mail: jorge.jose.abbud.momma@gmail.com; gonzalo@grpss.ssr.upm.es

Electronic Navigation Research Institute (ENRI), *Air Traffic Management and Systems*, Lecture Notes in Electrical Engineering 290, DOI 10.1007/978-4-431-54475-3_10,

cooperative surveillance system. The intention is to gradually migrate from Secondary Surveillance Radar (SSR) towards Wide Area Multilateration (WAM), to enhance surveillance integrity [3] for en-route applications.

Given the fast deployment of ADS-B, a promising solution is to reuse its ground stations as WAM base stations. Each base station will send the measured Time of Arrival (TOA) together with the ADS-B information to the Air Traffic Control (ATC) center. Multilateration is performed by processing the TOAs [3].

In a recent paper [4], authors have characterized two main issues affecting aircraft position estimation based on Time Difference of Arrival (TDOA): synchronization among ground stations and propagation errors. They have demonstrated that using opportunity traffic, accurate horizontal position estimates of aerostatic targets can be obtained.

This paper goes further in the use of opportunity traffic, presenting an aircraft tracking method that corrects the effect of systematic errors.

This method consists of two interdependent Kalman filters: one for the aircraft state vector estimate and the second one for the estimation of the parameters of the systematic error. This way, the effect of the systematic error is fed as a correction in order to provide a more accurate estimate of the aircraft position.

The paper is structured as follows: Sect. 2 states the problem of position determination with WAM, characterizing the effect of systematic errors. Section 3 presents the architecture of the system and its implementation. Section 4 analyzes the performance gain obtained with the use of the presented method.

2 Characterizations of Systematic Errors in WAM Systems

In WAM, the aircraft position is determined by means of the Time Difference of arrival (TDOA) of the signal at the different base stations. A method based on hyperbolic location as described in [5] can be used to obtain an initial solution.

Each base station measures the TOA of the same signal travelling from the target aircraft, as the time of reception (defined by the ground station clock).

The accuracy of the position estimate is therefore determined by the errors in the TOA estimates. From a data processing perspective, these errors can be grouped into three main categories [3]: white noise, propagation effects and synchronization issue among ground stations.

2.1 Impact on the TOA Measurement

The TOA of a signal travelling from aircraft j located at (x_j, y_j, z_j) to the base station i located at (x_i, y_i, z_i) can be represented by (1):

$$TOA_i = \tau_i^j = \frac{1}{c}\sqrt{(x_i - x_j)^2 + (y_i - y_j)^2 + (z_i - z_j)^2} + \frac{1}{c}\Delta P_i^j + T_e + \Delta T_i + n_i \quad (1)$$

and can be rewritten as:

$$TOA_i = \tau_i^j = \frac{1}{c} R_{ij} + \frac{1}{c} \Delta P_i^j + T_e + \Delta T_i + n_i \tag{2}$$

where R_{ij} stands for the slant range separating beacon and aircraft, $\Delta P_i{}^j$ represents the effect of atmospheric propagation, T_e represents the uncertainty affecting the signal emission time, ΔT_i is the synchronism error, and n_i the white noise random error. In order to eliminate the uncertainty in the signal emission time, the aircraft position will be assessed based on Time Difference of Arrival (TDOA). This means that all available TOAs for a single emission are referenced to the TOA measured by one of the base stations. Thus, the TOA equation system is now replaced by a TDOA equation-system, with one less unknown, as well as one less equation, as follows:

$$\begin{aligned} TDOA_i^j = \Delta\tau_{i,m}^j = \tau_i^j - \tau_m^j = \frac{1}{c}\left(R_{ij} - R_{mj}\right) + \frac{1}{c}\left(\Delta P_i^j - \Delta P_m^j\right) \\ + \left(\Delta T_i - \Delta T_m\right) + \left(n_i - n_m\right) \end{aligned} \tag{3}$$

where the reference base station is the mth station.

For the following sections, it is interesting to bring up the concept of pseudorange, noted ρ_{ij}, expressed as the product of the TOA multiplied by the speed of light in vacuum.

The effect of white noise is not critical for the typical S/N values in WAM. Propagation effects will be analyzed and modeled within this section. This is required in order to ensure that the accuracy does not suffer from degradation, especially in scenarios with poor Dilution of Precision. Finally, synchronism errors are considered to be approximately constant during an estimation interval, i.e. clock drift among beacons is out of scope.

2.2 Slant-Range Dependency of Propagation Effect

Let us characterize the propagation effect. The vertical gradient of the atmospheric refractive index "bends" the signal propagation trajectory and changes the velocity of light, thus delaying its arrival to the base station. Figure 1 represents this propagation error with respect to the slant range for aircraft flying at altitudes between 3,000 and 14,000 m AMSL, using path-integration with the ISA model. The base station is considered to be at sea level. Note that the obtained values are only applicable below the red dashed curve, representing the radio-wave Earth horizon.

Two relevant characteristics can be observed concerning this propagation error. First, for a given aircraft altitude, a second-degree polynomial seems to be a good fit for modeling the range bias with respect to the slant-range. This is:

$$\Delta P_i^j \left(R_{ij}, z_j\right)\Big|_{z_j = z_0} \approx \alpha_1 R_{ij} + \alpha_2 R_{ij}^2 \tag{4}$$

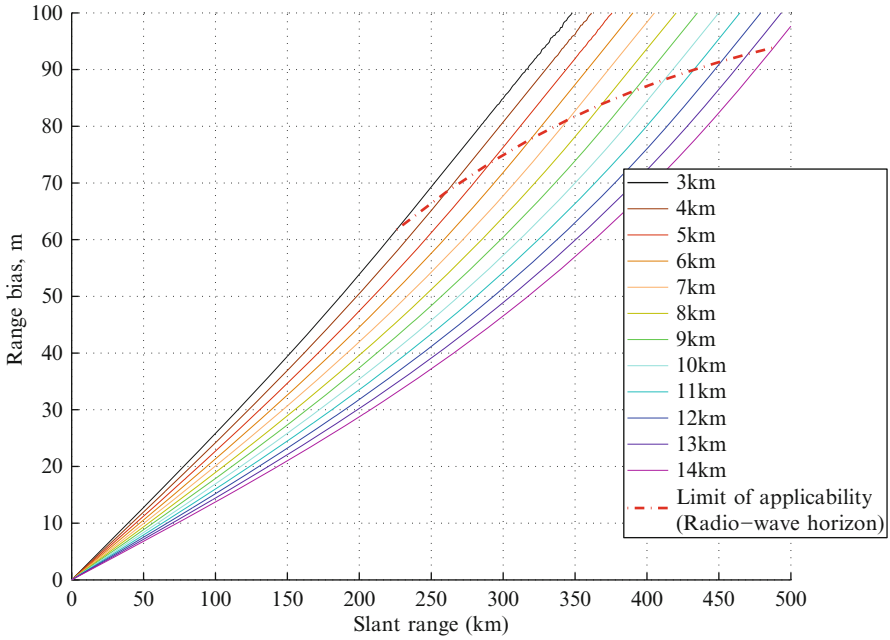

Fig. 1 Systematic error (range bias) due to radio wave propagation for a standard atmosphere

Second, although second-degree polynomials seem to be equally applicable to characterize the range bias for all aircraft altitudes, different coefficients are deemed necessary. This altitude dependency limits the applicability of the second-degree polynomial to a narrow layer (1–2 km) in height. This observation suggests an altitude dependency of the range bias, which will be analyzed in Sect. 2.3.

2.3 True Altitude Dependency

Section 2.2 has revealed the possibility of modeling the range bias through a family of second-degree polynomials using the slant-range as the independent variable, one per altitude layer. However, a relationship between these polynomials needs to be established in order to provide a general expression of the range bias.

Figure 2 shows the ratio between the range bias obtained when an aircraft is flying at a given altitude, compared to when flying at 14 km AMSL but at the same slant range from the beacon. Again, note that the obtained values are only applicable below the red dashed curve, representing the radio-wave Earth horizon.

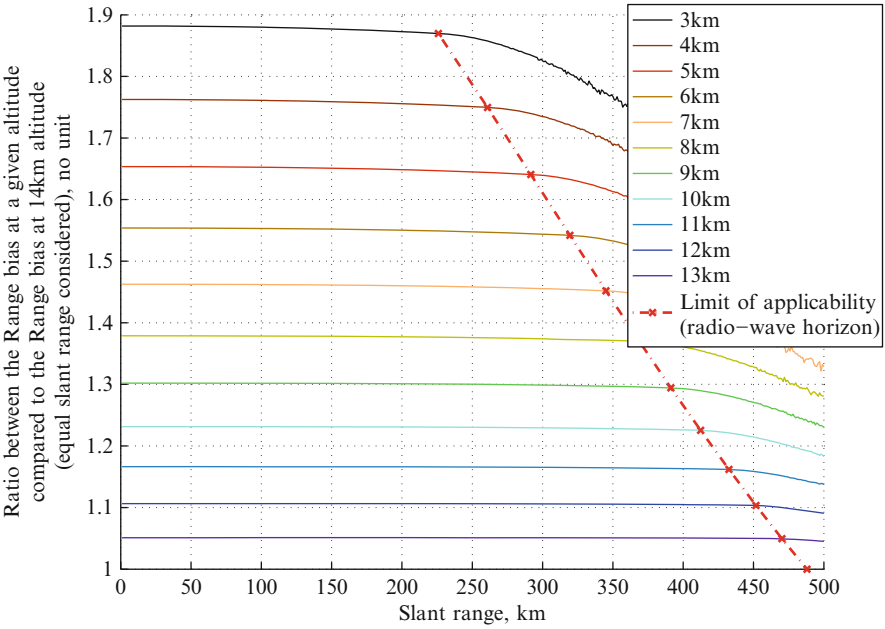

Fig. 2 Ratio between range biases for aircraft flying at a given altitude compared to at 14 km AMSL but equal slant-range

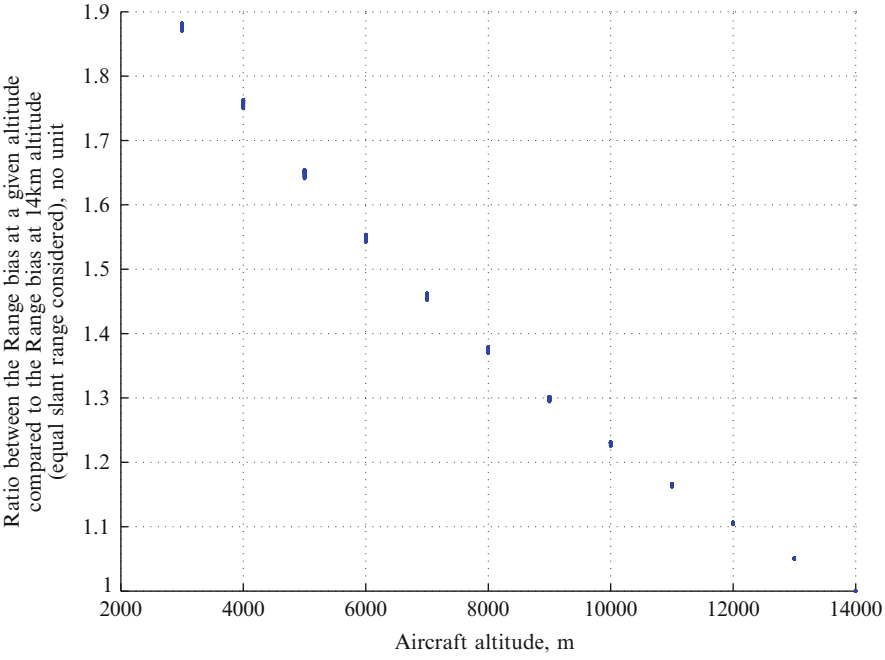

Fig. 3 Ratio between range biases for aircraft flying at a given altitude compared to when flying at 14 km AMSL but equal slant-range

$$C(z_j) = \frac{\Delta P_i^j\left(R_{ij}, z_j\right)|_{\rho_{ij}=\rho_k}}{\Delta P_i^j\left(R_{ij}, z_0\right)|_{\rho_{ij}=\rho_k}} \approx 1 + \alpha_3\left(1 - \frac{z_j}{z_0}\right) \tag{5}$$

Observations made in Sect. 2.2 and this section lead to the following proposal to approximate the range bias as a combined function of the aircraft altitude and the slant-range between the aircraft and the beacon. This is obtained as the product of (4) and (5).

The three-parameter model of the range bias is therefore as follows:

$$\Delta P_i^j\left(R_{ij}, z_j\right) \approx \Delta P_i^j\left(R_{ij}, z_j\right)\Big|_{z_j=z_0} \cdot C\left(z_j\right) \approx \left(\alpha_1 R_{ij} + \alpha_2 R_{ij}^2\right) \cdot \left[1 + \alpha_3\left(1 - \frac{z_j}{z_0}\right)\right] \tag{6}$$

It is assumed that variations in atmospheric propagation can be modeled with this expression. However, different values will apply with respect to the ones used in the case of the standard atmosphere.

This way, combining (3) and (6), a generic equation within the system is:

$$\begin{aligned} TDOA_i^j = {} & \frac{1}{c}\left(R_{ij} - R_{mj}\right) + \frac{1}{c}\left[\alpha_1\left(R_{ij} - R_{mj}\right) + \alpha_2\left(R_{ij}^2 - R_{mj}^2\right)\right]\left[1 + \alpha_3\left(1 - \frac{z_j}{z_0}\right)\right] \\ & + \left(\Delta T_i - \Delta T_m\right) + \left(n_i - n_m\right) \end{aligned} \tag{7}$$

We are now in a position to establish a system of TDOA equations in order to determine the aircraft position. It is important to mention that the number of unknowns has increased due to the characterization of propagation effects and relative synchronization errors. Therefore, the solution of the system shall not only contain the aircraft coordinates, but also the parameters used to model the propagation effect and the clock synchronization errors.

In order to avoid an indeterminate system of non-linear equations, a set of new independent equations must be obtained with the use of opportunity traffic, as presented in [4].

3 Target Tracking with Correction of Systematic Errors

The simplest approach for estimating the systematic errors is to assume that the parameters characterizing them are constant in time. This would mean that their estimation could be performed offline. However, the systematic errors under study change in time: propagation effects due to the constant changes in the atmosphere and clock synchronization due to the existing drift among the base stations' clocks. It is therefore required to perform a dynamic estimation of these errors, in parallel with the maintenance of target tracks.

This way, in theory, the filter equations of the systematic errors are coupled to the track maintenance equations for each target. However, an approach to decouple filter

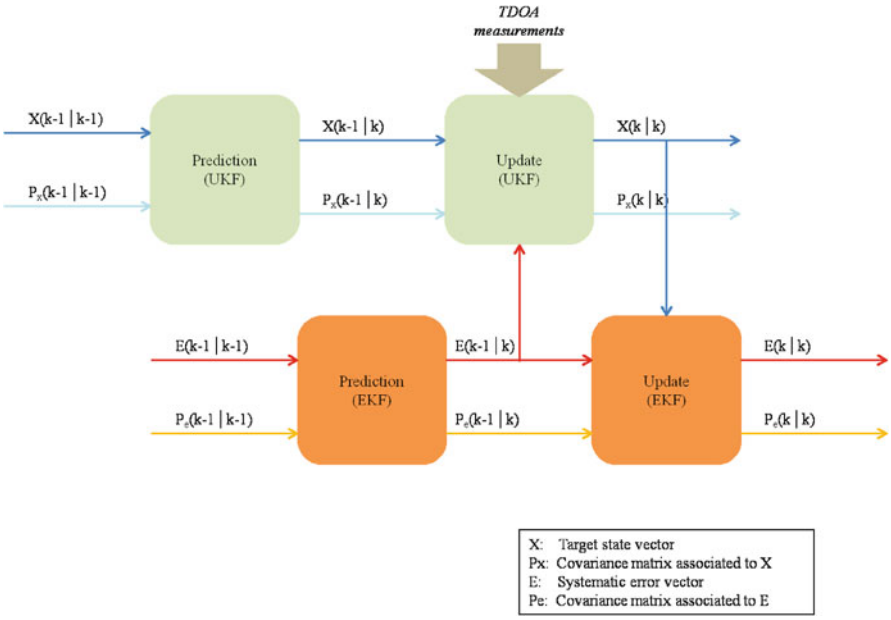

Fig. 4 Joint target tracking and systematic error correction for WAM

equations for systematic error estimation from the track maintenance filter equations is presented in [7]. This paper presents how this philosophy can be applied to a WAM target tracking system.

3.1 Design Architecture

In order to estimate the target position based on TDOA measurements, a system capable of correcting the systematic errors is required, as per in [7]. This way, it is not only needed to estimate the target state vector, but to estimate the effect of systematic errors (as characterized in Sect. 2) as well, in order to correct it. Figure 4 shows the design architecture aimed at performing this task. It consists of two Kalman filters that are interdependent in the update phase.

An UKF [8] is used for target tracking, given the non-linearity of TDOA measurements with respect to the target position. The prediction step of the UKF uses the previous combination of target state vector (position, velocity and acceleration) and its associated covariance matrix in conjunction with a Singer acceleration model [6]. The update step combines this prediction with the obtained TDOA measurements and the systematic error estimate.

On the other hand, the tracking of the systematic error model is performed via EKF. The estimation phase of EKF uses the previous combination of state vector

and its associated covariance matrix. In this case, the state vector contains the clock synchronization errors and the three parameters of the propagation error model described in Sect. 2 (α_1, α_2 and α_3).

It should be noted that the initialization phase of this system requires a set of observations based on TDOA measurement and hyperbolic location [5]. A second degree polynomial fit of the position estimate is performed for each target, in order to feed the tracking system with an initial set of state vectors.

3.2 Implementation

In this paper, all positions are defined as relative ranges to a fixed point in the centre of the WAM constellation. The target state vector $\boldsymbol{X}$ is therefore composed by the combination of range, velocity and acceleration (in all three axes) of each aircraft (M in total). The target covariance matrix $\boldsymbol{P_X}$ will initially be a block diagonal matrix. These are respectively:

$$\begin{cases} X = \left[X_1 \ \ldots \ X_j \ .. \ X_M \right]^T \\ P_X = diag\left(P_{X_1} \ \ldots \ P_{X_j} \ .. \ P_{X_M} \right) \end{cases} \tag{8}$$

where:

$$\begin{cases} X_j = \left[x_j \ \dot{x}_j \ \ddot{x}_j \ y_j \ \dot{y}_j \ \ddot{y}_j \ z_j \ \dot{z}_j \ \ddot{z}_j \right]^T \\ P_{X_j} = diag\left(\sigma^2_{x_j} \ \sigma^2_{\dot{x}_j} \ \sigma^2_{\ddot{x}_j} \ \sigma^2_{y_j} \ \sigma^2_{\dot{y}_j} \ \sigma^2_{\ddot{y}_j} \ \sigma^2_{z_j} \ \sigma^2_{\dot{z}_j} \ \sigma^2_{\ddot{z}_j} \right) \end{cases} \tag{9}$$

Likewise, the systematic error state vector $\boldsymbol{E}$ is composed by the three parameters used in the range bias model (Sect. 2) and the $N-1$ clock synchronization errors, where N is the number of WAM stations. Thus, the systematic error state vector and its associated covariance matrix $\boldsymbol{P_E}$ are defined as follow:

$$\begin{cases} E = \left[\alpha_1 \ \alpha_2 \ \alpha_3 \ c\Delta T_{2,1} \ c\Delta T_{3,1} \ \cdots \ c\Delta T_{i,1} \ \cdots \ c\Delta T_{N,1} \right]^T \\ P_E = diag\left(\sigma^2_{\alpha_1} \ \sigma^2_{\alpha_2} \ \sigma^2_{\alpha_3} \ \sigma^2_{c\Delta T_{2,1}} \ \sigma^2_{c\Delta T_{3,1}} \ \cdots \ \sigma^2_{c\Delta T_{i,1}} \ \cdots \ \sigma^2_{c\Delta T_{N,1}} \right) \end{cases} \tag{10}$$

3.2.1 Prediction Step (Target)

The prediction step for the target is performed in three stages (Fig. 5): the first stage consists of generating the augmented state vector. The second stage performs the prediction of the state vector associated to each sigma point, based on the Singer acceleration model. The last stage consists of generating the state vector and the covariance matrix associated to the prediction step.

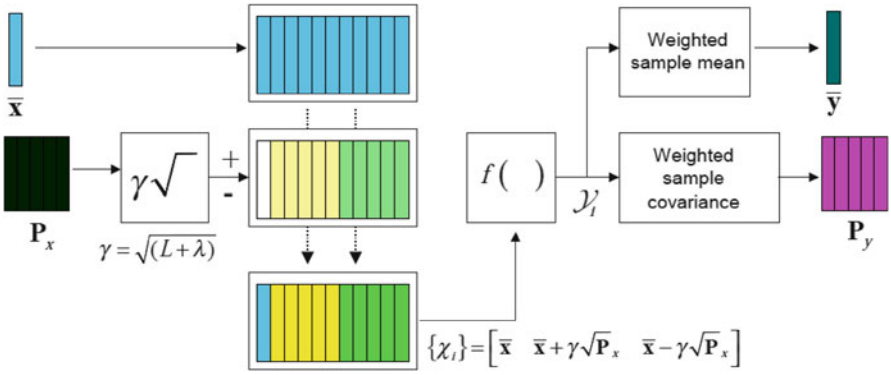

Fig. 5 Block diagram of the target prediction step

In this paper, since the state vector of each aircraft is composed by nine elements, the amount of sigma points is $18M+1$.

These sigma points χ are obtained as follow:

$$\begin{cases} \chi^0(k-1|k-1) = X^0(k-1|k-1) \\ \chi^q(k-1|k-1) = X^0(k-1|k-1) + \gamma\sqrt{P_{X^0(k-1|k-1)}}, q = 1,\ldots,9M \\ \chi^q(k-1|k-1) = X^0(k-1|k-1) - \gamma\sqrt{P_{X^0(k-1|k-1)}}, q = 9M+1,\ldots,18M \end{cases} \tag{11}$$

where:

$$\gamma = \alpha\sqrt{(9M+\kappa)} \tag{12}$$

The tuning parameter α determines the spread of the sigma points around the mean value and is usually set to a small positive value (10^{-3} in this paper). κ is a secondary scaling parameter which is usually set to 0.

The second stage consists of obtaining the predicted target vector associated to each sigma point $\overline{\chi}^q(k|k-1)$, based on the maneuvering model. The experiment presented in this paper uses the Singer acceleration model, thoroughly explained in [6].

The third stage computes the predicted mean and the predicted covariance as follow:

$$\begin{cases} X(k|k-1) = \sum_{q=0}^{18M} W_m^q \chi^q(k|k-1) \\ P_X(k|k-1) = \sum_{q=0}^{18M} W_c^q [\chi^q(k|k-1) - X(k|k-1)][\chi^q(k|k-1) - X(k|k-1)]^T \end{cases} \tag{13}$$

where

$$W_m^q = \begin{cases} 9M\left(\alpha^2 - 1\right), & \text{if } q = 0 \\ \frac{1}{18M\alpha^2}, & \text{if } q \neq 0 \end{cases} \tag{14}$$

and

$$W_c^q = \begin{cases} 9M\left(\alpha^2 - 1\right) + \left(1 - \alpha^2 + \beta\right), & \text{if } q = 0 \\ \frac{1}{18M\alpha^2}, & \text{if } q \neq 0 \end{cases} \tag{15}$$

The tuning parameter β is used to incorporate prior knowledge of the distribution of $\boldsymbol{X}$. A value of 2 is optimal for Gaussian distributions.

3.2.2 Prediction Step (Systematic Error)

Due to changes in the atmospheric conditions, as well as in the synchronization errors, the systematic errors may certainly vary in time. In this paper, we assume the linear Gaussian system presented in [7] to be an appropriate dynamic error model. This way, the prediction equations are:

$$\begin{cases} E\left(k|k-1\right) = E(0) + A\left[E\left(k-1|k-1\right) - E(0)\right] \\ P_E\left(k|k-1\right) = P_E(0) + A\left[P_E\left(k-1|k-1\right) - P_E(0)\right]A^T \end{cases} \tag{16}$$

The setting of $\boldsymbol{E}(\mathbf{0})$ and $\boldsymbol{P_E}(\mathbf{0})$ follows from off-line systematic error evaluations. Based on the typical values of α_1, α_2, as well as the synchronization errors obtained during the experiments performed in [4], the values of $\boldsymbol{E}(\mathbf{0})$ and $\boldsymbol{P_E}(\mathbf{0})$ have been chosen as follow:

- $\boldsymbol{E}(\mathbf{0})$ is set to a null vector
- $\boldsymbol{P_E}(\mathbf{0})$ is such that each diagonal value is two orders of magnitude greater than the square of its associated parameter

It is to be noted that based on the results in Fig. 3, the value of 10^{-3} has been chosen as typical for α_3. The weight matrix $\boldsymbol{A}$ is used to tune the sensitivity of the prediction step.

At this stage, we have obtained the predictions for target and systematic error.

3.2.3 Update Step (Target)

The update step for the target is performed in two phases. Phase one consists of obtaining the TDOA estimate using the philosophy depicted in Fig. 5. This way, the augmentation process described in (11) is applied to $\boldsymbol{X}(k \mid k-1)$, yielding $\boldsymbol{\chi^q}(k \mid k-1)$. The observation model described in (7) is then applied to

$\chi^{q}(k \mid k-1)$, q ranging from 0 to $18M$. We will note the result of this process as $\overline{\Delta\tau}^{q}(k|k-1)$, in order to highlight that the result for each sigma point is a vector of TDOA estimates. Please note that the values associated to this observation model are included in $E(k|k-1)$. Finally, $\overline{\Delta\tau}^{q}(k|k-1)$ is averaged as per (14) in order to obtain the vector of TDOA estimates $\overline{\Delta T}(k|k-1)$.

The second stage consists of updating the target state using the TDOA measurements, as defined in the expression below:

$$\begin{cases} X(k|k) = X(k|k-1) + K\left(\Delta T - \overline{\Delta T}(k|k-1)\right) \\ P_X(k|k) = P_X(k|k-1) - KP_{\Delta T,\Delta T}K^T \end{cases} \tag{17}$$

where:

$$K = P_{X,\Delta T}P_{\Delta T,\Delta T}^{-1}$$

$$P_{\Delta T,\Delta T} = \sum_{q=0}^{18M} W_c^q \left[\overline{\Delta\tau}^{q}(k|k-1) - \overline{\Delta T}(k|k-1)\right]\left[\overline{\Delta\tau}^{q}(k|k-1) - \overline{\Delta T}(k|k-1)\right]$$

$$P_{X,\Delta T} = \sum_{q=0}^{18M} W_c^q \left[\chi^{q}(k|k-1) - X(k|k-1)\right]\left[\overline{\Delta\tau}^{q}(k|k-1) - \overline{\Delta T}(k|k-1)\right]$$

3.2.4 Update Step (Systematic Error)

Finally, the update step of the systematic error is performed following the process described in [9]. Hence, the update equations are:

$$\begin{cases} E(k|k) \approx E(k|k-1) + P_E(k|k)v \\ P_E(k|k) \approx P_E(k|k-1) - P_E(k|k-1)VP_E^T(k|k-1) \end{cases} \tag{18}$$

Vector $\boldsymbol{v}$ is the "row-wise" sum of matrix $\boldsymbol{v_m}$. $\boldsymbol{v_m}$, in its turn, is obtained as follows:

$$v_m = \left[F_l F_\Delta - F\right]^T E^{-1} F_l \left[TDOA - \overline{\Delta T}(k|k-1)\right] \tag{19}$$

with

$$F_l = \left(F_s^T F_s\right)^{-1} F_s^T \tag{20}$$

$$F_S = \left[fs_{2,1}fs_{2,2}\ldots fs_{2,M}fs_{3,1}\ldots fs_{3,M}\ldots fs_{N_S,1}\ldots fs_{N_S,M}\right]^T \tag{21}$$

$$f_{S_{i,j}} = \left[\frac{\partial \left(TDOA_i^j \right)}{\partial x_j}, \frac{\partial \left(TDOA_i^j \right)}{\partial y_j}, \frac{\partial \left(TDOA_i^j \right)}{\partial z_j} \right] \tag{22}$$

$$F_\Delta = \left[f_{\Delta_{2,1}} f_{\Delta_{2,2}} \cdots f_{\Delta_{2,M}} f_{\Delta_{3,1}} \cdots f_{\Delta_{3,M}} \cdots f_{\Delta_{N_S,1}} \cdots f_{\Delta_{N_S,M}} \right]^T \tag{23}$$

$$f_{\Delta_{i,j}} = \left[\frac{\partial \left(TDOA_i^j \right)}{\partial \alpha_1}, \frac{\partial \left(TDOA_i^j \right)}{\partial \alpha_2}, \frac{\partial \left(TDOA_i^j \right)}{\partial \alpha_3}, \frac{\partial \left(TDOA_i^j \right)}{\partial \left(\Delta T_{2,1} \right)}, \ldots, \frac{\partial \left(TDOA_i^j \right)}{\partial \left(\Delta T_{N_s,1} \right)} \right] \tag{24}$$

$$F = F_l F_\Delta \tag{25}$$

$$E = F_l R F_l^T + P_S \tag{26}$$

where $\boldsymbol{R}$ is the diagonal matrix containing the covariance of the TDOA measurement errors. $\boldsymbol{P_S}$ is the sub-matrix composed by the elements of $\boldsymbol{P_x}(k \mid k)$ associated to the target positions.

On the other hand, matrix $\boldsymbol{V}$ is obtained as follows:

$$V = \left[F_l F_\Delta - F \right]^T E^{-1} \left[F_l F_\Delta - F \right] \tag{27}$$

4 Assessment of the Proposed Method

4.1 Experiment

In order to assess the technique presented in this paper, Monte Carlo experiments involving a hypothetical WAM scenario with eight aircraft and six base stations have been performed. The performance of the technique is measured through the accuracy and precision of the target position estimates along the experiment run time.

4.2 Assumptions

The following assumptions have been made:

Table 1 Aircraft motion

Aircraft	Initial x position (km)	Initial y position (km)	Height AMSL (km)	Ground-speed (m/s)	Bearing (°)
1	−150	60	10	250	90
2	100	70	9	200	270
3	80	−80	8	270	270
4	−120	−70	10	230	90
5	20	80	7	190	270
6	−30	−90	8	210	90
7	−30	90	8	200	90
8	−120	−60	9	260	90

Table 2 Base station coordinates

Base station	x position (km)	y position (km)	Height AMSL (km)
1	−50	50	0
2	0	50	1
3	50	50	0.2
4	−50	−50	0.5
5	0	−50	0.4
6	50	−50	0.3

- All aircraft have constant groundspeed along a specified bearing and a specified height AMSL. Due to the Earth curvature, this does not mean that the velocity vector remains constant.
- The range bias due to propagation effects has been modeled following the path integration method presented in [9].
- Clock synchronization errors and white noise have been modeled via zero-mean Gaussian distributions.

4.3 Settings

The aircraft motion settings are compiled in Table 1, whereas the base station coordinates are compiled in Table 2. Each aircraft emits its signal every 4 s. The receiver noise has been modeled through a Gaussian distribution with zero mean and a standard deviation of 3 m. The run time of the experiment is 15 min.

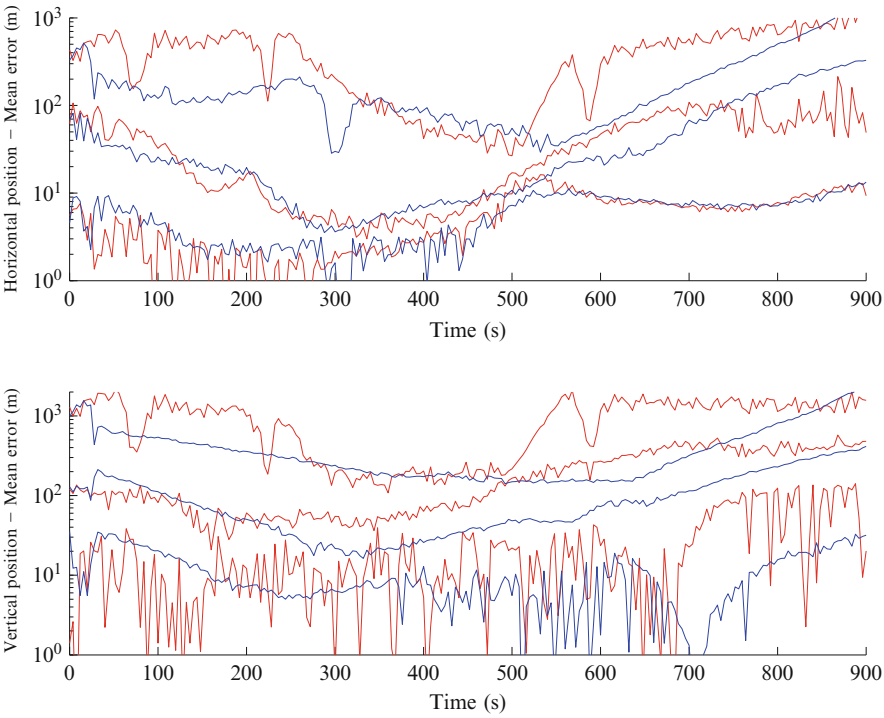

Fig. 6 Mean values of horizontal and vertical positioning error

5 Results

5.1 Legend

Figure 6 displays the mean error of the position estimate, whereas Fig. 7 displays the standard deviation. In both figures, the red plots show the minimum, median and maximum values of the respective magnitudes achieved when using the hyperbolic method. On the other hand, the blue plots display the achieved performance using the method presented in this paper.

5.2 Discussion

Concerning the accuracy of the position estimates (Fig. 6), the mean value of the error is reduced down to one fourth of the error obtained when using the hyperbolic location alone. The most significant improvements can be seen in the worst case scenario (maximum error curve).

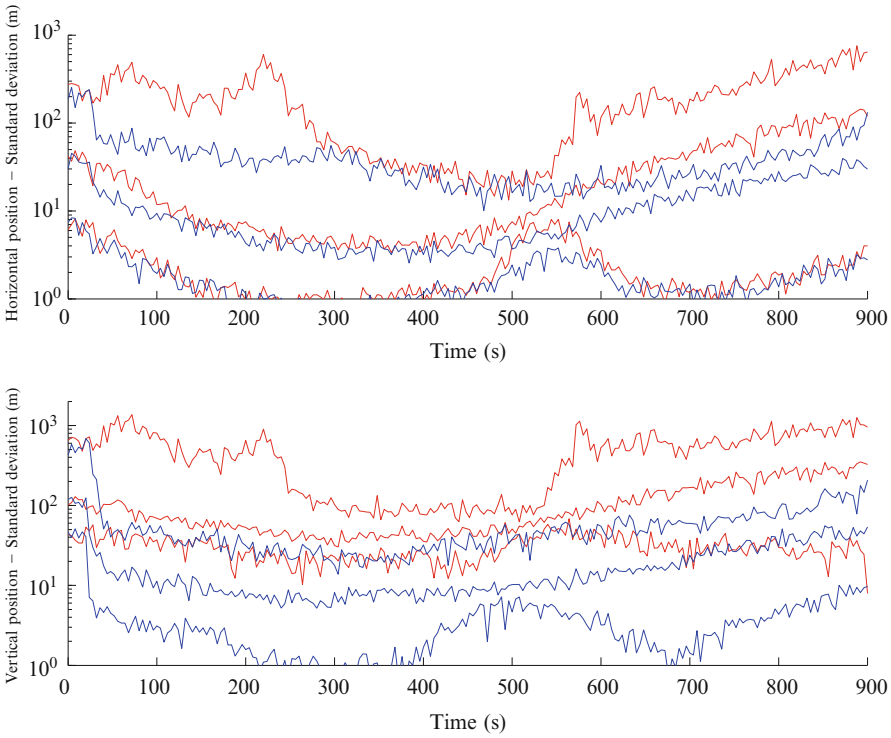

Fig. 7 Standard deviation of horizontal and vertical positioning error

The precision of the position estimates (Fig. 7) can be improved up to one order of magnitude, limiting the standard deviation of both horizontal and vertical positioning errors to 100 m during the entire run.

Figures 8 and 9 display respectively the HDOP and VDOP derived from the constellation defined in Table 2, for aircraft flying at a true altitude of 7 km AMSL. Note that the calculations have been performed assuming hyperbolic location in an error-free environment, following the method described in [10].

The algorithm used in this paper ensures that the horizontal precision of the position estimate does not exceed the predictable standard deviation based on the product of GDOP (without systematic error) and sensor error. The tracking filter ensures a vertical precision better than the GDOP-based expectation.

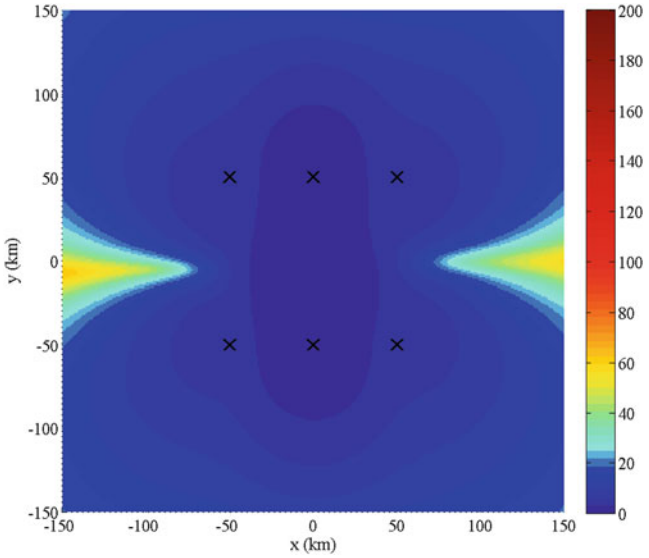

Fig. 8 HDOP for the constellation used in the experiment (an aircraft altitude of 7 km AMSL is used)

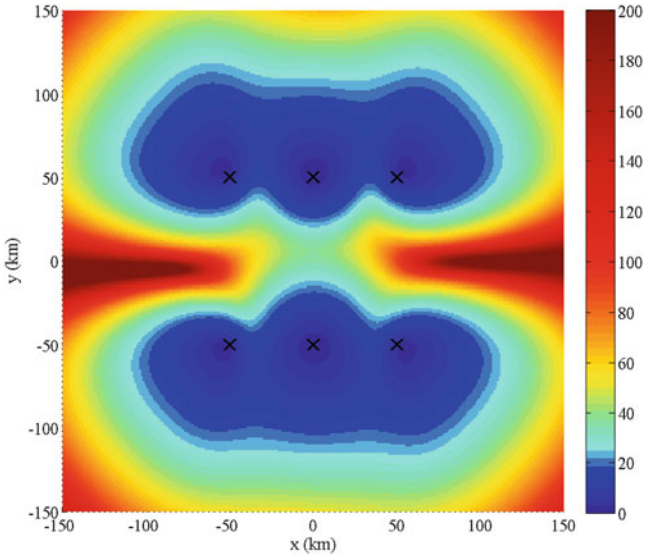

Fig. 9 VDOP for the constellation used in the experiment (an aircraft altitude of 7 km AMSL is used)

6 Conclusions

The method presented in this paper takes advantage of opportunity traffic to correct the systematic errors affecting WAM performance. Significant gains in both accuracy and precision are obtained for target tracking, especially in scenarios with poor GDOP.

Acknowledgment This work has been financed by the Spanish Science and Technology Office under projects TEC-2011-28626.

References

1. EUROCONTROL (2010) Introduction to the mission trajectory, ed. 1.0, May 2010
2. EUROCONTROL (2009) EUROCONTROL specification for the application of the Flexible Use of Airspace (FUA), ed. 1.1, October 2009
3. SESAR Consortium (2007) SESAR definition phase – deliverable 3: the ATM target concept, September 2007
4. Abbud J, De Miguel G, Besada JA (2011) Correction of systematic errors in wide area multilateration. In: Proceedings of the enhanced surveillance of aircraft and vehicles, Capri, September 2011
5. Chan YT, Ho KC (1994) A simple and efficient estimator for hyperbolic location. IEEE Trans Signal Process 42(8):1905–1915
6. Li XR, Jilkov VP (2003) Survey of maneuvering target tracking. Part I: Dynamic models. IEEE Trans Aerosp Electron Syst 39(4):1333–1364
7. Bar-Shalom Y (ed) (1992) Multitarget–multisensor tracking: applications and advances, vol II. Artech House Inc., Norwood
8. Simon JJ, Uhlmann JK (2004) Unscented filtering and nonlinear estimation. Proc IEEE 92(3)
9. Barton DK (2005) Radar system analysis and modeling. Artech House Inc., Norwood
10. Torrieri DJ (1984) Statistical theory of passive location systems. IEEE Trans Aerosp Electron Syst 20(2):183–198

Study of Ionospheric Delay Gradient Based on GPS Monitoring Stations Near Suvarnabhumi Airport in Thailand

Sarawoot Rungraengwajiake, Pornchai Supnithi, Susumu Saito, Nattapong Siansawasdi, and Apitep Saekow

Abstract The ionospheric delay gradient is an important parameter for the planning of ground-based augmentation system (GBAS) in a region. When it is beyond the limit, the integrity and safety for landing approach of CAT II/III may be compromised. In order to maintain the availability and safety requirement of the system, the ionospheric threat models have been developed in several countries during the past few years. However, the ionospheric delay gradient associated with plasma bubble in low latitude region has not been studied well. In this work, we present some analytical results of ionospheric delay gradient based on three GPS monitoring stations near Suvarnabhumi airport in Thailand. The stations are located on the campus of King Mongkut's Institute of Technology Ladkrabang (13.7278°N, 100.7726°E), Stamford University (13.7356°N, 100.6612°E) and Suvarnabhumi airport (13.6945°N, 100.7608°E). The analyzed results on 1st September 2011 show that the ionospheric delay gradient varies from −95.23 to 107.7 mm/km during the occurrence of the plasma bubbles.

Keywords GBAS • Ionospheric delay gradient • Slant TEC

S. Rungraengwajiake (✉) • P. Supnithi
Faculty of Engineering, King Mongkut's Institute of Technology Ladkrabang, Bangkok 10520, Thailand
e-mail: sarawootersky@gmail.com

S. Saito
Communication, Navigation and Surveillance Department, Electronic Navigation Research Institute, Tokyo, Japan

N. Siansawasdi
Air Navigation Radio Aids Department, Aeronautical Radio of Thailand, Bangkok, Thailand

A. Saekow
Faculty of Science and Technology, Stamford International University, Bangkok, Thailand

Electronic Navigation Research Institute (ENRI), *Air Traffic Management and Systems*, Lecture Notes in Electrical Engineering 290, DOI 10.1007/978-4-431-54475-3_11,

1 Introduction

The global navigation satellite system (GNSS) has become a powerful component for aeronautical navigations. However, the ionospheric delay is still the largest source of errors and degrades the accuracy of GNSS receivers. To improve the accuracy and availability of the system, the differential techniques have been developed to mitigate such error. For aeronautical navigation, the Satellite-Based Augmentation System (SBAS) and Ground-Based Augmentation System (GBAS) have been developed to support all navigation operational levels of the aircrafts. These augmentation systems provide the differential corrections and integrity information to the GNSS receivers that are equipped in the aircrafts. It is now well known that the severe ionospheric disturbances such as the storm-enhanced density (SED) can cause a large ionospheric delay gradient, which affects the availability and integrity requirement of the systems especially for landing approach of GBAS CAT II/III. The previous study in [1] has shown the extreme ionospheric delay gradient observed in U.S. on 20th November 2003 during the geomagnetic storm. It can reach 413 mm/km over the 40–100 km baselines. Therefore, the ionospheric anomaly monitoring and ionospheric threat model for GBAS are developed based on GPS receivers of CONUS (Conterminous U.S.), emphasizing on this extreme event located only in U.S. [2]. In order to protect the safety level requirements for worldwide operation, however, the local ionospheric threat model needs to be developed for other concerned regions. For equatorial and low-latitude regions, particularly, the equatorial anomaly and plasma bubble are common phenomena which can cause the ionospheric delay gradient as well as ionospheric scintillation [3]. However, the ionospheric delay gradients associated with plasma bubble in these regions have not been well studied [4].

In this work, we investigate the ionospheric delay gradient obtained from GPS monitoring stations near Suvarnabhumi airport in Bangkok, Thailand. We have analyzed a sample set of data during September equinox with the plasma bubble occurrence. In addition, we show a simple concept to calibrate the receiver biases suitable for the satellite pass during plasma bubble occurrence.

2 Theoretical Background

The largest error source of GNSS such as Global Positioning System (GPS) measurements is the ionospheric delay (I), which is a proportional to the amount of electrons in terms of slant total electron content (STEC), i.e.,

$$I = \frac{40.3}{f^2} STEC \tag{1}$$

where f is the frequency of the satellite signal and *STEC* is a number of electrons found in 1-m^2 column along the satellite-receiver propagation path, generally expressed in TEC unit or TECU (1 TECU $= 10^{16}$ electron/m^2). For GPS system, the slant TEC can be derived from dual-frequency GPS receivers based on the combination of pseudorange ($STEC_P$) or carrier phase ($STEC_L$) measurements given by

$$STEC_P = K(P_2 - P_1) \tag{2}$$

and

$$STEC_L = K(L_1 - L_2) \tag{3}$$

where P_1, P_2, L_1 and L_2 are the pseudorange and carrier phase (expressed in range) measurements at the L1 (1575.42 MHz) and L2 frequency (1227.60 MHz), respectively. The constant $K = 9.5196$ m^{-1} TECU for *STEC* expressed in TECU (1 TECU $= 10^{16}$ electrons/m^2). For the L1 and L2 frequency, 1 TECU is equivalent to 16 and 27-cm time delay. Note that the $STEC_P$ still includes the inherent satellite and receiver inter-frequency bias (IFB) which comes from the differential extra delay time between L1 and L2 frequencies due to the internal electronic circuit of receiver front-end and also some from satellite antenna path. Although the slant TEC derived from the pseudorange measurements is noisier than that derived from the carrier phase measurements, the carrier phase measurement contains initial phase ambiguities, which frequently cause the slant TEC to have some negative values. In order to keep the precise slant TEC from carrier phase measurement and also remove the initial phase ambiguities, the $STEC_L$ is adjusted to the $STEC_P$ level. For a simple approach, the $STEC_L$ is adjusted to the mean value of corresponding $STEC_P$ for each continuous arc, which can be expressed as

$$STEC_{adj} = STEC_L + \left(\overline{STEC_P - STEC_L}\right)_{arc} \tag{4}$$

where $\bar{x}$ represents the mean of x. However, the satellite and receiver IFB still needs to be accounted for. The adjusted slant TEC ($STEC_{adj}$) can therefore be given by

$$STEC_{adj} = STEC + B_S + B_R \tag{5}$$

where B_S and B_R are the satellite and receiver IFB, respectively. To compute the ionospheric delay gradient, the differential $STEC_{adj}$ of the kth satellite between two monitoring stations is first computed. Therefore, the satellite IFB will be eliminated. Figure 1 shows the concept of ionospheric delay gradient computation. However, the differential receiver IFB ($B_{R1} - B_{R2}$) still remains as a significant offset, i.e.,

$$dSTEC^k = \left(STEC_1^k - STEC_2^k\right) + (B_{R1} - B_{R2}) \tag{6}$$

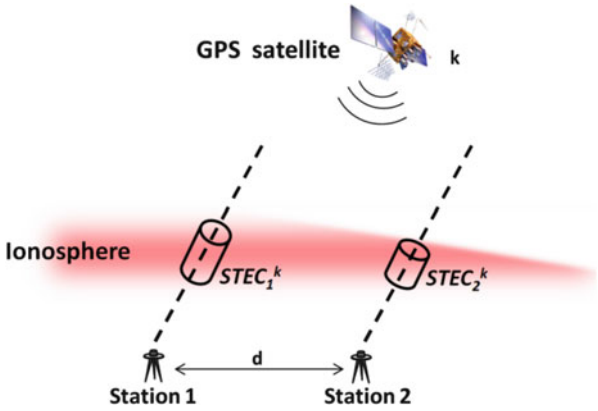

Fig. 1 Illustration of ionospheric delay gradient monitoring stations

The next step is to remove the differential receiver IFB ($B_{R1} - B_{R2}$). We apply the principle that the slant TECs of a short baseline monitoring stations are similar during the quiet ionospheric condition. Also, we assume that the receiver IFBs do not vary in one day. Therefore, the constant of the differential $STEC_{adj}$ is just the differential receiver IFB ($B_{R1} - B_{R2}$). This method is simpler than the methods in [5, 6]. Finally, the ionospheric delay gradient (∇I) can be estimated by dividing the differential $STEC_{adj}$ between two stations by the baseline distance (d) between two receivers at each epoch t, i.e.,

$$\nabla I(t) = \frac{40.3}{f^2}\left(\frac{STEC_1^k(t) - STEC_2^k(t)}{d}\right) \tag{7}$$

3 Experimental Setup

The slant TECs are derived from RINEX (Receiver Independent Exchange Format) data of three dual-frequency GPS receivers at the monitoring stations near Suvarnabhumi airport in Bangkok, Thailand. One is located on the runway of the airport (AERO: 13.6945°N, 100.7608°E). The others are located at King Mongkut's Institute of Technology Ladkrabang (KMIT: 13.7278°N, 100.7726°E) and Stamford International University (STFD: 13.7356°N, 100.6612°E) which are shown in Fig. 2. The pseudorange and carrier phase measurements are made at a 1-Hz sampling interval. In the pre-processing step, the cycle slips in the carrier phase measurements are detected and repaired using the algorithm in [7]. In this work, we select the data on 1st September 2011 for the analysis, which has the solar 10.7 cm radio flux index (F10.7) equal to 112, and we found the *STEC* fluctuations during nighttime.

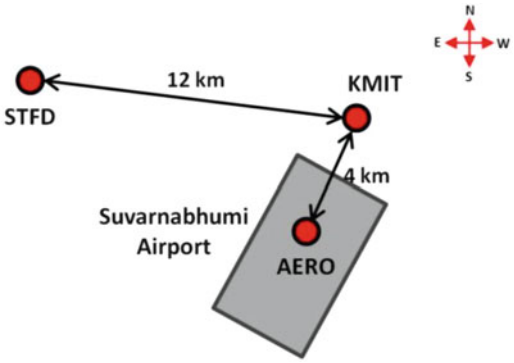

Fig. 2 Three GPS monitoring stations near Suvarnabhumi airport

4 Results and Discussions

In Fig. 3, we show the *STEC* of three stations on 1st September 2011. Note that the satellite and receiver IFBs are not calibrated and there are no *STEC* data from AERO station during 00:00–05:00 UT due to the receiver problems. The *STEC* of all stations evidently fluctuate during 14:00–19:00 UT or 21:00–02:00 LT (UTC + 7). The *STEC* fluctuation observed at low-latitude regions during nighttime are possibly caused by plasma bubbles. There are five satellites (PRN2, PRN9, PRN14, PRN21 and PRN29), which are affected by the STEC disturbances during this time.

In Fig. 4, we show the differential *STEC* (*dSTEC*) of these satellites aligning in the STFD-KMIT and AERO-KMIT directions or west–east and south–north direction, which can be considered zonal and meridional baselines, respectively. The different colors indicate the *dSTEC* of the visible satellites. The *dSTEC*s also evidently start the fluctuation during 14:00–19:00 UT in both directions. The dSTECs in the STFD-KMIT baseline has higher fluctuation than the AERO-KMIT baseline, probably caused by the longer baseline and the zonal drift of plasma bubble. The *dSTEC* values are relatively constant during 09:00–13:00 and 19:00–24:00 UT. This constant level can be regarded as the differential receiver IFBs. The average of the constant level of *dSTEC*s is considered the differential receiver IFBs which is then subtracted from the original *dSTEC*s. However, a slight offset exists in the AERO-KMIT direction due to the uncertainty in the adjustment process as detailed in [8]. The differential receiver IFBs should therefore be considered for each satellite. The differential receiver IFBs can vary from 4.28 to 5.12 TECU for STFD-KMIT receiver and 5.18 to 6.78 TECU for AERO-KMIT receiver. After the bias calibration, the ionospheric delay gradient (∇I) with respect to the L1 frequency is shown in Fig. 5.

The ∇I trends of both directions look similar with the fluctuation starting around 13:30 UT and becoming flat at 20:00 UT. The maximum ∇I can reach 107.7 mm/km at AERO-KMIT direction observed from PRN29 around 14:30 UT. For STFD-KMIT direction, the PRN21 gives the maximum $\nabla I = -95.23$ mm/km at 16:00 UT. In addition, the ∇I fluctuation of some satellites (for example, PRN9 (green)

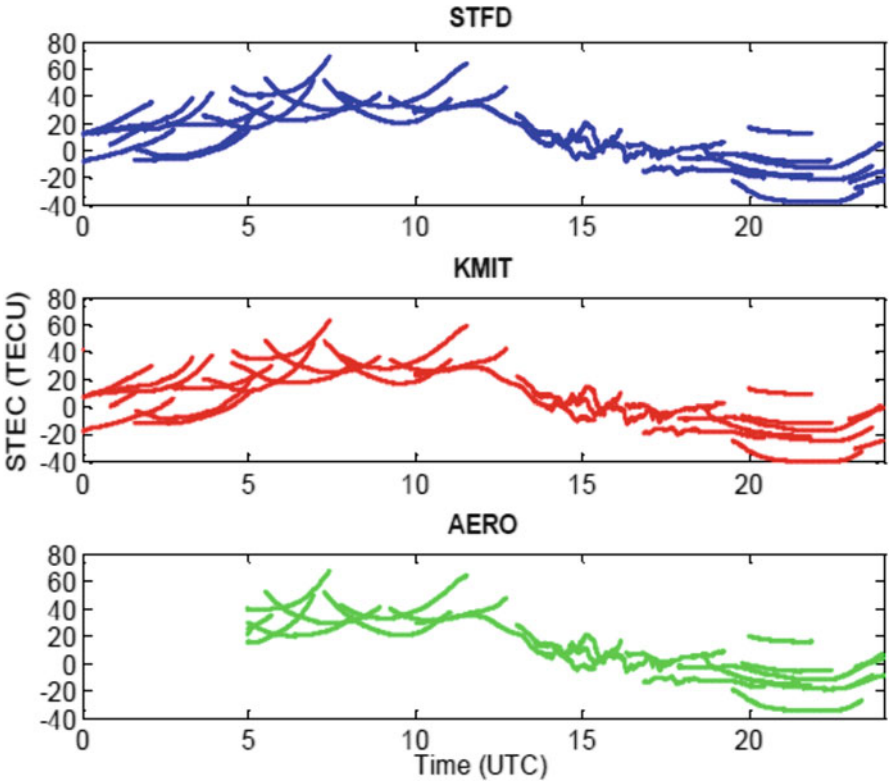

Fig. 3 Overall slant TECs of three stations (satellite and receiver IFBs are not calibrated)

and PRN14 (pink)) evidently show the different patterns. This can be due to the combination effect of IPP (Ionospheric Pierce Point) motions and plasma bubble movement. In order to evaluate the effects of plasma bubble on GBAS, the current plasma bubble model applies a rectangular depletion shape of electron density to simulate the worst case of positioning error [4]. However, the ∇I results show that they have the complicated variation corresponding to the complex shapes of plasma bubble. Figure 6 shows the probability mass functions (PMFs) of the ionospheric delay gradient (∇I) of both directions. The average and standard deviation of ∇I in STFD-KMIT and AERO-KMIT directions are 1.16 and -1.36 mm/km, 12.52 and 7.81 mm/km, respectively. The distribution centers of both directions are close to zero. The deviation of both directions look symmetrical with the STFD-KMIT direction showing more deviation than AERO-KMIT direction, probably cause by the moving of plasma bubble in the zonal direction. In order to support all possibilities of ionospheric delay gradient on this day, the local ionospheric threat model should cover the lower and upper bound of these PMFs, which are -95.23 to 107.7 mm/km. For the GAST-D (GBAS Approach Service Type D), which is the single-frequency GBAS support for CAT II/III, the current SARPs (Standards

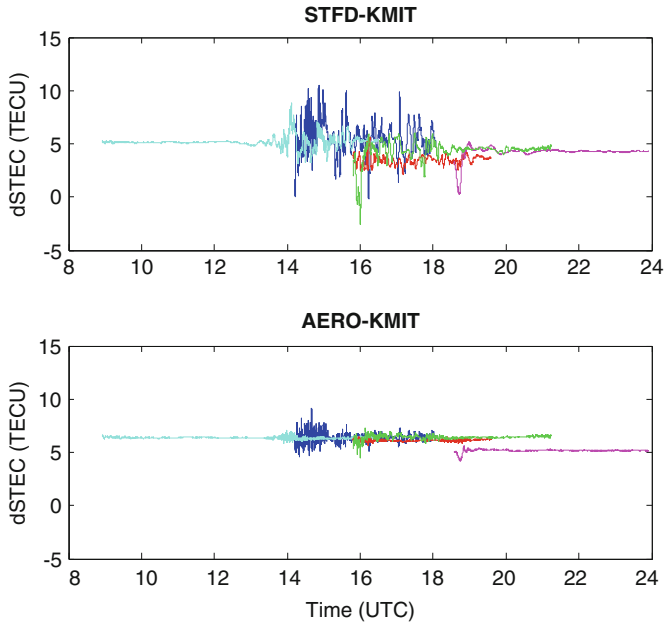

Fig. 4 Differential *STEC* (*dSTEC*) align in STFD-KMIT (*top*) and AERO-KMIT (*bottom*) direction

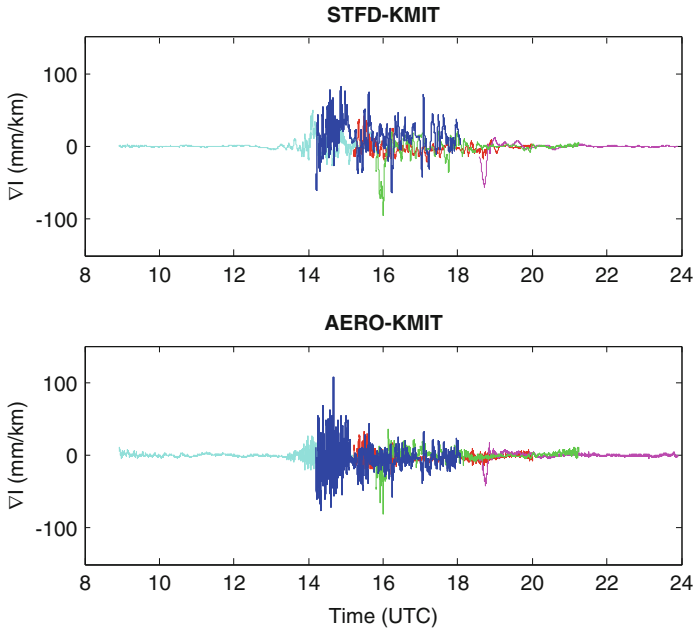

Fig. 5 Ionospheric delay gradient (∇I) align in STFD-KMIT (*top*) and AERO-KMIT (*bottom*) direction

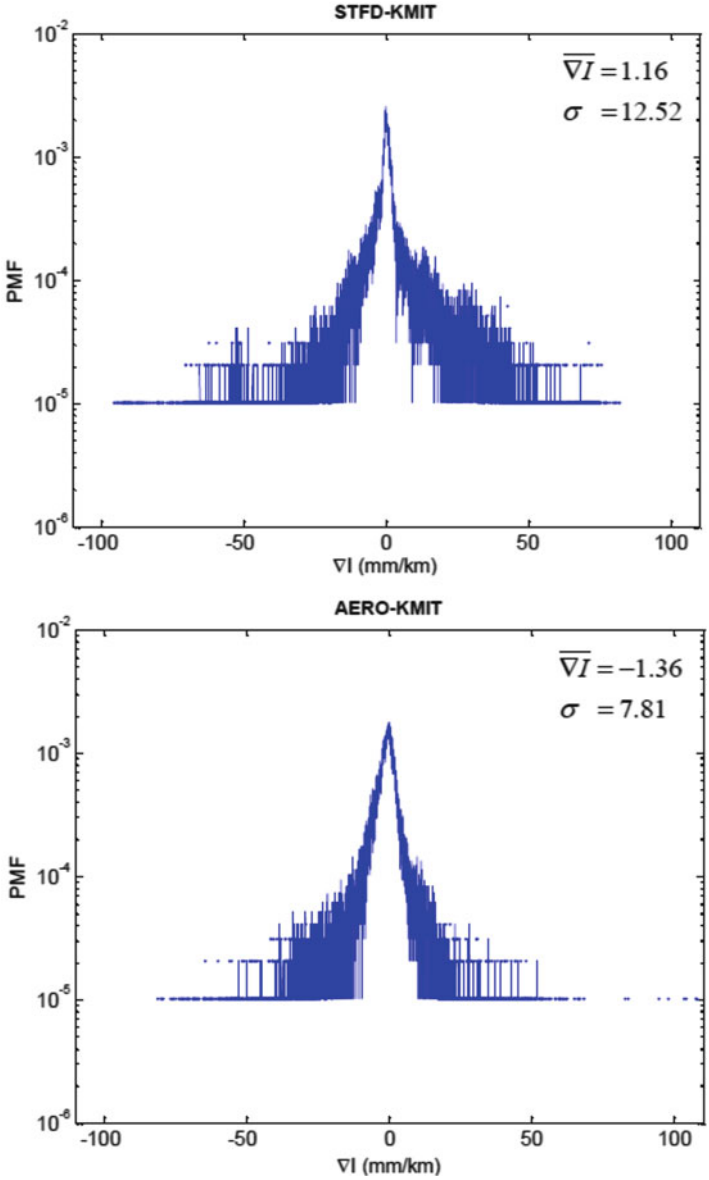

Fig. 6 Probability mass functions (PMFs) of ionospheric delay gradient (∇I) in STFD-KMIT (*top*) and AERO-KMIT (*bottom*) direction

and Recommended Practices) requires the ionospheric delay gradient shall be less than 300 mm/km [9]. Although, the observed ionospheric delay gradients during plasma bubble occurrence in this study are lower than the requirement threshold, the monitoring stations should continue to investigate more data sets to identify the possible extreme events within this region.

5 Conclusion

The ionospheric delay gradient is an important parameter for integrity and availability monitoring of GBAS. The equatorial and low-latitude regions are well known to have the plasma bubble phenomenon which may potentially degrade the GBAS system performance. In this work, we have analyzed the ionospheric delay gradient from three monitoring stations near Suvarnabhumi airport in Bangkok, Thailand. The results show the ionospheric delay gradient at the west–east and south–north directions can vary from −95.23 to 107.7 mm/km on the studied day in September equinox.

Acknowledgments The authors are grateful to Aeronautical Radio of Thailand, KMITL and Stamford International University for providing the location and facilities for the GPS receiver installation. This work is partially funded by National Research Council of Thailand and KMITL Research Fund.

References

1. Datta-Barua S, Lee J, Pullen S, Luo M, Ene A, Qiu D, Zhang G, Enge P (2010) Ionospheric threat parameterization for local area GPS-based aircraft landing systems. J Aircr 47:1141–1151
2. Lee J, Jung S, Bang E, Pullen S, Enge P (2010) Long term monitoring of ionospheric anomalies to support the local area augmentation system. In: Proceeding of ION GNSS 2010, pp 2651–2660
3. Yoshihara T, Fujii N, Matsunaga K, Hoshinoo K, Sakai T, Wakabayashi S (2007) Preliminary analysis of ionospheric delay variation effect on GBAS due to plasma bubble at southern region in Japan. In: Proceeding of the 2007 National Technical Meeting of ION 2007, pp 1065–1072
4. Saito S, Yoshihara T, Fujii N (2009) Study of effects of the plasma bubble on GBAS by a three-dimensional ionospheric delay model. In: Proceeding of ION GNSS 2009, pp 1141–1148
5. Ma G, Maruyama T (2003) Derivation of TEC and estimation of instrumental biases from GEONET in Japan. Ann Geophys 21:2083–2093
6. Rideout W, Coster A (2006) Automated GPS processing for global total electron content. GPS Solutions 10:219–228
7. Blewitt G (1990) An automatic editing algorithm for GPS data. Geophys Res Lett 17:199–202
8. Ciraolo L, Azpilicueta E, Brunini C, Meza A, Radicella SM (2007) Calibration errors on experimental slant total electron content (TEC) determined with GPS. J Geod 81:111–120
9. Murphy T, Harris M, Pullen S, Pervan B, Saito S, Brenner M (2010) Validation of ionospheric anomaly mitigation for GAST-D. In: ICAO NSP Working Group of the Whole (WGW) meeting, Montreal

Part V
Tutorial: Mathematical Model

Mathematical Models for Aircraft Trajectory Design: A Survey

D. Delahaye, S. Puechmorel, P. Tsiotras, and E. Feron

Abstract Air traffic management ensures the safety of flight by optimizing flows and maintaining separation between aircraft. After giving some definitions, some typical feature of aircraft trajectories are presented. Trajectories are objects belonging to spaces with infinite dimensions. The naive way to address such problem is to sample trajectories at some regular points and to create a big vector of positions (and or speeds). In order to manipulate such objects with algorithms, one must reduce the dimension of the search space by using more efficient representations. Some dimension reduction tricks are then presented for which advantages and drawbacks are presented. Then, front propagation approaches are introduced with a focus on Fast Marching Algorithms and Ordered upwind algorithms. An example of application of such algorithm to a real instance of air traffic control problem is also given. When aircraft dynamics have to be included in the model, optimal control approaches are really efficient. We present also some application to aircraft trajectory design. Finally, we introduce some path planning techniques via natural language processing and mathematical programming.

Keywords Aircraft trajectory design • B-spline • Principal component analysis • Bézier • Homotopy • Optimal control • Air traffic management • Strategic planning • Pre-tactical planning • Tactical planning

D. Delahaye (✉) • S. Puechmorel
Applied Mathematics Laboratory, French Civil Aviation University, Toulouse, France
e-mail: delahaye@recherche.enac.fr; puechmor@recherche.enac.fr

P. Tsiotras • E. Feron
School of Aerospace Engineering Georgia Institute of Technology, Atlanta, GA, USA
e-mail: tsiotras@gatech.edu; feron@gatech.edu

Electronic Navigation Research Institute (ENRI), *Air Traffic Management and Systems*, Lecture Notes in Electrical Engineering 290, DOI 10.1007/978-4-431-54475-3_12,

1 Introduction

Aircraft trajectory is one of the most fundamental objects within the frame of ATM. However, partly due to the fact that aircraft positions are most of the time represented as radar plots, the time dependence is generally overlooked so that many trajectory statistics conducted in ATM are spatial only. Even in the most favorable setting, with time explicitly taken into account, trajectory data is expressed as an ordered list of plots labeled with a time stamp, forgetting the underlying aircraft dynamics. Furthermore, the collection of radar plots describing the same trajectory can have tenths more samples, nearly all of them redundant. From the trajectory design point of view, this redundancy is real handicap for the optimization process. In this survey, alternative trajectory representations are presented with a description of their advantages and limits. Such new approaches may be applied in many areas:

Aircraft Trajectories Data Compression. As it has been previously mentioned, ATM system manage aircraft trajectories and control them in order to guarantee safety and airspace capacity. Currently those trajectories are represented by the mean of plot lists which are manipulated by ATM software. Every day, all aircraft trajectories are registered into large database for which huge capacity is needed. Based on this new trajectory representation for which redundancy has been removed, the trajectories database may be strongly improved from the capacity point of view. This compressed trajectory format may also be used for improving the trajectories transmission between ATM entities.

Aircraft Trajectories Distance Computation. Although trajectories are well understood and studied, relatively little investigation on the precise comparison of trajectories is presented in the literature. A key issue in performance evaluation of ATM decision support tools (DST) is the distance metric that determines the similarity of trajectories. Some proposed representation may be used to enhance trajectory distance computation.

Aircraft Model Inference. All aircraft models are based on ODEs (Ordinary Differential Equation), including tabular ones. Control input includes condition and model parameters. The model refinement (and computational complexity) ranges from tabular to many degrees of freedom. The aircraft model inference consists in answering the following question: Given a parametrized model and a goal trajectory, can we infer the best parameter values? A model can be viewed as a mapping from the control space into the trajectory space. The way to answer the previous question is then given by the closest model to the goal trajectory.

Trajectory Prediction. Air traffic management research and development has provided a substantial collection of decision support tools that provide automated conflict detection and resolution [13,24,78], trial planning [46], controller advisories for metering and sequencing [19, 75], traffic load forecasting [45, 47], weather impact assessment [25, 41, 74]. The ability to properly forecast future aircraft trajectories is central in many of those decision support tools. As a result, trajectory

prediction (TP) and the treatment of trajectory prediction uncertainty continue as active areas of research and development (e.g. [49, 50, 61, 71, 76]). Accuracy of TP is generally defined as point spatial accuracy (goal attainment) or as trajectory following accuracy. The last one can be rigorously defined by the mean of trajectory space. The first one is a limit case of the second by adding a weight function in the energy functional. Since we may prescribe smoothness accuracy of a simplified model relative to a finer one, may be computed.

Major Flows Definition. When radar tracks are observed over a long period of time in a dense area, it is very easy to identify major flows connecting major airports. The expression "major flows" is often used but never rigorously defined. Based on an exact trajectory distance and a learning classifier, it is possible to answer the following questions: Given a set of observed trajectories, can we split it into "similar" trajectory classes? If yes, classes with highest number of elements will rigorously define the major flows. Given those classes and a new trajectory, can we tell if it belongs to a major flow and which one? The principle of the major flows definition is to use shape space to represent trajectory shapes as points and to use a shape distance (the shape of a trajectory is the path followed by an aircraft, that is the projection in the 3D space of its 4D trajectory. The speed on the path has no impact).

Trajectory Planning. To improve Air Traffic Management, projects have been initialized in order to compel the aircraft in position and in time (4D trajectory) so as to avoid potential conflict and allow for some optimality with respect to a given user cost index, environmental criteria (noise abatement, pollutant emission ...). Depending on the time horizon, several kind of plannings can be designed:

- At a strategical level, only macroscopic indicators like congestion, mean traffic complexity, delays can be taken into account, considering the high level of uncertainty;
- at a pre-tactical level, the accuracy of previous indicators, specially congestion and complexity increases while at the same time early conflict detection can be performed;
- finally, at the tactical level, conflict resolution is the major concern and optimality of the trajectories is only marginally interesting.

As we can see, there are many areas of ATM where trajectories are the main objects that have to be manipulate.

The second part of this survey presents some relevant features of aircraft trajectories. The third part, presents dimension reduction tricks for optimization approaches. The fourth part describes approaches based on wave front propagation in isotropic and anisotropic environments. The fifth part presents automatic control approaches with some application to air traffic control. Finally, the sixth part introduces some path planning techniques via natural language processing and mathematical programming. Finally, the seventh part gives some air traffic management applications of such trajectory design approaches.

2 Some Trajectories Features

In the following all aircraft trajectories will be described as mappings from a time interval $[a,b]$ to a state space E with E either $\mathbb{R}^3$ or $\mathbb{R}^6$ depending on whether speed is assumed to be part of aircraft state or not. Extension to trajectories on a sphere (typically long haul flights) will be sketched only.

2.1 Notations and Terminology

The reference for this section is [6]. Let $\gamma[a,b] \to E$ be a trajectory. The origin of the trajectory is $\gamma(a)$ and the destination is $\gamma(b)$. Those two points are called the endpoints of the trajectory. All trajectories are assumed to be at least continuously differential (class C^1) so that the length of a trajectory $\gamma[a,b] \to E$ is well defined as:

$$l(\gamma) = \int_a^b \|\gamma'(t)\| dt \tag{1}$$

If $\|\gamma'(t)\| = 0$ for some $t \in (a,b)$ the point t is said to be singular. A parametrized curve of class C^p (or more concisely a C^p curve) will be a C^p mapping from an **open** time interval (a,b) to the state space E with no singular points. Any C^1 curve can be parametrized by arc length. Let $\gamma(a,b) \to E$ be such a curve. Defining the mapping $s(a,b) \to (0,l(\gamma))$ by:

$$s(t) = \int_a^t \|\gamma'(t)\| dt \tag{2}$$

We see that by the non-singularity assumption on γ, $s'(t) = \|\gamma'(t)\| > 0$ for any $t \in (a,b)$, so that s is an invertible mapping. Now, $\gamma \circ s^{-1}$ is a mapping from the open interval $(0,l(\gamma))$ to E satisfying:

$$\|(\gamma \circ s^{-1})'\| = \|(\gamma' \circ s^{-1}) \circ (s^{-1})'\| = 1 \tag{3}$$

In the following, we will simply write $\gamma(s), s \in (0,l(\gamma))$ for a curve parametrized by arc length, dropping the variable t.

Remark 1. One must be careful with the respective definitions of trajectories and curves: a curve is defined on an open interval and thus has no endpoints. Nevertheless, any trajectory $\gamma[a,b] \to E$ has an associated curve, namely $\gamma(a,b) \to E$. It is generally more convenient to deal with curves to avoid special treatment of the endpoints.

Remark 2. The non singularity assumption on the underlying curve is very natural when dealing with aircraft trajectories in $\mathbb{R}^3$ since it is not possible for an aircraft to stop except at the endpoints of the trajectory.

Remark 3. While the case $E = \mathbb{R}^3$ is very natural and intuitive, care must be taken when $E = \mathbb{R}^6$ since all the preceding definitions apply in a completely different setting: for example, the non singularity assumption does not implies nowhere zero speed, but only that speed and acceleration cannot both vanish at the same time. The arc length parametrization allows to define very important geometrical quantities when $E = \mathbb{R}^3$.

Definition 1. Let:

$$\gamma(0,l) \to \mathbb{R}^3 \tag{4}$$

be a C^1 curve parametrized by arc length. The unit tangent vector to γ at $s \in (0,l)$ is:

$$\tau(s) = \gamma^{'}(s) \tag{5}$$

It is clear from the definition of parametrization by arc length that $\tau(s)$ is a unit vector.

Definition 2. Let:

$$\gamma(0,l) \to \mathbb{R}^3 \tag{6}$$

be a C^2 curve parametrized by arc length. The curvature of γ at $s \in (0,l)$ is:

$$K(s) = \|\gamma^{''}(s)\| \tag{7}$$

The curvature can be explicitly computed even if the curve γ is not parametrized by arc length. The general formula is:

$$K(t) = \frac{\|\gamma^{'}(t) \wedge \gamma^{''}(t)\|}{\|\gamma^{'}(t)\|^3} \tag{8}$$

with $\wedge$ the vector cross product. Curvature is of primary importance for ATM related studies since as mentioned before aircraft trajectories are mainly made of straight lines and arcs of circle and so have piecewise constant curvature. If at point t the curvature is not zero, the curve is said to be biregular at t. For a curve γ parametrized by arc length, the unit normal vector $\nu(s)$ is defined at all biregular points by:

$$\nu(s) = \frac{\gamma^{''}(s)}{K(s)} \tag{9}$$

Remark 4. A straight line has everywhere zero curvature. However, it is clearly possible to define a unit normal vector. At a biregular point, $\tau(s)$ and $\nu(s)$ are well defined. Taking their cross product gives a new vector $\beta(s) = \tau(s) \wedge \nu(s)$. If the curve γ is assumed to be C^3, it can be shown that $\dot{\beta}(s)$ and $\nu(s)$ are collinear:

$$\beta(s) = T(s).\nu(s) \tag{10}$$

The real number $T(s)$ is called the torsion of the curve at s and represents an obstruction for the curve to be planar. As for the curvature, it is possible to compute the torsion even if the curve is not parametrized by arc length:

$$T(t) = -\frac{det(\gamma'(t), \gamma''(t), \gamma'''(t))}{\|\gamma'(t) \wedge \gamma''(t)\|^2} \tag{11}$$

Torsion is not so useful as curvature for en-route data analysis since only a few number of trajectories have non zero torsion. However, it is very relevant in terminal areas.

Remark 5. The $E = \mathbb{R}^6$ case is again very different, since the geometric meaning of curvature and torsion is not obvious in this setting. Furthermore, the extra degrees of freedom will impose using higher order derivatives in order to build up an equivalent description. A complete treatment goes beyond the scope of the present paper and has little interest for our purpose (in practical applications, the speed information, when available, is used to improve estimates of curvature and torsion and not to study a trajectory in $\mathbb{R}^6$).

3 Trajectory Models for Optimization

This section presents some dimension reduction tricks in order to reduce the dimension of the state space for which an optimization process is searching for an optimal vector of parameter.

This approach is summarized by Fig. 1.

The optimization process controls the parameter vector which is then used to build the trajectory γ for evaluation.

Each coordinate can be considered separately in order to build a given trajectory: $\gamma(t) = [x(t), y(t), z(t)]^T$.

In this section, several trajectory models are presented and compared. Simple models are first presented.

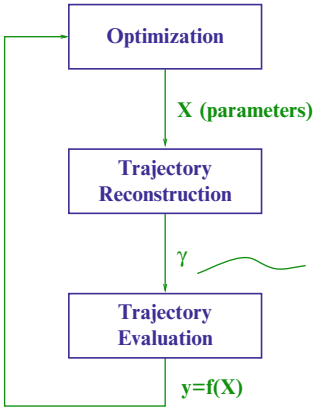

Fig. 1 The optimization process control the X vector in order to build a trajectory γ for evaluation

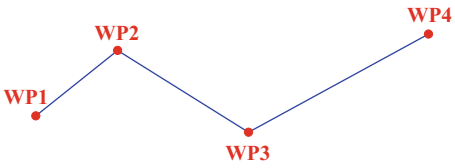

Fig. 2 Trajectory defined by four way points connected by *straight lines*

3.1 Straight Line Segments

One of the easiest way to design trajectory is to use way points connected by straight lines (see Fig. 2). This easy principle ensures continuity for the trajectory but not for its derivatives. If one want to approximate trajectory with many shape turns, one have to increase the number of way points in order to reduce the error between the model of the real trajectory.

In order to improve concept Lagrange interpolation process adjust a polynomial function to a given set of way points.

3.2 Lagrange Interpolation

Given $n+1$ real numbers $y_i, 0 \leq i \leq n$, and $n+1$ distinct real numbers $x_0 < x_1 < \ldots < x_n$, *Lagrange polynomial [39] of degree n* ($L_n(x)$) associated with $\{x_i\}$ and $\{y_i\}$ is a polynomial of degree n solving the interpolation problem:

$$L_n(x_i) = y_i, \ 0 \leq i \leq n \tag{12}$$

$$L_n(x) = \sum_{i=0}^{n} y_i . l_i(x) \tag{13}$$

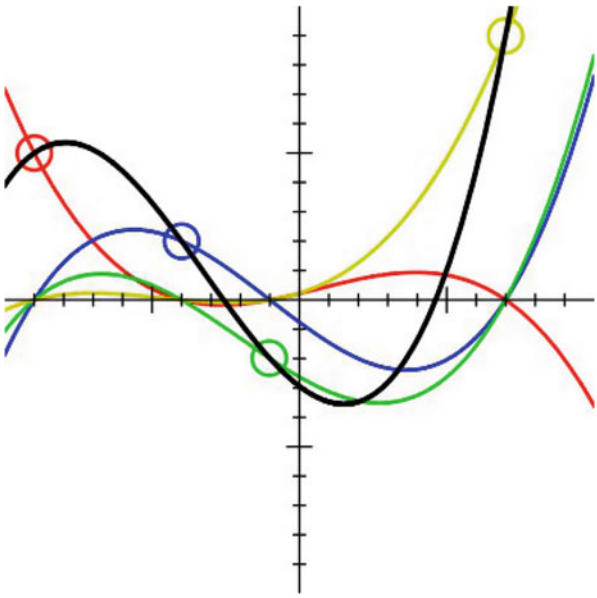

Fig. 3 $L_n(x)$ is represented by the *black curve*. The *other curves* are the polynomials $l_i(x)$

where

$$l_i(x) = \prod_{j \neq i} \frac{(x - x_j)}{(x_i - x_j)} \tag{14}$$

An example of Lagrange interpolation is given in Fig. 3 for which four points are interpolated by the black curve which represents $L_4(x)$. The four polynomial functions $\{l_0(x), l_1(x), l_2(x), l_3(x)\}$ are also given by the red, blue, green and yellow curves.

When derivatives have also to be interpolated, Hermite interpolation has to be used.

3.3 Hermite Interpolation

Hermite interpolation [3] generalizes Lagrange interpolation by fitting a polynomial $(H(x))$ to a function f that not only interpolates f at each knot but also interpolates a given number of consecutive derivatives of f at each knot. This means that the first derivative of the polynomial $H(x)$ have to fit the first derivatives of the function $f(x)$:

$$\left[\frac{\partial^j H(x)}{\partial x^j}\right]_{x=x_i} = \left[\frac{\partial^j f(x)}{\partial x^j}\right]_{x=x_i} \tag{15}$$

for all $j = 0, 1, \ldots, m$ and $i = 1, 2, \ldots, k$

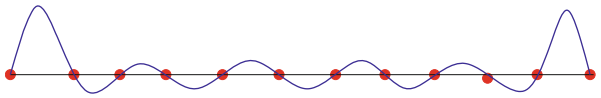

Fig. 4 Lagrange interpolation result for a set of aligned points

This means that $n(m+1)$ values

$$\begin{array}{llll} (x_0,y_0), & (x_1,y_1), & \ldots, & (x_{n-1},y_{n-1}), \\ (x_0,y_0'), & (x_1,y_1'), & \ldots, & (x_{n-1},y_{n-1}'), \\ \vdots & \vdots & & \vdots \\ (x_0,y_0^{(m)}), & (x_1,y_1^{(m)}), & \ldots, & (x_{n-1},y_{n-1}^{(m)}) \end{array} \tag{16}$$

must be known, rather than just the first n values required for Lagrange interpolation. The resulting polynomial may have degree at most $n(m+1)-1$, whereas the Lagrange polynomial has maximum degree $n-1$.

These interpolation polynomials seem attractive but they both induce oscillations between interpolation points (*Runge's phenomenon*). Runge's phenomenon is a problem of oscillation at the edges of an interval that occurs when using polynomial interpolation with polynomials of high degree (which is the case for Lagrange and Hermite interpolation). An example of such Runge's phenomenon is given in Fig. 4 for which Lagrange interpolation has been used.

We can conclude that interpolation with high degree polynomial is risky. In order to avoid this drawback of high degree polynomial interpolation one must use piecewise interpolation.

3.4 Piecewise Linear Interpolation

This is the simplest piecewise interpolation method.

Given $n+1$ real numbers y_i,$0 \leq i \leq n$, and $n+1$ distinct real numbers $x_0 < x_1 < \ldots < x_n$, we consider the n linear curves $lin_i(x) = a_i x + b_i$ on the intervals $[x_i, x_{i+1}]$ for $i = 0, \ldots n-1$ ($lin_i(x)$ represent linear functions for which a_i is the slope and b_i a constant).

Each $l_i(x)$ has to connect two points $((x_i,y_i),(x_{i+1},y_{i+1}))$

$$y_i = a_i x_i + b_i x_i \text{and} y_{i+1} = a_i x_{i+1} + b_i x_{i+1} \tag{17}$$

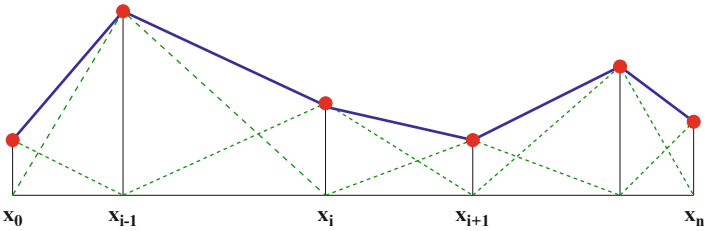

Fig. 5 Piecewise linear interpolation

In order to associate a piecewise formulation of this interpolation method, the following "tent" functions are defined:

$$\psi_i(x) = \begin{cases} \frac{x-x_{i-1}}{x_i-x_{i-1}} & if x \in [x_{i-1}, x_i] \\ \frac{x_{i+1}-x}{x_{i+1}-x_i} & if x \in [x_i, x_{i+1}] \\ 0 & elsewhere \end{cases} \tag{18}$$

Then,

$$f(x) = \sum_{i=0}^{i=n} y_i . \psi_i(x) \tag{19}$$

An example of such a linear piecewise interpolation is given in Fig. 5.

The derivative of the resulting curve is not continuous. In order to fix this drawback, one can use piecewise quadratic interpolation

3.5 Piecewise Quadratic Interpolation

We consider the n quadratic curves $\psi_i(x) = q_i(x) = a_i x^2 + b_i x + c_i$ on the intervals $[x_i, x_{i+1}]$ for $i = 0, \ldots n-1$. Each $q_i(x)$ has to connect two points $((x_i, y_i), (x_{i+1}, y_{i+1}))$; $\Rightarrow y_i = a_i x_i^2 + b_i x_i + c_i$ and $y_{i+1} = a_i x_{i+1}^2 + b_i x_{i+1} + c_i$. Furthermore, on each point, the derivative of the previous quadratic has to be equal to the derivative of the next one; $\Rightarrow 2a_i + b_i = 2a_{i-1} + b_{i-1}$. For the first segment the term $2a_{i-1} + b_{i-1}$ is arbitrarily chosen (this will affects the rest of the curve). An example of piecewise quadratic interpolation is given in Fig. 6. The main drawback of piecewise quadratic interpolation is linked to the effect induced on the curve by moving on point. As a matter of fact moving one point may totally change the shape of the interpolating curve. The piecewise cubic interpolation avoid this drawback.

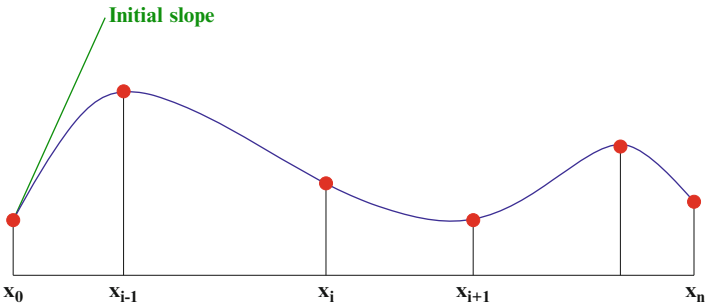

Fig. 6 Piecewise quadratic interpolation. The shape of the entire curve depend of the choice of the initial slope. Between two points, a quadratic polynomial is fitted

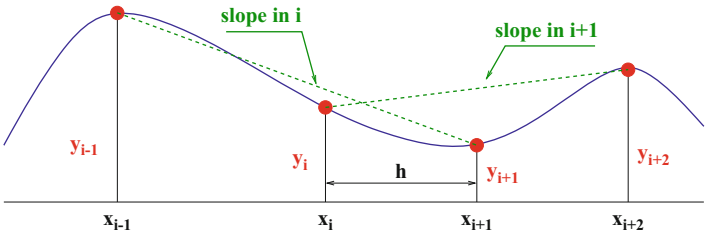

Fig. 7 Piecewise cubic interpolation. The derivative at point x_i is given by *line* joining the point (x_{i-1}, y_{i-1}) and (x_{i+1}, y_{i+1}). Between two points, a cubic polynomial is fitted. The term h represents the distance two consecutive points

3.6 Piecewise Cubic Interpolation

This interpolation is also called Hermite cubic interpolation [33]. For this interpolation:

$$\psi_i(x) = C_i(x) = a_i x^3 + b_i x^2 + c_i x + d_i \tag{20}$$

and we have the following constraints:

$$C_i(x_i) = y_i \qquad C_i(x_{i+1}) = y_{i+1} \tag{21}$$

$$C_i'(x_i) = y_i' = \frac{y_{i+1} - y_{i-1}}{x_{i+1} - x_{i-1}} \; C_i'(x_{i+1}) = y_{i+1}' = \frac{y_{i+2} - y_i}{x_{i+2} - x_i} \tag{22}$$

An example of piecewise cubic interpolation is given in Fig. 7.

Moving a point do not affect all the curve which is the main advantage of this interpolation. The resulting curve is C^1 but not C^2 (the second derivative is not

continuous). The curvature radius of a curve may be expressed by the following expression:

$$R = \frac{1 + \left(\frac{df(x)}{dx}\right)^{\frac{3}{2}}}{\left|\left(\frac{d^2 f(x)}{dx^2}\right)\right|} \tag{23}$$

The piecewise cubic interpolation do not insure that trajectory curvature is continuous which is not adapted for aircraft trajectory mainly in TMA[1] areas and cubic spline interpolation has to be used.

3.7 Cubic Spline Interpolation

This method has been developed by General Motor in 1964 [12]. For this piecewise interpolation $\psi_i(x) = S_i(x)$ with the following constraints:

$$\begin{array}{ll} S_i(x_i) = y_i & S_i(x_{i+1}) = y_{i+1} \\ S_i^{'}(x_i) = S_{i-1}^{'}(x_{i+1}) & S_i^{'}(x_{i+1}) = S_{i+1}^{'}(x_{i+1}) \\ S_i^{''}(x_i) = S_{i-1}^{''}(x_{i+1}) & S_i^{''}(x_{i+1}) = S_{i+1}^{''}(x_{i+1}) \end{array} \tag{24}$$

One can show that $S_i(x)$ for $x \in [x_i, x_{i+1}]$ is given by:

$$\begin{array}{rl} S_i(x) = & \frac{\sigma_i}{6} \cdot \frac{(x_{i+1}-x)^3}{x_{i+1}-x_i} + \frac{\sigma_{i+1}}{6} \cdot \frac{(x-x_i)^3}{x_{i+1}-x_i} \\ & + y_i \cdot \frac{x_{i+1}-x}{x_{i+1}-x_i} - \frac{\sigma_i}{6} \cdot (x_{i+1}-x_i)(x_{i+1}-x) \\ & + y_{i+1} \cdot \frac{x-x_i}{x_{i+1}-x_i} - \frac{\sigma_{i+1}}{6} \cdot (x_{i+1}-x_i)(x-x_i) \end{array} \tag{25}$$

where

$$\sigma_i = \frac{d^2 S_i(x)}{dx^2} \tag{26}$$

An example of such interpolation is given in Fig. 8.

Such spline is also called natural spline because it represents the curve of a metal spline constrained to interpolate some given points.

When interpolation is not a hard constraint, one can use some control points which change the shape of a given trajectory without forcing this trajectory to go through such control point; such approach is called approximation for which one of the famous methods is the Bézier curve.

[1] TMA: "Terminal Maneuvering Area".

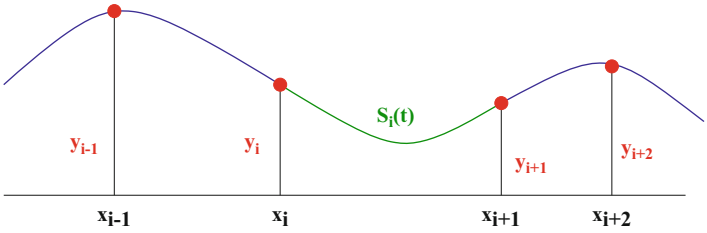

Fig. 8 Cubic spline interpolation

Fig. 9 Bézier curve with two points

3.8 Bézier Approximation Curve

Bézier curves[28] were widely publicized in 1962 by the French engineer Pierre Bézier, who used them to design automobile bodies. But the study of these curves was first developed in 1959 by mathematician Paul de Casteljau using de Casteljau's algorithm [27], a numerically stable method to evaluate Bézier curves. A Bézier curve is defined by a set of control points P_0 through P_n, where n is called its order ($n = 1$ for linear, 2 for quadratic, etc.). The first and last control points are always the end points of the curve; however, the intermediate control points (if any) generally do not lie on the curve. Given points P_0 and P_1, a linear Bézier curve $B(t)$ is simply a straight line between those two points (see Fig. 9). The curve is given by:

$$B(t) = P_0 + t(P_1 - P_0) = (1-t)P_0 + tP_1 \ , t \in [0,1] \tag{27}$$

With four points (P_0, P_1, P_2, P_3), a Bézier curve of degree three can be built. The curve starts at P_0 going towards P_1 and arrives at P_3 coming from the direction of P_2. Usually, it will not pass through P_1 or P_2; these points are only there to provide directional information (see Fig. 10).

Properties

- The polygon formed by connecting the Bézier points with lines, starting with P_0 and finishing with P_n, is called the Bézier polygon (or control polygon).
- The convex hull[2] of the Bézier polygon contains the Bézier curve.

[2]The convex hull or convex envelope of a set X of points in the Euclidean plane or Euclidean space is the smallest convex set that contains X.

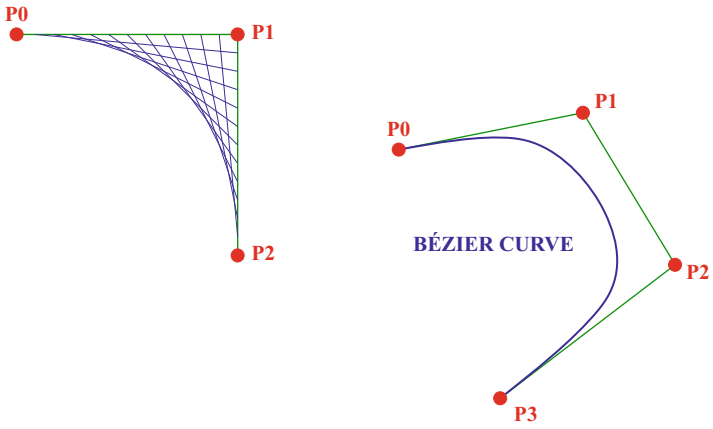

Fig. 10 Cubic Bézier curve

- The start (end) of the curve is tangent to the first (last) section of the Bézier polygon.

  The explicit form of the curve is given by:

$$B(t) = (1-t)^3 P_0 + 3(1-t)^2 t P_1 + 3(1-t) t^2 P_2 + t^3 P_3 \, , t \in [0,1]. \tag{28}$$

$$B(t) = \sum_{i=0}^{n} b_{i,n}(t) P_i, \quad t \in [0,1] \tag{29}$$

where the polynomials

$$b_{i,n}(t) = \binom{n}{i} t^i (1-t)^{n-i}, \quad i = 0, \ldots n \tag{30}$$

are known as Bernstein basis polynomials of degree n. So, if there are many points, one has to manipulate polynomials with high degree. In order to circumvent this weak point one must use Basis-Splines.

3.9 Basis Splines

A B-spline [21] is a spline function that has minimal support with respect to a given degree, smoothness, and domain partition. B-splines were investigated as early as the nineteenth century by Nikolai Lobachevsky. A fundamental theorem states that every spline function of a given degree, smoothness, and domain partition, can

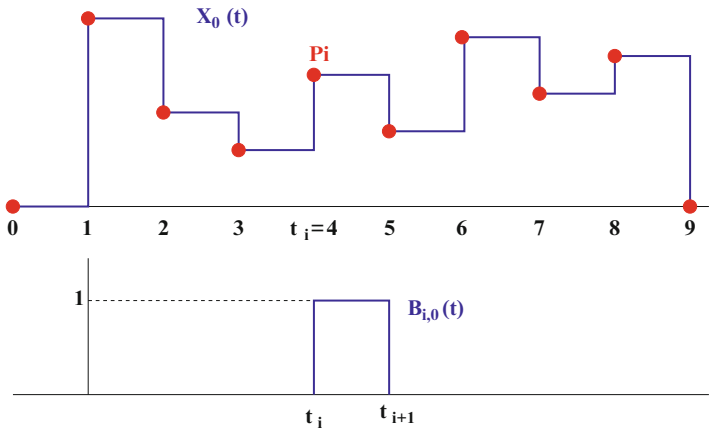

Fig. 11 Uniform B-splines of degree zero

be uniquely represented as a linear combination of B-splines of that same degree and smoothness, and over that same partition. It is a powerful tool for generating curves with many control points, B stands for basis. A single B-spline can specify a long complicated curve and B-splines can be designed with sharp bends and even "corners". B-Spline interpolation is preferred over polynomial interpolation because the interpolation error can be made small even when using low degree polynomials for the spline. Furthermore, spline interpolation avoids the problem of Runge's phenomenon which occurs when interpolating between equidistant points with high degree polynomials.

3.9.1 Uniform B-Splines of Degree Zero

We consider a node vector $T = \{t_0, t_1, \ldots, t_n\}$ with $t_0 \leq t_1 \leq, \ldots, \leq t_n$ and n points P_i. One want to build a curve $X_0(t)$ such that:

$$X_0(t_i) = P_i \tag{31}$$

$\Rightarrow X_0(t) = P_i \; \forall t \in [t_i, t_{i+1}]$.

$$X_0(t) = \sum_i B_{i,0}(t).P_i \tag{32}$$

where

$$B_{i,0}(t) = \begin{cases} 1 \text{ if} t \in [t_i, t_{i+1}] \\ 0 \text{ elsewhere} \end{cases} \tag{33}$$

The shape of the $X_0(t)$ function in one dimension is given in Fig. 11.

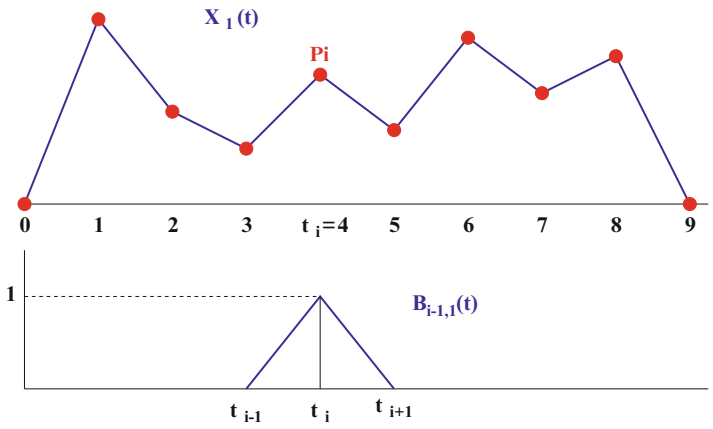

Fig. 12 Uniform B-splines of degree one

3.9.2 Uniform B-Splines of Degree One

We are searching for a piecewise linear approximation $X_1(t)$ for which:

$$X_1(t) = \left(1 - \frac{t - t_i}{t_{i+1} - t_i}\right) P_{i-1} + \left(1 - \frac{t - t_i}{t_{i+1} - t_i}\right) P_i \quad \forall t \in [t_i, t_{i+1}] \tag{34}$$

One can write $X_1(t)$:

$$X_1(t) = \sum_i B_{i,1}(t).P_i \tag{35}$$

where

$$B_{i,1}(t) = \begin{cases} \frac{t - t_{i-1}}{t_i - t_{i-1}} & \text{if } t \in [t_{i-1}, t_i] \\ \frac{t_{i+1} - t}{t_{i+1} - t_i} & \text{if } t \in [t_i, t_{i+1}] \\ 0 & elsewhere \end{cases} \tag{36}$$

The shape of the $X_1(t)$ function in one dimension is given in Fig. 12.

3.9.3 Uniform B-Splines of Degree Three

Those B-Splines have been developed at Boeing in the 1970s and represent one of the simplest and most useful cases of B-splines. Degree 3 B-Spline with $n + 1$ control points is given by:

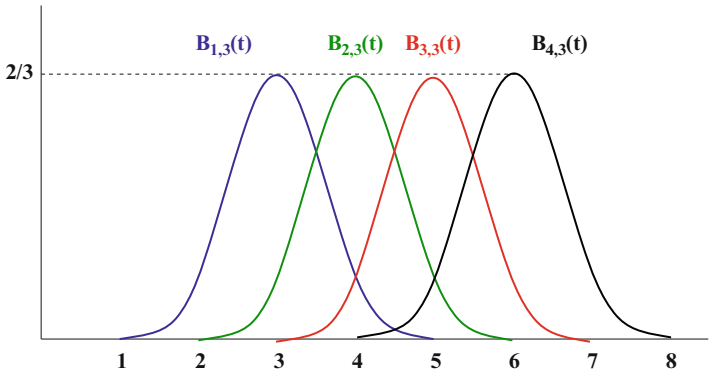

Fig. 13 Order 3 basis function

$$X_3(t) = \sum_{i=0}^{n} B_{i,3}(t).P_i \ 3 \leq t \leq n+1 \tag{37}$$

where $B_{i,3}(t) = 0$ if $t \leq t_i$ or $t \geq t_{i+4}$.

$$X_3(t) = \sum_{i=j-3}^{j} P_i.B_{i,3}(t) \ t \in [j, j+1], \ 3 \leq j \leq n \tag{38}$$

When a single control point P_i is moved, only the portion of the curve $X_3(t)$ is changed (with $t_i < t < t_{i+4}$) insuring local control property. The basis functions have the following properties:

- They are translates of each other i.e. $B_{i,3}(t) = B_{0,3}(t-i)$
- They are piecewise degree three polynomial
- Partition of unity $\sum_i B_{i,3}(t) = 1$ for $3 \leq t \leq n+1$
- The functions $X_i(t)$ are of degree 3 for any set of control points

$$B_{i-2,3}(t) = \frac{1}{h} \begin{cases} (t-t_{i-2})^3 \ \text{ if } t \in [t_{i-2}, t_{i-1}] \\ h^3 + 3h^2(t-t_{i-1}) + 3h(t-t_{i-1})^2 - 3(t-t_{i-1})^3 \\ \text{ if } t \in [t_{i-1}, t_i] \\ h^3 + 3h^2(t_{i+1}-t) + 3h(t_{i+1}-t)^2 - 3(t_{i+1}-t)^3 \\ \text{ if } t \in [t_i, t_{i+1}] \\ (t_{i+2}-t)^3 \text{ if } t \in [t_{i+1}, t_{i+2}] \\ 0 \text{ otherwise} \end{cases} \tag{39}$$

where h is the distance between two consecutive points.

Those basis functions are shown in Fig. 13.

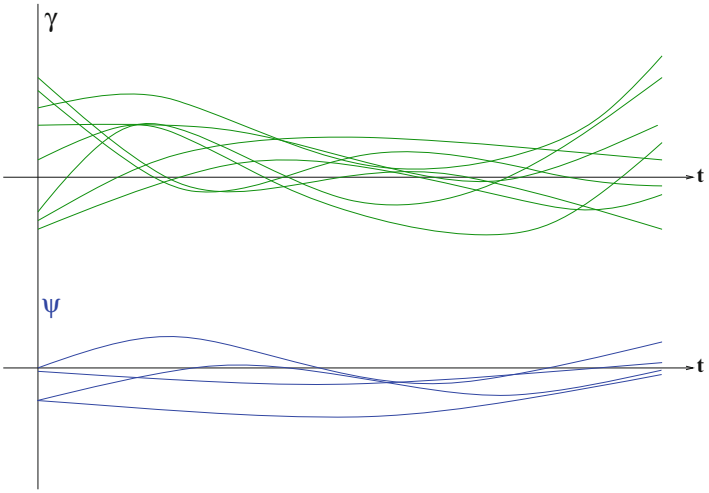

Fig. 14 The *black* trajectories represent registered samples for which four principal components are extracted (in this artificial example) for minimum error reconstruction process

3.9.4 Principal Component Analysis

When trajectories samples are available (from radar for instance), one can build a dedicated bases which will minimize the number of coefficient for trajectory reconstruction. Principal component analysis (PCA) is a mathematical procedure that uses an orthogonal transformation to convert a set of observations of possibly correlated variables into a set of values of linearly uncorrelated variables called principal components. The number of principal components is less than or equal to the number of original variables.

In the example presented in Fig. 14 a set of trajectories $\gamma_i(t), i = 1 \ldots n$ are used to build $K = 4$ principal components $(\psi_k(t))$ which can be used to reconstruct the initial trajectories.

$$\gamma_i(t) = \sum_{k=1}^{k=K} a_{ik} \psi_k(t) \tag{40}$$

When probability density functions of the coefficient a_{ik} can be identified, one can use this trick to plug a stochastic optimization process which generates random coefficients in order to produce relevant random trajectory. More information about Functional PCA can be found in [56].

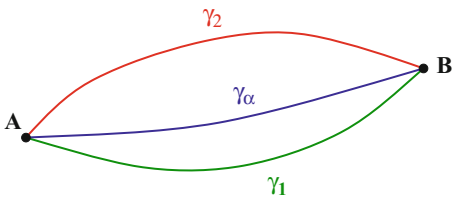

Fig. 15 One new trajectory is built by using a weighted sum of two reference trajectories

3.9.5 Homotopy Trajectory Design

An easy way to build trajectory is to used reference trajectory (regular trajectories used by aircraft) and to compute a weighted sum of such reference trajectories to build a new one. If we consider two (or more) references trajectories joining the same origin destination pair (see Fig. 15) (past flown trajectories may be considered):

$$\gamma_1, \gamma_2 \tag{41}$$

One can create a new trajectory γ_α by using an homotopy:

$$\gamma_\alpha = (1-\alpha)\gamma_1 + \alpha\gamma_2 \tag{42}$$

In this example only one coefficient α has been used but one can extend this principle to several parameters.

All the models described in this section, may be used in an optimization process for which dimension reduction is needed. Depending on the targeted properties of the designed trajectories one must select the most adapted representations for the underlying application.

After having review algorithms based on optimization, the next section presents wave front propagation approaches.

4 Wavefront Algorithms

4.1 Generalities

It is a well-known fact in physics that waves of high frequencies tend to propagate along the path whose traveling (or propagation) time is shortest (such minimum time path are called geodesic). The knowledge of the wave velocity at each point of space allows for the computation of wave fronts that are the set of all points reached by the wave at a given time, assuming it has started at a point source. The principle of the wavefront propagation algorithms is to simulate such physical propagation model in order to find optimal path based on a criterion that has to be optimized. As an example, congestion will be taken into account by velocity reduction, so that paths

crossing congested areas will be penalized. Depending on the fact that the metric is or not isotropic (the later case being the one to be investigated when the wind is used into the criterion and has a non negligible velocity), two classes of algorithms are used.

4.2 Fast Marching Algorithms

The *Fast Marching* method, presented by Sethian [66] is a part of the more general methods called *Level Set* [53]. These techniques are designed to track the evolution of interfaces. The evolution of the wavefront can be compared to deform a curve or a surface from a partial differential equation. The *Fast Marching* method is used in the particular case where the wavefront speed is isotropic. It can still be applied if the anisotropy is low enough. For air traffic applications, this last assumption is valid in some areas of the airspace (of course it is not the case in the vicinity of jet streams).

In the particular case where the Fast Marching method is applicable, the calculus of the minimum time T to reach any points of the environment from the initial point is equivalent to solve the Eikonal equation of the form:

$$|\nabla T(x)| = \frac{1}{F(x)}, \qquad F(x) > 0, \qquad \text{and} \qquad \mathrm{T}(\mathrm{x}_{\mathrm{initial}}) = 0 \tag{43}$$

where $x \in \mathbb{R}^2$ represents the position in space, $T \in \mathbb{R}$ the minimum time and $F : \mathbb{R} \to \mathbb{R}$ the speed of propagation.

In free space, the wave speed F is equivalent to the aircraft speed. When we have forbidden areas, we force the propagation speed at zero in order to get a barrier value since the time to reach this point will be equal to infinity. Thereby, we have guaranteed avoidance property for those areas. For the congestion, the method is different, we want to penalize some areas where the congestion is high but we do not want to ban aircraft from driving through these areas. We just need to reduce the propagation speed. Thus, the time is increased proportionally to the congestion value, penalizing the crossing.

To design the optimal path between the arrival point and the departure point, we can then perform a gradient descent using the calculated values of T on the space, from the arrival point to the initial point. There is no risk to get stuck on a local minimum since the function T has only one optimum which is global.

The numerical resolution is like the graph search algorithms. However, in opposition to these graph search algorithms, the *Fast Marching* method is consistent since when the grid is refined, the obtained solution converges on the exact solution of the Eikonal equation [66] that is a geodesic curve.

4.3 Ordered Upwind Algorithm

When wind is to be taken into account and has a non negligible speed with respect to the one of the aircraft, the propagation is no longer isotropic. The speed of the wavefront depends on the position and the directions of wind. A specific algorithm, called *Ordered Upwind*, has been developed to overcome this problem in [67], at the expense of a higher algorithmic complexity. Basically, an extra parameter, the anisotropy ratio, is considered: it is the ratio of the fastest to slowest propagation speed for each points. Given a point in space, the algorithm first considers the points on the current wavefront that are closest to it: it gives a time to travel when taking as propagation speed the slowest. Now, the other points to be considered are located no farther than the anisotropy ratio times the minimal distance. By maintaining a list of potential points contributing to the information at the point of interest, the ordered upwind algorithm can still be implemented in a single pass.

In order to keep the efficiency of the *Fast Marching* algorithm, Petres proposed an extension of the algorithm *Fast Marching* in [55], he assumed the field is smooth. He applied this extension to plan a path for autonomous underwater vehicles taking underwater currents into account. We propose here a similar extension to Petres's method of the *Fast Marching* method, our extension is specific to aircraft trajectories.

In the next section, we present an example of application of such wave propagation algorithm for air traffic management problem.

4.4 Light Propagation Algorithm

In geometric optics, light behavior is modeled using rays. Light emitted from a point is assumed to travel along such a ray through space. In an effort to explain the motion through space taken by rays as they pass through various media, Fermat (1601–1665) developed his *principle of least action* [29]:

The path of a light ray connecting two points is the one for which the time of transit, not the length, is a minimum.

In the framework of geometrical optics, light propagates through space respecting Descartes' Law:

Let n_1 be the index of refraction of medium 1 in which the incident ray propagates and n_2 that of the medium in which the refracted ray propagates (medium 2). We obtain:

$$\begin{cases} n_1.\sin(\theta_1) = n_2.\sin(\theta_2) \\ v_1 = \frac{c}{n_1}, v_2 = \frac{c}{n_2}, \end{cases} \tag{44}$$

where v_1,v_2 are the speed values in media 1 and 2, θ_1 the angle of incidence, θ_2 the angle of the refracted ray and c the speed of light in a vacuum.

We can make several observations as a result of Fermat's principle:

- In a homogeneous medium, light rays are rectilinear. That is, within any medium where the index of refraction is constant, light travels in a straight line.
- In an in-homogeneous medium, light rays follow smooth geodesic curves with minimum transit time.

Light therefore tends to avoid high index areas where rays are slowed down. Light reaches lowest speed for the highest encountered index.

Based on this principle of least action, we introduce an optimal path planning algorithm which computes smooth geodesic trajectories in environments with static or dynamic obstacles.

For a given mobile, we wish to find the shortest path between two points of $\mathbb{R}^n$, taking account of a given metric (time, distance etc.) whilst avoiding obstacles and respecting speed constraints. The trajectories produced must also respect a regularity criterion characterized by a maximum curvature value.

This algorithm mimics light propagation between a starting point towards a destination point, with obstacles modeled by high-index areas. By controlling the index landscape, it is possible to ensure that the computed trajectories meet the speed constraints and remain at a specified minimum distance from obstacles.

We begin by positioning a light source at the departure point (origin) which emits rays in a hemisphere oriented towards the destination point (this restriction prevents the generation of unrealistic trajectories which begin by turning 180° before turning back towards the destination). The path followed by the first beam to reach the arrival point corresponds to the geodesic trajectory we wish to obtain (see Fig. 16).

5 Optimal Control for Trajectory Generation

5.1 Optimal Trajectory Generation

In the physical space, a trajectory is occasionally represented as a four-dimensional flight path, following the tradition of air traffic control [18], with time as the fourth dimension, in addition to the normally used three-dimensional representation of a path. Generating *time-parameterized* paths necessitates the incorporation of the aircraft dynamics and/or kinematics, which makes the problem much more difficult than simply finding a path that avoids obstacles in the physical three-dimensional space. Path-planning is a term commonly used in the robotics and artificial intelligence communities to refer to the problem of generating an obstacle-free path to be followed by a vehicle (robot, aircraft, vehicle, etc.) in a two or three dimensional space containing obstacles [42].

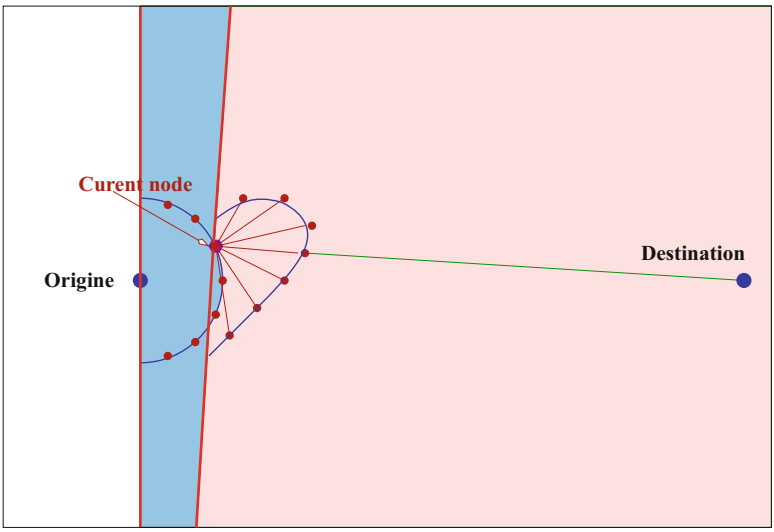

Fig. 16 Launching rays from the departure point. Geodesic computation (A^* like algorithm or Triangle mesh algorithm)

Because the vehicle dynamics are not taken into account in these path-planning methods (the solution of which only considers the geometric constraints of the problem) it is often the case that the resulting path is infeasible, that is, it cannot be followed exactly or even closely by the vehicle. One way to ensure that the resulting paths correspond to feasible trajectories satisfying the vehicle dynamics, is to use optimal control theory. The objective of optimal control theory is to determine the control input(s) that will cause a process (i.e., the response of a dynamical system) to satisfy the physical constraints, while, at the same time, minimize (or maximize) some performance criterion. Feasibility of the trajectories is automatically ensured using this approach. The typical optimal control problem (OCP) can be stated as follows:

Given initial conditions x_0, final conditions $x_f \in \mathscr{X}$, and an initial time $t_0 \geq 0$, determine the final time $t_f > t_0$, the control input $u(t) \in \mathscr{U}$ and the corresponding state history $x(t)$ for $t \in [t_0, t_f]$ which minimize the cost function

$$J(x,u) = \int_{t_0}^{t_f} L(x(t),u(t))\,\mathrm{d}t, \tag{45}$$

where $x(t)$ and $u(t)$ satisfy, for all $t \in [t_0, t_f]$ the differential and algebraic constraints:

$$\dot{x}(t) - f(x(t),u(t)) = 0, \tag{46}$$

$$C(x(t),u(t)) \leq 0. \tag{47}$$

Optimal control has its roots in the theory of calculus of variations, which originated in the seventeenth century by Fermat, Newton, Liebniz, and the Bernoullis, and was subsequently further developed by Lagrange, Weirstrass, Legendre, Clebsch and Jacobi and others in the eighteenth and nineteenth centuries [26]. Calculus of variations deals with the problem of minimizing (45) subject to the simple differential equality constraint of the form $\dot{x}(t) - u(t) = 0$, and is not able to handle more complicated differential equality constraints such as (46) or algebraic constraints such as (47). It was not until the middle of the twentieth century when the Soviet mathematician L.S. Pontryagin developed a complete theory that could handle constraints such as (46) and (47). Simply put, Pontryagin's celebrated Maximum Principle [54] states that the optimal control for the solution of the problem (45)–(47) is given as the pointwise minimum of the so-called Hamiltonian function, that is,

$$u_{\text{opt}} = \text{argmin}_{u \in U} H(t, x, \lambda, u), \tag{48}$$

where $H(t, x, \lambda, u) = L(x, u) + \lambda^T f(x, u)$ is the Hamiltonian, and λ are the co-states, computed from

$$\dot{\lambda}(t) = -\frac{\partial H}{\partial x}(x(t), \lambda(t), u(t)). \tag{49}$$

subject to certain boundary (transversality) conditions on $\lambda(t_f)$. Unfortunately, an analytic solution to the previous problem is difficult. The optimal control formulation of a trajectory optimization problem using Pontryagin's Maximum Principle (PMP) leads to a Two-point Boundary Value Problem (TBVP), or a Multi-point Boundary Value Problem (MBVP) when the optimal trajectory is composed of multiple phases. Numerical techniques such as shooting and multiple shooting methods can be applied to solve accurately these TBVP and MBVP, but their convergence is very sensitive to the choice of an initial guess for the solution. A software that solves the optimal control problem using this approach is BNDSCO [51]. BNDSCO is an example of a class of numerical optimization methods which are often referred to as indirect methods. The term indirect reflects the fact that in these methods a solution is sought not by maximizing (or minimizing) the cost (45) but, rather, by computing potential optimizers by solving the corresponding necessary optimality conditions (48)–(49).

In recent years, direct methods have become increasingly popular for solving trajectory optimization problems, the major reason being that direct methods do not require an analytic expression for the necessary conditions, which for complicated nonlinear dynamics can be intimidating. Moreover, direct methods do not need an initial guess for the co-states whose time histories are difficult to predict a priori. As mentioned earlier, direct methods, do not try to satisfy the necessary conditions of optimality from PMP, instead, they minimize directly (45) subject to (46)–(47).

The main idea behind direct methods is to discretize the states and controls of the original continuous-time optimal control problem in order to obtain a

finite-dimensional nonlinear programming problem (NLP). The solution of this NLP, which consists of discrete variables, is used to approximate the continuous control and state time histories. Typical direct methods are collocation methods, which discretize the ordinary differential equations (ODEs) of the problem using collocation or interpolation schemes [23, 32, 60, 79]. They introduce the collocation conditions as NLP constraints together with the initial and terminal conditions. The so-called pseudospectral methods use orthogonal polynomials to choose the collocation points and are very efficient, exhibiting superlinear convergence when the solution is smooth. Numerical optimal control software packages that implement direct methods for the solution of OCPs include SOCS [8], RIOTS [65], DIDO [59], PSOPT [4], GPOPS [57], MTOA [36] and DENMRA [83] among many others. A recent survey of numerical optimal control techniques for trajectory optimization can be found in [7].

In all these direct methods, the convergence rate and the quality of solution depends on the grid used to discretize the equations, the cost and the problem constraints. Uniform or fixed grid methods tend to perform poorly, especially when the problem has several discontinuities or irregularities. Not surprisingly, adaptive grid methods have been developed to accurately capture any discontinuities or switchings in the state or control variables. The main idea behind all these adaptive grid methods is to use a high resolution (dense) grid only in the vicinity of control switches, constraint boundaries etc., and a coarse grid elsewhere. Examples of such adaptive gridding techniques for the solution of optimal control problems are [9–11, 30, 37, 65].

A major issue with almost all current trajectory optimization solvers (direct or indirect) is the fact that their computational complexity is high and their convergence dependents strongly on the initial conditions, unless certain rather stringent convexity conditions hold. As a result, the solution of trajectory optimization problem in *real-time* is still elusive. A common line of attack for solving trajectory optimization problems in real time (or near real time) is to divide the problem into two phases: an offline phase and an online phase [38, 44, 69, 81]. The offline phase consists of solving the optimal control problem for various reference trajectories and storing these reference trajectories onboard for later online use. These reference trajectories are used to compute the actual trajectory online via a neighboring optimal feedback control strategy typically based on the linearized dynamics. Another strategy for computing near-optimal trajectories in real-time is to use a receding horizon (RH) approach [5, 52, 80]. In a receding horizon approach a trajectory that optimizes the cost function over a period of time, called the *planning horizon*, is designed first. The trajectory is implemented over the shorter *execution time* and the optimization is performed again starting from the state that is reached at the end of the execution time. A third approach is to use a two-layer architecture, where first an acceptable (in terms of length, safety, etc.) path is computed using common path-planning techniques, and then an *optimal* time-parameterization is imposed on this path to yield a feasible trajectory. As mentioned earlier such an approach needs to be carefully designed to ensure compatibility of the resulting path with the vehicle dynamics. However, when successful, such an approach is numerically very efficient

and can be implemented in real-time with current computer hardware. Even if the resulting trajectory is not exactly feasible, it is often close to a feasible trajectory, or it can be made as such using smoothing techniques [85]. As a result, alternatively, the final trajectory can be used as a good initial guess for a follow-up optimal trajectory generator. The next section summarizes this approach for applications related to aircraft maneuvering under strict time and fuel constraints. For more details the interested reader is referred to [2, 82, 84].

5.2 *Emergency Aircraft Trajectory Design*

Aircraft maneuvering was one of the first areas where optimal control theory was used to generate optimal trajectories. Not surprisingly, traditionally, most work has been focused on military aircraft. Relevant references on this subject are too many to enumerate here. We just mention the work on fuel and range optimization studied in [31, 68, 70], and the minimum-time, three-dimensional aircraft trajectory optimization problem considered in [64]. In the latter, an approximation of the aircraft dynamics using an energy state was used to reduce the dimension of the problem for better convergence. This type of model reduction technique is commonly used for aircraft trajectory optimization [40].

Some of these results have been extended to commercial airline operations. For example, the work of [16] deals with the problem of minimum-fuel trajectories with fixed time-of-arrival (TOA) for several civil aviation aircraft including B737, B747 and B767. Trajectory planning problems have also been studied in the context of air traffic management (ATM) and automation. Jackson et al. [34] performed a sensitivity analysis of trajectory prediction for ATM. The aircraft trajectory synthesis problem is studied in [71] to provide some basic tools for air traffic automation. Somewhat related is the recent work of Sridhar [72], in which he considered the generation of wind-optimal trajectories for cruising aircraft while avoiding the regions of airspace that facilitate persistent contrails formation. A shooting method was employed to solve the associated optimal control problem by minimizing a weighted sum of flight time, fuel consumption, and a term penalizing the contrail formation. The airspace avoidance problem has also been considered in [35]. In that reference, the avoidance of restricted airspace is formulated as a non-convex constrained trajectory optimization problem; it is claimed that with a feasible starting guess, the efficiency of the optimization algorithm is not degraded too much by the non-convex airspace constraints. Finally, some researchers have used ideas from *stochastic* optimal control to deal with issues related to the unpredictability of future trajectory, wind effects, presence of additional aircraft in the ATM airspace etc. [43, 77].

In this work we deal with the problem of *efficiently* generating minimum-time and minimum-fuel (with fixed TOA) landing trajectories for commercial aircraft. The former problem is of relevance in case of an on-board emergency where the pilot has to land the airplane quickly and safely to the closest airport or airfield;

the latter problem is of interest for typical terminal ATC phase applications. Prior work in emergency landing includes the abort landing problem in the presence of windshear [14, 15, 48], and emergency landing during loss of thrust [73]. The latter references generate feasible trajectories using segments of trajectories corresponding to selected trim condition maneuvers. The search results are however limited to those that can be generated by connecting trim state trajectory segments with stable transitions. Because the unstable flight conditions are not considered in the search, the algorithm cannot identify any feasible trajectories containing unstable flight modes. Furthermore, the path length is used as the search criterion, which is less appropriate when compared to flight time for emergency landing, or fuel consumption for normal flight. Related work includes the investigation of Atkins et al. [1], where the problem of emergency landing due to the loss-of-thrust was studied using a hybrid approach. A two-step landing-site selection/trajectory generation process was adopted to generate safe emergency plans in real time under situations that require landing at an alternate airport. In the trajectory generation routine, a heuristic path planner was used to generate a three-dimensional trajectory connecting the current position of the aircraft to the runway, which consists of straight lines and circular arcs. This method is fast and simple. However, it is limited to conservative aircraft maneuvers (typically Dubins paths) in order to reduce the chance of obtaining an infeasible trajectory. As a result, the optimality of the generated trajectory could be unacceptable for emergency landing, and further research is necessary to reduce such a conservatism.

In our approach, we start with the assumption that the path to be followed by the aircraft is given. Note that this does not mean that the *trajectory* to be followed is given. A trajectory requires a time-parameterized path and it is, indeed, the main goal of this approach to provide such a time parameterization so as to meet feasibility along with certain optimality specifications. The assumption that the path is given is not as unusual or atypical as one may initially think. Commercial airliners during the terminal landing phase, are required to follow strict Air Traffic Control (ATC) rules, which guide the airplanes to follow "virtual" three-dimensional corridors all the way to the landing strip. Furthermore, since our approach leads to very fast computation of feasible trajectories, one can use the approach over new, locally modified paths repeatedly till a satisfactory path is found.

To this end, let a path in the three-dimensional space, parameterized by the path coordinate s, be given as follows: $x = x(s)$, $y = y(s)$, $z = z(s)$, where $s \in [s_0, s_f]$. The main objective is to find a time-parameterization along the path, i.e., a function $s(t)$, where $t \in [0, t_f]$ such that the corresponding time-parameterized trajectory $(x(s(t)), y(s(t)), z(s(t)))$ minimizes either the flight time t_f (emergency landing case) or fuel (terminal landing operation). As shown in [82] all control (thrust, angle of attack, load factor, etc.) constraints can be mapped into constraints involving the specific kinetic energy of the aircraft, $E = v^2/2$ where v is the aircraft velocity of the form

$$\underline{g}_w(s) \leq E(s) \leq \overline{g}_w(s),$$

for some path-dependent functions $\underline{g}_w(s)$ and $\overline{g}_w(s)$. The original problems therefore reduce to the following simplified problems:

For the Minimum-Time Problem we have

$$\min_T \quad \int_{s_0}^{s_f} \frac{\mathrm{d}s}{\sqrt{2E(s)}} \tag{50a}$$

$$\text{subject to } E'(s) = \frac{T(s)}{m} - D(E(s),s) - g\sin\gamma(s), \tag{50b}$$

$$\underline{g}_w(s) \leq E(s) \leq \overline{g}_w(s), \tag{50c}$$

$$T_{\min} \leq T(s) \leq T_{\max}, \tag{50d}$$

and for the Minimum-fuel Problem with fixed TOA we have

$$\min_T \quad \int_{s_0}^{s_f} T(s)\,\mathrm{d}s, \tag{51a}$$

$$\text{subject to } E'(s) = \frac{T(s)}{m} - D(E(s),s) - g\sin\gamma(s), \tag{51b}$$

$$t'(s) = \frac{1}{\sqrt{2E(s)}}, \tag{51c}$$

$$\underline{g}_w(s) \leq E(s) \leq \overline{g}_w(s) \tag{51d}$$

$$T_{\min}(s) \leq T(s) \leq T_{\max}(s), \tag{51e}$$

where $D(E(s),s)$ is the drag, T is the thrust, γ is the flight-path angle, and where prime denotes differentiation with respect to path length s. The main advantage of these problem formulations is the dimensionality reduction of the problem that can be leveraged to solve both of these problems very efficiently and reliably. In fact, these OCPs are simple enough so that the optimal switching structure of the optimal solution can be unraveled using the necessary conditions from PMP. For the minimum-fuel problem the switching structure varies depending on the given TOA. However, for a given path and a fixed TOA, the structure is uniquely determined. This helps tremendously the convergence properties of the algorithm.

The overall architecture for optimal on-line trajectory generation is shown in Fig. 17. As shown in this figure, the method first generates a trajectory by assigning an optimal time parameterization along the path given by the geometric path planner via the solution of one of the previous two optimization problems. If the trajectory is feasible, then it is used as an initial guess for the numerical optimal control solver. Meanwhile, such a feasible trajectory is also stored as a back-up plan in case of the failure of the NLP solver. If the trajectory generated by the time-optimal path tracking method is not feasible, then the path is revised using the path smoothing method described in [85], and the optimization is applied again to the smoothed path. The process is repeated until either the trajectory is feasible, or the maximum number of iterations is reached. If no feasible trajectory can be

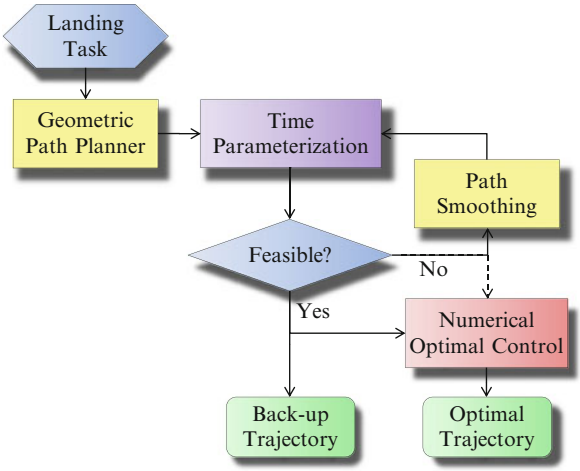

Fig. 17 Schematic of landing trajectory optimization

obtained after reaching the iteration limit, the infeasible trajectory is passed to the numerical optimal control algorithm, which makes a last attempt to produce a feasible trajectory. If this last attempt is not successful, then it does not exist a feasible trajectory that solves the problem.

6 Path Planning Techniques via Natural Language Processing and Mathematical Programming: A Paradigm for Future Aircraft Trajectory Management

Aircraft trajectory planning has reached enough maturity to shift the trajectory planning problem from the mathematical optimization of the aircraft trajectory to the automated parsing and understanding of desired trajectory goals, followed by their re-formulation in terms of a mathematical optimization program. To a large extent, we propose a possible evolution of the Flight Management System currently used on all transport aircraft to become a full-fledged autonomous logic that may also be used on unmanned aerial vehicles as an alternative to the current -and bulky- Remotely-Piloted Vehicle (RPV) paradigm. What follows is a direct extension of work originally presented in [63].

The overall proposed architecture is shown in Fig. 18. It consists of several nested feedback loops. At the operator level, the information is presented to the operator in the form of sentences expressed in natural language (e.g. that used by air traffic control phraseology). At the level of trajectory planning automation, the information is presented as a mix of continuous parameters (aircraft position and speed), and discrete parameters describing mission status (completed tasks, tasks remaining to be completed). The operator formulates the vehicles's goals (e.g. flight plans) using natural language. A natural language interpreter and task scheduler

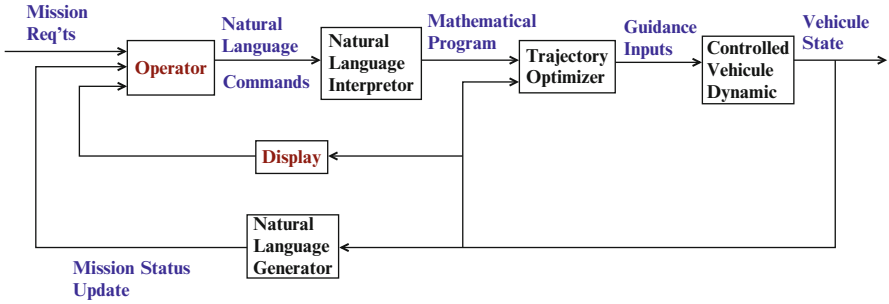

Fig. 18 Basic autonomous mission management loop for future aircraft and UAVs

transforms the operator's requirements into tractable mathematical optimization programs that may be executed by the vehicle through its flight control computer. The vehicle's innermost dynamics (that consist of raw vehicle dynamics and stability augmentation system), although critical to vehicle stability, are not shown.

6.1 Natural Language Parsing and Generation

The main goal of using a Natural Language Interface (NLI) for interacting with a computer-based system is to minimize the workload on the operator. Using normal English sentence commands and reports indeed allows an operator to communicate efficiently and effectively with an aircraft, as if it were a human pilot. The NLI module that we have developed for demonstration purposes consists of two major components. The first one takes sentence commands from the operator (presumably an air traffic controller) and turns them into a formally coded command that looks like the formulation of an optimization problem. The second component takes a coded command set from the aircraft and generates natural language responses for the air traffic controller to interpret. A sample dialog between the human operator and the machine could be as follows:

Controller: *Flight AA1234, this is Air Traffic Control.*
Aircraft: *Go ahead, Air Traffic Control.*
Controller: *Add new waypoint. Proceed to waypoint Echo-Charlie 5 in minimum time. and wait for further instructions after the task is completed*
Aircraft: *Roger. Acknowledge task information - proceeding to waypoint Echo-Charlie 5.*
Controller: *AA1234, out.*

The NLI module analyzes the natural sentences produced by the air traffic controller using parsing, which is the process of converting an input sentence, e.g. "Proceed to waypoint Echo-Charlie 5 in minimum time," into a formal representation. The latter is typically a tree structure which can in turn be translated

into an explicit formal command. In our system, parsing consists of first applying entity extraction to all the individual concepts (e.g. “Flight AA1234” or “Echo-Charlie 5”) and then combining these concepts through cascades of finite-state transducers using techniques derived from those described in [58]. While natural language processing represents our progress so far, it is easy to imagine that it could now be completed by a voice recognition device to further ease the level of communication between controller (or operator) and aircraft.

6.2 Task Scheduling and Communications Interfacing

The task scheduling and communications processing components are designed to centralize all of the aircraft mission processing in one module. Together with the Natural Language Interface, it provides flexibility for an operator to insert and change flight plan during the flight. The aircraft software keeps track of the flight tasks, waypoint locations and known obstacles to pass on to the guidance algorithm. The communications processing component provides the air traffic controller or operator with the authority to send commands and receive status updates, threat or obstacle avoidance information and acknowledgement messages. It also provides remote pilots monitoring the flight with the ability to override the guidance system in the event of an emergency or error. The system sends threat and override information to the air traffic controller before any status or update information in an effort to send the most important data relevant to the demonstration before any auxiliary information. Input/Output data are processed every 1 Hz frame before the task planner and guidance step to ensure that the most up-to-date information is used by the aircraft trajectory planner. The task scheduling component operates like a Flight Management System and allows the aircraft operator or the air traffic manager to enter a flight plan using a pre-defined list or as programmed during a mission. Many additional features may be added to such a task scheduler, such as orders to follow loiter patterns, “take me home” or low-emission approaches functionalities. In addition, he or she has the option of providing (in real- time via the NLI) the optimization metric used by the trajectory generation algorithm (i.e. minimum time, minimum fuel, or the amount of time to finish the flight). Next, the operator can either give the aircraft a new plan or change the current plan it is performing. A “New Plan” command is added to the end of the aircraft task list and is executed after all of the tasks currently scheduled have been completed. A “Change Plan” command, on the other hand, modifies the current task performed by the aircraft. Once a task is completed, it is removed from the list. After each of these actions, an acknowledgement is sent to the air traffic controller and the updated task information is included in the data sent to the Trajectory Generation Module.

6.3 Trajectory Planning

After the Natural Language Interface and Flight Planning and Scheduling components have converted the flight plan into a series of tasks for the aircraft to perform, the Trajectory Generation Module guides the vehicle from one task to the next, i.e. from an initial state to a desired one, through an obstacle field while optimizing a certain objective. The latter can be to minimize time, fuel or a combination of both. Much of the functionality described below becomes increasingly available in today's avionics systems, and also include such real-world factors as weather and wind conditions. For our purposes, 2D scenarios were considered in which special-use airspace and other no-fly zones are viewed as "obstacles" and detected while the flight proceeds. The environment is always fully characterized inside a certain detection region D around the aircraft. The resulting formulation can, however, be easily generalized to account for any detection shape, such as a radar cone, and for unknown areas within that shape. Since trajectories must be dynamically feasible, the aircraft dynamics and kinematics should be accounted for in the planning problem. For optimization purposes, the vehicle is characterized by a discrete time, linear state space model (A,B) in an inertial 2D coordinate frame (east-north). As such, the state vector $\mathbf{x}$ consists of the east-north position (x,y) and corresponding inertial velocity $(\dot{x},\dot{y})$. Depending on the particular model, the input vector u is an inertial acceleration or reference velocity vector. In both cases, however, combined with additional linear inequalities in x and u, the state space model must capture the closed-loop dynamics that result from augmenting the aircraft with a waypoint tracking controller. Since the environment is only partially-known and further explored in real-time, a receding horizon planning strategy is used to guide the vehicle towards the desired destination.

The destination is denoted by x_f and is an ingress/egress state of a waypoint with a corresponding inertial velocity vector. At each time step, a partial trajectory from the current state towards the goal is computed by solving the trajectory optimization problem over a limited horizon of length T. Because of the computation delay, the initial state $\mathbf{x}_0 = (x_0, y_0, \dot{x}_0, \dot{y}_0)$ in the optimization problem should be an estimate $\mathbf{x}_{\text{estim}}$ of the position and inertial velocity of the aircraft when the plan is actually implemented. The solution to the optimization problem provides a sequence of waypoints (x_i, y_i) and corresponding inertial reference velocities $(\dot{x}_i, \dot{y}_i)$ to the aircraft for the next T time steps. Typically, however, only the first waypoint and reference velocity of this sequence are given to the waypoint follower, and the process is repeated at the next time step. As such, new information about the state of the vehicle and the environment can be taken into account at each time step. By introducing a cost function J_T over the T time steps, the general trajectory optimization problem can be formulated as to

$$\text{Minimize}_{\mathbf{x}_i,u_i} J_T = \sum_{i=1}^{T} f_i(\mathbf{x}_i,u_i,\mathbf{x}_f) + f_T(\mathbf{x}_T,\mathbf{x}_f)$$

$$\text{Subject to} \begin{cases} \mathbf{x}_{i+1} = A\,\mathbf{x}_i + Bu_i, \;\; i = 0,\ldots,T-1 \\ \mathbf{x}_0 = \mathbf{x}_{\text{estim}} \\ \mathbf{x}_i \in \mathscr{X}_0, \;\; i = 1,\ldots,T \\ u_i \in \mathscr{U}_0, \;\; i = 0,\ldots,T-1 \\ (x_i,y_i) \in \mathscr{D}_0, \;\; i = 1,\ldots,T \\ (x_i,y_i) \notin \mathscr{O}_0, \;\; i = 1,\ldots,T \end{cases}$$

The objective function consists of stage costs $f_i(\mathbf{x}_i,u_i,\mathbf{x}_f)$ corresponding to each time step i, and a terminal cost term $f_T(\mathbf{x}_T,\mathbf{x}_f)$ that accounts for an estimate of the cost-to-go from the last state $\mathbf{x}_T$ in the planning horizon to the goal state $\mathbf{x}_f$. The sets $\mathscr{X}_0$ and $\mathscr{U}_0$ represent the (possibly non-convex) constraints on the vehicle dynamics and kinematics, such as bounds on velocity, acceleration and turn rate. Here, the 0-subscript denotes the fact that these constraints can be dependent on the initial state. Lastly, the expressions $(x_i,y_i) \in \mathscr{D}_0$ and $(x_i,y_i) \notin \mathscr{O}_0$ capture the requirement that the planned trajectory points should lie inside the known region $\mathscr{D}_0$, but outside the obstacles $\mathscr{O}_0$ as given at the current time step $i = 0$. Note that they are assumed to hold for $\mathbf{x}_0$; if not, the trajectory optimization problem would be infeasible from the start. As demonstrated in [62], however, despite the detection region and avoidance constraints, the above receding horizon strategy has no safety guarantees regarding avoidance of obstacles in the future. Namely, the algorithm may fail to provide a solution in future time steps due to obstacles that are located beyond the surveillance and planning radius of the vehicle. For instance, when the planning horizon is too short and the maximum turn rate relatively small, the aircraft might approach a no-fly zone too closely before accounting for it in the trajectory planning problem. As a result, it might not be able to turn away in time, which translates into the optimization problem becoming infeasible at a future receding horizon iteration. In [62], a safe receding horizon scheme was therefore proposed based on maintaining a known feasible trajectory from the final state $\mathbf{x}_T$ in the current planning horizon towards an obstacle-free holding pattern. The latter must lie in the region $\mathscr{D}_0$ of the environment that is fully characterized at the current time step, and is computed and updated online. Assuming that the planned trajectories can be accurately tracked, at each time step, the remaining part of the previous plan together with the holding pattern can then always serve as an a priori safe backup or "rescue" plan. In practice, we have found that formulating the problem of finding the nominal and rescue trajectories optimization as mixed-integer programs (MIP) works very well in practice, though such choices are not mandatory and may be replaced by the other techniques discussed in this paper.

7 Application to Air Traffic Management

Aircraft trajectory design can be applied in many areas of air traffic managements like strategic planning, pre-tactical planning, tactical planning, SID-STAR design, emergency trajectory design, etc.. . . In the following three Air Traffic Management applications are presented for which trajectory design is critical. The first one presents the strategic aircraft trajectory planning (optimization approach), the second one the pre-tactical and tactical planning by light propagation algorithm (wave propagation approach) finally the last one describes Emergency trajectory design by optimal control (optimal control approach).

7.1 Strategic Aircraft Trajectory Planning

The aim of strategic planning is to reduce airspace congestion by modifying takeoff slots and routes for a set of flights on a country-wide scale.We thus considered a sectorized airspace and a set of flight plans for a given day. For each flight, we defined a set of alternative routes and a set of possible takeoff slots. Our goal was to produce an optimal assignment to minimize airspace congestion. Our problem can be presented as follows:

- We consider all of the flight plans associated with the airspace of a country.
- For each airplane k, we suppose that the following elements are known:
  - a set of possible routes (+ associated costs)
  - a set of possible takeoff times (+ associated costs)
  - the set of flights connected with flight k at departure and arrival points (hub phenomenon)

We wish to obtain the configuration which allows us to reduce airspace congestion, minimize cost and respect connection plans.

The architecture of the chosen approach (see Fig. 19) is made up of a traffic simulator and a genetic algorithm (GA).

The simulator is used in pre-treatment to obtain the data needed for optimization. It receives flight plans (airplane identification, airplane type, origin-destination, departure time, flight profile, route as a set of beacons) and constructs airplane trajectories, while saving the necessary data (sector input and output, flight position and direction every minute, etc.).

Genetic algorithms simulate the process of natural selection in a hostile environment linked to the problem under consideration [20]. They use a vocabulary similar to that found in natural genetics, without neglecting the fact that the underlying principles involved in the two domains are considerably more complex in their natural context. We thus refer to individuals in a population, and often individuals will be reduced to a single chromosome. These chromosomes themselves are made up of genes which contain the hereditary characteristics of the individual. We also use principles of selection, crossing (crossover), mutation etc.

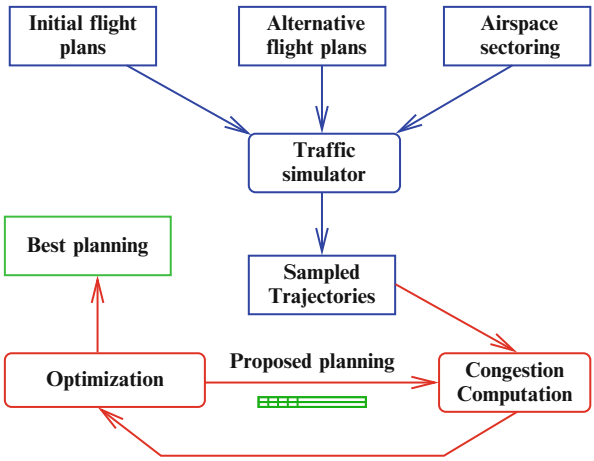

Fig. 19 Optimization structure

In the context of optimization, each individual represents a point in the state space to which we associate the value of the criterion to optimize. We then randomly generate a population of individuals from which the genetic algorithm aims to select the best specimens while ensuring efficient exploration of the state space.

The optimization algorithm then manipulates possible plannings, represented by disturbances, in terms of routes and slots, to the initial flight plans.

The optimization generates plannings which are increasingly efficient in terms of minimizing congestion. The best planning is then put forward as the result of the optimization process.

This approach has been successfully applied for removing conflict in European airspace with 32000 aircraft. The purpose of this research is to design a gate-to-gate conflict free planning by adding way points (inducing a maximum of 10 % extra-distance) and/or by shifting the time on departure (maximum shift: ± 30 min). The optimal altitude profiles have been used. Direct route planning induces $\simeq$400,000 interactions between trajectories. Figure 20 shows the European traffic with interaction in red.

Figure 21 represents the conflict free traffic after optimization.

More information about this work may be found in [17].

7.2 Pre-tactical and Tactical Planning by Light Propagation Algorithm

The objective of the proposed method, based on an analogy with optics, is to find an optimal 4D trajectory for each aircraft which avoids congestion or conflicts and minimizes a criterion based on a local metric.

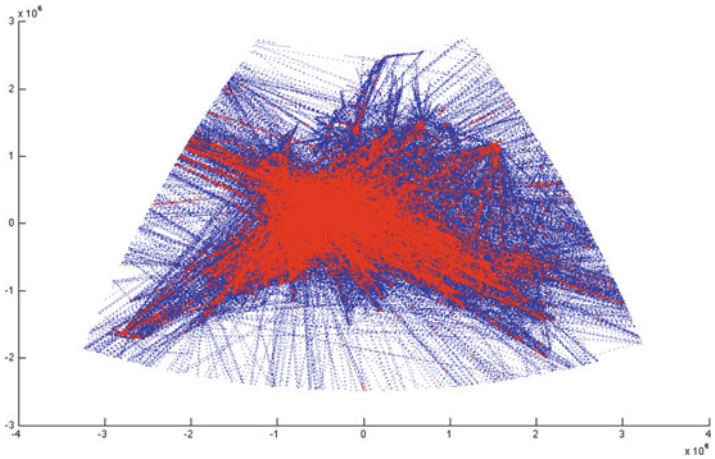

Fig. 20 Direct route traffic over Europe

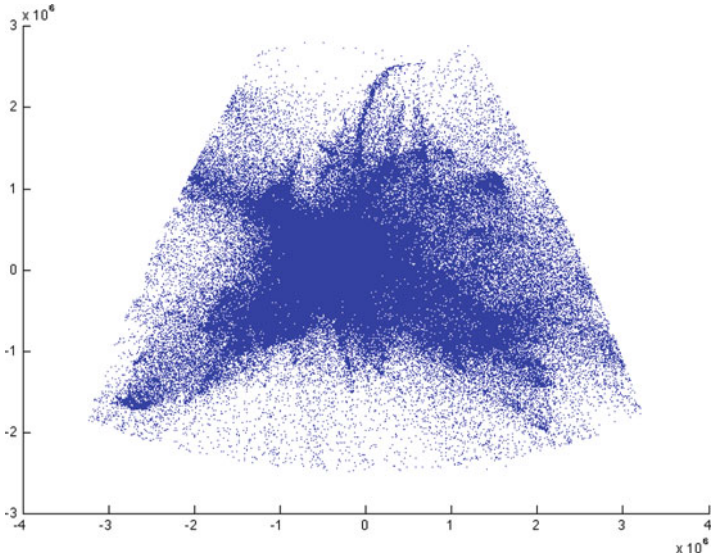

Fig. 21 Traffic picture after optimization

Congestion and the *protection zone* (volume surrounding the aircraft where no other aircraft may enter) of other aircraft will be modeled as high-index areas. Our *light propagation algorithm* (LPA) is designed from a particular aircraft point of view. It is assumed that the aircraft knows the surrounding aircraft trajectories (the set of trajectories of the other aircraft is a given input of the algorithm).

Some examples of geodesic trajectories computation are given on the following Fig. 22 for which the red areas contain high index values.

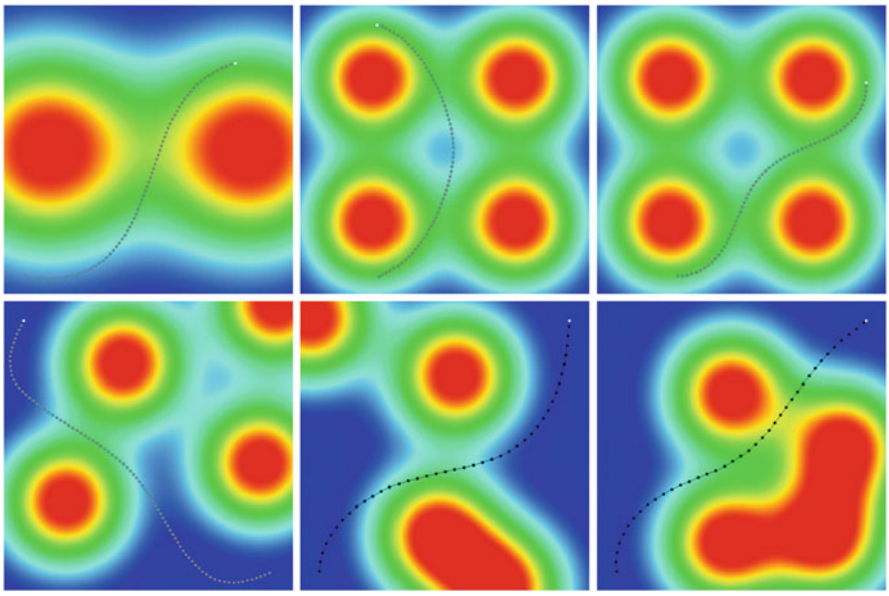

Fig. 22 Example of optimal geodesic curves. The *red color* indicate high index areas

This algorithm has also been used at tactical phase in order to produce conflict free trajectories. To generate a trajectory, we use a wavefront propagation algorithm in 2D + time (in order to conform to operational practice, we carry out resolution in terms of heading, but with a detection method which takes account of altitude) with temporal sampling (the wave is propagated with a time step dt).

Real flight plans of 12 August 2008 with about 8,000 flights have been used to produce reference trajectories. The initial trajectories (before conflict resolution) induce a total number of around 4,000 conflicts. Based on a sliding time window, trajectory segments are extracted in order to built conflict cluster for which LPA is applied. To address the conflict resolution, LPA is sequentially applied to aircraft. We assign a trajectory to the first aircraft disregarding the other aircraft (without considering any constraints). Then, LPA looks for a trajectory for the subsequent aircraft by considering the trajectory of the first aircraft as a constraint, and so on, up to the m^{th} aircraft which considers the $m-1$ previous aircraft trajectories as constraints. In practice, some operational criteria may also be used in order to select a specific sequence (for instance: first-come first-served rule, some aircraft may have higher priority, trajectory length, etc.). The time window is then shifted and the process is applied again.

The algorithm nearly solves all conflicts, with only 28 situations for which conflict-free trajectories have not been found. However, these situations correspond to some aircraft being already in conflict at the beginning of the simulation, for instance at their starting point. Only 1,501 trajectories have been modified to reach such a conflict-free planning. In many cases, the new computed trajectories are

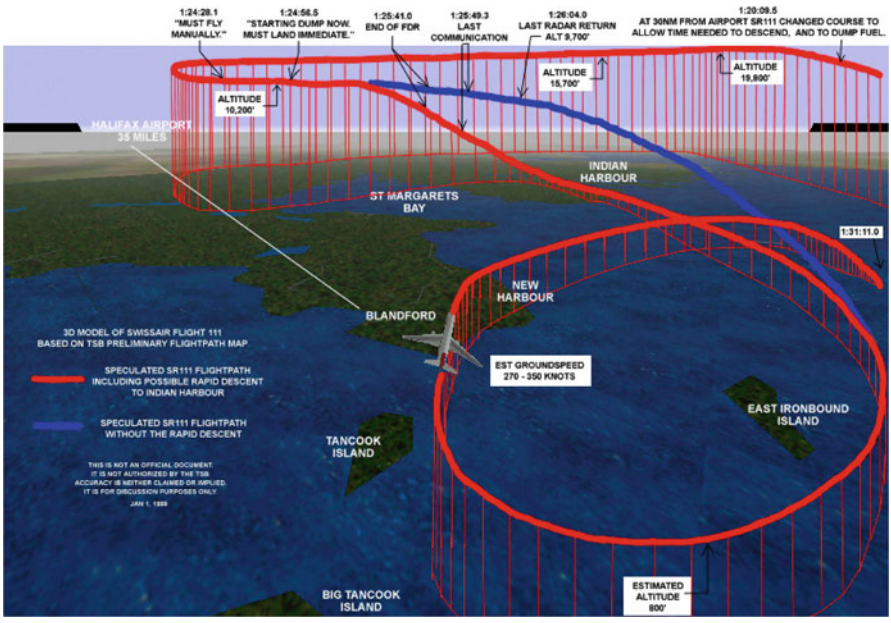

Fig. 23 Swissair 111 trajectory reconstruction

shorter than the initial ones (those that follow waypoints), due to the fact that LPA is searching for the shortest path trajectories and proposes direct routes when possible. More information about this work may be found in [22].

7.3 Emergency Trajectory Design by Optimal Control

This work presents an application of optimal control for computing backup trajectories in case of emergency. In such a situation, one must be able to design backup landing trajectories for aircraft that have lost having loose their thrust. The proposed algorithm begin to find a flyable path to avoid obstacles (Dubins paths generation with continuous descent), then find a feasible trajectory to follow along this path.

This requires the solution of optimal time parametrization (or velocity generation) problem. The latter is a one-dimensional optimal control problem that can be solved very efficiently.

Two cases are presented in the following, the first one is link to the Swissair 111 crash and the second one to the US Air 1549 crash.

On Wednesday, 2 September 1998, the Swiss Air 111 flight crashed into the Atlantic Ocean southwest of Halifax International Airport (due to fire on board).

The Swissair 111 trajectory is given in Fig. 23.

The algorithm has been applied to this case and has produced several backup trajectories bringing back the aircraft at Halifax airport as it can be shown in Fig. 24.

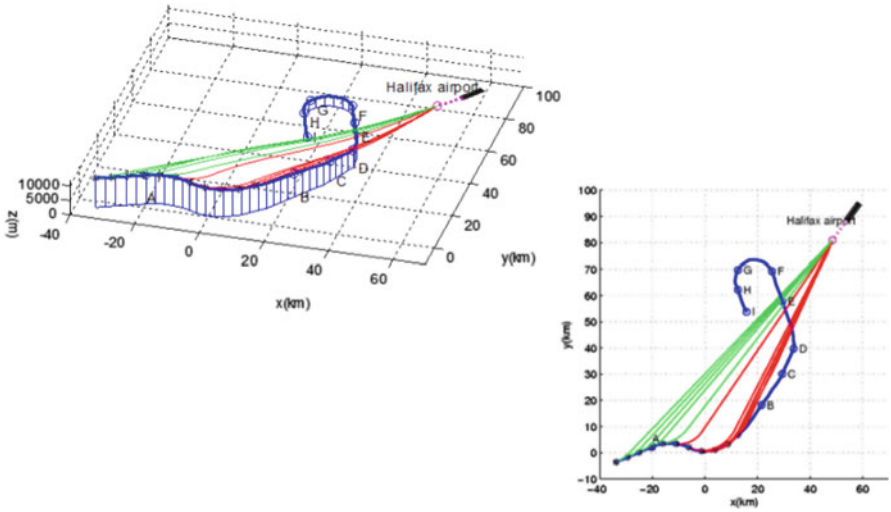

Fig. 24 Swissair 111 case backup trajectories generation in *green*. The *blue* trajectory represent the real flown trajectory

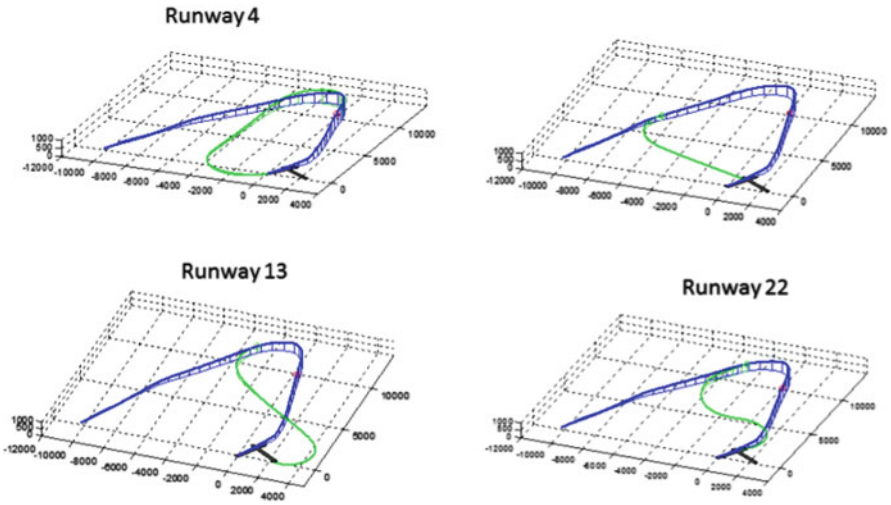

Fig. 25 US Air 1549 backup trajectories in *green*. The *blue* trajectory represent the real flown trajectory ending in Hudson river

This algorithm has also been applied to the US Air 1549 case. On January 15, 2009, the US Air 1549 flight struck a flock of Canada Geese during its initial climb out, lost engine power, and ditched in the Hudson River off midtown Manhattan. Again, the algorithm found four backup trajectories bringing back safely the aircraft the Laguardia airport (see Fig. 25).

8 Conclusion

This survey has shown several approaches for trajectory modeling. As it has been mentioned, trajectories are belonging to infinite dimension space for which dimension reduction has to be implemented. Using trajectory samples vectors is really redundant and inefficient. After having presented some definitions and some features of aircraft trajectories, some dimension reductions methods have been presented in order to be included in an optimization process. Interpolation and approximation technique have been presented and some information have also been given about Principal Component Analysis and Homotopy. The next section has presented wave front propagation approaches and gives some details on Fast Marching Algorithms, Ordered upwind algorithms and the light propagation algorithm (LPA). The fourth part has focused on methods coming automatic control for which vehicle dynamics are explicitly included in the models. Some applications to air traffic management have also been presented. The sixth part has presented an original path planning techniques mixing natural language processing and mathematical programming. Finally, some air traffic management applications have been presented for realistic cases.

References

1. Atkins EM, Portillo IA, Strube MJ (2006) Emergency flight planning applied to total loss of thrust. J Guid Control Dyn 43(4):1205–1216
2. Bakolas E, Zhao Y, Tsiotras P (2011) Initial guess generation for aircraft landing trajectory optimization. In: AIAA guidance, navigation, and control conference. AIAA
3. Bartels RH, Beatty JC, Barskyn BA (1998) An introduction to splines for use in computer graphics and geometric modeling. Computer graphics. Morgan Kaufmann, San Francisco
4. Becerra VM (2011) Psopt optimal control solver user manual. Tech. report
5. Bellingham J, Kuwata Y, How J (2003) Stable receding horizon trajectory control for complex environment. In: AIAA guidance, navigation, and control conference and exhibit. AIAA
6. Berger M, Gostiaux B (1988) Differential geometry: manifolds, curves and surfaces. Springer, New York
7. Betts JT (1998) Survey of numerical methods for trajectory optimization. J Guid Control Dyn 21(2):193–207
8. Betts JT, Huffman WP (1997) Sparse optimal control software SOCS. Tech. report, Mathematics and Engineering Analysis Technical Document MEALR-085, Boeing Information and Support Services, The Boeing Company
9. Betts JT, Huffman WP (1998) Mesh refinement in direct transcription methods for optimal control. Optim Control Appl Methods 19(1):1–21
10. Betts JT, Biehn N, Campbell SL, Huffman WP (2000) Compensating for order variation in mesh refinement for direct transcription methods. J Comput Appl Math 125:147–158
11. Binder T, Blank L, Dahmen W, Marquardt W (2000) Grid refinement in multiscale dynamic optimization. Tech. report, RWTH Aachen
12. Birkhoff G, de Boor C (1964) Piecewise polynomial interpolation and approximation. In: Proceeding of the general motors symposium of 1964. General Motors

13. Brudnicki DJ, McFarland AL (1997) User request evaluation tool (uret) conflict probe performance and benefits assessment. In: Proceeding of the air traffic management seminar, FAA/Eurocontrol
14. Bulirsch R, Montrone F, Pesch HJ (1991) Abort landing in the presence of windshear as a minimax optimal control problem. Part I: necessary conditions. J Optim Theory Appl 70(1):1–23
15. Bulirsch R, Montrone F, Pesch HJ (1991) Abort landing in the presence of windshear as a minimax optimal control problem. Part II: multiple shooting and homotopy. J Optim Theory Appl 70(2):223–254
16. Burrows JW (1983) Fuel-optimal aircraft trajectories with fixed arrival times. J Guid Control Dyn 6(1):14–19
17. Chaimatanan S, Delahaye D, Mongeau M (2012) Conflict free strategic planning. In: Proceeding of the 2012 interdisciplinary science for innovative air traffic management conference. ERAU
18. Chakravarty A (1985) Four-dimensional fuel-optimal guidance in the presence of winds. J Guid Control Dyn 8(1):16–22
19. Coppenbarger R, Lanier R, Sweet D, Dorsky S (2004) Design and development of the enroute descent advisor (eda) for conflict-free arrival metering. In: Proceeding of the AIAA-2004-4875 AIAA GNC conference. AIAA GNC
20. Davis L (1991) Handbook of genetic algorithms. Van Nostrand Reinhold, New York
21. de Boor C (1978) A practical guide to splines. Springer, New York
22. Dougui N, Delahaye S, Puechmorel D, Mongeau M (2012) A light-propagation model for aircraft trajectory planning. J Glob Optim 56:873–895
23. Enright PJ, Conway BA (1992) Discrete approximation to optimal trajectories using direct transcription and nonlinear programming. J Guid Control Dyn 15:994–1002
24. Erzberger H, Paielli RA, Isaacson DR, Eshowl MM (1997) Conflict detection in the presence of prediction error. In: Proceeding of the air traffic management seminar, FAA/Eurocontrol
25. Evans J et al (2003) Reducing severe weather delays in congested airspace with weather support for tactical air traffic management. In: Proceeding of the air traffic management seminar, FAA/Eurocontrol
26. Ewing GM (1969) Calculus of variations with applications. Norton, New York, reprinted by Dover, 1985
27. Farin G (1993) Curves and surfaces for computer aided geometric design. A practical guide. Academic, San Diego
28. Farin G, Hansford D (2000) The essentials of CAGD. A K Peters, Natick
29. Giancoli DC (1989) Physics for scientists and engineers with modern physics, 2nd edn. Prentice-Hall, Englewood Cliffs
30. Gong Q, Fahroo F, Ross IM (2008) Spectral algorithm for pseudospectral methods in optimal control. J Guid Control Dyn 31(3):460–471
31. Grimm W, Well K, Oberle H (1986) Periodic control for minimum-fuel aircraft trajectories. J Guid Control Dyn 9(2):169–174
32. Hargraves CR, Paris SW (1992) Direct trajectory optimization using nonlinear programming and collocation. J Guid Control Dyn 15:994–1002
33. Heath MT (2002) Scientific computing, an introductory survey. Computer graphics. McGraw-Hill, New York
34. Jackson MR, Zhao Y, Slattery RA (1999) Sensitivity of trajectory prediction in air traffic management. J Guid Control Dyn 22(2):219–228
35. Jacobson M, Ringertz UT (2010) Airspace constraints in aircraft emission trajectory optimization. J Aircraft 47:1256–1265
36. Jain S, Tsiotras P (2008) Multiresolution-based direct trajectory optimization. J Guid Control Dyn 31(5):1424–1436
37. Jain S, Tsiotras P (2008) Trajectory optimization using multiresolution techniques. J Guid Control Dyn 31(5):1424–1436
38. Jardin MR, Bryson AE (2001) Neighboring optimal aircraft guidance in winds. J Guid Control Dyn 24:710–715

39. Jeffreys H, Jeffreys BS (1988) Methods of mathematical physics. Cambridge University Press, Cambridge
40. Kelley HJ (1973) Control and dynamic systems: advances in theory and applications. Academic, New York
41. Kirk DB et al (2001) Problem analysis resolution and ranking (parr) development and assessment. In: Proceeding of the air traffic management seminar, FAA/Eurocontrol
42. LaValle SM (2006) Planning algorithms. Cambridge University Press, Cambridge
43. Liu W, Hwang I (2012) Probabilistic aircraft mid-air conflict resolution using stochastic optimal control. IEEE Intell Transp Syst Trans Mag
44. Lu P (1999) Regulation about time-varying trajectories: precision entry guidance illustrated. J Guid Control Dyn 22:784–790
45. Masalonis A et al (2004) Using probabilistic demand prediction for traffic flow management decision support. In: Proceeding of the AIAA-2004-4875 AIAA GNC conference. AIAA GNC
46. McNally BD, Bach RE, Chan W (1998) Field test evaluation of the ctas conflict prediction and trial planning capability. In: Proceeding of the AIAA-1998-4480 AIAA GNC conference. AIAA GNC
47. Meckiff C, Chone R, Nicolaon JP (1998) The tactical load smoother for multi-sector planning. In: Proceeding of the air traffic management seminar, FAA/Eurocontrol
48. Miele A (1990) Optimal trajectories and guidance trajectories for aircraft flight through windshears. In: Proceedings of the 29th IEEE conference on decision and control. IEEE
49. Mondoloni S, Bayraktuta I (2005) Impact of factors, conditions and metrics on trajectory prediction accuracy. In: Proceeding of the air traffic management seminar, FAA/Eurocontrol
50. Mondoloni S, Pagli SM, Green S (2002) Trajectory modeling accuracy for air traffic management decision support tools. In: Proceeding of the ICAS conference. ICAS, Toronto
51. Oberle HJ, Grimm W (1989) BNDSCO - a program for the numerical solution of optimal control problems. Tech. report. Institute for Flight System Dynamics, German Aerospace Research Establishment Oberpfaffenhofen
52. Ohtsuka T (2002) Quasi-Newton-type continuation method for nonlinear receding horizon control. J Guid Control Dyn 24:685–692
53. Osher S, Sethian JA (1988) Fronts propagating with curvature-dependent speed: algorithms based on Hamilton-Jacobi formulations. J Comput Phys 79(1):12–49
54. Pontryagin LS, Boltyanski VG, Gamkrelidze RV, Mischenko EF (1962) The mathematical theory of optimal processes. Interscience, New York
55. Pêtrès C, Pailhas Y, Patron P, Petillot Y, Evans J, Lane D (2007) Path planning for autonomous underwater vehicles. IEEE Trans Robot 23(2):331–341
56. Ramsay JO, Silverman BW (2005) Functional data analysis. Springer series in statistics. Springer, New York
57. Rao AV, Benson D, Huntington GT (2011) User's manual for GPOPS version 4.x: a matlab package for software for solving multiple-phase optimal control problems using hp-adaptive pseudospectral methods. Tech. report
58. Roche E (1997) Parsing with finite-state transducers. In: Roche E, Schabes Y (eds) Finite-state language processing. MIT Press, Cambridge
59. Ross IM (2005) User's manual for DIDO: a MATLAB application package for solving optimal control problems. Tech. report, Naval Postgraduate School
60. Russell RD, Shampine LF (1972) A collocation method for boundary value problems. Numerische Mathematik 19:13–36
61. Ryan HF, Paglione M, Green S (2004) Review of trajectory accuracy methodology and comparison of error measure metrics. In: Proceedings of the AIAA-2004-4787 AIAA GNC conference. AIAA GNC
62. Schouwenaars T, How J, Feron E (2004) Receding horizon path planning with implicit safety guarantees. In: American control conference, Boston, MA, June 2004, pp 5576–5581
63. Schouwenaars T, Valenti M, Feron E, How J, Roche E (2006) Linear programming and language processing for human/unmanned-aerial-vehicle team missions. AIAA J Guid Control Dyn 29(2):303–313

64. Schultz RL (1990) Three-dimensional trajectory optimization for aircraft. J Guid Control Dyn 13(6):936–943
65. Schwartz A (1996) Theory and implementation of numerical methods based on runge-kutta integration for solving optimal control problems. Ph.D. thesis, Université Montpellier II, France
66. Sethian JA (1999) Fast marching methods. SIAM Rev 41(2):199–235
67. Sethian JA, Vladimirsky A (2003) Ordered upwind methods for static Hamilton-Jacobi equations: theory and algorithms. SIAM J Num Anal 41:325–363
68. Seywald H (1994) Long flight-time range-optimal aircraft trajectories. J Guid Control Dyn 19(1):242–244
69. Seywald H, Cliff EM (1994) Neighboring optimal control based feedback law for the advanced launch system. J Guid Control Dyn 17:1154–1162
70. Seywald H, Cliff EM, Well K (1994) Range optimal trajectories for an aircraft flying in the vertical plane. J Guid Control Dyn 17(2):389–398
71. Slattery RA, Zhao Y (1997) Trajectory synthesis for air traffic automation. J Guid Control Dyn 20(2):232–238
72. Sridhar B, Ng HK, Chen NY (2011) Aircraft trajectory optimization and contrails avoidance in the presence of winds. J Guid Control Dyn 34:1577–1583
73. Strube MJ, Sanner RM, Atkins EM (2004) Dynamic flight guidance recalibration after actuator failure. In: AIAA 1st intelligent systems technical conference. AIAA
74. Sud V et al (2001) Air traffic flow management collaborative routing coordination tools. In: Proceeding of the AIAA-2001-4112 AIAA GNC conference. AIAA GNC
75. Swensen HN et al (1997) Design and operational evaluation of the traffic management advisor at the forth worth air route traffic control center. In: Proceeding of the air traffic management seminar, FAA/Eurocontrol
76. Swierstra S, Green S (2003) Common trajectory prediction capability for decision support tools. In: Proceeding of the air traffic management seminar, FAA/Eurocontrol
77. Tomlin C, Pappas GJ, Sastry S (1998) Conflict resolution for air traffic management: a study in multi-agent hybrid systems. IEEE Trans Automat Control 43:509–521
78. Vink A (1997) Eatchip medium term conflict detection: part 1 eatchip context. In: Proceeding of the air traffic management seminar, FAA/Eurocontrol
79. Weiss R (1974) The application of implicit Runge-Kutta and collocation methods to boundary value problems. Math Comput 28:449–464
80. Williams P (2004) Application of pseudospectral methods for receding horizon control. J Guid Control Dyn 27:310–314
81. Yan H, Fahroo F, Ross IM (2002) Real-time computation of neighboring optimal control laws. In: AIAA guidance, navigation, and control conference and exhibit. AIAA
82. Zhao Y (2011) Efficient and robust aircraft landing trajectory optimization. Ph.D. thesis, School of Aerospace Engineering, Georgia Institute of Technology
83. Zhao Y, Tsiotras P (2010) Density functions for mesh refinement in numerical optimal control. J Guid Control Dyn 34(1):271–277
84. Zhao Y, Tsiotras P (2010) Time-optimal parameterization of geometric path for fixed-wing aircraft. In: Infotech@Aerospace. AIAA, Atlanta
85. Zhao Y, Tsiotras P (2011) Stable receding horizon trajectory control for complex environment. In: American control conference (ACC), San Francisco, CA